

Investigation of Strategies for Risk Minimisation of Adverse Alkali-Silica Reaction in Concrete

by

Elsie Nsiah-Baafi

Thesis submitted in fulfilment of the requirements for
the degree of

Doctor of Philosophy

under the supervision of

Dr. Kirk Vessalas

Dr. Paul Thomas

Professor Vute Sirivivatnanon

University of Technology Sydney
Faculty of Engineering and Information Technology

February 2021

Certificate of Original Authorship

I, *Elsie Nsiah-Baafi* declare that this thesis, is submitted in fulfilment of the requirements for the award of *Doctor of Philosophy* in the *School of Civil and Environmental Engineering, Faculty of Engineering and Information Technology* at the University of Technology Sydney.

This thesis is wholly my own work unless otherwise referenced or acknowledged. In addition, I certify that all information sources and literature used are indicated in the thesis.

This document has not been submitted for qualifications at any other academic institution.

This research is supported by the Australian Government Research Training Program.

Production Note:
Signature removed prior to publication.

Signature: Elsie Nsiah-Baafi

Date: February 23, 2021

ACKNOWLEDGMENTS

Foremost, I wish to extend my deepest gratitude to my supervisors: Dr. Kirk Vessalas, Dr. Paul Thomas, and Professor Vute Sirivivatnanon. Words cannot express how much I appreciate the guidance and training you have given me throughout my doctoral study. I always count myself blessed for the opportunity to study under your supervision. ***Thank you!***

I would also like to acknowledge the support I have received throughout my research work from the UTS Science Technical Officers: Dr. Alex Angeloski, Dr. Mark Lockrey, and Dr. Herbert Yuan for their support with the analytical and characterisation studies carried out in their respective laboratory. I am also grateful to the FEIT Laboratory Technical Officers: Johir Mohammed, Rami Haddad, Mulugeta Hailu, and the UTS Service life facilities Technical Support Assistant, Ann Yan. I truly appreciate all the assistance I have received from you. ***Dankie!***

I also acknowledge the assistance I have received from the School of Civil and Environmental Engineering Academic Officer, Van Le, for ensuring all the documentation surrounding my candidature is submitted to the university on time.

Salamat!

My gratitude also goes out to Muans Abdulnebe of Boral Materials and Technical Services for supplying the non-reactive Australian aggregates used, facilitating the work done in the initial stages of this study, and allowing my involvement in some industrial laboratory concrete mixing for essential training purposes. ***Mahalo!***

I sincerely thank ARC Nanocomm Hub for the financial support during my doctoral study. Similarly, I am grateful to Sue Freitag of WSP Opus and James Mackechnie of Concrete NZ for providing financial support and the New Zealand aggregates used in this study. I salute their very informative discussions on the codes of practice in New Zealand and their contribution to reviewing some of the published results from this study. ***Medaase!***

I am thankful to my family for their support and encouragement through this journey. I truly could not have done this without you. ***Merci!***

Finally, to my research mates, thank you for making this study a memorable one. ***Xièxiè!***

LIST OF PUBLICATIONS

E., Nsiah-Baafi, K., Vessalas, P., Thomas and V., Sirivivatnanon, 2018, Mitigating Alkali-Silica Reactions in the Absence of SCMs: A Review of Empirical Studies. Proceedings, 5th International fib Congress, 7-11 October 2018, Melbourne, Australia.

E.Nsiah-Baafi, K., Vessalas, P., Thomas and V., Sirivivatnanon, 2019, Investigating Reactive Aggregate Combination for Alkali-Silica Reaction Risk-Free Concretes, Concrete Institute of Australia's Biennial National Conference, 8-11 September 2019, Sydney, Australia

E., Nsiah-Baafi, K., Vessalas, P., Thomas and V., Sirivivatnanon, 2019, Investigation of Alkali Threshold Limits and Blended Aggregate in ASR Risk-free Concretes, Concrete NZ conference, 10-12 October, Dunedin, New Zealand.

E., Nsiah-Baafi, K., Vessalas, P., Thomas and V., Sirivivatnanon, 2020, Protocols for Investigating Reactivity of Aggregates and Alkali thresholds for ASR Prevention, 16th International Conference on Alkali Aggregate Reaction in Concrete (ICAAR), October 2021, Lisboa, Portugal.

E., Nsiah-Baafi, K., Vessalas, P., Thomas and V., Sirivivatnanon, 2020, Mitigation of ASR using Aggregate Fines as Alternative for SCMs, 16th International Conference on Alkali Aggregate Reaction in Concrete (ICAAR), June 2021, Lisboa, Portugal.

TABLE OF CONTENTS

CERTIFICATE OF ORIGINAL AUTHORSHIP	II
ACKNOWLEDGMENTS	III
LIST OF PUBLICATIONS	V
TABLE OF CONTENTS	VI
LIST OF FIGURES	XI
LIST OF TABLES	XXII
ABSTRACT	XXV
CHAPTER 1. INTRODUCTION	1
1.1 Research Aims	6
1.2 Research Objectives	6
1.3 Significance of Research	7
1.4 Organisation of Thesis	8
CHAPTER 2. LITERATURE REVIEW	11
2.1 Overview	11
2.2 Alkali-Silica Reaction (ASR)	11
2.3 Pre-requisites for ASR	13
2.3.1 Reactive Aggregates	14
2.3.2 Alkali content	16
2.3.2.1 Potential Internal Sources of Alkali	17
2.3.3 Moisture	19
2.4 Environmental Influence on ASR	21
2.5 Mechanism of ASR	23
2.5.1 Chemical Mechanism of ASR	23
2.5.1.1 Factors Affecting the Formation of Alkali-Silica Gel	25
2.5.2 Pore Solution Alkali Cations	26
2.5.2.1 Role of Calcium Hydroxide	28
2.5.3 Characteristics of Alkali-Silica Gel and Expansion Mechanism	30
2.5.3.1 Expansion Mechanism of Alkali-Silica Gel	32

2.6	Symptoms and Effects of ASR.....	35
2.7	Test Methods for Assessing ASR.....	41
2.7.1	Standard Test Methods for Assessing ASR.....	44
2.7.1.1	Petrography.....	45
2.7.1.2	Chemical Reactivity Test.....	47
2.7.1.3	Concrete Prism Test (CPT).....	50
2.7.1.4	Accelerated Concrete Prism Test (ACPT).....	51
2.7.2	Limitations of CPT.....	53
2.8	Mitigation and Control of ASR.....	55
2.8.1	Use of Non-Reactive Aggregates.....	56
2.8.2	Restricting Moisture Access.....	56
2.8.3	Limiting Alkali Content.....	57
2.8.3.1	Using Low Alkali Content Cement.....	58
2.8.3.2	Alkali Limits in Concrete.....	59
2.8.3.3	Addition of Supplementary Cementitious Materials (SCMs).....	61
2.8.4	Addition of Ground Siliceous Particles.....	67
2.8.5	Use of a Non-Expansive Aggregate Combination.....	71
	Chapter Summary.....	72
CHAPTER 3. MATERIALS AND METHODS FOR ASSESSING AGGREGATE REACTIVITY AND ALKALI-SILICA REACTION.....		75
3.1	Overview.....	75
3.2	Materials.....	75
3.2.1	Aggregates.....	75
3.2.2	Cement.....	76
3.2.3	Reagents.....	77
3.3	Methods.....	78
3.3.1	Physical Expansion Test Methods.....	78
3.3.1.1	Accelerated Mortar Bar Test (AMBT).....	78
3.3.1.2	Concrete Prism Tests.....	83
3.3.2	RILEM Recommended Methods for Determining Alkali Limits of Aggregates.....	88
3.3.3	Chemical Tests.....	90
3.3.3.1	ASTM C289.....	90
3.3.3.2	Dissolution Test.....	91
3.3.3.3	Ground Aggregate Slurry Test (GAST).....	92

3.3.3.4	Ground Aggregate Paste Test (GAP).....	94
3.3.4	Characterization Techniques.....	95
3.3.4.1	Petrography.....	95
3.3.4.2	Microstructural and Elemental Compositional Analysis.....	98
3.3.4.3	Sample Preparation.....	101
3.3.4.4	X-Ray Diffraction Analysis (XRD).....	104
3.3.4.5	X-Ray Fluorescence Spectroscopy (XRF).....	107
3.3.4.6	Thermogravimetric Analysis (TGA).....	108
3.3.5	Microwave Plasma Atomic Emission Spectroscopy (MP-AES).....	111
3.3.6	Laser Diffraction Particle Size Analysis.....	114
3.3.7	Compressive and Flexural Strength Tests.....	115
	Chapter Summary.....	116

CHAPTER 4. INVESTIGATING ALKALI LIMITS AND AGGREGATE BLENDS FOR MITIGATING DELETERIOUS ASR IN CONCRETES..... 117

4.1	Overview.....	117
4.2	Experimental Plan.....	119
4.2.1	Materials.....	119
4.2.2	Methods.....	121
4.3	Results and Discussion.....	124
4.3.1	Petrographic Assessment of Aggregates.....	124
4.3.2	Chemical Tests.....	129
4.3.3	Expansion Tests.....	134
4.3.3.1	Accelerated Mortar Bar Test (AMBT).....	134
4.3.3.2	Concrete Prism Test (CPT).....	138
4.3.3.3	Accelerated Concrete Prism Test (ACPT).....	141
4.3.3.4	Potential Correlation between Test Methods.....	142
4.3.4	Determination of Alkali Limits.....	143
4.3.4.1	Determination of Alkali Limits at 24 Months.....	146
4.3.4.2	Minimizing the risk of ASR using sand blends (WT ¹ and WT ²).....	149
4.3.5	Petrographic Analysis of Mortar and Concrete Samples.....	149
4.3.5.1	Mortar Bars.....	149
4.3.5.2	Concrete Prisms.....	157
	Chapter Summary.....	165

CHAPTER 5. CORRELATIONS BETWEEN ASR TEST METHODS USED FOR ASSESSING POTENTIAL REACTIVITY OF AGGREGATES 168

5.1	Overview.....	168
5.2	Experimental Plan	169
5.2.1	Statistical Analysis	169
5.2.1.1	Pearson's Correlation Coefficient Method	169
5.2.1.2	Factorial Analysis	170
5.2.2	Leachate Assessment of CPT Expansion Tests	172
5.3	Results and Discussion	174
5.3.1	Reliability of Existing Test Methods for Aggregate Reactivity Determination	174
5.3.2	Correlation between Expansion Test Methods	178
5.3.2.1	Accelerated Mortar Bar Test (AMBT) and Concrete Prism Test (CPT).....	178
5.3.2.2	Concrete Prism Tests at 38°C (CPT) and 60°C (ACPT)	182
5.3.3	Leachate Assessment for Concrete Prism Expansion Tests.....	185
5.3.4	Assessment of Factors that Affect ASR Expansion.....	193
5.3.4.1	Principal Component Analysis (PCA).....	193
5.3.4.2	Analysis of Variance.....	195
	Chapter Summary	198

CHAPTER 6. INVESTIGATING THE ASR MITIGATION POTENTIAL OF GROUND REACTIVE AGGREGATE FINES.....200

6.1	Overview.....	200
6.2	Experimental Plan	202
6.2.1	Materials	202
6.2.1.1	Ground Reactive Aggregate Fines (GRAFs)	202
6.2.1.2	Reference Aggregates.....	205
6.2.2	Methods.....	205
6.2.3	Chemical Tests.....	207
6.2.3.1	Dissolution of Silicon and Aluminium from GRAF in Alkaline Solution.....	207
6.2.3.2	Paste Studies	207
6.2.4	Expansion Tests	211
6.2.4.1	Accelerated Mortar Bar Test (AMBT)	211
6.2.4.2	Concrete Prism Tests (CPT) and Accelerated Concrete Prism Tests (ACPT).....	212
6.3	Results and Discussion	213
6.3.1	Determination of Silicon and Aluminium released from Ground Reactive Aggregate Fines (GRAFs) in Alkali solution	213
6.3.1.1	Characterisation of reaction products	216

6.3.2	Influence of Ground Reactive Aggregate Fines (GRAFs) on the Pore Solution Chemistry of Pastes.....	223
6.3.2.1	Alkalinity (pH) of Pore Solutions	223
6.3.2.2	Ion Concentration of Pore Solutions.....	226
6.3.3	Expansion Test Results	233
6.3.3.1	Effect of Ground Reactive Aggregate Fines on ASR Expansion of Mortar Bars ...	234
6.3.3.2	Effect of Ground Reactive Aggregate Fines on ASR Expansion of Concrete Prisms	241
6.3.4	Thermogravimetric Analysis (TGA) of Pastes containing GRAFs.....	244
6.3.5	Influence of Ground Reactive Aggregates on Mechanical Properties of Concrete	248
6.3.6	Evaluating ASR Mitigation Mechanism of Ground Reactive Aggregates through Post-Expansion Characterisation of Concrete Prisms	251
	Chapter Summary	265
	CHAPTER 7. CONCLUSION.....	267
7.1	Overview.....	267
7.2	Investigation of Alkali Limits and Aggregate Blends for Mitigating Deleterious ASR in Concretes (Chapter Four).....	267
7.3	Correlation between Test Methods for Assessing Potential ASR of Aggregates (Chapter Five)	272
7.4	Investigating the ASR Mitigating Potential of Ground Reactive Aggregate Fines (Chapter Six)	276
	CHAPTER 8. RECOMMENDATION FOR FUTURE STUDIES.....	280
	REFERENCES.....	283
	APPENDIX A.....	321
	APPENDIX B.....	323
	APPENDIX C	330

LIST OF FIGURES

Figure 2.1 Schematic representation of ASR and Thomas Stanton in 1940 with a bridge parapet wall showing evidence of ASR (Thomas, Fournier & Folliard 2013)	12
Figure 2.2 A typical two dimensional schematic of the silicate structure showing (a) crystalline silica and (b) amorphous silica (Brown 2012)	15
Figure 2.3 A typical example of alkali (sodium) within an amorphous silica structure (Callister & Rethwisch 2014)	19
Figure 2.4 Effects of water-to-cement ratio on ASR expansion of concrete specimens (Stark 1995).....	20
Figure 2.5 Schematic representation of (a)-(b) the hydrolisation of silica and to form silanol (c) alkali charge balancing resulting in the formation of alkali silicate (Pignatelli, Comi & Monteiro 2013)	25
Figure 2.6 Effect of solution alkalinity (pH) on the concentration of silica dissolved (Cs) (Vogelsberger, Seidel & Rudakoff 1992)	26
Figure 2.7 Changes in the expansion of mortar bars in 0.05M NaOH solution as a function of SiO ₂ /Na ₂ O ratio of the ASR gel formed (Glasser & Kataoka 1981).....	28
Figure 2.8 Schematic molecular model of a typical ASR gel (Vayghan, Rajabipour & Rosenberger 2016)	30
Figure 2.9 Schematic diagram of DDLs mechanism of ASR gel expansion (reconstructed from(Pignatelli, Comi & Monteiro 2013)).....	34
Figure 2.10 Symptoms of ASR. (a) map cracking (b) efflorescence and exudation of ASR gel from concrete cracks (c) aggregate pop-out (d) surface discoloration and ASR gel exudation from map cracks (Thomas, Fournier & Folliard 2013).....	36

Figure 2.11 The Chickamauga lock and dam showing extensive cracking due to ASR (dominating mechanism) and ACR (Smith et al. 2017).....	37
Figure 2.12 ASR affected concrete showing (a) cracks, exudation, efflorescence, and discoloration on a bridge beam, (b) longitudinal crack on a concrete beam, and (c and d) misalignment of concrete members (Thomas, Fournier & Folliard 2013)	39
Figure 2.13 The Los Angeles sixth street viaduct showing signs of significant ASR (Muscato 2017)	40
Figure 2.14 Recommended protocol for assessing the reactivity of aggregates to minimize the risk of ASR. (Standards Australia 2015)	42
Figure 2.15 (a) Examples of SCMs. <i>From left to right</i> ; fly ash (Class C), metakaolin, silica fume, fly ash (Class F), slag and calcined clay, and (b) image of the Nant-y-Moch Dam (a 60-year-old bridge) containing reactive aggregates and 50% fly ash (Thomas, Fournier & Folliard 2013).....	62
Figure 2.16 Effects of (a) SCM addition on the expansion of mortar bars (Tapas et al. 2019) and (b) SCM composition on dosage requirement for effective ASR mitigation in concrete(Thomas 2011).....	64
Figure 2.17 Effect of SCM fineness and dosage on the compressive strength. Data from (Chindaprasirt, Jaturapitakkul & Sinsiri 2005).....	66
Figure 2.18 Linear distribution of elements (Ca, Si and Na) along a partly reacted finely ground glass grain, showing evidence of a pozzolanic reaction to form (Na-C-S-H) ASR gel(Afshinnia & Rangaraju 2015b).....	68
Figure 2.19 SEM micrographs of concrete sample containing (a) 100% cement and (b) 30% glass powder. <i>Note: 1= Aggregate; 2= ASR gel</i> (Afshinnia & Rangaraju 2015b)	69
Figure 2.20 Influence of particle size on the reactivity of reactive silica (Thomas 2011)	70

Figure 3.1 AMBT procedure showing (a) Horbat mixer (b) AMBT moulds (c) initial curing of mortar bars in a humidity cabinet (d) water curing of mortar bars at 80°C (e) ageing in 1M NaOH hot bath at 80°C, and (f) horizontal comparator for measuring expansion at respective ages	80
Figure 3.2 Concrete mixing procedure.....	85
Figure 3.3 Concrete mixing with principal supervisor and laboratory technicians, for CPT and ACPT, and schematic and photograph of prism storage method (showing absorbent polypropylene rope) during curing for CPT and ACPT.....	86
Figure 3.4 38°C environmental chamber for CPT and the horizontal comparator for CPT and ACPT prism expansion measurements carried out in this study.....	87
Figure 3.5 ASTM C289 standard curve for identifying reactivity of aggregates	91
Figure 3.6 Procedure for GAST method (a) ring mill for grinding aggregates to micron-sized powders (b) ground aggregate slurries in 80°C oven and (c) ground aggregate slurry after day 1 of testing.....	93
Figure 3.7 Petrographic slides for mortar bars studied	96
Figure 3.8 SEM-EDS instrument used in this study	98
Figure 3.9 Electron interactions and resulting emissions during SEM. <i>Modified image from</i> (Mazumder et al. 2018)	99
Figure 3.10 Labotom15 cutting machine for mortar and concrete sectioning	102
Figure 3.11 Set-up for mounting and polishing specimens for SEM-EDS analysis....	103
Figure 3.12 Prepared powder samples for XRD analysis	105
Figure 3.13 Schematic of θ - θ Bragg-Brentano configuration and Burker X-ray diffraction instrument used in this study.....	106
Figure 3.14 Atomic model explaining the principle of XRF analysis (Francisco; 2018)	107

Figure 3.15 General TGA curve for hydrated cement (Singh et al. 2015).....	109
Figure 3.16 Thermal analyser used for TGA in this study.....	110
Figure 3.17 4200 Agilent Technologies MP-AES instrument with an autosampler....	113
Figure 3.18 Malvern MasterSizer 3000 laser diffraction particle size analyser.....	114
Figure 4.1 Plane polarised petrographic images of aggregate (a) aggregate WT, (b) GW, (C) RT, and (d) PR. Note: Q= Quartz; Q''= Quartz veining through aggregate particle; F= Feldspar; G= Indurated greywacke in aggregate RT (notice the resemblance to aggregate GW); P= Pumice, and epidote vein cutting across the meta-greywacke fragment of aggregate GW	128
Figure 4.2 Classification of aggregates according to the dissolution test (as per ASTM C289).....	130
Figure 4.3 Compiled dissolution test from (Freitag 2003) for aggregate AS (x). Modified from (Black 2009).....	132
Figure 4.4 TG-DTG results of 28 days GAST test on aggregates	133
Figure 4.5 AMBT expansion results for aggregates at (a) 0.6 M, (b) 0.8 M and (c) 1.0 M NaOH alkali concentration.....	136
Figure 4.6 12 months CPT expansion results for the selected aggregates (a) including aggregate AS and (b) excluding aggregate AS at 38°C and 5.25 kg/m ³ Na ₂ O _e alkali content. <i>Note: Initial expansion (Day 0/Month 0) is 0.00%. Graphs represent expansion measurements from Day 7 (Month 0.25)</i>	139
Figure 4.7 6 months ACPT expansion results for aggregates at 60°C and 5.25 kg/m ³ Na ₂ O _e alkali content. <i>Note: Initial expansion (Day 0/Month 0) is 0.00%. Graphs represent expansion measurements from Day 7 (Month 0.25)</i>	142
Figure 4.8 12-month CPT expansion of aggregates at varying alkali content (Na ₂ O _e)	145
Figure 4.9 24-month CPT expansion of aggregates at varying alkali content (Na ₂ O _e)	146

Figure 4.10 Petrographic images of mortar bar WT showing (a) photograph of cut-off dyed block surface (*image width= approx. 20mm*), (b) fine crack joining two acid volcanic fragments and showing porosity in a glassy shard and acid volcanics, (c) ASR induced open crack passing through an acid volcanic and porous depleted glassy shard, as well as through quartz grains and (d) ASR gel lining an air bubble leading from micro-cracks within a beta-form quartz grain (*Note: SCALE= 200µm*) 152

Figure 4.11 Petrographic images of mortar bar GW_F showing (a) polished and dyed cut-off blocks from the mortar bars (*image width= approx. 20mm*), (b) ASR gel lining air bubbles and open micro-cracking in greywacke clast, (c) micro-cracks pass through and connecting greywacke clasts and, (d) an ASR-filled crack passing through a greywacke fragment (*Note: SCALE= 200µm*) 154

Figure 4.12 Petrographic images of mortar bars containing aggregate WT¹ showing (a) cut-off block from the mortar bar with fine porosity and micro-cracks occurring in and around WT grains and in the cement matrix (*image width= approx. 20mm*), (b) micro-cracks passing through silica depleted (porous) acid volcanic and glassy shard fragments (c) a crack passing through acid volcanic fragment. *Note the remnants of ASR gel in the cracks* and, (d) ASR gel lining an air bubble and, many micro-cracks emanating from the edge of the air bubble into the cement matrix (*Note: SCALE= 200µm*)..... 156

Figure 4.13 Petrographic images of the mortar bars containing aggregate WT² showing (a) dyed cut-off mortar blocks (*image width= approx. 20mm*), (b) conspicuous ASR-filled crack passing through an acid volcanic fragment and a silica-depleted (porous) acid volcanic fragment, (c) a micro-crack through a greywacke fragment and along an ovoid air bubble lined with ASR gel and (d) ASR gel lining air bubbles with associated micro-

cracks passing into cement matrix. *Note the internal cracking and depletion-induced porosity in a glassy acid volcanic clast (Note: SCALE= 200µm)* 157

Figure 4.14 Plane and cross-polarized transmission light images of WT¹ CPT prism showing (a) ASR gel lining an air bubble (inner rim), outlined by fibrous ettringite (outer rim) and micro-crack passing through glassy acid volcanic clasts and, (b) ASR gel lining an air bubble replaced by fibrous ettringite. *Note micro-cracks passing through cement matrix and alongside a quartz grain into the gel lined air bubble. (Note: SCALE= 200µm)* 159

Figure 4.15 Plane and cross-polarized transmission light images of WT¹ ACPT prism showing (a) an air bubble lined with fibrous ettringite and ASR gel in micro-cracks passing through cement paste and quartz grain and (b) ASR gel lining an air bubble that is thinly outlined by low birefringent ettringite. Basaltic PR_C can also be seen *(Note: SCALE= 200µm)* 160

Figure 4.16 Plane and cross-polarized transmission light images of WT² CPT prism showing (a) fine cracking running alongside meta-greywacke fragments suspected to be bleeding gaps, (b) micro-crack joining two quartz grains and running alongside a glassy volcanic clast (c) an air void (pore) lined by remnants of a clear ASR gel and associated micro cracks around the air bubble and, (d) a micro-crack joining a glassy fragment and a meta-greywacke fragment *(Note: SCALE= 200µm)* 162

Figure 5.1 Selected variables for factorial analysis..... 171

Figure 5.2 (a) Filtration and (b) dilution of sampled CPT and ACPT storage water for MP-AES analysis 174

Figure 5.3 Relationship between GAST after 56 days and 12 months CPT expansion test 177

Figure 5.4 Relationship between AS 1141.60.1 AMBT and AS 1141.60.2 CPT test methods	180
Figure 5.5 Related studies on the comparison of AMBT and CPT results for several aggregates from various projects	181
Figure 5.6 Correlation between AMBT and CPT for different aggregates assessed under AS 1141.60.1 and AS 1141.60.2 test methods.....	182
Figure 5.7 Correlation between 12 months CPT and 3 months ACPT expansion tests.	184
Figure 5.8 Alkali leaching from prisms tested under CPT condition (38°C). <i>Note: All concrete prisms have initial alkali content of 5.25 kg/m³ Na₂O_e</i>	186
Figure 5.9 Alkali leaching from prisms tested under ACPT condition (60°C). <i>Note: All concrete prisms have initial alkali content of 5.25 kg/m³ Na₂O_e</i>	186
Figure 5.10 Alkali leaching from prisms containing only cement, tested under CPT and ACPT. <i>Note: All concrete prisms have initial alkali content of 5.25 kg/m³ Na₂O_e</i>	188
Figure 5.11 Alkali leaching for one prism tested under standard CPT condition at varying alkali contents (total alkali measured divided by three).....	191
Figure 5.12 Scree plot of extracted principal components and related eigenvalues	194
Figure 5.13 Loading plot for variables in principal component analysis.....	195
Figure 5.14 Effect of varying alkali and temperature on measured expansion.....	197
Figure 6.1 A typical example of GRAFs used and the particle size distribution of cement, GRAFs, and FA.....	204
Figure 6.2 SEM micrograph and elemental mapping of fractured hardened paste surface showing (a) GRAFs in paste and (b-c) well-dispersed GRAFs (Si) in paste (<i>Note: Paste contains 25% RH_G</i>)	208

Figure 6.3 Photographs of paste specimens during curing phase for pore solution analysis	209
Figure 6.4 Illustration of pore solution extraction device	210
Figure 6.5 Photograph of (a) concrete specimens cast for the various tests and (b) concrete cylinder during 28 days compressive strength testing.....	213
Figure 6.6 Concentration of silicon released by GRAFs and FA in 1M NaOH at 80°C	214
Figure 6.7 Concentration of aluminium released by GRAFs and FA in 1M NaOH at 80°C	216
Figure 6.8 Microstructure of (a) unreacted FA and (b-d) FA treated in 1M NaOH alkali solution at 80°C after 28 days	217
Figure 6.9 Schematic showing the zeolitization process of FA (Fansuri, Pritchard & Zhang 2008)	218
Figure 6.10 Microstructure of (a) unreacted WT _G and (b-d) WT _G treated in 1M NaOH alkali solution at 80°C after 28 days	219
Figure 6.11 Microstructure of (a) unreacted GW _G and (b-d) GW _G treated in 1M NaOH alkali solution at 80°C after 28 days	220
Figure 6.12 Microstructure of (a) unreacted RH _G and (b-d) RH _G treated in 1M NaOH alkali solution at 80°C after 28 days	221
Figure 6.13 XRD diffraction patterns of GRAFs and FA (a) untreated and (b) treated in 1M NaOH at 80°C after 28 days.....	222
Figure 6.14 Effect of temperature on the measured pH of pore solutions of pastes containing GRAFs after 28 days.....	224
Figure 6.15 Effect of age on the measured pH of pore solutions of pastes containing GRAFs at 38°C	225

Figure 6.16 Total alkali concentration of the pore solution after 28 days and varying temperatures	227
Figure 6.17 Total alkali concentration of the pore solution at 38°C and varying ages	229
Figure 6.18 Ca/Si ratio of the pore solution of pastes after 28 days and varying temperatures	230
Figure 6.19 Concentration of Al in the pore solution of pastes after 28 days and varying temperatures	230
Figure 6.20 AMBT expansion results of aggregates used as GRAFs.....	234
Figure 6.21 Effect of GRAFs on AMBT expansion of mortar bars with reactive test aggregates WT (a-c) and RT (d-f).....	237
Figure 6.22 AMBT results of mortar bars containing GRAFs and FA at 25% cement replacement level	238
Figure 6.23 AMBT expansion results for mortar bars containing reference aggregate WT and ground non-reactive aggregate PR (PR _G).....	239
Figure 6.24 Mortar bar expansions as related to three cement alkali contents in 1M NaOH 80°C test solution (Islam et al. 2016)	240
Figure 6.25 Expansion results of 12 months CPT at 38°C for concrete prisms containing GRAFs and FA. <i>Note: Initial expansion (Day 0/Month 0) is 0.00%. Graphs represent expansion measurements from Day 7 (Month 0.25)</i>	241
Figure 6.26 Expansion results of ACPT (CPT at 60°C) for concrete prisms containing GRAFs and FA. <i>Note: Initial expansion (Day 0/Month 0) is 0.00%. Graphs represent expansion measurements from Day 7 (Month 0.25)</i>	243
Figure 6.27 Microstructure of fractured paste samples containing (a) FA (2000x) and GRAFs (WT _G) (1000x) cured at 60°C after 28 days (<i>Note the presence of ettringite (Ett)</i> ,	

<i>portlandite (CH), calcium silicate hydrate (C-S-H), calcium aluminium silicate hydrate (C-A-S-H), and aluminate ferrite monosulfate (AFm)</i>	244
Figure 6.28 Portlandite content in pastes containing GRAFs at different dosages after 28 days curing at 80°C	245
Figure 6.29 (a) Full range DTG curves and (b) partial range DTG curves showing portlandite content in pastes with 25% cement replacement after 28 days at CPT temperature (38°C) <i>Note: Area under portlandite curve represents the amount of portlandite present in the system</i>	247
Figure 6.30 (a) Full range DTG curves and (b) partial range DTG curves showing portlandite content in pastes with 25% cement replacement after 28 days at ACPT temperature (60°C) <i>Note: Area under portlandite curve represents the amount of portlandite present in the system</i>	247
Figure 6.31 Effect of GRAFs and FA on the compressive and flexural strengths of concrete after 28 days.....	249
Figure 6.32 Appearance of concrete prisms after 8 months ACPT (<i>Note micro-cracks (within red squares) and map cracking on the surface of control samples (OPC)</i>)	252
Figure 6.33 SEM-BSE micrograph and elemental mapping of ASR gel found in the control sample (WT- control) after 8 months (242x) (<i>Note: aggregate has higher Na alkali content</i>)	254
Figure 6.34 Morphology of crystalline ASR gel after 8 months (a) forming on the surface of the aggregate particle in the control prisms (5000x) (b) ASR gel at a higher magnification (10000x).....	256
Figure 6.35 SEM-SEI micrograph and elemental mapping of ASR gel found in concrete prism containing 25% WT _G after 8 months (400x)	257

Figure 6.36 SEM-SEI micrographs of the concrete prisms containing 25% GW_G showing ASR gel in cracks after 8 months (a) along the aggregate-paste interface (500x) and (b) within the paste (250x).....260

Figure 6.37 SEM-SEI micrograph and elemental mapping of ASR gel found in concrete prism containing 25% GW_G after 8 months (1000x)261

Figure 6.38 SEM-SEI micrographs of concrete prisms containing 25% RH_G at (a) 200x (b) 200x (c) 250x and (d) 500x, showing extensive cracking and presence of ASR gel after 8 months (*Note red arrows in (c) indicate the reaction rim of aggregate*)263

LIST OF TABLES

Table 2.1 Composition of ASR gel identified in different studies	31
Table 2.2 Examples of concrete structures around the world that have suffered effects ASR.....	39
Table 2.3 Laboratory Test methods for ASR assessment.....	44
Table 2.4 ASR susceptible minerals in aggregates (Islam & Akhtar 2013).....	47
Table 2.5 Variations in adopted AMBT test methods (Golmakani 2013)	49
Table 2.6 Expansion limits and reactivity classification as per the different current CPT methods	51
Table 2.7 Alkali limits specified in CSA A23.2-27A (Canadian Standards Association 2000)	60
Table 3.1 Description of all the aggregates used in this study	76
Table 3.2 The chemical composition of the cement used, as determined by XRF analysis	77
Table 3.3 Grading requirement for manufactured fine aggregates in AMBT according to AS 1141.60.1.....	79
Table 3.4 AMBT aggregate reactivity classification by AS1141.60.1 test method	82
Table 3.5 Coarse aggregate grading requirement for CPT and ACPT under AS 1141.60.2	84
Table 3.6 Classifications of aggregate reactivity levels in accordance with RILEM AAR 3.2.....	89
Table 3.7 Selected wavelengths of the desired elements for MP-AES analysis	113
Table 4.1 Aggregates and sand blends selected for investigating alkali limits	119

Table 4.2 Summary of the test program showing the different test methods used, the sample description and test conditions.....	122
Table 4.3 Mortar bars and concrete prisms selected for post-expansion petrographic assessment.....	124
Table 4.4 Mineralogical composition and reactivity classification of aggregates selected for investigating alkali limits, as determined by petrography.....	125
Table 4.5 ASTM C1778 Classification of Aggregate Reactivity.....	138
Table 4.6 RILEM AAR-3.2 reactivity categories and recommended alkali limits as per RILEM AAR-7.1	148
Table 4.7 Summary of aggregate reactivity classifications based on various expansion tests and suggested alkali limits	148
Table 4.8 ASR causative minerals in the respective aggregates and their mortar bars	151
Table 5.1 Comparison of reactivity classification by various test methods	175
Table 5.2 Correlation between 12 months CPT results and ACPT results at different ages	183
Table 5.3 Alkali leaching (Na_2O_e) for three concrete mixes, during CPT and ACPT expansion tests	187
Table 5.4 Effect of alkali content on alkali leaching during CPT per prism (total alkali measured divided by three).....	190
Table 5.5 Percentage of alkali in safety margin and leached alkali per prism at alkali content of $4.0 \text{ kg/m}^3 \text{ Na}_2\text{O}_e$	192
Table 6.1 Details of the ground reactive aggregates used in this study determined by petrography	203
Table 6.2 Chemical composition of GRAFs, FA, and cement determined by XRF	203
Table 6.3 Particle Size distribution of GRAFs, cement, and FA	204

Table 6.4 Summary of the test program for investigating the ASR mitigation potential of GRAFs	206
Table 6.5 Sodium and potassium ion concentration in the pore solution of pastes after 28 days as a function of temperature	228
Table 6.6 MP-AES results of pore solution of pastes containing GRAFs and FA at different ages.....	233
Table 6.7 EDS Analysis of ASR gels in concrete prisms after eight months (Atomic weight percentages have been normalized relative to oxygen).....	259

ABSTRACT

In recent decades, many structures worldwide have suffered damage due to alkali-silica reaction (ASR). This reaction is one of the most recognised chemical reactions leading to the deterioration of concrete. ASR is largely an alkali-activated process that causes the concrete to expand with time. To minimise the risk of expansion, a large focus has been placed on reducing the alkali content in the concrete when non-reactive aggregates are not available to use as part of the mix design. Restricting the alkali content can be achieved by: (i) imposing a generalised alkali limit of 0.6% Na_2O_e in cement and limiting the total alkali content in concrete to 2.5-2.8 kg/m^3 Na_2O_e ; and (ii) adding supplementary cementitious materials (SCMs) for partial replacement of the cement to limit and bind the amount of alkali available. While these practices have shown desired outcomes in the past, recent challenges surround the implementation of these practices, such as a shortage of SCM supply in the foreseeable future and the economic cost associated with using such solutions.

In addition, owed to the several limitations identified, the validity of classifying the reactivity status of aggregates against current short-term laboratory test methods employed for assessing ASR is under conjecture by researchers. This has left the concrete and cement industry with the inconvenient option of performing long-term tests extending up to 24 months to obtain a reliable prediction of an aggregate's reactivity. As a consequence, a delay in decision-making leading to a decrease in productivity is likely.

For these reasons, this study has been undertaken to explore sustainable and novel techniques for mitigating ASR that also encourage the conservation of natural

resources. Aggregates of different mineralogical compositions and reactivity potentials sourced from Australia and New Zealand were studied using a suite of test methods comprised of petrography, chemical tests, expansion tests, and analytical techniques.

The effect of varying alkali content on the expansion behaviour of selected aggregates was investigated via accelerated mortar bar test (AMBT), concrete prism test (CPT), and accelerated concrete prism test (ACPT) to establish specific alkali limits respective to the mineralogical composition and reactivity classification of the aggregate. Subsequently, the potential of using ground reactive aggregate fines (GRAFs) as alternative additives for mitigating ASR was evaluated. Pastes, mortar, and concrete specimens containing varying cement replacement levels of GRAFs were studied and compared against control and fly specimens using expansion tests, thermogravimetric analysis (TGA), and microwave plasma atomic emission spectroscopy (MP-AES) analysis carried out on extracted pore solutions. The effect of GRAFs on some mechanical properties of concrete was also measured. Furthermore, the correlation between the various test methods was investigated via a statistical approach involving the use of Person's correlation coefficient method and a modified factorial analysis approach to assess the validity of the different test methods and to determine the effects and interactions of ASR factors on expansion.

The results showed that a generalised alkali limit imposed on all aggregate types may not be necessary. It is further illustrated that the current alkali limits could be relaxed to accommodate the use of cement containing slightly higher alkali content with aggregates that are compatible, or revised from the current 2.5 to 2.8 kg/m³ Na₂O_e set in concrete. The efficacy of GRAFs in mitigating ASR as potential SCMs was

established as pozzolanicity was identified from the GRAFs investigated. Although the mechanical properties of concretes containing GRAFs were found to be lower than control concrete strength after 28 days, the GRAFs satisfied the ASTM C618 strength requirement for natural pozzolans revealing pozzolanicity for the coarser particle-sized GRAFs compared to fly ash and cement particle fineness. The findings also showed consistency in the reactivity prediction by the different methods. A positive correlation was found between CPT, chemical tests, and AMBT. Moreover, a correlation coefficient of $r= 0.9$ was found between 12 months CPT and three months ACPT, indicating that ACPT could be used as a reliable short-term test method for early predictions of the reactivity potential of aggregates.

CHAPTER 1. Introduction

Concrete is undoubtedly one of the most widely used materials for construction. The versatility of concrete is attributed to its economic benefits and the material's ability to be formed into impressive design shapes (Young, Mindess & Darwin 2002). A well-designed, manufactured, and placed concrete possesses several desired properties such as strength and stiffness. These macroscopic properties influence the durability of concrete, that is, its ability to withstand degradation (Berke, Hicks & Folliard 1997). Other factors that affect concrete durability include cement content, aggregate quality, permeability, and chemical deterioration mechanisms such as sulphate attack, delayed ettringite formation (DEF), and alkali-aggregate reaction (AAR).

Alkali aggregate reaction (AAR) refers to a group of reactions that occur in concrete between certain reactive minerals in the aggregate and hydroxide ions in the pore solution. These reactions are slow evolving and occur internally in concrete structures, leading to expansions that cause concrete damage (Islam & Akhtar 2013). Visible deterioration due to AAR is usually observed 10-15 years after concrete placement; however, in some instances, the damage to the concrete structure can occur earlier.

Generally, AAR describes two types of chemical reactions: (i) alkali carbonate reaction (ACR) and (ii) alkali-silica reaction (ASR). It has been established that ACR occurs in specific argillaceous dolomitic limestone aggregates, which are rare in most regions of the world (Katayama 2010). In contrast, there are many reported ASR cases worldwide, including New Zealand and Australia (Sims & Poole 2017), making ASR the most common form of AAR and the subject of this study.

Since 1940, ASR has become a matter of utmost concern for concrete manufacturers and the topic for discussion in many studies (Fournier & Bérubé 2000; Rowe & Freitag 1991; Sims; Nixon 2003; Stanton 1940). Literature establishes that the equilibrium triangle for ASR contains: the presence of reactive aggregate; high alkali content; and, sufficient moisture (Rajabipour et al. 2015). ASR occurs in the pore solution of concrete between dissolved silica from reactive aggregates, and alkali ions (Na^+ and K^+), and calcium from cement. The reaction leads to the formation of a hygroscopic ASR gel that expands upon the adsorption of moisture. The expansion of ASR gel usually results in distress of the concrete structure with cracks formed that can be deleterious or exacerbated by the synergy of applied stresses from other phenomena such as dynamic loads and cycles of freezing and thawing, thus increasing the rate of structural damage (Rajabipour et al. 2015; Stanton 1940).

Currently, there are limited options available for repairing ASR-affected structures. Once the ASR has manifested itself in field structures, the rate of deterioration may be mitigated by applying waterproofing products to reduce moisture ingress to the reaction site located within the concrete matrix. Owing to the severity of the reaction, precautions have been introduced to prevent ASR occurrence before the placement of concrete (Bérubé & Fournier 1993; Nixon & Sims 2016a). Feasible ASR mitigation techniques are usually targeted at eliminating one or more of the essential factors required for the reaction to proceed (Young, Mindess & Darwin 2002). Consequently, the common methods employed to mitigate ASR involve avoiding the use of reactive aggregates and modifying the composition of the pore solution by limiting alkalis and adding supplementary cementitious materials (SCMs). Further to this, an established recommendation by RILEM (Nixon & Sims 2016b) proposes that ensuring the use of non-reactive aggregates in concretes combined with the set alkali limits increases the

likelihood of successfully mitigating ASR in concretes, especially when the test method for assessing the aggregate's reactivity is inconclusive.

Although these methods have proven sufficient for mitigating ASR (Thomas et al. 2006), there are some recent emerging challenges associated with their implementation. For one, the preferred use of non-reactive aggregates may be impractical and costly, especially since non-reactive aggregates may not be readily and logistically available. Due to the rejection of supposed potentially reactive aggregates, there is a high demand for aggregate sources deemed acceptable. This is an increasing concern for the concrete industry worldwide as depletion of these acceptable sources is imminent.

Similarly, to reduce the amount of alkali made available to react with ASR susceptible aggregates, guidelines have been imposed on the allowable alkali content in concrete. Alkali limits are set as $2.8 \text{ kg/m}^3 \text{ Na}_2\text{O}_e$ in Australia (Standards Australia 2015) and $2.5 \text{ kg/m}^3 \text{ Na}_2\text{O}_e$ in New Zealand (CCANZ 2012). These limits are strict and generalized for all aggregates regardless of their mineralogical compositions. To achieve these limits, an additional alkali limit of $0.6\% \text{ Na}_2\text{O}_e$ has been imposed on cements in Australia and New Zealand (Standards Australia 2015; Standards New Zealand 2009a; Thomas et al. 2006). Cements with low alkali contents ($\leq 0.6\% \text{ Na}_2\text{O}_e$) can be challenging to achieve due to the limited availability of resources for cement production and the new methods used in clinker manufacturing. It is most likely that the manufacturer may have to discard kiln dust to achieve such low alkali percentages, making low alkali cements expensive to manufacture; therefore, presenting both environmental and economic challenges to the industry. Nonetheless, applying these limits does not guarantee that ASR will not occur. In fact, there are reported instances

where concrete structures containing low alkali cement have still experienced ASR (Fournier & Bérubé 2000; Stark & Bhatta 1986; Thomas et al. 2006). This is associated with the potential alkali contribution from certain minerals in aggregates (Rajabipour et al. 2015), as well as other external parameters that promote the expansion reaction to continue. Evidently, the alkali content that will initiate ASR is fundamentally dependent on the mineralogical composition of the aggregate used in the concrete (Thomas et al. 2006) and would typically vary from one aggregate to the next.

Undoubtedly, the most common ASR mitigating method involves the addition SCMs such as fly ash and granulated blast furnace slag. When added in appropriate amounts, SCMs effectively hinder deleterious ASR by reducing the amount of alkalis in the pore solution through a pozzolanic reaction (Chappex & Scrivener 2012; Diamond 1989), among other hydration reactions. The effectiveness of SCMs in this role is well documented (Duchesne & Bérubé 1994; Saha et al. 2018; Shafaatian et al. 2013; Skibsted & Snellings 2019; Thomas 1996a). However, in some countries, the use of SCMs in concrete is difficult and costly as SCMs are not locally obtainable (Durant, Bigley & Milestone 2013). Besides, SCMs are essentially by-products of other industrial processes, so their availability is much dependent on the operation of these industries. Therefore, where SCMs are routinely used in concrete for ASR mitigation, their availability could become limited in the untold future.

With the depleting sources of known compatible aggregate combinations for concrete structures, the need for testing both new and existing aggregate sources to ascertain their likelihood to ASR before incorporating them in concrete is crucial. At present, the most recognised laboratory test methods for ASR involve petrography, chemical

tests, and expansion tests like accelerated mortar bar test (AMBT), concrete prism test (CPT), and accelerated concrete prism test (ACPT). The reliability of these methods has been a topic of major discussion by several investigations for the past decade (Bérubé & Fournier 1992; Lu, Fournier & Grattan-Bellew 2006; Schouenborg, Åkesson & Liedberg 2008; Shayan 2001; Sirivivatnanon, Mohammadi & South 2016; Thomas et al. 2006). Related studies report on the limitations of the different test methods, especially when used unaccompanied to assess the reactivity level of an aggregate (Thomas et al. 2006). Due to these limitations, some test methods may provide false indications of an aggregate's reactivity level resulting in the rejection of so-called reactive aggregates. This, in turn, increases the burden on using acceptable aggregate sources only, leading to quicker depletion of these resources. The CPT test method, which is known to provide reliable results comparable to field performance, is a long-term test (12 to 24 months) and could be inconvenient for industry and practitioners when outcomes are needed within a much shorter timeframe for decision making.

In light of these challenges, this study investigates sustainable and alternative mitigation and testing protocols for reducing the risk of ASR occurrence in concretes that ensure the full utilisation of available aggregate and cement resources, thus conserving natural resources while improving the durability of concrete structures.

1.1 Research Aims

The aims of this study are to:

- ✚ Determine the alkali thresholds of aggregates with different mineralogical compositions and reactivity classification, to propose new and flexible alkali limits for aggregates based on their composition and reactivity.
- ✚ Identify and make recommendations on the reliability and correlation between the different test methods to suggest alternative accelerated test methods that offer comparable results to trusted long-term tests.
- ✚ Establish globally sustainable alternative mitigation strategies for ASR in the absence of conventional SCMs.

1.2 Research Objectives

To achieve the set aims, three principal objectives have been identified for this study.

- ✚ Investigate the effect of increasing alkali concentration on the reactivity of aggregates and ASR using expansion tests, and propose alkali limits as per RILEM recommended methods.
- ✚ Assess the correlation between the chemical and physical test methods using statistical methods, and identify the best age (test duration) at which ACPT expansion results are most comparable to 12 months of CPT.
- ✚ Evaluate the efficacy of ground reactive aggregates fines (GRAFs) as additives in concrete to reduce the risk of ASR occurrence.

- ✚ Explore the potential use of sand blends in concrete to decrease the amount of reactive silica available, thus reducing the risk of ASR.

1.3 Significance of Research

The findings from this study will contribute to both research and industry knowledge by providing recommendations for the safe use of potentially reactive aggregates in concrete in the foreseeable future. The determination of specific alkali limits for respective aggregates types will provide outcomes that could form the framework for revising the current single alkali limit that is used in concrete, particularly in New Zealand and Australia. Thus, alkali limits may be relaxed or customized for specific aggregate types. This will provide some flexibility for cement manufactures to utilise available resources and newer clinker manufacturing processes. The recommendations made in this study could also be adopted globally to accommodate available aggregate sources ensuring ASR risk-free concrete mixes are utilised in field structures.

Furthermore, the concept of incorporating GRAFs for ASR mitigation will introduce a circular economic opportunity to re-utilise aggregates that are highly reactive and otherwise unsafe for use in concrete. This strategy is globally achievable and will reduce the waste being designated to landfill sites. At present, the standard procedures for concrete mix design require a specific aggregate size grading where fine aggregate particles $\leq 125 \mu\text{m}$ are discarded (ASTM 2008; Nixon & Sims 2016c; Standards Australia 2014e). Therefore quarries that produce manufactured sand

discard large amounts of aggregate fines that result from the crushing of larger rocks, which could be repurposed for ASR mitigation.

Additionally, this work will also elaborate on the relationship between the different test methods for assessing ASR and provide evidence to support the validity of the short-term ACPT in ASR assessment. This will reduce the cost incurred from long-term testing and, more importantly, provide concrete industry with reliable data within a relatively short period for decision making.

1.4 Organisation of Thesis

This thesis consists of eight chapters. In this chapter (**Chapter One**), the background for this research, the research objectives, the research significance, and the thesis structure are presented. For the subsequent chapters, an overview describing the purpose of each chapter and a chapter summary outlining the key issues discussed are given.

Chapter Two provides a detailed review of the chemistry and mechanism of ASR, the effect of this reaction on concrete structures, the current test methods for assessing ASR and their respective limitations, and finally, the challenges associated with the existing techniques for mitigating ASR. Related studies on unconventional ASR mitigation techniques will also be discussed. This chapter aims to provide the reader with the necessary technical background knowledge on ASR, which is vital in understanding the significance and outcomes of this study.

Chapter Three presents the selected methods employed in this study to evaluate the ASR potential of aggregates and assess the proposed preventive measures addressed. A brief discussion on the principles behind the analytical techniques, the operating parameters, and test conditions for the different test methods used is presented.

The results from the exploratory work carried out in this thesis are specified in **Chapters Four, Five, and Six**. The principal objectives identified in Section 1.1 are addressed separately in the individual chapters. Each chapter begins with a description of the experimental plan, including the specific materials and methods used for achieving the set objective. This is followed by a thorough discussion of the results supported by literature.

In Chapter Four, the work done on the determination of alkali limits for different aggregate types is presented. This chapter also considers the potential of using sand blends to mitigate ASR in concretes, and explores the mechanism of ASR expansion as a function of temperature and alkali content.

Chapter Five submits the work carried out using statistical methods to evaluate correlations between the petrography, chemical, and physical expansion test methods. In this chapter, the alkali leaching effect in CPT and ACPT is addressed. Further, the effect of factors that influence ASR and related expansion is assessed.

The effectiveness of using ground reactive aggregate fines (GRAFs) to mitigate ASR is evaluated in **Chapter Six**. The findings of the work carried on slurries, pastes, mortar bars, and concrete prisms using a suite of analytical, chemical, and physical expansion test methods are given. This chapter also presents the characterisation of ASR products and the impact of the product's composition and concrete expansion.

Finally, based on the significant findings of this research, some suitable conclusions are made in **Chapter Seven**. Additionally, recommendations for future research are suggested in **Chapter Eight**, followed by a list of references supporting the claims made in this thesis.

CHAPTER 2. Literature Review

2.1 Overview

This chapter provides a comprehensive review of literature relating to the fundamentals of ASR in concrete, the primary factors influencing ASR, and the common symptoms and effects of the reaction. The dynamics of ASR and theories surrounding the expansion mechanism of ASR gel are also discussed. This chapter will also address the recognised test methods for assessing ASR and the start-of-the-art ASR mitigating strategies employed in industry. At the end of the chapter, some emerging studies on proposed alternative ASR mitigation techniques will be evaluated.

2.2 Alkali-Silica Reaction (ASR)

The reaction between reactive silica from aggregates and alkalis in the pore solution of mortar and concrete is referred to as alkali-silica reaction (ASR). ASR results in the formation of a permeable alkali-silica gel (ASR gel) with a varying amount of calcium and the ability to absorb moisture, which expands and causes distress in concrete (Fournier & Bérubé 2000). The principal effect of ASR is the formation of cracks induced by the expansion of the ASR gel. These cracks allow further permeation of moisture in the concrete, which causes more ASR gel expansion leading to additional cracking. Cracks may also provide the pathway for other reactants such as chloride and sulphates to diffuse into the concrete structure and

cause further damage. ASR cracks can be deleterious on their own; however, in most cases, the cracks serve as the underlying cause for severe concrete damage through other reactions like corrosion of steel reinforcement, chloride and sulphate attack, and freeze-thaw cycling.

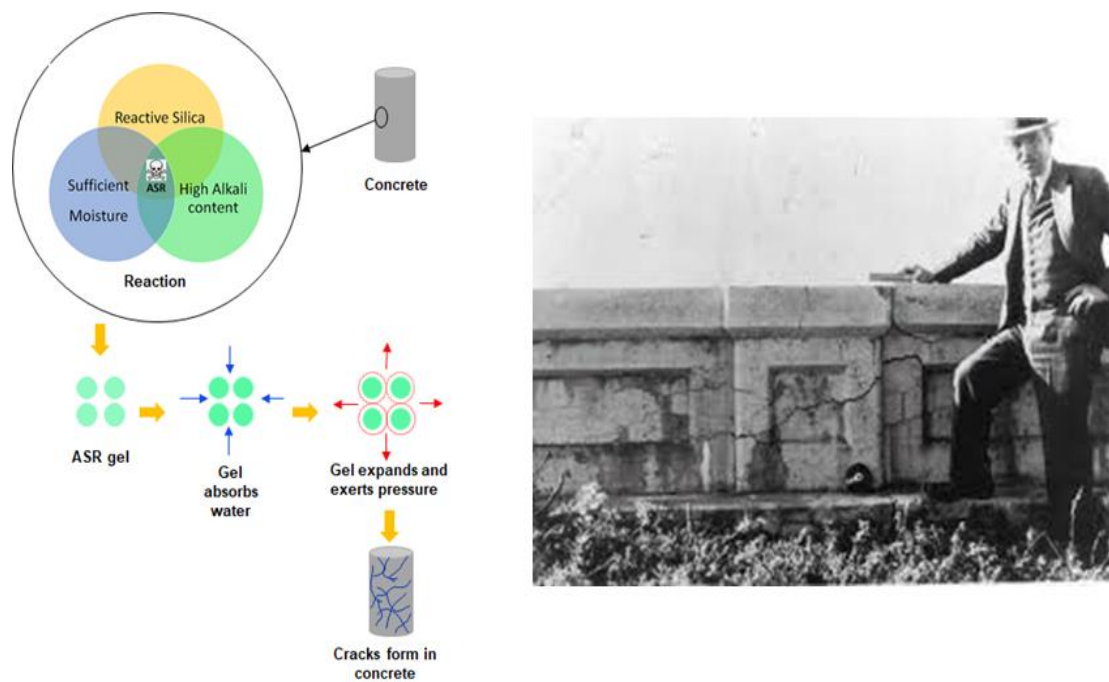


Figure 2.1 Schematic representation of ASR and Thomas Stanton in 1940 with a bridge parapet wall showing evidence of ASR (Thomas, Fournier & Folliard 2013)

Eighty years after ASR was first documented (Stanton 1940) (Figure 2.1), much has been reported in literature regarding the chemistry of ASR, the factors that contribute to the reaction, and the mechanism of expansion (Diamond 2000; Duchesne & Bérubé 1994; Kawamura & Iwahori 2004; Lindgård et al. 2012; Wang & Noguchi 2020). However, it is agreed that ASR is not well understood regarding the reaction products and different morphologies that transpire (Diamond 1997). Although the basic concepts are well documented, ASR cases differ from one location

to the other and are dependent on several factors, including environmental influence, which the reader will agree is difficult to control. Furthermore, once ASR begins in placed concrete, it is challenging to arrest the reaction (Ferrara et al. 2018). ASR can be slowed down by employing chemical treatments and stress relief and restraint methods (Fournier et al. 2005). Occasionally, post-hardening finishes such as patching are practiced to seal the cracks induced by ASR; nevertheless, the reaction will proceed until the eventual deterioration of the concrete. This is why ASR has also been termed “concrete cancer” (Kazmi et al. 2017; Wang & Noguchi 2020), and thus the need for research to continue to understand its varying morphological stages better.

2.3 Pre-requisites for ASR

From the description of ASR (also shown in Figure 2.1), it is clear that the conditions for the reaction to occur are:

- ✚ Presence of high alkali concentration in the pore solution
- ✚ Availability of reactive forms of silica
- ✚ Presence of sufficient moisture

The absence of one of the factors required to initiate deleterious ASR reduces the likelihood of ASR-induced expansion (Hobbs 1988).

2.3.1 Reactive Aggregates

With the exception of a few mono-mineralitic rocks, such as igneous anorthosites (composed solely of plagioclase feldspar), the majority of the aggregates used in concrete contain a significant amount of silica (SiO_2), usually in the form of quartz. Nonetheless, not all polymorphs of silica are reactive towards ASR. Metastable forms and forms of silica that show disorder in their crystal structure are usually ASR reactive. The extent of reactivity is dependent on the degree of disorder. Typical examples of reactive forms of silica include cherts, opal, volcanic glass, chalcedony, and tridymite. These minerals, as well as other constituents that may contribute to ASR, can be identified through petrographic examination of aggregates performed by qualified petrographers. However, the mineralogy of aggregates alone is inadequate in determining the extent of their reactivity. Therefore, standard laboratory testing is necessary to classify the ASR potential and reactivity level of aggregates.

Other reactive forms of silica include amorphous and strained quartz. Typically, the molecular geometry of silica compounds exists as a tetrahedral network consisting of one central silicon atom (Si^{4+}) bonded at each silicate corner by oxygen atoms, as shown in Figure 2.2 (Leming et al. 1996).

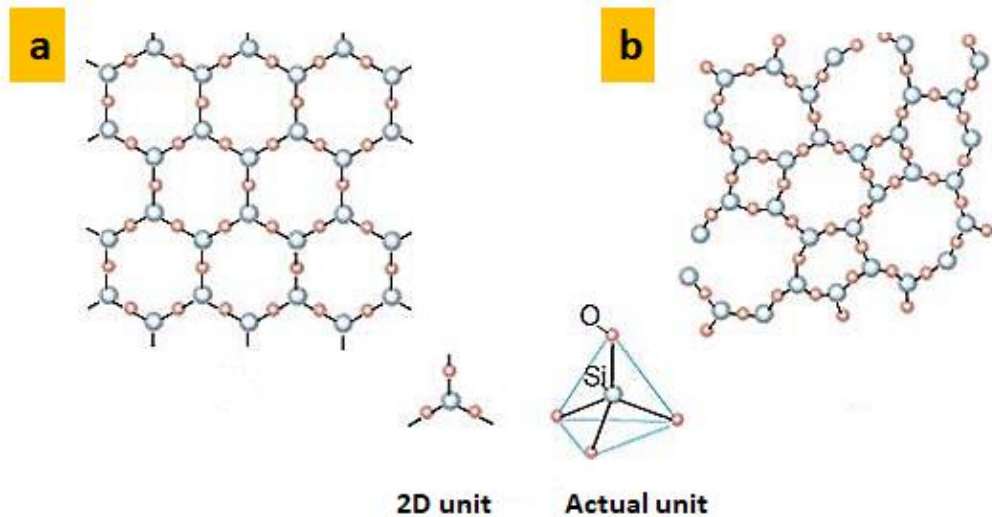


Figure 2.2 A typical two dimensional schematic of the silicate structure showing (a) crystalline silica and (b) amorphous silica (Brown 2012)

A crystalline (non-reactive) silica structure is formed when a repetition of the tetrahedral structure occurs in an ordered manner of 3D space (Touma, Fowler & Carrasquillo 2001). The outcome of this is that each oxygen atom becomes attached to two silicon atoms; thus, electrical neutrality is achieved within the structure while the surface remains negatively charged for minimal reaction (Leming et al. 1996), as shown in Figure 2.2a. Contrary to crystalline silica structures, amorphous silica structures (Figure 2.2b) result from a disarray of the silica tetrahedral arrangement. These structures have a porous network where electrical neutrality is unsatisfied, creating a reactive ion migration pathway. The porous network provides a larger reactive surface area for ASR to occur. As such, aggregates comprising amorphous silica are particularly very reactive (Bérubé & Fournier 1993).

Studies on the effects of internal grain size of aggregates on the degree of ASR have been carried out (Diamond & Thaulow 1974; Lindgård et al. 2012; Multon et al. 2010; Poyet et al. 2007; Wigum 2012). It has been reported that fine aggregates are

more susceptible to ASR. Due to their large surface area, fine aggregate exposes more silica for alkali attack (Hobbs 1988). While this may be true, other researchers have challenged that larger aggregates particles showed higher ASR expansion (Multon et al. 2008; Poyet et al. 2007). Perhaps, the contradictory results obtained by these studies did not consider the influence of a possible physical mechanism of ASR expansion in concrete. For instance, ASR expansion from fine-sized aggregates will not exert the same amount of expansive forces as observed for coarse-sized aggregates. Indeed, the theory surrounding the rate of reactions agrees with the observation that fine aggregates show more reactivity; however, more importantly, the type and amount of reactive silica present in aggregates is responsible for the extent of its ASR reactivity regardless of the size of the aggregate. For most aggregates, the amount of silica that causes deleterious ASR, also known as the pessimum amount, is small and may vary from 2-10% (Forster et al. 1998a), dependent on the type of reactive silica mineral present.

2.3.2 Alkali content

High alkali concentration in concrete is critical to the onset and progression of ASR (Rajabipour et al. 2015). Alkali ions are present in the pore solution as metal ions of sodium (Na^+) and potassium (K^+). At high alkalinity, the rate of silica dissolution is increased; thus, ASR proceeds rapidly. This implies that the maximum alkali content that will not initiate ASR in concrete, known as the alkali threshold, is dependent on the reactivity of the aggregate used (Thomas et al. 2006).

The majority of the alkalis available for ASR in concretes is supplied by the cement. This has influenced the decision from specifiers worldwide to impose alkali limits

on acceptable alkali contents in cement and subsequently concretes, as a precaution against ASR (Bérubé et al. 2002; Leming & Nguyen 2000).

The alkalis in cement (clinker) are unavoidable and derived from the clay or sulphate constituents of the raw materials used, such as shale. Over the years, the alkali content of Portland cement has increased due to changes in the manufacturing process of cement, as well as differences in the composition of the raw materials sourced for the manufacture of clinker (Diamond 1975). Typically, the alkali content in cement ranges from 0.2 – 1.1% by weight of oxide. Alkalis are released during cement hydration and become available in the pore solution as hydroxides of sodium (Na) and potassium (K) ions. ASR is dependent on the total alkali ion concentration. Thus, the alkali content in the concrete is defined as a sodium equivalent (Na_2O_e) of Na and K, expressed as:

$$Na_2O_e = Na_2O + 0.658K_2 \dots\dots\dots \text{Eqn 2.1}$$

Other sources of alkali to concrete include supplementary cementitious materials (SCMs), aggregates, chemical admixtures, de-icing agents, unportable mix water, and external sources such as the service environment.

2.3.2.1 Potential Internal Sources of Alkali

Supplementary Cementitious Materials (SCMs)

SCMs usually contain alkalis that can potentially slowly release into the concrete pore solution over time, thereby contributing to the formation of deleterious ASR at a later stage (Rajabipour et al. 2015; Shafaatian et al. 2013). The effect of the alkalis released from SCMs is dependent on the presence of reactive alumina ions and the

amount of free silica available in the respective SCM. SCMs with low alumina ion content have lower alkali binding properties (Chappex & Scrivener 2012; Hüniger, Hübner & Scholz 2016). Therefore, the alkalis present in such SCMs are not bound when released, causing an increase in the alkali content of the concrete with time. Studies on the use of fly ash (FA) for ASR mitigation report that FA with high calcium content tends to have high alkali contents and thus poor ASR mitigating capabilities (Chen, Soles & Malhotra 1993; Shafaatian et al. 2013). That said, neither the amount nor rate of alkalis released from SCMs in the lifetime of a concrete structure in service is certain (Rajabipour et al. 2015).

Aggregates

Another internal source of alkali that is equally difficult to quantify is the potential alkalis released from the aggregates. Consequently, instances occur where ASR expansions are still observed when low alkali content cement has been used (Grattan-Bellew 1995; Olague, Wenglas & Castro 2003; Stark & Bhatta 1986). Both reactive and non-reactive aggregates may contain releasable alkalis (Rajabipour et al. 2015); nevertheless, the amount of alkalis from aggregates that potentially contribute to the pore solution's alkalinity is challenging to quantify. At present, a reliable method for assessing the amount of alkalis released by aggregates is under investigation by RILEM Technical Committee 219-ACS (Nixon & Sims 2016a).

Typically, aggregates containing minerals such as quartzite, feldspar, zeolite, and dawsonite have the tendency to release alkalis into the pore solution when used in concrete (Bérubé 2004). The alkalis in aggregates may be encapsulated within the meta-stable silica structure of the aggregate, as shown in Figure 2.3, and slowly

released as the silica structure is dissolved (Rajabipour et al. 2015). Under severe conditions, some aggregates release alkalis equivalent to 10% of the total alkalis present in the Portland cement (Islam 2010). For example, the Witwatersrand quartzite in South Africa can release about 0.7% Na_2O_e of alkalis (Blight et al. 1981). Additionally, aggregates from marine sources and coastal locations such as limestone may be contaminated with sea salts. Sodium chloride (NaCl) that has been adsorbed by the aggregates from these environments can contribute to the alkali content when used in concrete.

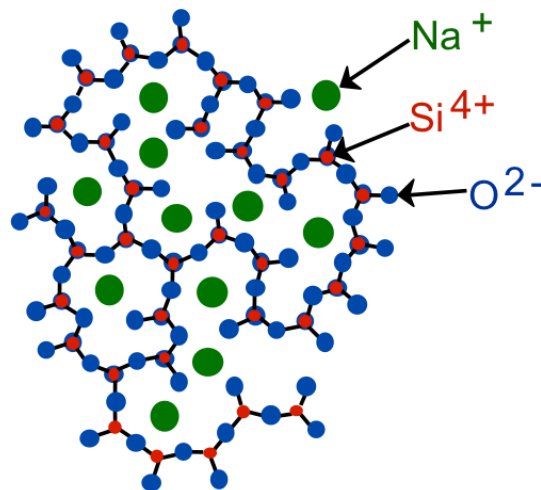


Figure 2.3 A typical example of alkali (sodium) within an amorphous silica structure (Callister & Rethwisch 2014)

2.3.3 Moisture

Moisture in concrete acts as both an ASR reactant and a transport medium for alkalis and other ions (Broekmans 2004) to infiltrate the concrete structure. From an understanding of the reaction sequence of ASR, it is clear that without sufficient

moisture, the ASR gels formed cannot exhibit deleterious expansion (Saouma & Perotti 2006). However, moisture is a challenging factor to control, especially in field structures. Usually, ASR gels absorb moisture from the mix water used in producing the concrete and the concrete's service environment. It goes without saying then, that the water-to-cement (w/c) ratio selected in the concrete mix design plays a crucial role in reducing the likelihood of ASR.

Figure 2.4 shows the results from a study on the influence of the w/c ratio on the ASR expansion of concrete prisms (Stark 1995). It can be observed that the level of expansion of aggregates increased with increasing w/c ratio. However, it is worth noting that a low w/c ratio in concrete indirectly implies a high cement content, resulting in high alkali content in the concrete (Shon, Zollinger & Sarkar 2002).

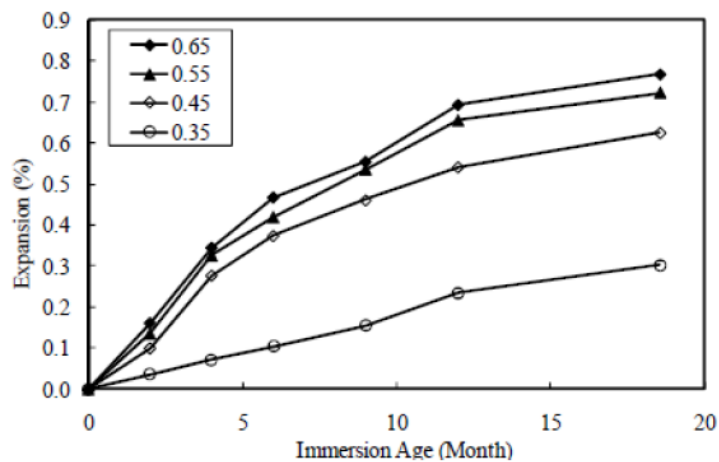


Figure 2.4 Effects of water-to-cement ratio on ASR expansion of concrete specimens (Stark 1995)

Usually, ASR gel expansion is exacerbated in environments with internal relative humidity above 85% (Fournier & Bérubé 2000). Restricting the moisture content to less than 70% relative humidity could effectively reduce deleterious ASR (Swamy

1991). A study conducted by Poole (Poole 1992) demonstrated, by drying concrete prisms, that ASR expansion decreases when ASR gel is partially dehydrated. It was further reported that upon rehydration, concrete prisms resumed expansion, except for specimens that were dried and carbonated prior to moisture contact. These outcomes also support the previous discussion that once ASR begins, it cannot be arrested.

For field concretes, a well thought-out structural design may allow the use of techniques such as tanking and cladding (Nixon & Sims 2016a) to reduce the concrete's access to moisture from the service environment. Yet, these methods are difficult to sustain for all weather conditions and can be costly.

2.4 Environmental Influence on ASR

The effect of environmental conditions on ASR is not well documented. This is mainly because the environmental conditions that affect ASR are not constant. Phenomena like changes in atmospheric temperature, excess moisture from rainfall, and other climate changes can increase the rate and degree of ASR. In designing and assessing the ASR risk of a concrete structure, one of the critical factors to consider is the environmental conditions to which the structure will be subjected (Nixon & Sims 2016a).

Several scientific experiments demonstrate that temperature acts as a catalyst for chemical reactions by increasing the kinetic energy and thus the rate of the reaction. Similarly, an increase in temperature can promote an increase in the rate of ASR,

especially at the onset of the reaction (Dolar-Mantuani 1983). However, the effect of temperature on the level of expansion achieved is dependent on the reactivity of aggregate (Young, Mindess & Darwin 2002). Even though concrete structures in warmer environments are more prone to ASR than structures in colder climates (Perenchio, Kaufman & Krause 1991), a reasonable degree of temperature can help maintain the surface of the concrete dry to prevent further the moisture needed for ASR gel expansion.

Laboratory tests conducted to determine the alkali reactivity of aggregates in concretes are usually performed at elevated alkali and temperatures to accelerate the reaction for timely results compared to field performance or exposure site tests. Consequently, the rate of ASR occurrence is more in laboratory test specimens; however, the reaction is likely to decline or approach a steady-state condition over time. Whereas in colder temperatures, a slow but longer reaction is expected. This effect of temperature on reaction is also observed among laboratory test methods that vary temperature, such as concrete prisms tests carried out at 38°C and 60°C. Accordingly, the analysis of an ASR affected concrete in Iceland revealed that the side of the concrete facing the sun experienced greater damages than the opposite side (Gudmundsson & Asgeirsson 1975) due to the differences in the degree of exposure temperature.

As discussed in Section 2.3.3, moisture is one of the requirements for ASR to occur. Moisture from the service environment depends mainly on weather changes such as rainfall; however, it could be subjective due to the atmospheric temperature. The drying and wetting cycles experienced by concrete structures in exposed environments is an essential factor to ASR. When temperature increases, the

amount of moisture (humidity) in the environment is expected to be minimal; thus, drying of the concrete surface and sub-surface could occur. This causes an increase in the concentration of alkalis in the drying zones, resulting in the dissolution of silica and higher ASR gel formation in these areas (Perenchio, Kaufman & Krause 1991). During the wetting cycle, usually caused by rainfall, excessive moisture dilutes the concentrated alkali pore solution and provides the moisture necessary for the expansion of the alkali-rich ASR gels formed during the drying cycle. This continuous cycle results in the formation of cracks that allow the permeation of moisture into the concrete structure to cause deleterious expansion and the eventual deterioration of the concrete.

2.5 Mechanism of ASR

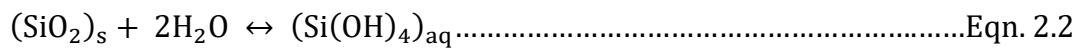
The mechanism of ASR has been described in-depth in several works (Glasser & Kataoka 1981; Helmuth et al. 1993; Rajabipour et al. 2015; Stanton 1940). The mechanism of ASR is described as a series of chemical reactions that occur continuously and simultaneously, from the dissolution of silica to the expansion of the ASR gel formed.

2.5.1 Chemical Mechanism of ASR

The chemical mechanism of ASR begins at the silica-pore solution interface with the dissolution of silica. Silica dissolution occurs in two distinct steps identified as: (i)

the hydrolysis of silica; also known as the hydroxyl ion attack and, (ii) the reaction of hydroxyl ions with the formed silanol structure (Glasser & Kataoka 1981). In crystalline silica, the breakdown of the lattice structure by alkali hydroxides is almost impossible; consequently, the silica is non-reactive.

When hydroxyl ions in the pore solution progressively attack the siloxane bond ($\equiv\text{Si-O-Si}$) of reactive silica, dissolution of the SiO_2 network results, causing the formation of silanol ($\equiv\text{Si-OH}$) bonds. Since the interatomic bond (Si-O-Si) is stronger than the hydrogen bond (O-H), the silica surface is left with a weak acidic character (Glasser & Kataoka 1981). The SiO_2 network dissolution reaction is further described in Equation 2.2 (Broekmans 2004; Walther & Helgeson 1977).



At high alkalinity, such as in concrete pore solution where alkali metal ions (Na^+ and K^+) are present, the OH^- ions penetrate the porous structure of reactive silica to dissolve $\text{Si}(\text{OH})_4$ further. This produces three Si-O^- species, thus creating a charge imbalance that is then satisfied by Na^+ and K^+ alkali ions in solution to form alkali silicates, as illustrated in Figure 2.5. The dissolution of silicate ions consumes OH^- ions resulting in a decrease in alkalinity (pH). As the pH decreases, the polymerisation reaction of the alkali silicate ions to form ASR gel begins.

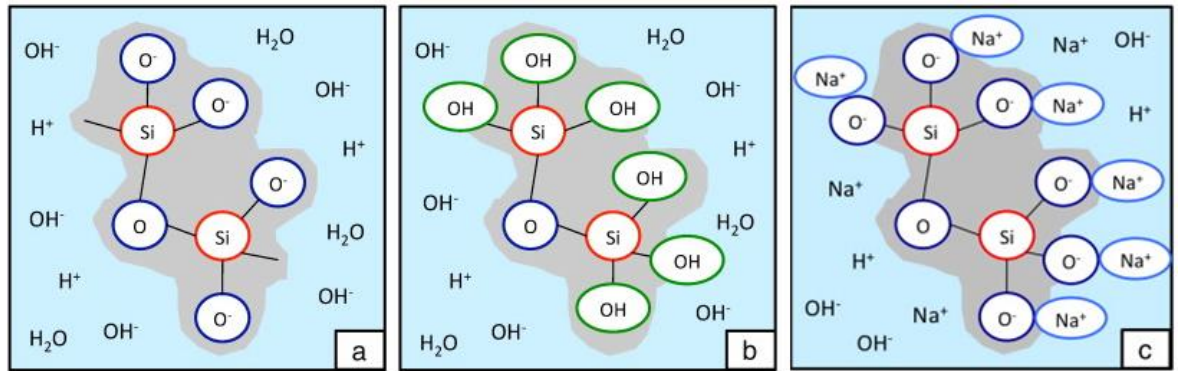


Figure 2.5 Schematic representation of (a)-(b) the hydrolisation of silica and to form silanol (c) alkali charge balancing resulting in the formation of alkali silicate (Pignatelli, Comi & Monteiro 2013)

2.5.1.1 Factors Affecting the Formation of Alkali-Silica Gel

Essential factors that influence ASR gel formation are: (i) the degree of solubility of silica at high pH; and (ii) the rate of silica dissolution. Usually, the forms of silica that exhibit a slow dissolution rate could potentially reduce the early onset of ASR.

Some studies have established that the silica dissolution rate, which is controlled by the reaction at the silica-solution interface, is linear with the pH of the pore solution (Helgeson, Murphy & Aagaard 1984; Holdren Jr & Berner 1979). However, a study using ground silica reported that the rate of silica dissolution is parabolic (Wirth & Gieskes 1979). Subsequent works have since provided data that suggest that the rate of silica dissolution may not exclusively be linear; instead, it is dependent on the surface reaction mechanism of the silica (Mazer & Walther 1994). These researchers further explained that silica dissolution is initially controlled by the diffusion of water through the silica network. Therefore, it can be concluded that surface area (particle size) and the degree of crystallinity of the silica are significant factors that alter the rate of silica dissolution and, thus, the formation of ASR gel.

Similarly, the solubility of reactive silica is affected by the pH of the pore solution (Vogelsberger, Seidel & Rudakoff 1992). Figure 2.6 summarises the result from a study carried out by Vogelsberger and co-workers.

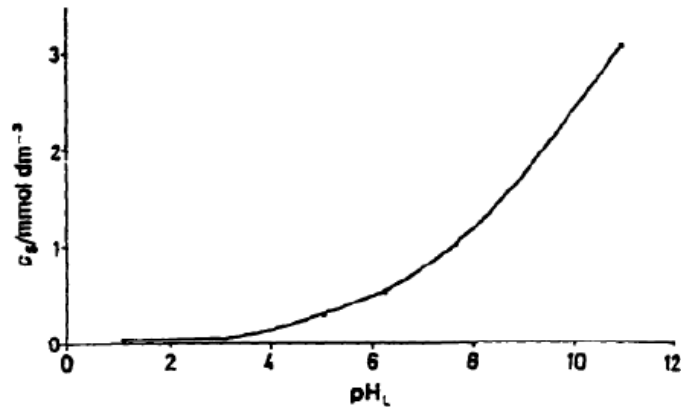


Figure 2.6 Effect of solution alkalinity (pH) on the concentration of silica dissolved (C_s) (Vogelsberger, Seidel & Rudakoff 1992)

The results from the study in Figure 2.6 show a parabolic relationship where an increase in silica concentration occurs as the pH of the solution increases. A parallel study presented by the same researchers (Vogelsberger, Seidel & Rudakoff 1992) stated that an increase in silica solubility occurs with an increase in temperature. Therefore, increasing the temperature increases the silica dissolution, as also observed in the work presented in this thesis (Figure 6.18).

2.5.2 Pore Solution Alkali Cations

The initial hydration of Portland cement releases calcium (Ca²⁺), potassium (K⁺), sodium (Na⁺), hydroxyl (OH⁻), and sulphate (SO₄⁻) ions. As the hydration reaction continues, Ca²⁺ and SO₄⁻ ions are decreased to trace concentrations while Na⁺ and K⁺

ions are increased. This decrease is associated with the precipitation of calcium silicate hydrates (C-S-H) and ettringite (Folliard et al. 2006). After approximately 24 hours, only alkali ions (Na^+ , K^+ , and OH^-) are present in noticeable concentrations in the pore solution (Nixon et al. 1987). After 30 days of hydration, the concentration of alkali ions in the pore solution approaches equilibrium (Diamond 1989).

Alkali cations (Na^+ and K^+) provide a better indication of the alkalinity of the pore solution. Typically, the total concentration of alkali in the pore solution depends on the alkali content of the cement; estimated at approximately 70 to 80% of the cement's alkali content (Diamond 1989). ASR usually occurs at $\text{pH} \geq 13.2$ (Mukhopadhyay 2013). Pore solutions with high Na^+ and K^+ ion concentrations are highly alkaline with typical pH values in the range of 13.2-13.9, dependent on the cement's alkali content and the concentration of Ca^{2+} ions in the pore solution. Usually, a decrease in the pore solution alkalinity is observed with an increase in Ca^{2+} . The role of calcium in the formation of ASR and its related expansion is discussed in Section 2.5.1.2.

Due to the limited diffusion that occurs in concrete, a saturation limit for dissolved silica is eminent when the alkali concentration of the pore solution is high. At silica saturation, the alkalinity of the pore solution decreases, and polymerisation of the dissolved silica into ASR gel begins. Aqueous alkali ions bond to negatively charged sites on the silica surface to form part of the ASR gel (Glasser & Kataoka 1981). Accordingly, ASR gel is composed of dissolved silica, alkali ions, and water. The ongoing process of silica dissolution and repolymerisation in the presence of water initiates the expansions that are associated with ASR. At a pessimum proportion of silica in the gel, the ratio of silica to alkali concentration is optimised to achieve the

highest ASR gel expansion. This is reported as a mole ratio of 6 for most reactive siliceous aggregates that exhibit a pessimum behaviour (Rajabipour et al. 2015). A similar conclusion has been arrived at by Glasser & Kataoka (Glasser & Kataoka 1981), as presented in Figure 2.7. From Figure 2.7, it can be that at a pessimum $\text{SiO}_2/\text{Na}_2\text{O}$ mole ratio of 5, the highest expansion in the studied mortar bars was measured.

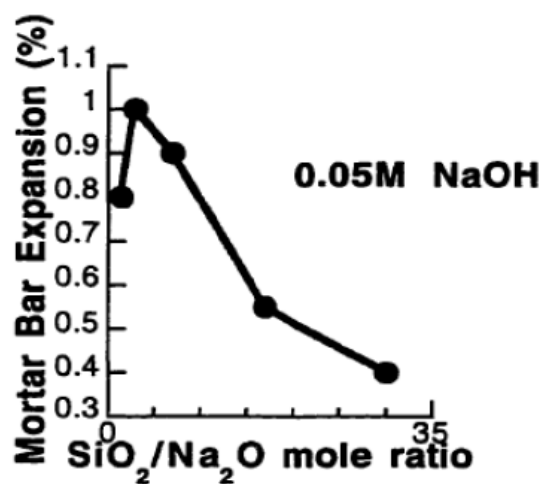


Figure 2.7 Changes in the expansion of mortar bars in 0.05M NaOH solution as a function of $\text{SiO}_2/\text{Na}_2\text{O}$ ratio of the ASR gel formed (Glasser & Kataoka 1981)

2.5.2.1 Role of Calcium Hydroxide

The effect of calcium ions on ASR raises much scrutiny and has been studied extensively. According to Powers & Steinour (Powers & Steinour 1955), the expansion produced by ASR gel is dependent on the ratio of Ca^{2+} to alkali ion concentration in the concrete pore solution. These researchers indicated that when the Ca^{2+} concentration is high, a non-swelling C-S-H gel is formed. Conversely, a lower Ca^{2+} concentration resulted in an expansive gel. On the other hand, while they

partly agree with the Power-Steinour theory, Wang and co-workers (Wang & Gillott 1991) argued that excess Ca^{2+} in pore solution promotes ASR. Ca^{2+} ions react to substitute some alkali ions in ASR gel and form a calcium-alkali-silica hydrate gel, which is the typical composition of ASR gel (Walther & Helgeson 1977). The substitution of Ca^{2+} ions releases alkali ions back into the pore solution hence allowing the regeneration of a high pH that results in the further dissolution of silica and the continuation of ASR formation.

A schematic molecular model of typical ASR gel is shown in Figure 2.8. In a study to understand the role of calcium in ASR gel expansion, it was observed that Ca^{2+} adheres to the gel to form a highly crystalline C-S-H network at the gel surface (Thomas 1998). Conversely, when the amount of Ca^{2+} ions in the solution was consumed, the reaction to form ASR gel was arrested. This observation indicates that calcium is necessary for the precipitation of ASR gel (Thomas 1998). However, it is worth mentioning that the total depletion of calcium is unlikely to occur. Portlandite ($\text{Ca}(\text{OH})_2$) crystals tend to form initially around aggregates in the concrete and later dissolve to replenish the consumed Ca^{2+} ions in the pore solution; therefore, acting as a buffer for the continuous precipitation of ASR gel (Glasser & Kataoka 1981).

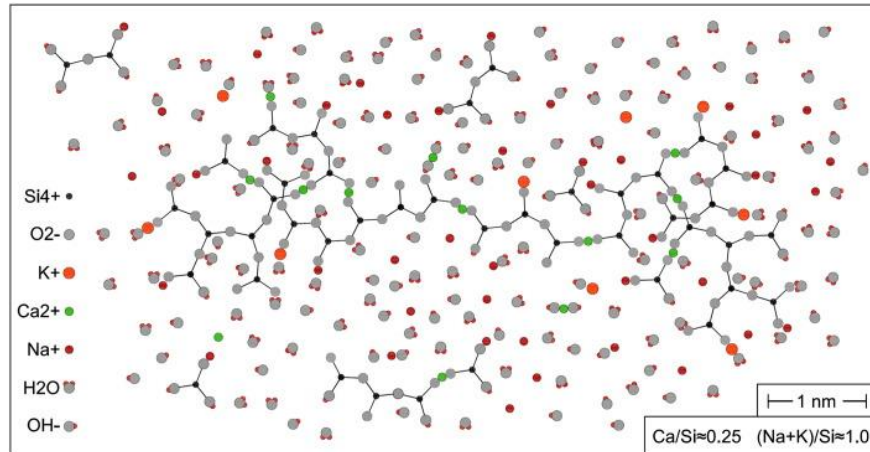


Figure 2.8 Schematic molecular model of a typical ASR gel (Vayghan, Rajabipour & Rosenberger 2016)

2.5.3 Characteristics of Alkali-Silica Gel and Expansion

Mechanism

ASR gel is composed predominantly of SiO_2 , with varying amounts of calcium and alkali oxides as well as water (Regourd-Moranville 1989). The chemical composition of ASR gel is not stoichiometric. It depends on the concentration of alkalis, calcium, and reactive silica present in the pore solution (Dolar-Mantuani 1983). Typical examples of the compositions of the ASR gel identified by various researchers are presented in Table 2.1. It can be seen from the table that the principal constituent of the ASR gel is SiO_2 and then alkali (Na and K). The amount of Ca in ASR gel varies significantly in comparison. It can also be noted that ASR gels that contain high amounts of alkali tend to have lower Ca content. This is as a result of alkali recycling (Rajabipour et al. 2015); a concept that will be discussed further in Section 6.3.6.

Table 2.1 Composition of ASR gel identified in different studies

% by mass					Reference
Na ₂ O	K ₂ O	SiO ₂	CaO	MgO	
12.9	---	53.9	2.9	0.6	Stanton (1942)
12.9	---	53.4	2.6	0.8	
14.9	5.2	61.7	0.6	---	Idorn (1961)
13.4	5.1	65.5	0.5	0.2	
12.4	4.9	69.9	0.3	0.5	
17.9	8.2	73.7	1.1	0.1	
9.4	4.1	72.8	1.3	0.2	
14.6	6.2	61.9	---	0.1	
16.2	5.7	56.8	---	---	
8.2	4.1	56.1	17.4	0.2	
8.3	5.0	28.5	22.4	0.2	
1.2	0.4	51.4	29.9	10.0	Poole (1975)
7.4	0.7	53.0	22.1	10.0	
1.5	13.9	38.9	27.3	---	Gutteridge and Hobbs (1980)
0.4	4.7	51.1	21.5	---	Regourd (1983)
---	0.6	27.9	35.2	---	
1.0	6.9	61.5	9.2	---	Oberholster (1983)
1.0	6.2	53.8	8.2	---	
1.8	5.5	49.9	12.8	---	
1.0	5.2	50.4	12.0	---	
1.4	9.0	62.9	12.5	---	
0.8	7.4	53.2	10.0	---	
1.2	4.1	66.5	6.5	---	Baronlo (1983)
3.7	12.9	43.3	21.8	0.8	Mullick and Samuel (1986)
3.9	11.7	49.4	15.9	0.5	
9.9	2.2	55.1	5.7	---	Sachlova, Prikryl and Pertold (2010)
10.4	0.2	50.5	4.7	2.2	
10.6	0.2	66.3	8.2	2.9	

Characterisation studies on the morphology of ASR gel indicate that the gel may possess either a less defined or textured structure (Shayan & Quick 1989). Less defined structured gels are typically seen as a dark reaction rim around the reactive silica particles and are usually the initial ASR gel formed (Regourd, Hornain & Poitevin 1981). An example of such ASR gels is shown in Figure 4.15. These ASR gels

are less expansive and tend to fill pre-existing cracks in the aggregates. In contrast, textured ASR gels evolve from the less defined ASR gels with age and are characterised as grainy, spongy, or foliated, depending on the concentration of Ca^{2+} present in the gel. The most common well-crystalline textured ASR gels are usually observed as rosette, lamella, and fibrous structures (Hu, Gautam & Panesar 2018; Shi et al. 2018).

2.5.3.1 Expansion Mechanism of Alkali-Silica Gel

The mechanism of ASR gel expansion is not well understood. However, it is generally established that osmotic pressure is generated upon moisture adsorption by ASR gel, which affects the surrounding cement paste and aggregate, resulting in expansion of the structure.

Currently, three theories surround the expansion mechanism of ASR gel. These are described as: (i) the Power-Steinour theory; (ii) the Chatterji's theory; and (iii) the electric double layers theory. Admittedly, several researchers agree with the Power-Steinour theory of ASR gel expansion (Powers & Steinour 1955). As discussed in Section 5.2.2, this theory postulates that the expansion of ASR gel is dependent on the amount of Ca^{2+} in its composition, such that gels with high Ca^{2+} content are less expansive. Ca^{2+} promotes cross-linking of the silicate structure, forming a more rigid structure with a lower capacity to expand (Shi & Lothenbach 2019). Furthermore, it is suggested that for porous reactive aggregates, when Ca^{2+} concentration is low, an increase in ASR gel formation within the aggregates occurs. This results in a discharge of gel from the reaction site (Pike 1958).

In contrast, Chatterji's theory (Chatterji et al. 1986) proposes a much complicated supposition that, at constant pH and ionic strength, absorption of OH⁻ ions decreases as the size of the associated hydrated cation (K⁺, Na⁺, Ca²⁺) increases. The OH⁻ absorbed cations will then penetrate reactive silica to attack the siloxane bonds, as discussed in Section 2.5.1. The authors further explain that this attack removes silica ions from their original sites and, thus, enables more diffusion of silica from the aggregate grains in a process controlled by the presence of Ca²⁺. At higher Ca²⁺ concentration, the diffusion of SiO₂ is reduced. That is, Ca(OH)₂ promotes the penetration of reaction ion molecules (including H₂O) into the reactive silica grain and hinders the diffusion of silicate ions. In this way, when there is a surplus amount of the reaction ions penetrating the reactive silica relative to the amount of silica leaving the grain, expansion occurs.

In the electric double layers (EDLs) theory (Rodrigues, Monteiro & Sposito 1999), the electrostatic repulsion between EDLs formed is accountable for generating the expansive forces exhibited by the ASR gel. This theory suggests that hydroxyl ions, which are negatively charged, react with the negatively charged surfaces of reactive silica to form ASR gel by exchanging electrical charges (Chatterji & Kawamura 1992). The ASR gel formed exhibits high negative charges on its surface. Consequently, cations in the solution are attracted to the gel, creating a diffuse electrical double layer of positive charges. This layer, also known as the Gouy-Chapman-Stern layer (Oldham 2008), is thin and derived from the ionic strength of the pore solution electrolytes. The EDLs formed are essentially part of a colloidal system composed of dissolved silicate particles surrounded by a diffuse layer of cations with excess anions dispersed in the pore solution. Therefore, the expansion

of the gel is determined by the particle-particle interface, as illustrated in Figure 2.9, showing the EDL layers discussed.

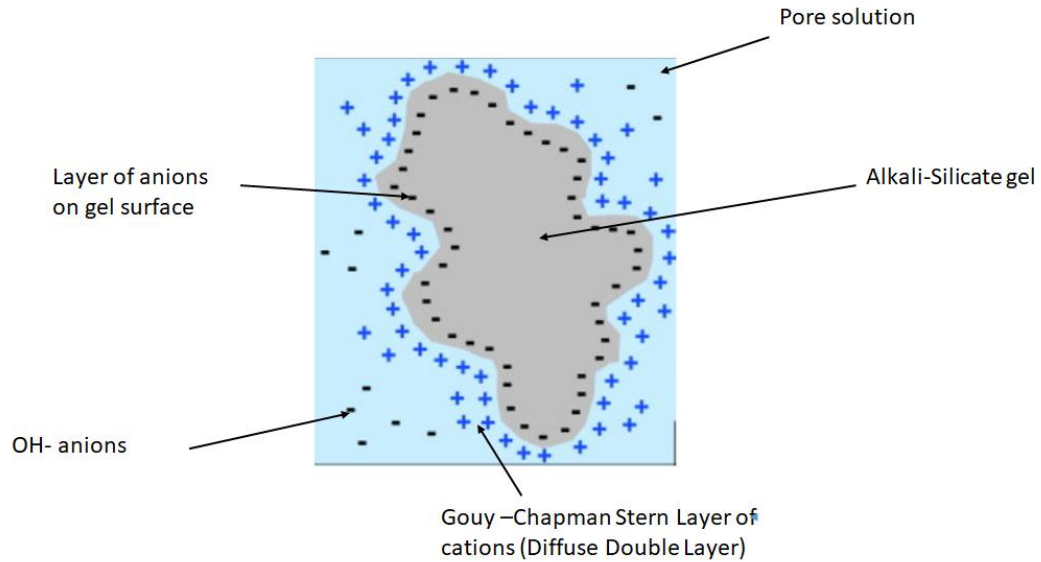


Figure 2.9 Schematic diagram of DDLs mechanism of ASR gel expansion (reconstructed from(Pignatelli, Comi & Monteiro 2013))

The EDLs theory clarifies the pre-requisite of moisture for ASR gel expansion. When the moisture content is low, the physical space between the colloidal particles is reduced until a maximum attraction energy is achieved such that it overpowers the repulsive electrostatic forces, and the ASR gel does not exhibit expansion. However, in the presence of sufficient moisture, layers of water molecules adhere to the gel surface; thus, increasing the distance between the particles. This creates an increase in the repulsive electrostatic force over the attraction energy resulting in the expansion of the gel.

2.6 Symptoms and Effects of ASR

Symptoms of ASR

The most conspicuous manifestation of internal distress due to ASR is cracking in concrete. Typically, concrete structures have relatively low tensile stress resistance. The expansion that occurs post ASR gel moisture absorption causes an increase in the tensile stress that may exceed the tensile strength of the concrete (Turanli et al. 2001). This results in the formation of micro-cracks that may be intensified by the differential expansion in concrete (Gillott & Asgeirsson 1975) or further ASR gel expansion, leading to the formation of macro and much larger cracks.

A characteristic configuration of the cracking visible for ASR affected concretes consists of connected horizontal and vertical cracks. This pattern is referred to as 'map cracking' and usually forms a pseudo-hexagonal shape depending on the loading of the concrete structure. ASR map cracking has been found to occur in unrestrained concrete. For reinforced concrete, cracks are observed to develop parallel to the reinforcement direction (Figg 1987; Hobbs 1988). The characteristics of ASR-induced cracks include longitudinal and block patterns.

Additionally, ASR may manifest itself as aggregate pop-out, misalignment of structural members due to irregular expansion, surface discoloration, and visible gel discharge and efflorescence from the formed cracks. When exudation occurs, ASR gel usually reacts with the environment to form a whitish appearance on the concrete surface, similar to carbonation. Typical examples of the aforementioned ASR indicators are shown in Figure 2.10.

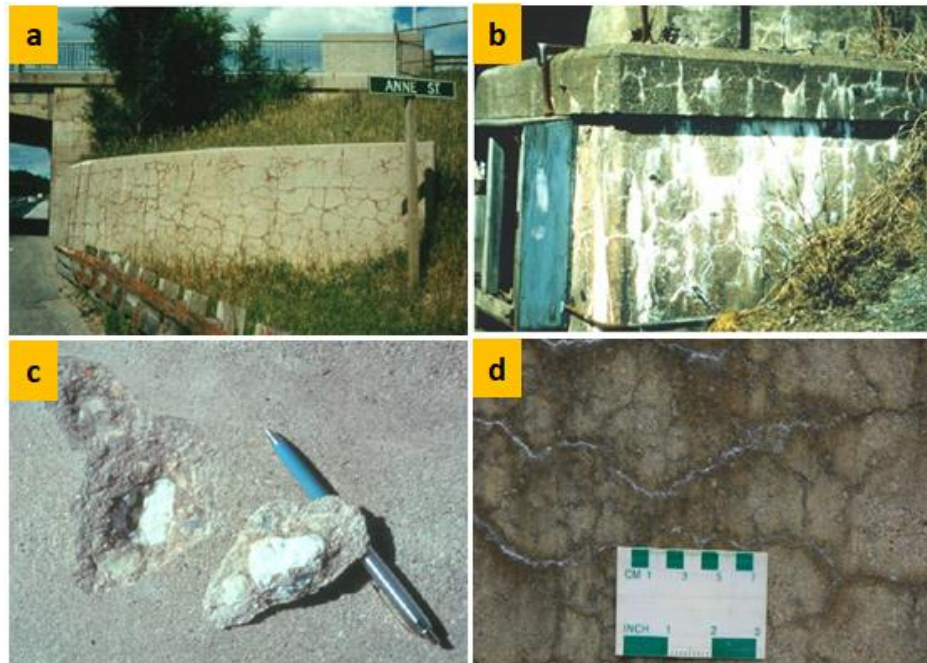


Figure 2.10 Symptoms of ASR. (a) map cracking (b) efflorescence and exudation of ASR gel from concrete cracks (c) aggregate pop-out (d) surface discoloration and ASR gel exudation from map cracks (Thomas, Fournier & Folliard 2013)

Even though the presence of cracks may indicate that ASR has occurred in a structure, it is worth noting that other chemical deterioration mechanisms in concretes such as DEF and ACR also result in concrete cracking. Therefore, it is essential to perform further microscopic characterisation studies to confirm the presence of expansive ASR gel as the root cause of distress. In some cases, expansion and cracking in concrete results from a dual attack of ASR and another chemical deterioration mechanisms. This is very common for ASR and DEF. There are several reports in literature where both ASR and DEF products have been identified in a concrete system (Bauer et al. 2006; Bouzabata et al. 2012; Czarnecki & Eng 2016; Stark & Bollmann 2000). However, the question of which reaction comes first is still a debate. Another example of the dual effects of distress reactions in concrete is the Chikamuaga lock and dam in the US (Figure 2.11). The initial petrographic

examination of concrete core samples from the dam (1957) identified the presence of brucite, indicating that expansions and related cracks observed were caused by ACR. However, over time, subsequent analysis showed significant amounts of ASR gel (1999) with diminishing brucite content, proposing that the leading cause of the later expansion observed was due to ASR (Smith et al. 2017).



Figure 2.11 The Chickamauga lock and dam showing extensive cracking due to ASR (dominating mechanism) and ACR (Smith et al. 2017)

It has been argued that ASR and ACR are not mutually exclusive and, thus, the cycling of these deterioration mechanisms in concrete is not uncommon (Grattan-Bellew & Chan 2013; Grattan-Bellew et al. 2010; Katayama 1992). The so-called ACR has been identified as the ASR of cryptocrystalline silica locked in dolomitic limestone (Katayama et al. 2011). Therefore, the deleterious expansion observed in ACR is actually ASR influenced by dedolomitization (Katayama 2004).

Effects of ASR

The aftermath of deleterious ASR is the depreciation of the concrete's properties, resulting in a loss of strength and durability. The cracks formed from ASR are essentially defects in the structure, which reduces the integrity and service life of the concrete. In some cases, ASR can cause buckling and misalignment of concrete. For structures that require precise alignment of adjacent members, such as turbines and lift bridges, misalignments render them useless. Typical examples of ASR affected concrete showing cracks and misalignment of adjacent members are presented in Figure 2.12.

Additionally, deleterious ASR expansion can lead to the premature failure and removal of concrete structures from the service, especially for high-profile structures such as dams and bridges. For ASR-affected structures that maintain their structural stability, complex and expensive concrete repair methods may be employed. Nonetheless, this is possible if ASR is detected early. Examples of known ASR affected structures around the world are given in Table 2.2

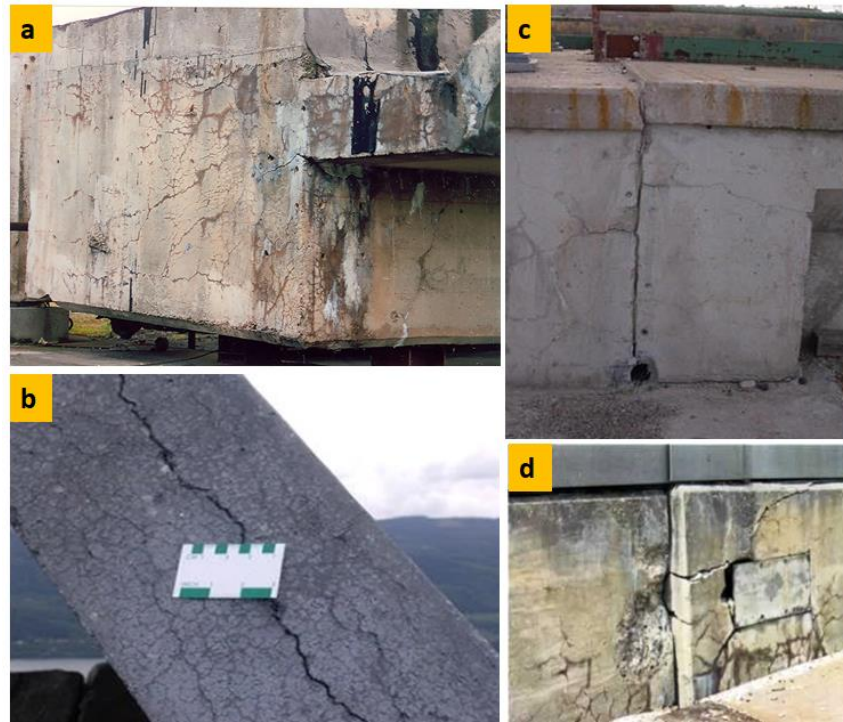


Figure 2.12 ASR affected concrete showing (a) cracks, exudation, efflorescence, and discoloration on a bridge beam, (b) longitudinal crack on a concrete beam, and (c and d) misalignment of concrete members (Thomas, Fournier & Folliard 2013)

Table 2.2 Examples of concrete structures around the world that have suffered effects ASR

Australia	
Kings Street Bridge (AKA Patalowanga bridge)	Progressively being demolished and replaced since 2011.
Centennial Hall	Demolished in 2007
Canada	
Interchange Robert Bourassa – Charest	Demolished in 2010
New Zealand	
Fairfield Bridge (Hamilton)	Repaired in 1991
United Kingdom	
Merafield Bridge	Demolished in 2016
Pebble Mill Studios	Demolished in 2005
United States	
Sixth Street Viaduct	Demolished in 2016
Chickamauga Dam	Requires constant repairs since 1997

The work done to repair and replace ASR affected structures is usually complicated, time-consuming, and costly. For example, maintenance and repair on the Chicamuaga dam require the intricate technique of temporarily slicing the dam at vantage points to release built-up stresses that result from the expansion of the gel (Alison Pryor 2020). As early as 1991, the cost of repairs for the Fairfield bridge in New Zealand was estimated as NZ\$ 1.1 million. Similarly, the cost of replacing the King street bridge in Glenelg, South Australia, is reported as AUD\$ 9 million (Ashley Walsh 2011). In 2016, it was announced that the cost of replacement for the Los Angeles sixth street viaduct, which is also an iconic landmark featured in several films and projects, was estimated at USD\$ 449 million (Muscato 2017). Figure 2.13 shows this iconic structure and the occurrence of ASR. The reconstruction project for the Los Angeles sixth street viaduct has been extended for an additional year. Evidently, the financial burden resulting from ASR is significant; therefore, emphasising the need to establish mitigating strategies for ASR prevention before the placement of the concrete in the field is a must.

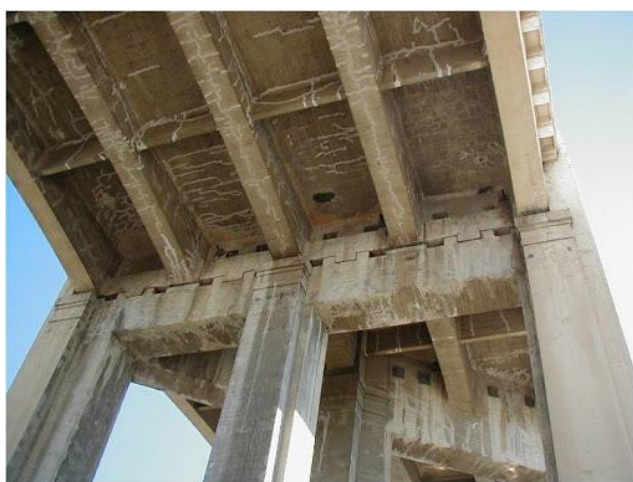


Figure 2.13 The Los Angeles sixth street viaduct showing signs of significant ASR (Muscato 2017)

2.7 Test Methods for Assessing ASR

Over the years, a variety of test methods have been developed to: (i) predict the ASR potential of aggregates; and, (ii) to evaluate preventive measures that allow the safe use of potentially reactive aggregates in concrete. A selection of these test methods have proven successful, some have been reported as failures, and others are rated somewhere in-between (Lindgård et al. 2012; Lindgård et al. 2013; Thomas et al. 2006). Through constant research and development, these test methods have evolved to increase their validity and reproducibility. At present, convergence has been reached on acceptable laboratory test methods for assessing ASR potential and preventive measures. These methods have been standardised and are categorised as characterisation tests, chemical tests and expansion test methods.

The Standards Australia Handbook SA HB 79 that provides guidance on minimising the risk of ASR damage in concretes suggests a scheme, similar to the recommendations by RILEM Technical Committee 219-ACS, for testing and performing quality control checks for the ASR reactivity potential of aggregates (Standards Australia 2015). Accordingly, the cement and concrete association of New Zealand (now Concrete NZ) has made provisions for aggregate testing to minimize the risk of ASR in their Technical Report 3 (TR3)(CCANZ 2012). The flow charts presented in Figure 2.14 describe the SA HB 79, and the RILEM Technical Committee 219-ACS recommended protocols for assessing the safe use of aggregates in concrete. From the flow chart, it is observed that the protocol comprises the use of different test methods and a decision on the reactivity potential not restricted to a single test method. This is particularly so to account for the

limitations and unknown errors from the individual test methods, as will be discussed throughout this study.

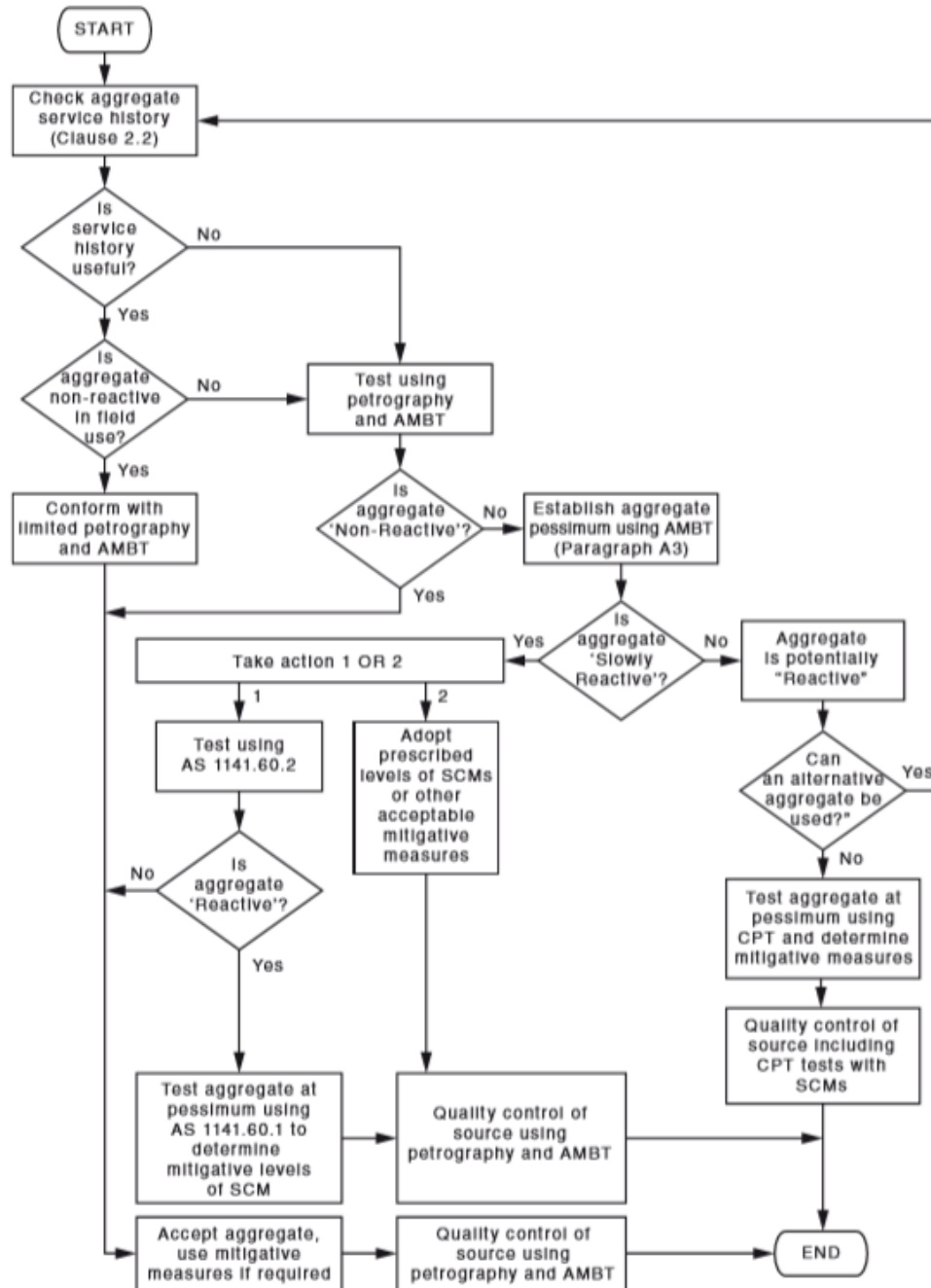


Figure 2.14 Recommended protocol for assessing the reactivity of aggregates to minimize the risk of ASR. (Standards Australia 2015)

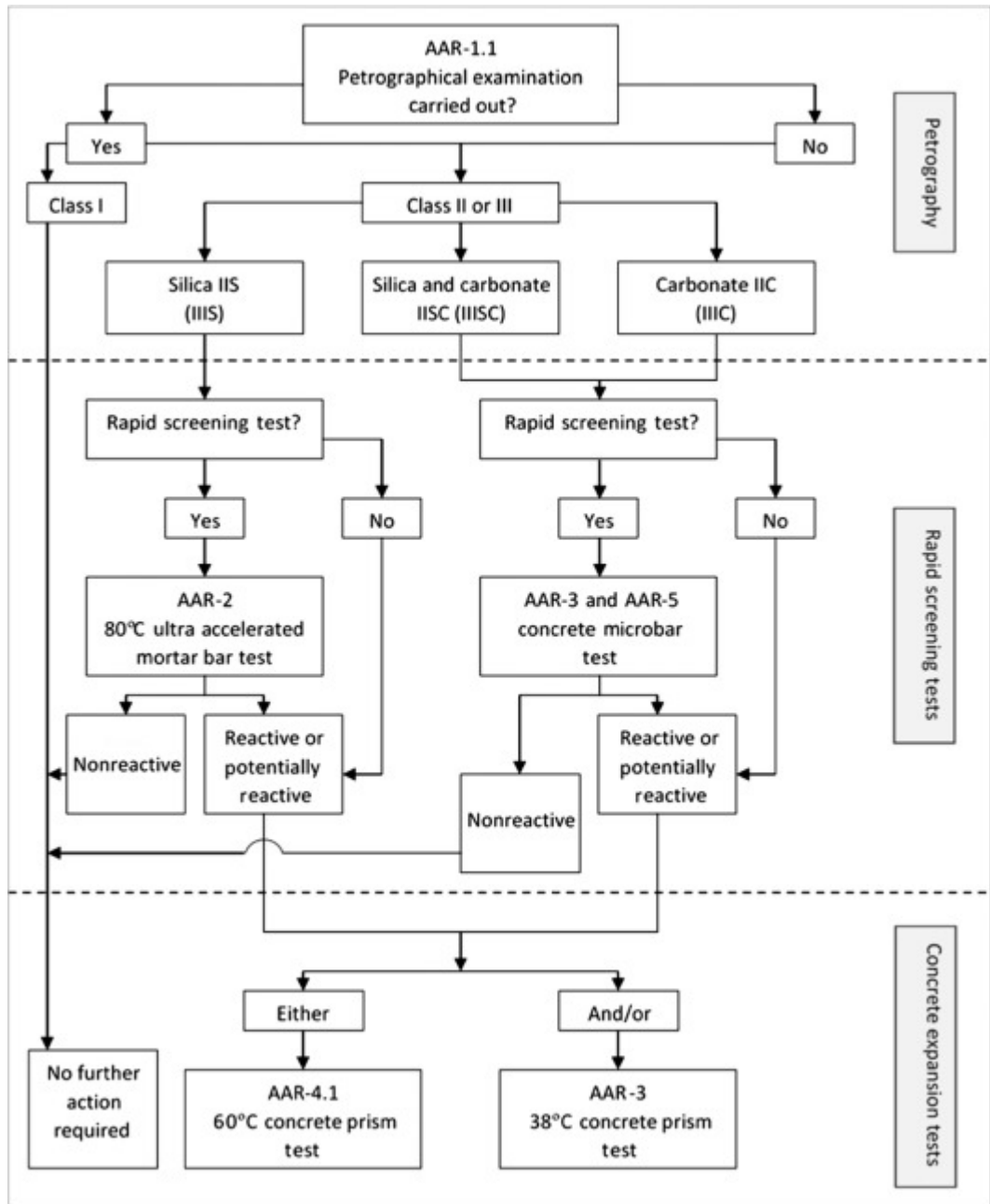


Figure 2.14b RILEM Technical Committee 219-ACS integrated scheme for assessing the reactivity of aggregates to minimize the risk of ASR (Nixon & Sims 2016b)

The SA HB79 testing scheme is similar to the RILEM protocol for aggregate testing in that both guidelines employ the use of petrography, AMBT, and CPT expansion tests. Likewise, there is no suggestion by both approaches, on an appropriate chemical test method amongst the suit of methods recommended, owed to the withdrawal of the once recognized ASTM C289 chemical test method. This has left a gap in these otherwise comprehensive aggregate testing schemes. Additionally, contrary to the SA HB 79, the RILEM protocol of aggregate testing introduces the CPT test method at 60°C (ACPT) as an alternative concrete prism test to assess the reactivity of aggregates. However, this test method is not yet standardized; however, there are on-going investigations to correlate the performance of ACPT to CPT. this present study addresses this knowledge gap as the main objective in Chapter five.

2.7.1 Standard Test Methods for Assessing ASR

Table 2.3 presents the standard test methods that are employed for assessing the ASR potential of aggregates and concrete mixes.

Table 2.3 Laboratory Test methods for ASR assessment

ASR Test Methods	
Petrography	ASTM C 295; AS 1141.65 ³ ; AAR-1
Chemical Reactivity Test	ASTM C 289 ²
Accelerated Mortar Bar Test (AMBT)	ASTM 1260; AS 1141.60.1; CSA A23.2-25A; AAR-2
Concrete Prism Test (CPT)	ASTM 1293; AS 1141.60.2; CSA A23.1-14A; AAR-3
Post-expansion Petrographic Examination and Assessments ¹	ASTM C856

1= Optional; 2= withdrawn in 2016; 3= withdrawn in 2020

The current laboratory test methods shown in the table have been adopted and standardised in several countries such as the US (ASTM), Canada (CSA), Australia (AS), and in Europe (AAR) (Rocker et al. 2015). Although these adaptations vary slightly regarding their acceptance limits and test duration, sample preparation and testing procedures are fundamentally similar.

Individually, the recognised methods may provide a good indication of the reactivity potential of the aggregates. However, neither is considered an 'ideal' test method. An ideal test method is expected to be rapid, reliable, and capable of determining the influence of: (i) the aggregates' reactivity; (ii) the performance of in service concrete mixes; and (iii) the influence of exposure conditions on ASR (Thomas et al. 2006). Indeed, the current test methods do not satisfy the requirements for an ideal test method as the tests become more conservative with shortened time, thus, their reliability typically reduces with the severity of the accelerated test duration. It is therefore recommended to use a collection of the test methods to limit variability in the test results (Nixon & Sims 2016b; Standards Australia 2015)

2.7.1.1 Petrography

Petrographic examination and assessment of aggregates are conducted to determine the presence and relative amounts of particular mineral constituents that are considered reactive to alkali (Mielenz 1954). An extensive list of alkali reactive minerals is included in the standard testing procedure and can be easily identified by skilled petrographers (Nixon & Sims 2016b; Standards Australia 2008). Petrographic examination and assessment also provides information on the essential physical characteristics of the aggregate, such as particle size and shape,

surface texture, pore dimensions, and the presence of unexpected foreign materials such as coatings. Table 2.4 gives examples of ASR reactive minerals in aggregates that can be identified by petrography.

Petrographic examinations are performed by analysing thin sections of aggregates under polarised light. Usually, the results obtained from petrography guide the selection of physical expansion tests required to specify the reactivity potential of aggregates. Petrographic assessment is completed by the point count method on a representative sample of the bulk aggregate source to determine the percentage of reactive minerals and, thus, the aggregate's ASR potential. Additionally, the identified and fundamental mineralogical composition of the aggregate can be compared to aggregates of similar characteristics whose field performance records are well documented (Wakizaka, Morita & Kawano 1987) to predict the behaviour of unfamiliar aggregates.

Table 2.4 ASR susceptible minerals in aggregates (Islam & Akhtar 2013)

Category (1)	Alkali-reactive poorly crystalline or metastable silica minerals, and volcanic or artificial glasses (Classical alkali-silica reaction)
Reactants	Opal, tridymite, cristobalite; volcanic glasses; artificial glasses, beekite
Rocks	Opal such as shales, sandstones, silicified carbonate rocks, some cherts, flints, and diatomite Volcanic rocks, such as rhyolites, dacites, latites, andesites, and their tuffs, perlites, obsidians; some basalts
Category (2)	Alkali-reactive quartz-bearing rocks
Reactants	Chalcedony; cryptocrystalline to microcrystalline quartz; quartz with deformed crystal lattice, rich in inclusions, intensively fractured or granulated; poorly crystalline quartz at grain boundaries; quartz cement overgrowths (in sandstones)
Rocks	Cherts, flints, quartz veins, quartzites, quartz-arenites, quartzitic sandstones which contain microcrystalline to cryptocrystalline quartz and/or chalcedony Volcanic rocks such as that in category (1) but with devitrified, cryptocrystalline to microcrystalline groundmass Micro-granular to macro-granular silicate rocks of various origins which contain microcrystalline to cryptocrystalline quartz: a) Metamorphic rocks: gneisses, quartz-mica schists, quartzites, hornfelses, phyllites, argillites, slates; b) Igneous rocks: granites, granodiorites, charnockites; c) Sedimentary rocks: sandstones, greywackes, siltstones, shales, siliceous limestones, arenites, arkoses;
	Sedimentary rocks (sandstones) with epitax

2.7.1.2 Chemical Reactivity Test

The chemical reactivity test is described as a quick test to assess the deleterious ASR potential of aggregate. This test method uses a decision chart that has been developed based on highly siliceous aggregates to predict the ASR reactivity of aggregates. Aggregates are treated in a highly alkaline solution (typically NaOH), and the amount of silica dissolved in the solution is compared to the decision chart, shown in Figure 3.5, to establish the reactivity status of the aggregate.

Over the years, there have been emerging concerns and debates surrounding the applicability of the decision chart (Turriziani 1986), among other limitations such as the test's inability to assess carbonated aggregates (Bérubé & Fournier 1992;

Vivian 1981). Consequently, the ASTM C289 test method has been withdrawn as a standardised test method for evaluating the reactivity potential of aggregates. Nonetheless, some recent studies (Bukhari 2019; Mo et al. 2020) still employ this technique, with caution, as a preliminary test to screen aggregates prior to further long-term expansion testing.

The withdrawal of this chemical test method has left the need for a quick and reliable chemical test method to assess the reactivity potential of aggregates. Consequently, this has encouraged the development of modified versions of the ASTM C289 test method (Knudsen 1987) as well as new chemical test methods such as the ground aggregate slurry test (GAST) and ground aggregate paste (GAP) test methods that have been developed and employed in this study (Sections 3.2.3.3 and 3.2.3.4)

2.7.1.3 Accelerated Mortar Bar Test (AMBT)

Initially developed in South Africa (Oberholster & Davies 1986; Shayan 2007), the AMBT test method is likely the most widely used standard test method for assessing ASR potential. This test method measures the expansion of mortar bars submerged in 1M NaOH solution at 80°C for a minimum duration of 14 days (Sirivivatnanon, Mohammadi & South 2016; Standards Australia 2014b).

AMBT is well known for its ability to provide quick results that help to decide the reactivity potential of aggregates within 14-21 days of testing. This is attributed to the conservative test conditions of the high alkaline solution and elevated temperature used. The reactivity classification for AMBT varies as per the different designations presented in Table 2.5, which summarises some of the differences in

classification criteria for the AMBT test methods in accordance with ASTM and CSA. The aggregate reactivity criteria for AS 1141.60.1 is presented in Table 3.4.

Table 2.5 Variations in adopted AMBT test methods (Golmakani 2013)

Test method	Mortar Preparation	Moist curing	Water curing	Subsequent storage	Proposed Limit
ASTM C 1260	<ul style="list-style-type: none"> • Autoclave expansion of cement <0.20% • W/C=0.47 • Sieve sequence of 2.35, 1.18, 0.6, 0.3, 0.15 mm 	24 h Moist cure in moulds, demould	24h in cold water up to 80°C	1.0 N NaOH, 80°C, 14d	<0.10% non-reactive 10%-0.20% uncertain >0.20% reactive
CSA A23.2-25A	<ul style="list-style-type: none"> • Alkali content of cement =0.9±10% • W/C=0.44,0.5 for crushed stone sand • Metric sieve series: 2.5, 1.25,0.63,0.315,and 0.16mm 	24 h Moist cure in moulds, demould	24h in cold water up to 80°C	1.0 N NaOH, 80°C, 14d	For quarried siliceous limestone:>0.10% reactive For other types:>0.15% reactive

Due to the high temperature and alkali environment of the AMBT method, a higher expansion resulting in the false indication of the alkali reactivity of some aggregates can occur (Latifee & Rangaraju 2015). This could lead to classifying the aggregate as reactive by the expansion limits prescribed for this method. Owing to this limitation, AMBT is recommended primarily as a rapid screening tool for identifying non-reactive aggregate from reactive aggregates (Thomas, Hooton & Rogers 1997). It is, therefore, common practice to also perform concrete prism tests and refer to field history where possible, for all aggregates that exhibit expansion exceeding the 0.10% limit in AMBT (Table 2.5).

2.7.1.3 Concrete Prism Test (CPT)

The CPT test (also referred to as standard CPT in this study) is by far the most reliable expansion test method capable of evaluating the reactivity potential of both alkali-silica and alkali-carbonate reactive aggregates. CPT is usually used to assess one reactive aggregate at a time; that is, one fraction of the aggregate proportion (be it the fine or coarse aggregate) must use an aggregate source of known reactivity (usually a non-reactive aggregate). However, the RILEM AAR-3 CPT test method allows for the assessment of aggregate combinations where the blend may also constitute unknown prior classification of reactivity potential.

CPT tests are conducted on 75 mm x 75 mm x 285 mm concrete prisms. The alkali content of the concrete is usually adjusted to 1.25% Na₂O_e by the addition of high purity NaOH in the concrete mix water. Concrete prisms are cured in a high humidity environment at 38°C for a minimum of 12 months. A detailed description of the test procedure is reported in several literature sources (ASTM 2008; Costa, Mangialardi & Paolini 2017; Nixon & Sims 2016c; Rivard et al. 2003; Standards Australia 2014e), and in Section 3.2.1.2.

The different CPT standards given in Table 2.3 follow the same procedure. However, there is variability in their suggested expansion limits for ASR assessment. Based on the measured expansion of the concrete prisms after 12 months of CPT, the aggregate or concrete mix can be classified as reactive (potentially reactive for AS) or otherwise, following the recommended expansion limit of the respective standard. The expansion limits and classification index stipulated by the different CPT standards are given in Table 2.6. Evidently, the AS CPT method adopts a conservative expansion limit compared to ASTM and RILEM.

Table 2.6 Expansion limits and reactivity classification as per the different current CPT methods

Interpretation	12 Months Expansion Limit (%)		
	AS1141.60.2	ASTM C1293	RILEM AAR-3
Non-reactive	< 0.03	< 0.04	< 0.05
Reactive/Potentially Reactive	≥ 0.03	≥ 0.04	≥ 0.05

The curing conditions for CPT provide expansion results that are deemed most reliable and comparable to actual field performance of siliceous aggregates (Fournier & Bérubé 2000; Sirivivatnanon, Mohammadi & South 2016). However, the relatively long test duration of 12 months for evaluating aggregate reactivity and 24 months for assessment of preventive measures poses an inconvenience in cases where the early prediction of potential ASR behaviour is required.

2.7.1.4 Accelerated Concrete Prism Test (ACPT)

The accelerated concrete prism test (ACPT) has gained much attention since 1990, as a practical alternative test method to the standard CPT, due to its efficiency in providing consistent results in a shortened time (Bollotte 1992; Ranc & Debray 1992). Despite the several studies that have been carried out on the reliability of ACPT (DeGrosbois & Fontaine 2000; Folliard et al. 2004; Fournier et al. 2004; Ideker et al. 2010; Rivard et al. 2003; Wallau et al. 2018), this test method has still not been acknowledged as a standard test method for ASR assessment.

The documented guideline for the ACPT test has been given by the State-of-the-Art Report of the RILEM Technical Committee 219-ACS and is referred to as AAR 4.1 (Nixon & Sims 2016d). ACPT uses the same sample preparation method as the standard CPT. However, in ACPT, concrete prisms are stored in a high humidity

environment at 60°C. Due to the higher curing temperature of ACPT, ASR expansion results can be obtained in a shorter period. At present, the test duration for ACPT is not decided. In RILEM AAR-4.1, a testing period of 4 months is suggested. However, subsequent studies conclude that 3 months of ACPT is sufficient to predict the reactivity potential of aggregates and concrete mixes (DeGrosbois & Fontaine 2000; Fournier et al. 2004). In contrast, when ACPT is used to assess ASR preventive measures, an extended test period of 6 months has been proposed (Touma, Fowler & Carrasquillo 2001).

Currently, there is no specific acceptance limit designated for ACPT, as the test method is yet to be accepted as a standardised test method. However, available data in literature indicates that ACPT results may correlate to standard CPT (Thomas et al. 2006), which is considered the most reliable test method. Reportedly, applying the acceptance limit of standard CPT, described in Table 2.6, after 3 months of ACPT generally gives the same indication of an aggregate's reactivity potential as that obtained after 12 months of the standard CPT (Fournier et al. 2004). However, in another sourced literature study, it is suggested that for aggregates classified as slowly reactive in initial tests, the standard CPT expansion limit after 5 months of ACPT provides a more reliable assessment of the ASR potential of the aggregate (Lindgård et al. 2010). That is, the specific expansion correlation age and performance criterion for ACPT to 12 months standard CPT is unclear.

2.7.2 Limitations of CPT

Alkali Leaching

Although the standard CPT method is the most reliable test method for ASR assessment, one of the major drawbacks of using this method is the apparent alkali leaching that occurs during the curing of prism samples. At high humidity and temperature, condensation of water vapour occurs on the surface of the prisms. This causes a localised reduction of alkali concentration in the surface pore solution; thus, inducing the transport of alkali from the inside of the prism towards the surface. When this occurs, excess water enriched with alkali drips down the prisms' surface into the water solution present at the bottom of the storage pail (Figure 3.3) (Rivard et al. 2007).

Alkali leaching potentially reduces the reliability of the CPT. It has been reported that approximately 35% of the total alkali in the concrete prism could be leached out by the end of the 12-months standard CPT test duration (Thomas et al. 2006), and a 20% loss is apparent after 90 days of curing. These are significant outcomes that should be taken into consideration, especially for aggregates that are classified as slowly reactive by CPT and during the assessment of ASR preventive measures. In a study to determine the long-term effectiveness of SCMs against ASR, researchers have found that the expansion curve begins to flatten out after 24 months test duration due to alkali loss through leaching (Duchesne & Bérubé 2001).

For ACPT, higher alkali leaching and increased sulphate content in the concrete pore solution have been reported. (Rivard et al. 2003). This is generally expected due to the higher curing temperature employed in ACPT. As a consequence, the main

expansion phase of ACPT is thought to be completed after 3 months (Fournier et al. 2004). This stems the recommended 3 months ACPT to 12 months CPT expansion correlation aforementioned. Additionally, there have been accounts of lower expansion recorded in ACPT (Ideker et al. 2010). This is as a result of higher alkali leaching in ACPT compared to the standard CPT test method. Admittedly, other factors that could affect the perceived lower expansions in ACPT may include the changes in pore solution at 60°C, such as the initiation of ettringite dissolution, which contributes sulphates to the pore solution at the expense of OH⁻ ions. This causes the lowering of pore solution pH and consequently ASR.

To reduce the effects of alkali leaching in concrete prism tests, new techniques like alkali-wrapping concrete prism test (AW-CPT) have been introduced in some studies (Kawabata et al. 2018; Yamada, Sagawa, et al. 2016). In this method, the concrete prisms under investigation are wrapped with a cloth that has been wetted in an alkaline solution with the same pH as the concrete pore solution. Indeed, this method has shown positive results towards reducing the alkali leaching in concrete prism tests (Yamada, Sagawa, et al. 2016). However, it has also been found that alkalis consumed in the formation of ASR gel in the prisms are replaced by some alkalis from wetted wrapped cloth (Yamada, Tanaka, et al. 2016). A similar emerging technique for limiting alkali leaching is to undertake the concrete prism tests by immersing the prisms in a solution having the same pH as the pore solution of the concrete prism (Tapas et al. 2021). This technique limits the alkali leaching but also provides an abundant supply of moisture for ASR gel formed to expand more; which raises the interesting question of the appropriate acceptance limit for reactivity classification based on CPT carried out with this technique. Undoubtedly, the problem of alkali leaching is a significant challenge in concrete prism tests. It is,

therefore, an issue to focus on in this study where CPT and ACPT correlation studies are concerned.

Heating/Cooling Cycles during Expansion Measurements

A recently highlighted limitation with the current concrete prism tests involves changes in temperature and humidity gradient during manual measurement of the concrete prisms. Before expansion measurements are taken, prisms are cooled down to room temperature inside their storage containers. This creates a heating-cooling cycle that causes stresses leading to expansion and cracks in the concrete. These cracks further promote the transport of alkalis, moisture, and ASR gel within the concrete during curing, thus results in an increase in prism expansion. In that case, the expansions observed may not be representative of the reactivity potential of the aggregate. Emerging studies suggest adopting a continuous measurement system using inductive sensors during concrete prism tests to minimise the cycling effect of heating and cooling (Wallau et al. 2018).

2.8 Mitigation and Control of ASR

As already established in Sections 2.1 and 2.2, once ASR begins, it cannot be arrested, and the replacement of ASR affected structures is costly. As such, precautions are put in place to avert the initiation of ASR before the placement of concrete in the service environment (Bérubé & Fournier 1993). ASR mitigation techniques aim to

eliminate one or more pre-requisites (Section 2.2) required for ASR to occur (Mindess, Young & Darwin 2002; Nixon & Sims 2016a).

2.8.1 Use of Non-Reactive Aggregates

Undoubtedly, using non-reactive aggregates in concrete is the most effective strategy to prevent ASR from occurring. However, avoiding the use of reactive aggregates in concrete structures may be impractical and unsustainable. Firstly, due to the depletion of available non-reactive aggregates sources, this option is not interminable. Likewise, where local sources of non-reactive aggregates are unavailable additional costs for transportation will be incurred, whereas other locally sourced aggregates could be obtained at a much lower cost. Occasionally, the rapid test methods for screening aggregates may provide inconsistent indications on the aggregates' reactivity. This indirectly creates a lack of confidence in the test results for so-called non-reactive aggregate, making this technique less feasible to implement. That said, if an aggregate source is readily obtainable and is confirmed to be truly non-reactive, this approach is the ultimate ASR mitigation strategy.

2.8.2 Restricting Moisture Access

Eliminating external moisture sources from concrete structures is a challenging task. For well-designed and placed structures, it might be possible to redirect the flow of excess water (drainage) away from the concrete, but the fact is most concrete structures spend their service life exposed to the environment; hence, rainfall and humidity. Applying surfacing protection like waterproof coatings (Putterill &

Oberholster 1985) on the concrete may reduce moisture ingress and delay expansion caused by ASR in low profile structures like non-structural concretes. However, on its own, this technique is less likely to succeed as the eventual formation of cracks in these coatings will expose any ASR gel that has formed to additional moisture leading to further expansion (Putterill & Oberholster 1985) if additional mitigation strategies have not been considered in the original supply specification of the concrete mix design. Other moisture preventative measures include spraying polyurethane sealants on concrete surfaces and cracks, and employing surface drying methods (Fournier et al. 2005). Nevertheless, these techniques should only be considered as a last resort in the application as maintenance procedures for concrete that has already experienced unexpected ASR in the field.

2.8.3 Limiting Alkali Content

Reducing the amount of alkali in the pore solution is considered the most practical technique in mitigating ASR. This is also the most commonly employed technique used by most concrete producers, as it is a relatively easy measure to apply and monitor. Although the majority of the alkalis in concrete can be accounted for, making this method relatively easy to implement, other alkali sources such as alkalis from aggregates and SCMs may be quite challenging to determine, as mentioned in Section 2.2.2.1. Notwithstanding, this is the preferred method recommended by RILEM Technical Committee 219-ACS to achieve the mitigation of ASR by modifying the pore solution (Nixon & Sims 2016a).

The alkali content in the pore solution can be reduced by:

- use of low alkali content cement
- implementation of alkali limits in concretes
- addition of SCMs

2.8.3.1 Using Low Alkali Content Cement

As discussed in Section 2.2.2, cement is the primary source of alkali in concrete although other sources may contribute to the total alkali in the pore solution. The alkalinity of the pore solution is thus dependent on the alkali content of the concrete mix.

The use of low alkali cement in concrete can be considered an effective technique to reduce the occurrence and effect of ASR in many cases. Low alkali cements are basically cements whose alkali content would typically fall below the fixed alkali limit of 0.6% Na_2O_e (Standards New Zealand 2009a; Thomas et al. 2006). This alkali limit for cement is used in Australia, New Zealand, and the United States of America. However, such low cement alkali contents can be challenging to achieve due to the changing composition of the available local resources and the depletion of low alkali content raw materials required to manufacture clinker. Furthermore, the current environmental requirements on cement manufacture and new methods used in the manufacturing clinker usually result in the volatilisation and condensation of high amounts of alkalis in the kiln; therefore, causing an increase in the alkali content of the cement produced. Low alkali cements are generally costly to manufacture for this reason, as the manufacturer may also reject the use of kiln dust to achieve the low alkali content required. Nonetheless, it is important to consider that the

behaviour of aggregates with alkali varies from one aggregate source to the next source due to differences in the mineralogical composition of the aggregates. Consequently, using low alkali cement does not guarantee that ASR will not occur.

The use of low alkali cement has been found to be effective in preventing ASR damage. A study carried out by Woolf on the reaction behaviour of different aggregates with low-alkali cement showed that for aggregates containing large amounts of alkali reactive minerals, the use of low alkali cements caused minimal expansion; whereas, an objectionable expansion was measured when aggregates comprising a small amount of reactive minerals were used with low alkali cement (Woolf 1952). Perhaps the work carried out by Woolf discovered the influence of pessimum amount on the alkali requirement for the safe use of aggregates. This presents a typical example of the effect of aggregate mineralogy on its reactivity behaviour with alkali, emphasising the need to assess aggregate and cement combinations in the proportions intended for use in actual concrete mixes.

Similarly, there are isolated instances reported in literature of concrete structures containing low alkali cement that have been impacted by the effects of ASR (Blaikie, Bowling & Carse 1996; Thomas et al. 2006). This can be attributed to other internal sources of alkali that contribute to an increase in the pore solution alkalinity. Therefore, a progressive approach of imposing alkali limits on the total allowable alkalis permitted for use in concretes has been established.

2.8.3.2 Alkali Limits in Concrete

At present, to reduce the risk of ASR, the allowable total alkali limit in concrete in New Zealand and Australia is fixed as $2.5 \text{ kg/m}^3 \text{ Na}_2\text{O}_e$ and $2.8 \text{ kg/m}^3 \text{ Na}_2\text{O}_e$,

respectively (CCANZ 2012). Alkali limits are usually set as per national guidelines to allow the full utilisation of available local aggregate sources. In Canada, the CSA A23.2-27A standard provides a ‘sliding scale’ of suitable alkali limits for reducing the risk of ASR depending on the identified prevention level of the aggregate. The recommended alkali limits in accordance with CSA A23.2-27A is shown in Table 2.7. These alkali limits offered by CSA A23.2-27A adopt a wide range of alkali limits from 1.8 -3.0 Kg/m³. This accommodates the use of a wide selection of aggregates.

Table 2.7 Alkali limits specified in CSA A23.2-27A (Canadian Standards Association 2000)

Level of prevention required	Alkali limit (Na ₂ O _e)	
	kg/m ³	lb/yd ³
Mild (W)	3.0	5.0
Moderate (X)	2.4	4.0
Strong (Y)	1.8	3.0
Exceptional (Z)	1.8 + SCM	3.0 + SCM

Conversely, in New Zealand and Australia, the 2.5 and 2.8 kg/m³ Na₂O_e alkali limits are fixed and generalised for all aggregate types regardless of the aggregate’s mineralogical composition or reactivity classification. Consequently, the rejection of aggregates that are deemed reactive at these alkali limits occurs, especially when the use of SCMs is not an option. Consequently, there is a needlessly high demand on using aggregate sources that ‘pass’ these limits causing increased depletion of using such sources in the future. Likewise, to adhere to these alkali limits in concrete, the 0.6% Na₂O_e alkali limit in cement must also be observed. This poses significant difficulties for both cement manufacturers and concrete producers in obtaining resources and adopting costly processes to maintain a strict alkali limit in cement, and using limited choices of aggregate sources, respectively.

In actual practice, the various classes of aggregates behave differently with alkali content. It is well established that ASR expansion is dependent on the nature and composition of the aggregate. This implies that for a specific aggregate, ASR may initiate below the current set limit or above. Therefore, it is essential to identify alkali limits for aggregates based on their composition and reactivity classification to ascertain their behaviour with alkali and allow their safe use in concrete.

2.8.3.3 Addition of Supplementary Cementitious Materials (SCMs)

The role of SCMs in mitigating ASR is well documented (Thomas 2011). SCMs partially replace the Portland cement and form part of the binder composition in concrete. Adding the correct amounts of SCMs is patently effective in hindering the chemical reactions leading to the formation of deleterious ASR by reducing the amount of alkalis that are available in the concrete pore solution (Diamond 1989). This is achieved through a pozzolanic reaction that occurs over time. Typical examples of SCMs used in concrete are shown in Figure 2.15. The most common SSCMs include fly ash, silica fume, slag, and metakaolin.

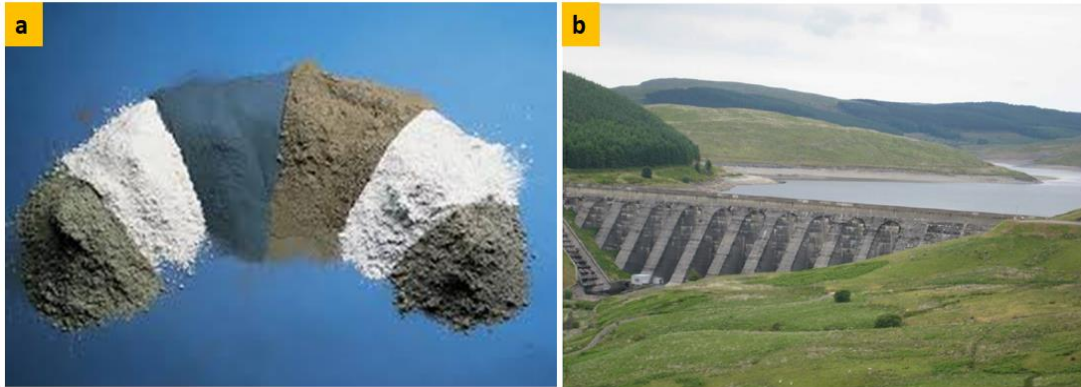


Figure 2.15 (a) Examples of SCMs. *From left to right; fly ash (Class C), metakaolin, silica fume, fly ash (Class F), slag and calcined clay, and (b) image of the Nant-y-Moch Dam (a 60-year-old bridge) containing reactive aggregates and 50% fly ash (Thomas, Fournier & Folliard 2013)*

Mitigation Mechanism of SCMs

The primary mitigation mechanism for SCMs involves alkali binding. SCMs react rapidly with available alkali in concrete pore solution, thus, consuming alkali and depriving aggregates of the alkalis required to form deleterious ASR (Thomas 2011).

SCMs also reduce ASR by:

- ✚ alkali dilution, as they replace part of the Portland cement, thus, reducing the total alkali in pore solution (Hobbs 1982);
- ✚ consumption of portlandite through a pozzolanic reaction to form secondary C-S-H phases that are non-expansive (Bleszynski & Thomas 1998);
- ✚ supplying soluble alumina that aids in the formation of C-A-S-H phases that are non-expansive and exhibit high alkali binding properties (Hong & Glasser 2002); and,
- ✚ modifying the composition of the ASR gel formed since the C-S-H and C-A-S-H phases bind alkalis and calcium from solution and, therefore,

forming ASR gels that have low alkali and calcium contents and high viscosity and less expansion capacity (Struble & Diamond 1981b).

Typically, SCMs with high SiO₂ and Al₂O₃ contents have high efficacy to mitigate ASR (Chappex & Scrivener 2012; Hüniger, Hübner & Scholz 2016). When the alkalis in the binder (cement and SCMs blend) are released, they can coexist as ions in the pore solution bound by hydration products or fused into the ASR gel (Lothenbach, Scrivener & Hooton 2011; Thomas 2011). At high pH, Al₂O₃ from the SCMs are released into the pore solution and react with silica to form aluminosilicate precipitates. Al³⁺ ions replace Si⁴⁺ ions in the tetrahedral network of the silica, causing a charge imbalance, which consumes alkali ions (Na⁺, K⁺) in the pore solution to reform the tetrahedral structure. As a consequence, the alkalinity of the pore solution is also reduced. Furthermore, the cement provides portlandite (Ca(OH)₂) that partially dissolves to supply Ca²⁺, aiding in the precipitation of secondary C-S-H and C-A-S-H gels that are non-expansive (Hong & Glasser 2002). A homogeneous distribution of SCMs in the concrete mix ensures a wide dispersal of the precipitated gels, thus, reducing the risk of deleterious expansion.

Typical examples of previous studies showing the effect of SCMs on mortar and concrete prisms are illustrated in Figure 2.16. Figure 2.16a (Tapas et al. 2019) shows the effect of different SCMs on the expansion behaviour of mortar bars after 28 days of AMBT. The addition of SCMs was observed to be effective in reducing ASR expansion. The various SCMs were studied at the same cement replacement level of 10% to ascertain their performance in mitigating ASR. It can be seen that the order of decreasing expansion is relative to the apparent silica content of the respective

SCM. Silica fume (SF), which is essentially pure reactive silica (96%), showed the least expansion. In contrast, slag (SL), which is known to contain high amounts of calcium oxide (CaO) and comparably lower silica, showed the most expansion among the SCMs studied by the authors. Conversely, metakaolin (MK), which contains high proportions of Al₂O₃ and SiO₂, exhibited a reduction in expansion comparable to SF. This is attributed to the high Al₂O₃ content in MK that likely reacts to form C-A-S-H phases or aluminosilicate layers on the surface of the aggregates preventing further silica dissolution and, consequently, ASR.

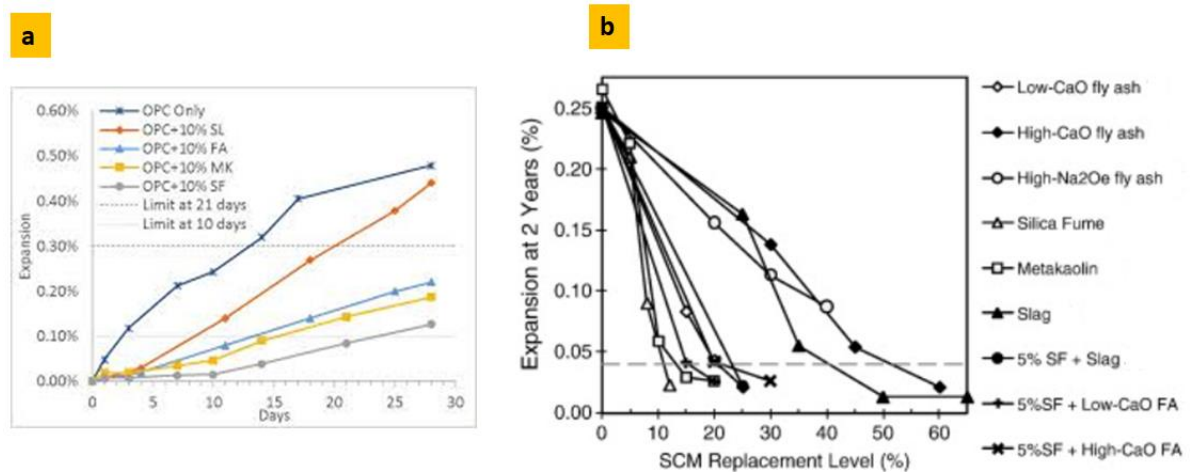


Figure 2.16 Effects of (a) SCM addition on the expansion of mortar bars (Tapas et al. 2019) and (b) SCM composition on dosage requirement for effective ASR mitigation in concrete(Thomas 2011)

Other workers also investigated the effect of SCM composition on the dosage requirement for effective ASR mitigation (Thomas 2011). Typically, the amount of SCM required to reduce the risk of ASR was found to be dependent on the reactivity potential of the aggregate needing mitigation (Rajabipour et al. 2015). However, the results from the authors mentioned above (Figure 2.16b) depict that the

composition of the SCM also influences the dosage requirement for ASR prevention. From Figure 2.16b, it can be seen that to achieve the same level of mitigation as 10% silica fume, approximately 50% of slag cement replacement is required. This observation is consistent with what is reported by the authors in Figure 2.16a and agrees with the recommended dosages for using these SCMs (Standards Australia 2015). Additionally, for the different classes of FA, which contains different amounts of CaO, a higher dosage is needed for FA containing high amounts of CaO. Likewise, FA comprising high alkali content also showed lower abilities in reducing the occurrence of ASR induced expansion. This is likely due to the alkalis in SCMs being released into the pore solution of the concrete over time, thus, increasing the total alkali content available for the aggregates to react (Rajabipour et al. 2015). However, some researchers argue that the silica released by SCMs is sufficient to bind the surplus of alkalis in the pore solution (Shafaatian et al. 2013).

SCMs also mitigate ASR in restricting the ingress of moisture in concrete by undergoing a pozzolanic reaction with the portlandite available in the pore solution. Pozzolanicity also increases the density of the structure and, thus, improves the hardened properties and durability of the concrete (Aldred et al. 2006), reducing the pathway for moisture ingress and ASR gel to move through the concrete. Moreover, the addition of SCMs maintains the desired compressive strength requirements of the concrete. Besides the micro-filling achieved by the fine particle size of SCMs, the C-S-H formed from the pozzolanic reaction of SCMs also contributes to a reduction in the porosity and permeability of the concrete (Rajabipour et al. 2015; Shafaatian et al. 2013; Thomas 2011).

The effect of SCM fineness on the compressive strength of paste specimens has been studied by Chindapasirt and co-workers using FA of particle size 19.1 μm (OFA) and the same FA treated to a particle size of 6.4 μm (CFA), at two dosages of 20% and 40% cement replacement (Chindapasirt, Jaturapitakkul & Sinsiri 2005). The compressive strength results from the Chindapasirt study are extracted and shown in Figure 2.17. From the Figure, it can be seen that a decrease in compressive strength was observed with an increase in the addition of the SCMs as a function of cement replacement level. However, except for the 7-day strength, the decrease observed with SCM addition at any given dosage for both SCMs is no more than 30% of the control's strength devoid of SCM (PC). Additionally, considering the effect of the particle size on the compressive strength, specimens containing SCM with the lower particle size (CFA) showed higher compressive strength. In fact, after 90 days, 20% CFA measured a similar compressive strength to PC.

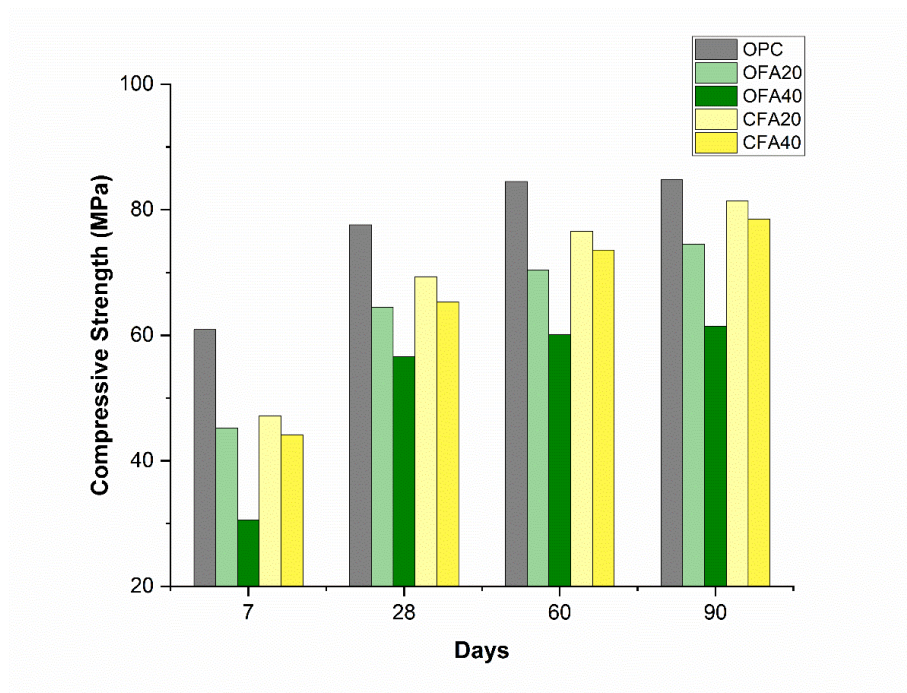


Figure 2.17 Effect of SCM fineness and dosage on the compressive strength. Data from (Chindapasirt, Jaturapitakkul & Sinsiri 2005)

It can thus be concluded that an effective SCM for ASR prevention is one that has high SiO₂ and Al₂O₃ content, low CaO, and alkali content, and very fine particle size. By understanding the characteristics and mechanism of SCMs, alternative materials can be developed as a substitute in the absence of using SCMs.

2.8.4 Addition of Ground Siliceous Particles

Few studies have explored the option of using various forms of ground reactive silica sources such as glass (Afshinnia & Rangaraju 2015b) and perlite (Bektas, Turanli & Monteiro 2005) for mitigating ASR. Supposedly, due to the increase in surface area, ground siliceous materials expose large amounts of reactive silica that rapidly react with calcium and alkali to form ASR gel ((Na, K)-C-S-H), thus, consuming alkali in the pore solution. Figure 2.18 shows the linear distribution of elements along a partly reacted glass grain. It can be observed that the outer rim of the glass grain showed the presence of higher amount of Ca and then Na. This is indicative that the fine glass particle has undergone a pozzolanic reaction to form the C-S-H phase that consequently bound some alkali in the pore solution. Subsequently, any reactive silica present in the fine and coarse aggregates used in a concrete mix is deprived of alkali minerals to react. This mechanism of mitigation is similar to the pozzolanic reaction exhibited by traditional SCMs (FA, silica fume, metakaolin, etc.). However, whereas the secondary C-S-H phases formed from the reaction with SCMs are non-expansive, ground siliceous aggregates tend to form ASR gel from their interaction with alkali (Zheng 2016). Nonetheless, the ASR gel formed is usually localised and small due to the fine particle size of the silica source; thus, they do not appear to

generate enough expansion to cause ASR distress in the concrete (Afshinnia & Rangaraju 2015b).

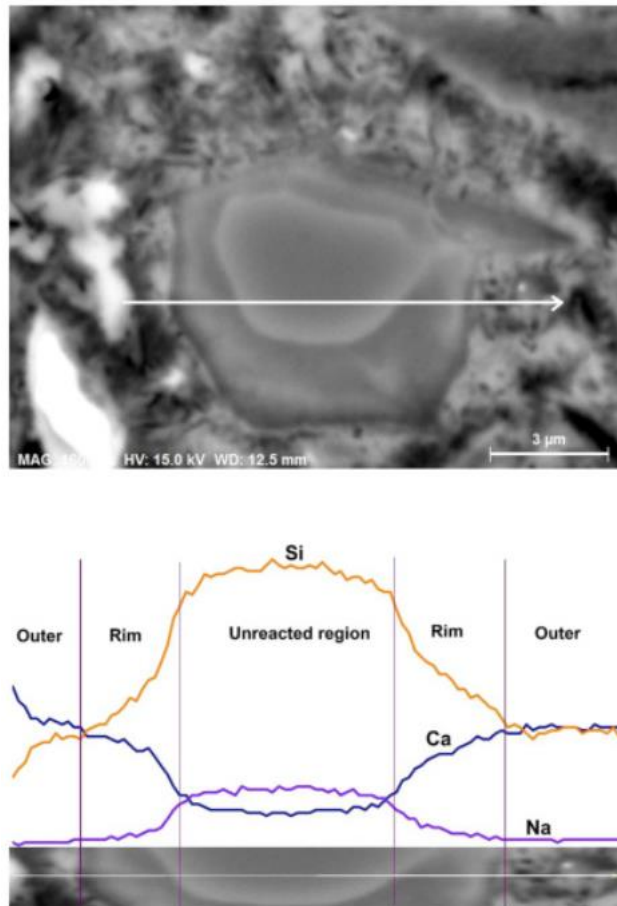


Figure 2.18 Linear distribution of elements (Ca, Si and Na) along a partly reacted finely ground glass grain, showing evidence of a pozzolanic reaction to form (Na-C-S-H) ASR gel (Afshinnia & Rangaraju 2015b)

Additionally, due to the consumption of alkalis by these ground siliceous additives, the reaction between fine or coarse-sized aggregate particles and the remaining alkalis in the pore solution results in the formation of relatively narrower ASR gels that exert less pressure upon expansion. The results of a study undertaken on the use of finely ground glass in mitigating ASR are shown in Figure 2.19. From the

Figure, it can be observed that the ASR gels formed in the coarse-sized aggregates of concrete samples with 100% cement (Figure 2.19a) are larger in width than the gels formed in the concrete systems containing 30% glass powder. This proposes that the gels in Figure 2.19 s have a greater expansion impact on the concrete. Additionally, it is clear that the frequency of the ASR gels in the concrete void of glass powder is higher, suggesting that the concrete has undergone significant ASR compared to the concrete samples with the glass powder.

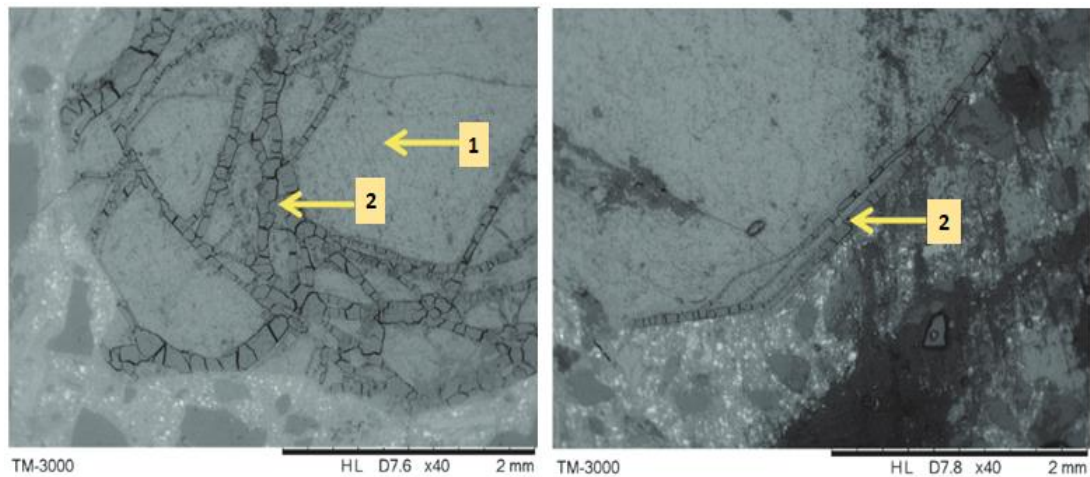


Figure 2.19 SEM micrographs of concrete sample containing (a) 100% cement and (b) 30% glass powder. *Note: 1= Aggregate; 2= ASR gel* (Afshinnia & Rangaraju 2015b)

Thomas demonstrated the effectiveness of ground siliceous material in reducing the expansion caused by ASR using a reactive vycor glass and less reactive quartz (Thomas 2011). The results from this study, presented in Figure 2.20. When the mortar bars composed of sand-sized vycor glass and 100% cement were studied, an expansion of approximately 0.4% was recorded. However, with the addition of the same material as a powder, at 20% cement replacement level, the expansion of the

mortar bars decreased to about 0.3%. This confirms that very reactive silica materials that show deleterious expansion as large particles have a high tendency to mitigate ASR expansion when used as ground particles at cement replacement levels. It is further explained that due to the small nature of the ASR gels formed from the reaction with finely ground silica, calcium readily exchanges with alkali in the gel over time (alkali recycling). Thus, the composition of the gel becomes similar to the non-expansive C-S-H formed from the pozzolanic reaction with SCMs and contributes to the lower expansion observed.

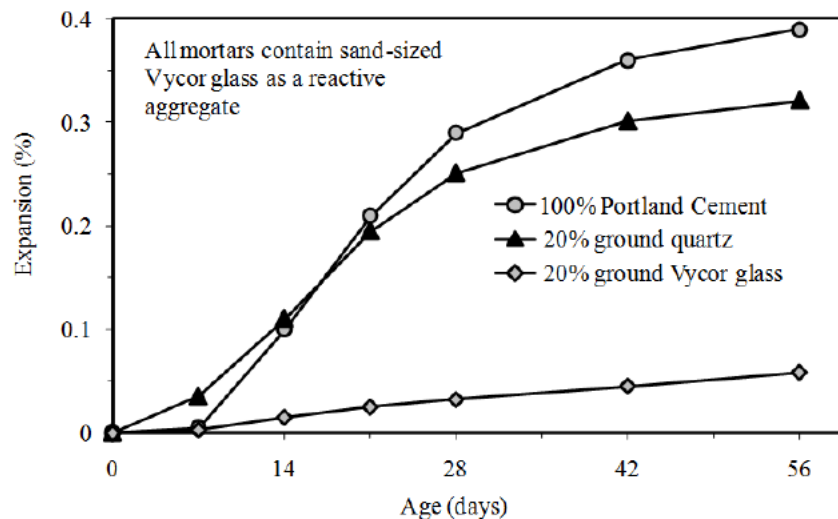


Figure 2.20 Influence of particle size on the reactivity of reactive silica (Thomas 2011)

At present, limited studies have evaluated the potential of using ground aggregates such as lightweight aggregates for ASR mitigation (Li, Thomas & Ideker 2018). However, the results available from the published studies are indeed promising. Therefore, it can be hypothesized that homogeneously mixing sufficient amounts of very fine reactive aggregate particles in concrete could also inhibit ASR in a pozzolanic reaction similar to the mechanism of SCMs. Equally, the fragmental C-S-H

formed could fill open pores in the concrete structure to increase the strength and the durability of the concrete (Ichikawa 2009).

2.8.5 Use of a Non-Expansive Aggregate Combination

Generally, the proportion of silica that will lead to the most damaging reaction will depend on the type of silica mineral present. When reactive aggregate is mixed with a non-reactive aggregate at different amounts, the proportion of reactive silica minerals in the aggregate blend that exhibits the most damaging ASR is referred to as the pessimum amount (Nixon & Sims 2016b).

Typically, the amount of reactive minerals needed for ASR in most aggregates could be as low as 2% or as high as 100% (Forster et al. 1998). With this in mind, ASR mitigation can be achieved by aggregate blending of highly reactive siliceous aggregates with non-reactive aggregates such that the pessimum amount is not reached (Nixon & Sims 2016a). This technique, when properly implemented, allows the safe use of potentially reactive aggregates to ensure full utilisation of local aggregate sources and conservation of natural resources.

Since the expansion behaviour of aggregate blends is unknown, it is crucial to evaluate the ASR reactivity of the desired aggregate blends using a comprehensive scheme of test methods such as the RILEM Technical Committee 219-ACS protocol and SA HB 79 (also supported by RILEM Technical Committee 219-ACS) shown in Figure 2.14, in the exact combination that is intended for use in real concrete. This will provide some indication of the compatibility of the aggregate blends in mitigating ASR in the field.

Chapter Summary

In this chapter, the chemistry of ASR has been explained in detail. The factors that are necessary for ASR to occur have been identified as sufficient reactive silica, abundant alkali, and moisture, all of which are unavoidable in concrete; thus, ASR is likely to occur when additional preventive measures are not taken. However, the degree of ASR can be deleterious or benign depending on the amounts of the reactants available.

It was discussed that ASR leads to the formation of alkali-silicate gel, which polymerises in the presence of calcium to form an alkali-calcium-silicate-hydrate gel, referred to as ASR gel. The gel formed is hygroscopic and thus absorbs moisture to expand, creating cracks in the concrete, among other symptoms such as misalignment and discoloration. The consequences of ASR are a decrease in the strength properties of concrete and economic challenges resulting from the repair and replacement costs of ASR-affected structures. It was also established that ASR is persistent, and once the reaction begins, it cannot be arrested. Therefore, the ASR reactivity of aggregates must be evaluated to decide on the mitigation method that provides the least likelihood of ASR.

The aggregate testing protocol used in Australia, also recommended by RILEM, was discussed as a practical scheme to identify aggregates' reactivity and minimise the risk of ASR in concrete. The protocol, which consists of several standard test methods such as petrography, AMBT, and CPT, is absent of chemical test methods as a quick ASR predictor test due to the limitation of the current standardised chemical method ASTM C289. Conversely, the strengths and limitations of the individual test methods were discussed, as was the non-standardised ACPT test method. ACPT is

an accelerated version of the standard CPT, carried out at 60°C. Although ACPT has been used for decades in assessing the ASR of aggregates, this test method has not yet been standardized. Meanwhile, the standardization of ACPT will benefit industry by providing concrete producers with an alternative reliable short-term test method to assess ASR in time-constrained scenarios. This will also save industry the cost incurred from long-term testing. The major drawback of both concrete prism tests was identified as alkali leaching. A detailed discussion on alkali leaching and the resulting effect on prism expansion observed in related studies was presented.

Further, the current practices for mitigating ASR were elaborated. It was discussed that feasible mitigation methods target removing or reducing one or more of the three essential ASR factors identified. However, the most commonly used method that is also the easiest to implement is limiting alkali in the pore solution. This can be achieved by using low alkali content cements, enforcing alkali limits, and the addition of SCMs. The process by which each of these techniques reduces the risk of ASR and the challenges associated with their use were addressed. In particular, the mechanism of SCM in ASR mitigation was discussed in detail. SCMs mitigate ASR primarily by reducing the alkali content through alkali dilution and subsequently binding alkali in the pore solution, through a pozzolanic reaction that results in the formation of C-S-H and C-A-S-H. Thus, it was established that SCMs with high silica and alumina content, low calcium and alkali content, and very fine particle size, were advantageous and the most effective in mitigating ASR, reducing concrete porosity and permeability, and maintaining the strength of concrete, all of which ensure durability. Although SCMs are patently effective in mitigating ASR, their availability for use in the future is uncertain.

Additionally, the challenges associated with imposing strict alkali limits on concretes were highlighted. It was mentioned that these alkali limits are strict and generalised for all aggregates. This has resulted in the rejection of aggregate sources that are deemed potentially reactive and caused depletion in the 'acceptable' aggregate sources, creating the need to investigate ways of incorporating available aggregate sources in concrete.

This chapter concluded with a discussion of emerging studies that employ alternative ground siliceous materials such as glass as additives to mitigate ASR. These studies have shown promising mitigation results on the use of ground reactive siliceous materials that are similar to the mitigation observed with SCMs. However, there is insufficient research material on the potential use of ground reactive aggregates for this purpose. Finally, a mitigation technique involving the use of aggregate blends in proportions that avoid the pessimum amount of the reactive silica mineral in the aggregate was introduced. This mitigation technique is thought to be less costly and ensures the full utilisation of locally available aggregate sources, thus, promoting the conservation of natural resources.

CHAPTER 3. Materials and Methods for Assessing Aggregate Reactivity and Alkali-Silica Reaction

3.1 Overview

This chapter outlines the different materials and experimental test methods used in this study to classify the potential ASR of aggregates and characterise new generation materials for ASR prevention. The experimental test methods employed have been categorised into characterization techniques, chemical tests, and physical expansion test methods. The tests were mostly carried out in accordance with relevant Australian and ASTM standards. In some instances, modified versions of these standards were adopted, as described, to achieve the aims and objectives of this study. The details of the general principle, the sample preparation, and test parameters for the individual tests undertaken are presented in the subsequent sections of this chapter.

3.2 Materials

3.2.1 Aggregates

Six different aggregates sourced from New Zealand and Australia were selected for the investigations carried out in this study. These aggregates were chosen based on their availability and the need for the New Zealand and Australian concrete

industry to fully utilize these aggregate sources. Table 3.1 list the various aggregates used in the empirical studies discussed in this study. Accordingly, the mineralogical composition of the aggregates is described in Section 4.3.1.

Table 3.1 Description of all the aggregates used in this study

Aggregate	Source	Nature of Aggregate	Symbol
Waikato	New Zealand	Natural river sand	WT
Greywacke		Manufactured coarse aggregate	GW _C
		Manufactured fine aggregate	GW _F
Rangitikei		Natural river sand	RT
Andesite		Manufactured fine aggregate	AS
Rhyolite	Australia	Manufactured fine aggregate	RH
Peats Ridge		Manufactured coarse aggregate	PR _C
		Manufactured fine aggregate	PR _F

Although most of the aggregates used were sourced from New Zealand, attention is given to the mineralogy and physical properties (shape and size) of the aggregates, which may be similar to other aggregates in other parts of the world. Further, the Australian aggregate chosen; Peats Ridge, is a non-reactive aggregate that is widely accepted as a reference aggregate by aggregate, cement, and concrete suppliers in Australia and New Zealand to assess reactivity levels of other aggregates.

3.2.2 Cement

General Portland (GP) cement supplied by GBC Winstone was chosen as the source of cement to use in all paste, mortar, and concrete mixes carried out in this work. As

determined by XRF in an external laboratory, the alkali content of the cement is 0.58% Na₂O_e, thus conforming to current alkali limits set for cement in New Zealand and Australia (Standards Australia 2015; Standards New Zealand 2009a). The alkali content determined was comparable with the chemical information supplied by the cement manufacturer. The chemical composition of the cement, showing the elements that could influence the reaction products formed during the hydration of the cement, is presented in Table 3.2.

Table 3.2 The chemical composition of the cement used, as determined by XRF analysis

Component	%	Component	%
CaO	64.55	Na ₂ O	0.25
SiO ₂	20.79	P ₂ O ₅	0.18
Al ₂ O ₃	3.80	SO ₃	2.25
Fe ₂ O ₃	2.52	TiO ₂	0.28
MgO	0.95	LOI	3.20
Mn ₂ O ₃	0.08	Total	99.35
K ₂ O	0.50	Total alkali (as Na ₂ O _e)	0.58

3.2.3 Reagents

The reagents used in this study are sodium hydroxide (NaOH) and calcium hydroxide (Ca (OH)₂). NaOH pellets of ≥ 98% purity supplied by Rowe Scientific Pty Ltd. were used in the physical expansion tests to increase the alkali content of the storage solution (for AMBT method) and concrete prisms (for CPT and ACPT methods). Alkali loading using NaOH for CPT and ACPT is represented as sodium equivalent (Na₂O_e) as per AS 1141.60.2, thus considering the potential influence of K⁺ expected from ordinary cement.

Similarly, Ca (OH) ₂ powder from Sigma-Aldrich was used as a reactant in the GAST method to assess the reactivity of ground aggregates based on the amount of portlandite remaining after the chemical reaction has been completed.

3.3 Methods

The description of the general methods employed throughout this study is given in Sections 3.3.1 - 3.3.4. However, for the experimental work undertaken to achieve the respective objectives (Chapters four, five, and six), a detailed account of the experimental plan; including the selected materials and the designed test program, is further elaborated in the respective chapter.

3.3.1 Physical Expansion Test Methods

Physical expansion test methods were used to determine the alkali reactivity classification of aggregates and aggregate-cement combinations. In particular, AMBT, CPT, and ACPT expansion methods were carried out following Australian standards for ASR assessment.

3.3.1.1 Accelerated Mortar Bar Test (AMBT)

AMBT on mortar bars was carried out as per AS 1141.60.1 (Standards Australia 2014b). Mortar bars were prepared with sand-sized aggregates of particle sizes

not exceeding 4.75mm. The aggregate grading used for manufactured (crushed) fine aggregates is shown in Table 3.3. For natural fine aggregates, except for discarding particle sizes above 4.75 mm, the aggregates were used without grading (Standards Australia 2014b).

Table 3.3 Grading requirement for manufactured fine aggregates in AMBT according to AS 1141.60.1

Sieve size		% by mass
Passing	Retained	
4.75	2.36	10
2.36	1.18	25
1.18	0.600	25
0.600	0.300	25
0.300	0.150	15

Sample Preparation and Mixing

The procedure carried out in AMBT in this work is shown in Figure 3.1. Mortar bars were prepared using a Hobart mixer in the mix composition of 990 g of aggregate to 440 g of cement. A water-cement (w/c) ratio of 0.47 by mass was incorporated for all mortar mixes. Mixing was achieved by first blending the cement and water at a speed of 140 r/min for 30 s. This ensures better dispersion and distribution of the cement particles during mixing. Without stopping the mixer, the aggregate portion was added slowly to cement paste within a period of 30 s. The mixture was continuously stirred at a higher speed of 270 ± 25 r/min for another 30s, after which it was allowed to rest for 90 s to allow the absorption of moisture by the particulates. Following the resting period, the mortar was stirred at 270 ± 25 r/min for an additional 60 s to mix any water that may have risen to the mortar surface during

the resting period, and to ensure a well-homogenized mix. The flow of the mortar was immediately measured using a flow table. During flow measurements, the flow table was dropped 25 times within 15 s, from a distance of 12mm. The mortar portion used for the flow test was added back into the mixing bowl and stirred for 10 s before moulding.



Figure 3.1 AMBT procedure showing (a) Horbat mixer (b) AMBT moulds (c) initial curing of mortar bars in a humidity cabinet (d) water curing of mortar bars at 80°C (e) ageing in 1M NaOH hot bath at 80°C, and (f) horizontal comparator for measuring expansion at respective ages

Moulding and Curing

AMBT bars were cast in a metal mould of dimensions 25 mm x 25 mm x 285 mm, laced with a release agent (WD-40), for easy demoulding of hardened mortar bars. Three bars were prepared for each mortar mix. After casting, the mortar bars were initially cured in the mould at 23°C for 24 hours in a humidity (vaporised water) controlled cabinet maintained at 70% relative humidity to allow the hardening of the mortar bars. Following the initial curing, the bars were demoulded, and the initial expansion was measured using a horizontal comparator (Figure 3.1). Subsequently, the bars were cured in water at 80 °C for an additional 24 hours. This curing step was employed to achieve an equilibration at 80°C for appropriate expansion measurement at 0 days (zero reading). After 24 hours of water curing, expansion measurements were taken and recorded as the zero reading. The mortar bars were then aged in a 1M NaOH hot bath maintained at 80°C (Figure 3.1) for the remainder of the test duration.

Expansion Measurement

Usually, in accordance with AS 1141.60.1, expansion measurements for mortar bars are taken up to 21 days at the standard age intervals of 1, 3, 7, 10, 14, and 21 days. However, in this study, measurements were continued up to a minimum of 28 days and at 7 days intervals for an extended test period of 56 days. This was done to ascertain the effect of age on the reactivity of the aggregates as well as to observe the reaction rate and reactivity levels of aggregates deemed as slowly reactive. For the AMBT studies carried out for the extended test period. The AS 1141.60.1 21-day limit was selected as the expansion limit at 56 days.

The aggregates' reactivity was thence determined by comparing the averaged percentage expansion to the acceptance criterion and reactivity classification stipulated in AS 1141.60.1 (shown in Table 3.4). The percentage expansion (En) of the mortar bars was determined Equation 3.1 (Standards Australia 2014b).

$$E_n (\%) = \left(\frac{L_n - L_z}{L_g} \right) \times 100 \dots\dots\dots \text{Eqn 3.1}$$

Where, L_n = Specimen length at measurement age n ; L_z = Specimen length at zero reading and L_g = Gauge length of 250 mm.

Subsequently, the reactivity classification of the cement-aggregate combination of the mortar bars was determined based on the expansion limits prescribed in AS 1141.60.1, as shown in Table 3.4.

Table 3.4 AMBT aggregate reactivity classification by AS1141.60.1 test method

Mean mortar bar expansion (E) %		Aggregate Reactivity classification
Duration of specimens in 1 mol/L NaOH at 80oC		
10 days	21 days	
-	$E < 0.10^*$	Non-reactive
$E < 0.10^*$	$0.10^* \leq E < 0.30$	Slowly reactive
$E \geq 0.10^*$	-	Reactive
-	$0.30 \leq E$	Reactive

* 0.15% for natural sand

3.3.1.2 Concrete Prism Tests

Concrete prism tests at 38°C (CPT) and 60°C (ACPT) were carried out following AS 1141.60.2 (Standards Australia 2014e) test method and a modified RILEM AAR-3.2 method. To improve concrete workability and strength, tailored mix designs, shown in Appendix B: Table B1 and B6, were prepared for each concrete mix under assessment.

Sample Preparation and Mixing

The grading requirement for coarse aggregate in the CPT mix design used in this work is shown in Table 3.5. Conversely, fine aggregates were used without any modification to the grading. Before concrete mixing, both fine and coarse aggregates were brought to a saturated surface dry condition (SSD) to ensure that much of the water used during is not absorbed by the aggregates, allowing enough free water to react with the cement to form the necessary hydration phases. Using the aggregates in the SSD condition also improves the workability of the concrete mix. SSD was achieved by soaking the aggregates in water for 24 hours prior to the mix date. For coarse aggregates, the water was drained after 24 hours, and the aggregate surfaces were wiped with a damp cloth to remove excess free water. SSD was achieved in fine aggregates by spreading the drained sand in a pan, which was then left uncovered in the laboratory mixing area for approximately 8 hours (or until all the free water has evaporated). Fine aggregates were stirred with a trowel every 2 hours during this time to help evaporate any free water. The cement and both aggregates were stored covered (to prevent further moisture loss) in the laboratory mixing area for approximately 12 hours before concrete mixing to equilibrate the

temperature of the material to the room. Moisture content tests were also carried on both fine and coarse aggregate before mixing, to establish the water of absorption of the aggregates as well as the appropriate w/c ratio that will produce the best workability of the concrete mix.

Table 3.5 Coarse aggregate grading requirement for CPT and ACPT under AS 1141.60.2

Sieve Size Passing	Sieve Size Retained	Aggregate Mass Portion
19.0	13.2	1/3
13.2	9.5	1/3
9.5	4.75	1/3

The proportions of coarse and fine aggregates used for each concrete batch were determined as per the procedure for concrete mix design (Standards Australia 2014e). A w/c ratio of 0.42- 0.45 was used in producing the concrete. Further, the alkali content in the concrete was boosted to 1.25% by 420 kg/m³ weight of cement, by adding high purity (>99%) NaOH in the concrete mix water.

Concrete mixing was done in a 50 l capacity mechanical mixer. 30 l of concrete was produced for each mix batch. Concrete mixing was carried out in accordance with the procedure described in AS 1012.2(Standards Australia 2014a). The mixing procedure used is shown in Figure 3.2. The proportion of the concrete used for the initial slump test (Figure 3.2) was returned to the mixer for the remainder of the mix sequence. The air content of the fresh concrete was also measured before concrete casting.

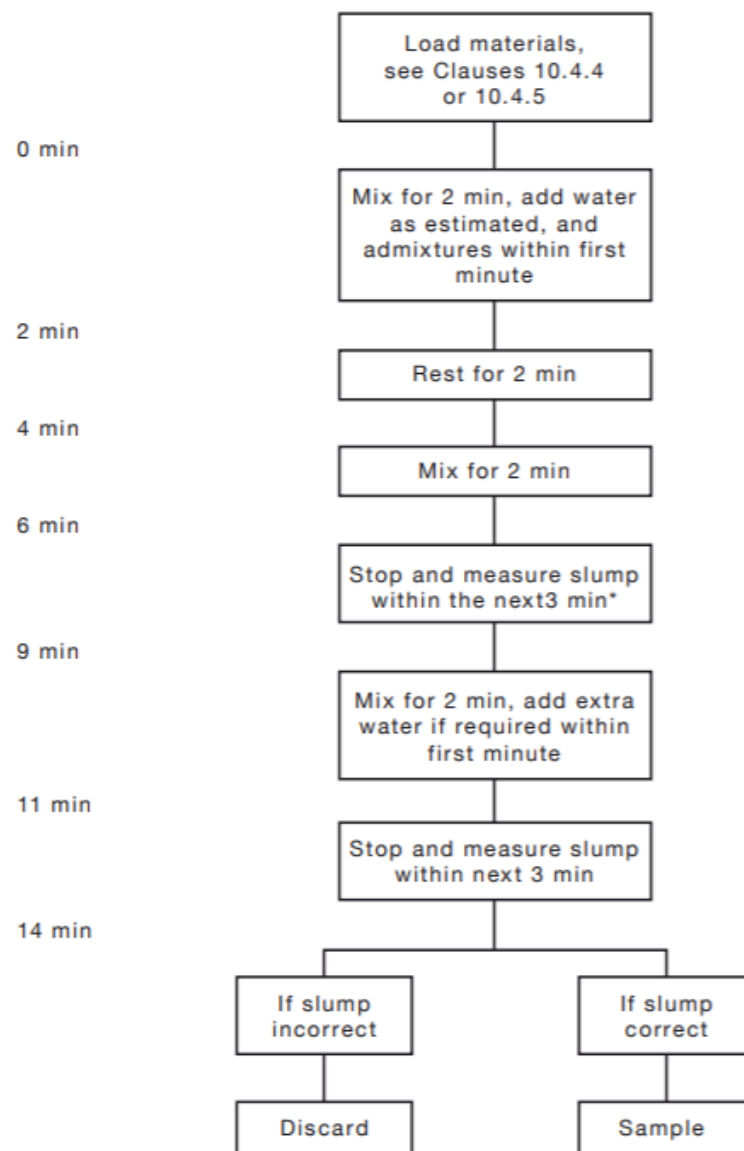


Figure 3.2 Concrete mixing procedure

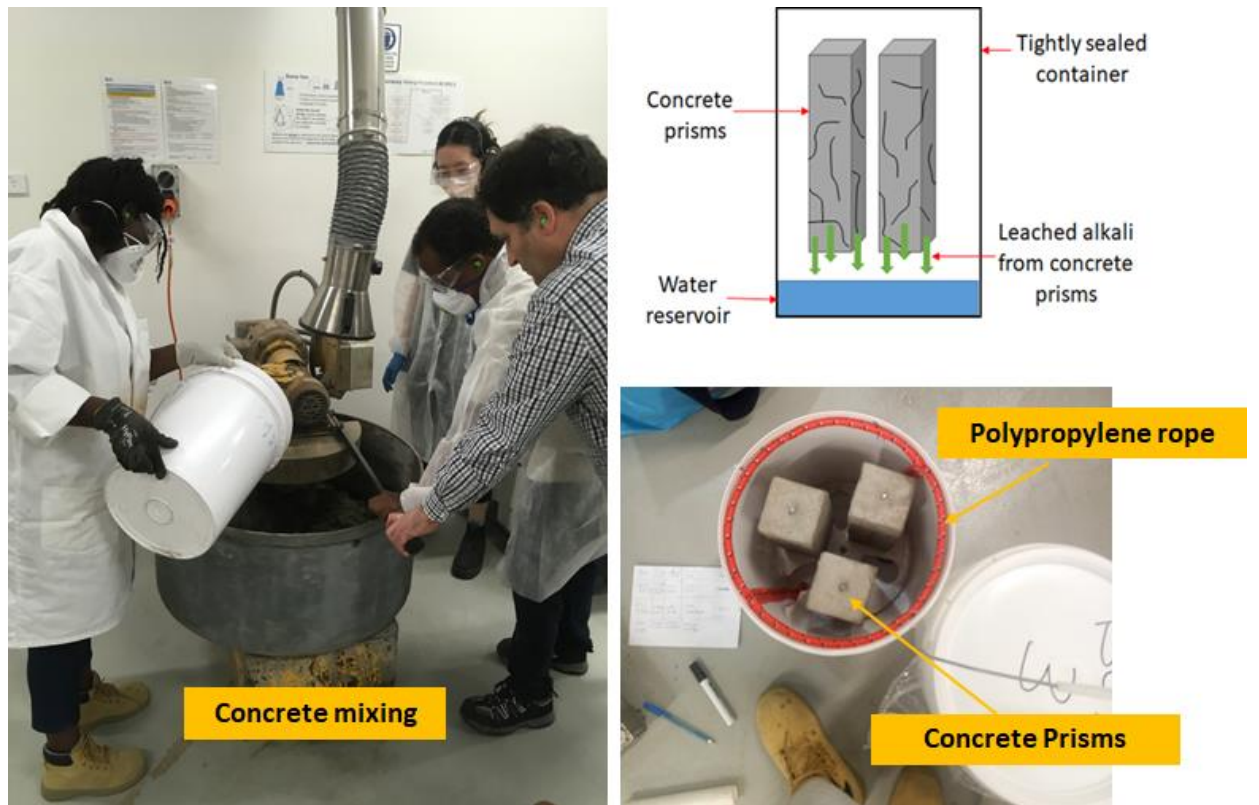


Figure 3.3 Concrete mixing with principal supervisor and laboratory technicians, for CPT and ACPT, and schematic and photograph of prism storage method (showing absorbent polypropylene rope) during curing for CPT and ACPT

Moulding and Curing

Concrete prisms were cast in a metal mould of 75 mm x 75 mm x 285 mm. The concrete was poured into the moulds and shaken on a vibration table at a medium frequency (approximately 50 Hz) to remove air bubbles and improve compaction. After casting, the concrete prisms were covered with plastic; to reduce moisture loss and cured in the mould at room temperature for 24 hrs. After that, the prisms were demoulded, and the initial mass and length measurements were taken with recorded. CPT was carried out by curing the concrete prisms vertically above a water reservoir (storage water) at 38°C in tightly sealed plastic pails lined with

polypropylene rope, as shown in Figure 3.3. This ensured a high humidity above 95% throughout the test duration. For ACPT, the concrete prisms were cured in the same manner; however, curing was achieved at 60°C in a laboratory oven. The temperature in the CPT environmental chamber (Figure 3.4) and ACPT ovens were continuously monitored and maintained throughout the test period

Expansion Measurements

CPT and ACPT expansion measurements were carried out with a horizontal length comparator (Figure 3.4) for a minimum of 12 months and 6 months, respectively, at the standard ages of 7 and 28 days, and then at monthly intervals for the remainder of the test duration. For slowly reactive aggregates and during the assessment of potential supplementary cementitious materials, an extended test period of 24 months for CPT (Sirivivatnanon, Mohammadi & South 2016) and 8 months for ACPT was considered.



Figure 3.4 38°C environmental chamber for CPT and the horizontal comparator for CPT and ACPT prism expansion measurements carried out in this study

Expansion measurements were taken in a temperature and humidity-controlled room, at 23°C ±5 and 50% RH. Concrete prisms were cooled in the same controlled environment while in their storage pails for 16±2 hours before measurements were taken. The length comparator for expansion measurement was set to zero before the start of measurements at each age. The percentage expansion of the prisms (En %) was then determined by Equation 3.2.

$$E_n (\%) = \left(\frac{L_n - L_i}{L_g} \right) \times 100 \dots\dots\dots \text{Eqn 3.2}$$

Where, L_n = Prism length after period n ; L_i = Initial length of the prism and L_g = Gauge length (usually 250 mm.)

The reactivity classification of the aggregates or concrete mix was further determined following the classification index given by AS1141.60.2 (Table 2.6). That is, concrete prisms that show expansion exceeding 0.03% after 12 months of CPT are classified as potentially reactive, whereas prisms that showed expansion below 0.03% after 12 months are considered non-reactive. For ACPT, the CPT expansion limit of 0.03% was applied to 3 months and 5 months of ACPT, unless otherwise stated.

3.3.2 RILEM Recommended Methods for Determining Alkali

Limits of Aggregates

The RILEM AAR-3.2 and AAR-7.1 methods were employed in this work to determine the alkali limits of aggregates and aggregate combinations. The RILEM AAR-3.2 describes a similar method to the AS 1141.60.2 CPT method, except that the alkali content of the concrete is increased at chosen intervals from 2 - 5 kg/m³

Na₂O_e using high purity NaOH in the mixing water. The sample preparation, moulding, and curing of concrete prisms for AAR-3.2 are comparable to the procedure described in 3.2.1.2. However, the varying alkali content allows for the determination of the alkali threshold, that is, the alkali highest alkali content at which there is no deleterious expansion of concrete prisms after 12 months of testing (Nixon & Sims 2016b). For the RILEM AAR-3.2 method, an expansion of 0.05% at 12 months is considered the limit for classifying potentially deleterious expansion. However, in this study, the AS 1141.60.2 expansion limit of 0.03% was used.

From the expansion results obtained after 12 months, the reactivity levels of the aggregates or aggregate combination were further be categorized as per the RILEM AAR-3.2 reactivity index, given in Table 3.6.

Table 3.6 Classifications of aggregate reactivity levels in accordance with RILEM AAR 3.2

Category	Explanation
Low	Aggregates that show no significant reaction from classification and expansion tests performed in accordance with petrographic assessment, AMBT, and CPT standards.
Medium	Aggregates that show an alkali threshold higher than 4.0 kg/m ³ alkali content,
High	Aggregates with low alkali threshold, typically below 4.0 kg/m ³ alkali content.

Further to this, proposed alkali limits for aggregates were determined by applying a safety margin as outlined in RILEM AAR-7.1(Nixon & Sims 2016a). Safety margins are based on benchmarked standard tests and local experience of several aggregates and account for the difference between laboratory and field specimens such as alkali

leaching (Section 2.7.2), potential alkali released from aggregates, and site batching variations. A safety margin is typically set at 1.0 to 1.5 kg/m³ Na₂O_e below the alkali threshold of the aggregate. For this study, the safety margin of 1.0 kg/m³ Na₂O_e was nominated to determine the alkali limits of the selected aggregates.

3.3.3 Chemical Tests

3.3.3.1 ASTM C289

The ASTM C289 chemical test method was employed as a rapid method to provide preliminary indications of the potential reactivity of aggregates. As discussed in Section 2.7.1.2, this method uses a ranked list that has been developed based on highly siliceous aggregates to determine the reactivity of aggregates in an alkaline environment (ASTM 2007).

In the present study, the aggregates under investigation were ground and sieved to pass a 300 µm sieve and be retained on a 150 µm sieve. The ground aggregates were reacted with 1M NaOH solution at 80°C for 24 hours. Subsequently, the amount of dissolved silica and the reduction in the alkalinity of the test solution was analysed using atomic emission spectroscopy to determine the reactivity of the aggregates based on the decision chart shown in Figure 3.5. The limitations of the ASTM C289 are discussed in Section 2.7.1.2; thus, the results from this method were considered as an initial predictor of aggregate reactivity prior to further comprehensive testing.

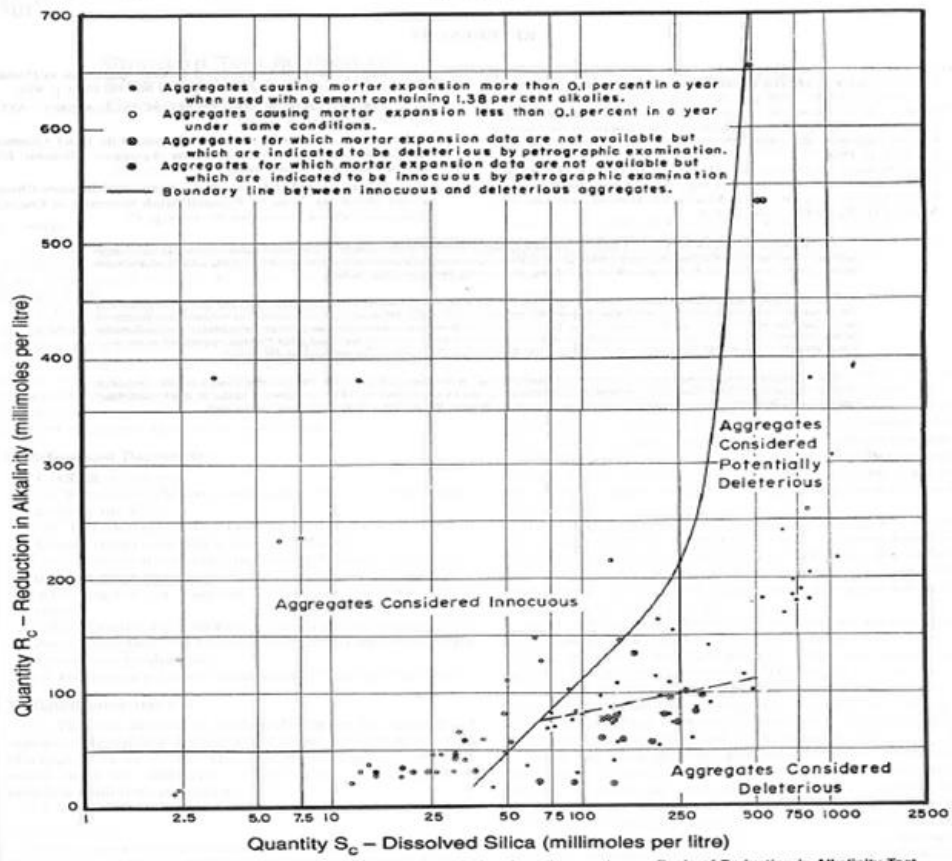


FIG. X1.1 Illustration of Division Between Innocuous and Deleterious Aggregates on Basis of Reduction in Alkalinity Test

Figure 3.5 ASTM C289 standard curve for identifying reactivity of aggregates

3.3.3.2 Dissolution Test

Additional dissolution tests were carried out on ground aggregate particles to determine the amount of soluble silica and alumina present in the aggregate. As aforementioned in Section 2.8.3, SCMs with high amounts of Si and Al have higher ASR mitigatory properties. Thus the dissolution tests were particularly undertaken to investigate the efficacy of GRAFs in ASR mitigation based on the amount of silicon (Si) and aluminium (Al) released by the ground aggregates despite the potential interaction by other ions.

Aggregates for dissolution tests were ground to fine powders of approximately 100 ± 10 μm particle size. The ground aggregates were placed in 1M NaOH solution at 80°C for 7, 14, 21, and 28 days. The concentration of Si and Al ions released into the test solution, as well as calcium, was analysed using microwave plasma atomic emission spectroscopy (MP-AES).

3.3.3.3 Ground Aggregate Slurry Test (GAST)

GAST is a chemical test method that has been devised in an attempt to resolve the limitations of ASTM C289 by increasing the test duration and incorporating $\text{Ca}(\text{OH})_2$ as a co-reactant. Although it has not yet been benchmarked, GAST has shown potential in effectively assessing the reactivity of aggregates (Thomas, Ha Hau, et al. 2019; Thomas, Roboredo, et al. 2019).

GAST tests were carried out by mixing 1.00 ± 0.01 g of finely ground aggregate (100 ± 10 μm particle size) with 1.00 ± 0.01 g of $\text{Ca}(\text{OH})_2$ in HDPE centrifuge tubes. 10 mL of 1.0 M NaOH was then added into the tubes and shaken to produce homogenous slurries. The HDPE tubes were placed in an 80°C oven for 1, 3, 7, 14, and 28 days (Figure 3.6). At the respective ages, the solids were recovered using a Buchner funnel, rinsed with 10 mL of methanol, and transferred to a new HDPE tube to dry in a vacuum oven at $48\pm 2^\circ\text{C}$ for 72 hours. The dry solids were further ground in a mortar with a pestle to remove lumps, transferred to a new HDPE tube, and stored in a $48\pm 2^\circ\text{C}$ vacuum oven until required for thermogravimetric analysis.

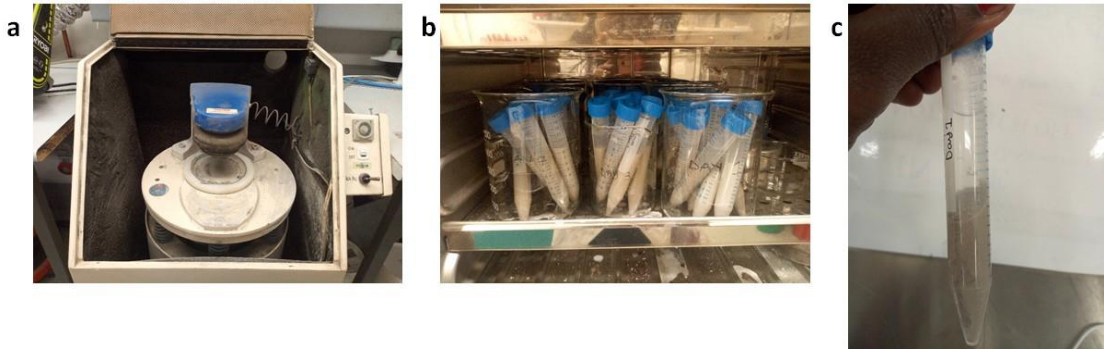


Figure 3.6 Procedure for GAST method (a) ring mill for grinding aggregates to micron-sized powders (b) ground aggregate slurries in 80°C oven and (c) ground aggregate slurry after day 1 of testing.

GAST can be considered a rapid test due to the high temperature (80°C) used to simulate the AMBT method. However, it can also be adopted at 38°C to simulate CPT conditions and 60°C for ACPT. The test method is primarily designed to evaluate the reactivity of aggregates by assessing their pozzolanic behaviour. This is determined by the effective reduction of portlandite in the slurry substrate after testing. The increased surface area of the aggregate enhances the dissolution of metastable silica in high alkalinity (1M NaOH) to form a weak silicic acid (Si(OH)₄). Si(OH)₄ becomes part of the pozzolanic reaction that leads to the formation of C-S-H gel in the reaction described in Equation 3.3.



As discussed in Section 2.3.1, aggregates that have high amounts of reactive silica exhibit high ASR reactivity. Therefore, a higher release of metastable silica results in a higher consumption of Ca(OH)₂ (portlandite) during the GAST.

The pozzolanic reaction is similar to the hydration reaction leading to the formation of ASR gels. However, the C-S-H gels formed from the pozzolanic reaction are

non-expansive due to the high calcium (Ca) content of the gel. Generally, at high alkalinity, as is usually the case in cement systems, Ca concentration in the pore solution is low. Therefore, C-S-H gels that precipitate tend to have a low Ca content and thus can cause expansive ASR.

The GAST method is a developing technique; therefore, there are some challenges associated with its execution. For instance, the partial dissolution of $\text{Ca}(\text{OH})_2$ in solution, as well as the segregation of the ground aggregate and $\text{Ca}(\text{OH})_2$ suspension that occurs over time due to the differences in densities. Additionally, the high temperature (80°C) at which the test is carried out may cause new calcium silicate phases to become stable, thus reducing available Ca in the solution for the reaction.

3.3.3.4 Ground Aggregate Paste Test (GAP)

Similar to the GAST method, the ground aggregate paste (GAP) test provides a quick method for assessing the reactivity of aggregates to alkali susceptibility (Boyd-Weetman & Thomas 2020). Nonetheless, rather than adding $\text{Ca}(\text{OH})_2$ and NaOH , this method uses cement to supply ground aggregates with calcium and alkali for the pozzolanic reaction (Eqn. 3.3). Generally, this test method is better suited for assessing binder systems containing mineral additions and SCMs of particle size comparable to the particle size of cement (Fanghui, Qiang & Jingjing 2015; Suraneni et al. 2018).

Consequently, the GAP test was used in this study to investigate the potential GRAFs as additives for mitigating ASR. For this purpose, pastes composed of cement and GRAFs at cement replacement levels from 10 to 40% in sealed HDPE tubes. 24 ± 0.5 g

of material (cement +GRAFs) was used for the GAP test with a water-binder ratio of 0.5. The HDPE tubes were stored at 38°C, 60°C, and 80°C to simulate CPT, ACPT, and AMBT conditions, respectively. The mass loss of portlandite, indicating the reactivity and thus mitigation potential of the respective GRAFs, was ascertained after 7, 14, 21, and 28 days of testing using thermogravimetric analysis.

3.3.4 Characterization Techniques

A variety of techniques are available to investigate the mineralogical and elemental composition of aggregates, the presence, and composition of ASR reaction products, phase morphologies developed, and the concentration of ions in solution. In this study, a combination of techniques was selected for characterization purposes. This includes petrography, scanning electron microscopy (SEM), x-ray diffraction (XRD) analysis, x-ray fluorescence (XRF) analysis, thermogravimetric analysis (TGA), and microwave plasma atomic emission spectroscopy (MP-AES) analysis. These techniques are discussed as follows.

3.3.4.1 Petrography

Petrographic assessment of aggregates as well as mortar bars and concrete prisms after the completion of expansion tests were carried out in this study. The principal objective of the petrographic assessment of aggregates is to identify the potential of siliceous-based minerals that react with hydroxyl ions from the cement pore solution to form ASR products (Nixon & Sims 2016b). Acceptance and reactivity classification of aggregates by petrography is usually dependent on the

petrographer, and is achieved by considering local experience of identified reactive constituents. This may vary in regional or national areas.

Sample Preparation




Macroscopic and thin section petrography were performed on the aggregates using a high lens magnifying glass and a binocular microscope equipped with accessories for identifying the optical properties of minerals, correspondingly. For mortar bars and concrete prisms, specimens were prepared by taking a random slice along the length of the bars and prisms. The slices were then impregnated with blue-dyed epoxy to stabilize existing voids and cracks. Thin sections from the stabilized slices were prepared for microscopic petrographic examination and assessments in transmitted polarized light. A sample of the petrographic slides prepared for this work is shown in Figure 3.7.



Figure 3.7 Petrographic slides for mortar bars studied

Test Procedure

Petrography following procedures outlined in ASTM C295 (ASTM 2003) and AS 1141.65 (Standards Australia 2008) were carried out on the aggregates used in this work. Additionally, specifications by AS 2758.1 and SA HB 79 (Standards Australia 2016) were also considered for identifying the potential reactivity of the aggregates. Conversely, the petrographic assessment of mortar bars and concrete prisms after completing the respective physical expansion test methods was carried according to ASTM C856 requirements (ASTM C856 2018). The approximate amount of the mineral constituents in the aggregate and the composition of the mortar bars and concrete prisms were determined by identifying and counting the components at each 100 widely spaced points within the thin section of each sample. Petrographic assessment of mortar and concrete prisms, under the ASTM C856 method, was carried out with attention to the following clauses:

-  **Clause 5.5.1:** To establish whether ASR has taken place, what aggregate constituents were affected, what evidence of the reaction exists, and what were the effects of the reaction on the concrete.
-  **Clause 5.5.3:** To establish whether any other cement-aggregate reaction has taken place. In addition to alkali-silica and alkali-carbonate reactions, these include hydration of anhydrous sulfates, rehydration of zeolites, wetting of clays, and reactions involving solubility, oxidation, sulfates, and sulphides.
-  **Clause 5.5.4:** To establish whether an aggregate used in a test has been contaminated by a reactive constituent when in fact, the aggregate was not reactive.

- 🚩 **Clause 5.5.6:** To determine the extent of reaction, the nature of reaction products, and effects of reaction produced in exposure to a chemically aggressive environment
- 🚩 **Clause 5.5.8:** By comparison with appropriate laboratory specimens, a petrographer may be able to substantiate the existence of a particular reaction in concrete or determine that the reaction cannot be detected.

3.3.4.2 Microstructural and Elemental Compositional Analysis

A scanning electron microscope (SEM), equipped with an energy dispersive x-ray spectrometer (EDS), is a useful tool for investigating the morphology, microstructure, and elemental composition of materials. In this study, a Zeiss Evo LS15 SEM with a resolution range of 2 μm at 20 keV was used. This SEM was equipped with a Bruker 127eV energy-dispersive x-ray detector to characterize the composition of the aggregate, paste, mortar, and concrete specimens investigated.

Figure 3.8 shows this setup in further detail.



Figure 3.8 SEM-EDS instrument used in this study

Principle of Technique

Generally, an SEM generates surface (and sub-surface) images of a specimen on a microscopic scale by scanning a specimen with a beam of high energy electrons in an optical column. When an incident electron beam interacts with the atoms on the surface of a specimen surface, elastic and inelastic scattering of the beam occurs that produces energy characteristic beams, as shown in Figure 3.9. These beams are analysed by attached detectors (in this case, EDS) to give specific information on the specimen.

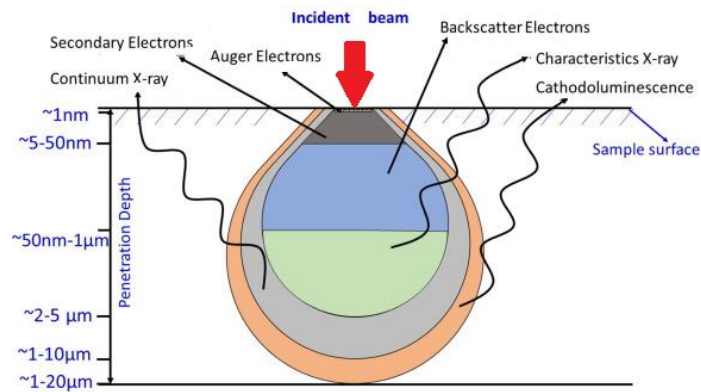


Figure 3.9 Electron interactions and resulting emissions during SEM. *Modified image from* (Mazumder et al. 2018)

For this study, a combination of secondary and backscattered electrons were used for the microstructural and elemental compositional analysis. Secondary electrons (SE) are formed from the inelastic collision of electrons from the incident beam and their interaction with the specimen, resulting in lower energy electrons that penetrate only a few nm from the specimen's surface (Figure 3.9). Due to this, SE discharged from the specimen typically provide information on the topological features of the specimen surface. In contrast, the elastic scattering of electrons

produces backscattered electrons (BSE) with high electron energy that penetrate the sample deeper to provide information on the elements present, based on their respective atomic number and phase differences in the specimen. Images generated from BSE are contrasted depending on the atomic number of the elements present in the specimen such that; regions of the specimen that contain elements with a high atomic number appear brighter during analysis (Lloyd 1987). A similar elastic collision takes place in the formation of characteristic x-rays (Figure 3.9). However, the energy of the beams generated is much higher with a greater depth of penetration to displace electrons from a lower-energy shell of an atom in an element, and emit x-rays that are characteristic of that element. Thus, the various elements and their respective amounts in a specimen can be obtained by the attached EDS detector.

Operating Parameters

SEM analysis was carried out in the SE and BSE imaging mode to obtain information on the surface features such as the morphology of GRAFs, and the presence of cracks and reaction products on the expanded mortar and concrete specimens. Electron acceleration voltages of 10 and 15 keV, depending on the conductivity of the surface coating achieved (Section 3.2.4.2.1), was used during both SE and BSE imaging.

Since x-rays are released from the atomic shell, a higher incident electron energy is required to ensure sufficient electrons are displaced to emit enough x-rays from the specimen surface for detection and analysis. Therefore, for EDS analyses, the electron acceleration voltage was increased to 20 keV. This high acceleration voltage also accounts for the depth of coating required to analyse non-conductive materials,

as discussed in Section 3.2.4.2.1. EDS point analysis and elemental compositional mapping methods were used for characterising the features of the specimens. During EDS analysis, the elements of interest were predetermined as Ca, Silicon (Si), potassium (K), sodium (Na), oxygen (O), Iron (Fe), magnesium (Mg), aluminium (Al), carbon (C), and sulphur (S).

3.3.4.3 Sample Preparation

All specimens were coated with gold-palladium to a depth of 20 nm for polished and fractured surfaces and 15 nm for ground aggregate fines, prior to SEM-EDS analyses. This step was carried out to eliminate electron-to-electron repulsion (charging) as the specimens were non-conductive. Specimen coating was achieved using a Leica EM ACE600 applicator.

Ground Aggregate Fines

Ground aggregate fines were mounted on a metal sample stud with carbon tape before coating and SEM-EDS analyses. Mounted specimens were further sprayed with compressed air to remove excess powders from the carbon tape and stud that may contaminate the SEM vacuum chamber and interfere with electrons during analysis.

Mortar and Concrete Specimens

The sample preparation for mortar and concrete specimens followed sequence sectioning, vacuum drying, mounting, and polishing before coating for SEM-EDS analyses.

Sectioning and Drying

Sectioning of mortar bars and concrete prisms was achieved with a Struers Labotom15 cutting machine, fitted with a diamond blade (shown in Figure 3.10). The cutting machine employed water as the cutting fluid. Sectioned specimens were soaked in 99% isopropanol for a period of 5 to 7 days to arrest hydration through a solvent exchange process, thus stopping any ongoing reaction from progressing (Knapen et al. 2006; Thomas 1989). Specimens were then dried in a vacuum oven at 38°C for CPT prism samples and 45°C for AMBT and ACPT samples for 72 hours prior to mounting.



Figure 3.10 Labotom15 cutting machine for mortar and concrete sectioning

Mounting and Polishing

Following drying, sectioned specimens were mounted using a vacuum impregnation technique and an epoxy resin (EpoFix) supplied by Struers. The surfaces of the mounted specimens were first manually polished on 360 grit SiC paper to remove any film of resin covering the surface to be examined. Fine polishing was then achieved mechanically with a Struers Laboforce-100 using composite magnetic discs with 9 μm , 3 μm , and 1 μm polycrystalline diamond suspension as the polishing aid and lubricant. This setup is shown in Figure 3.11.

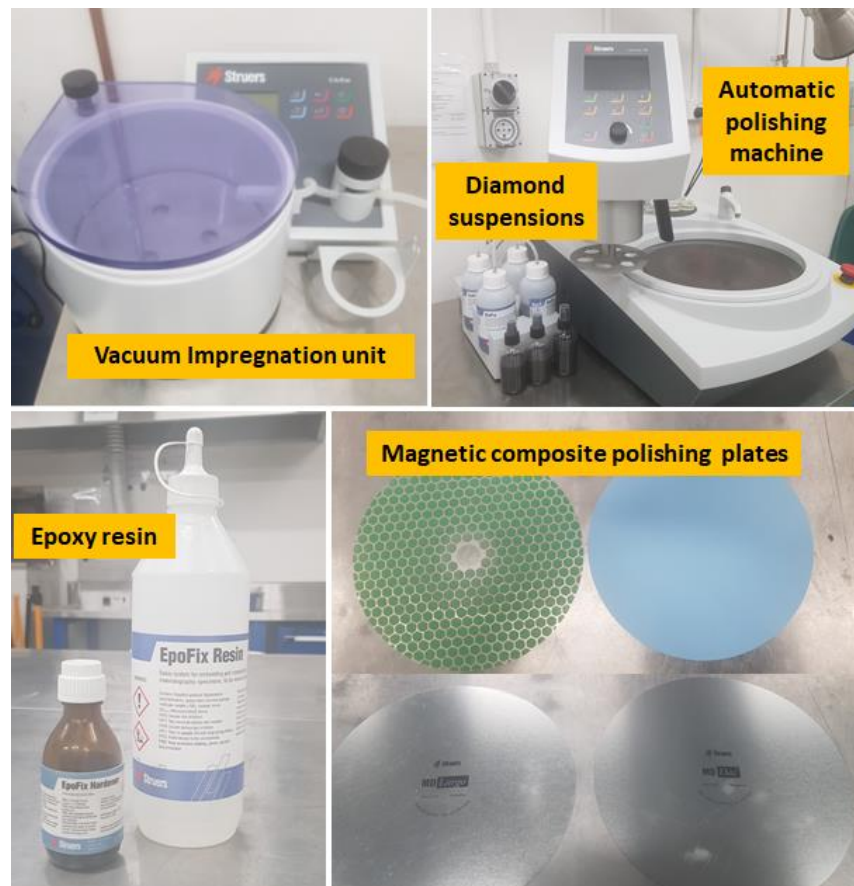


Figure 3.11 Setup for mounting and polishing specimens for SEM-EDS analysis

The Laboforce-100 mechanical polisher was programmed to follow a sequence of 10 mins of polishing on MD largo plates with 9 μm diamond suspension, after which 3 μm diamond suspension was used for an additional 15 mins. The polishing plate was rinsed with deionized water at the end of each polishing stage to remove the larger diamond particle size (9 μm) that may continue to scratch the surface of the specimen. Fine polishing was achieved on the MD Darc neoprene cloth plate with 1 μm diamond suspension for 30 mins. During polishing, a consistent speed of 300 rpm and 25 kN load was applied on the mounted specimen. After fine polishing, specimens were ultrasonicated for 5 mins in isopropanol to remove any diamond or paste debris on their surfaces. Further, the specimens were dried in a vacuum oven at 38°C for 3 days and stored in a vacuum desiccator at 23 ± 2°C until the time for analysis.

3.3.4.4X-Ray Diffraction Analysis (XRD)

Principle of Technique

X-ray diffraction (XRD) is a non-invasive qualitative characterization technique for determining features such as atomic and crystal structure, as well as phases in materials. XRD is mostly used for investigating crystalline materials. XRD operates on the principle of the Braggs law described in Equation 3.4 (Pope 1997).

$$2d \sin\theta = n\lambda \dots\dots\dots\text{Eqn. 3.4}$$

Typically, when incident monochromatic x-rays with wavelength (λ) interact with the atoms in a particle, they are elastically scattered and remitted with an intensity that is dependent on the atomic number of the atoms present. In crystalline

materials, the remitted x-rays are reflected off planes of an orderly array of atoms, resulting in predominately destructive interference. However, according to Bragg's law, at certain diffraction angles, the spacing between the planes (d) corresponds to several wavelengths, resulting in constructive interference that leads to the formation of peaks in a diffraction pattern. For this reason, in amorphous materials where the average spacing between the reflection planes is disordered, a decrease in constructive interference occurs, resulting in lower diffraction signals that are exhibited as broad peaks (sometimes referred to as a 'halo') above the background (noise) of the diffraction pattern obtained (Kőrösy et al. 2013).

Sample Preparation

All specimens for XRD analysis were ground to a fine powder in a mortar and pestle and dried in a vacuum oven at 45 ± 2 °C for 24 hours. Before carrying out XRD analysis, the powders were packed firmly to level in a sample holder, as demonstrated in Figure 3.12.



Figure 3.12 Prepared powder samples for XRD analysis

Operating Parameters

The powder diffraction method was used for XRD analysis. The analysis was carried out with a Cu K α radiation of wavelength 1.5418 Å. The diffraction patterns presented in this study were obtained using a Bruker D8 Discover XRD operating in a θ - θ Bragg-Brentano configuration (Figure 3.13). In this scan formation, the sample position is fixed on a stage while the x-ray tube and x-ray detector move along a diffractometer circle in a synchronized motion (Cline et al. 2019). For all XRD analyses, the instrument was fitted with a knife edge (Figure 3.13) to reduce the background 'noise' during low angle scanning.

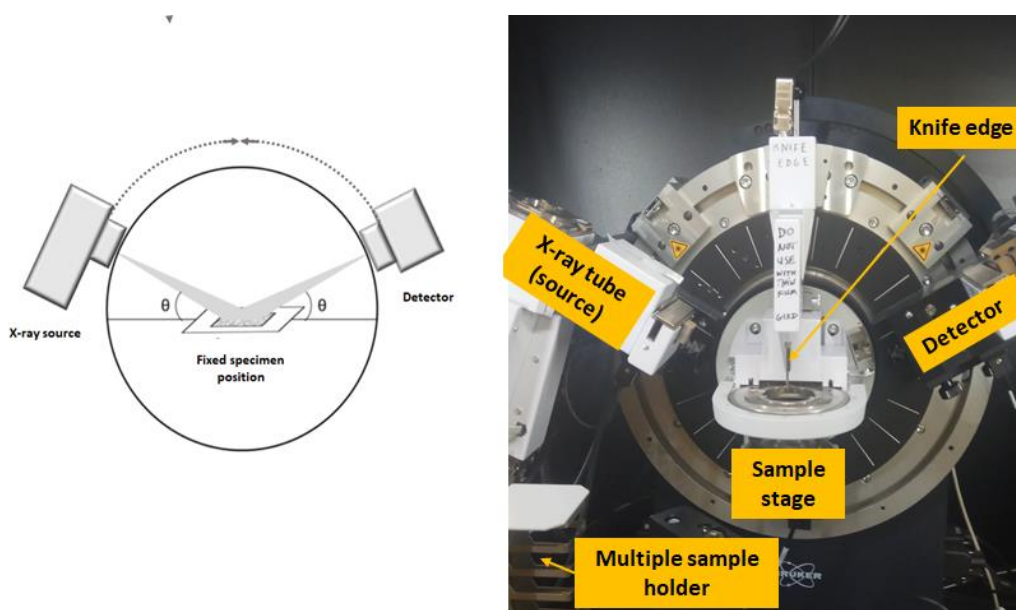


Figure 3.13 Schematic of θ - θ Bragg-Brentano configuration and Bruker X-ray diffraction instrument used in this study

Diffraction patterns were taken from 2θ angle of 5° to 80° , at a scan rate of 0.02° per second. A search-match routine was then performed with DIFFRACT.EVA software and ICDD PDF 4+ database for phase identification.

3.3.4.5 X-Ray Fluorescence Spectroscopy (XRF)

Principle of Technique

The XRF characterisation technique is similar to EDS except that a high energy incident x-ray (rather than incident electrons in EDS) dislodges the electrons in the specimens' atomic structure, and the detected signals are fluorescent (or secondary) x-rays. Accordingly, the elements present in the specimen are identified by the characteristic energy of the fluorescent x-rays emitted when an electron from a higher energy shell in an atom replaces a hole in a lower energy shell due to electron displacement upon x-ray interaction. Depending on the energy state of the electron shell, K_{α} or K_{β} x-ray fluorescence will be emitted (Figure 3.14). Quantitative analysis of identified elements is determined by counts of x-ray photons emitted.

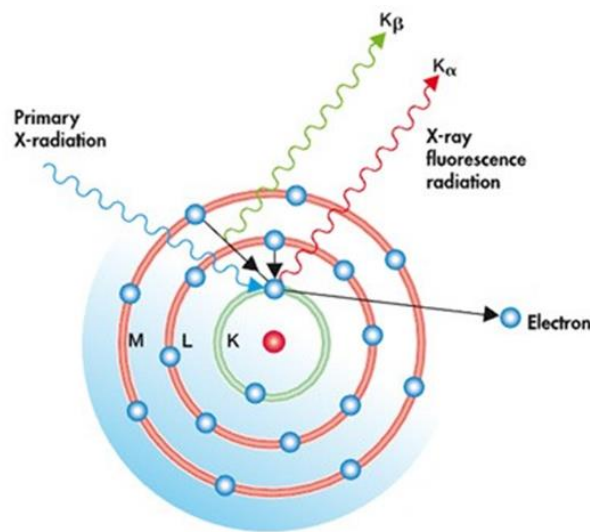


Figure 3.14 Atomic model explaining the principle of XRF analysis (Francisco; 2018)

All XRF analysis were carried out at the University of New South Wales (UNSW). XRF analysis was carried out on the finely ground aggregate (100±10 μm), fly ash, and cement materials using a Philips PW2400 XRF complete with

SUPERQ software with a detection level of 0.01%. The equipment was calibrated using certified reference materials (CRMs) sourced from Malvern Panalytical. The calibration was achieved by measuring the sample three times to estimate the standard of deviation; this was found to be 0.02%, suggesting that the measurement obtained are reproducible.

3.3.4.6 Thermogravimetric Analysis (TGA)

Principle of Technique

Thermal analysis is one of the most widely used techniques in cement chemistry for identifying hydration phases through thermal decomposition. In TGA, changes in a material's physical and chemical properties are observed by monitoring mass loss in the material as temperature is increased at a constant heating rate in a controlled environment. For cement materials, the extent of hydration and other reactions are assessed by measuring the dehydration of hydrate phases, the dehydroxylation of portlandite, and the decarbonation of calcite (Scrivener et al. 2015), which occur at specific temperature ranges. A general TGA curve for hydrated cement- showing the temperatures at which the dehydration, dehydroxylation, and decarbonation decomposition steps may occur, is shown in Figure 3.15. It is worth noting that the exact temperatures at which the decomposition steps occur may vary depending on the bound water of the additives in the cement if present (Deboucha et al. 2017).

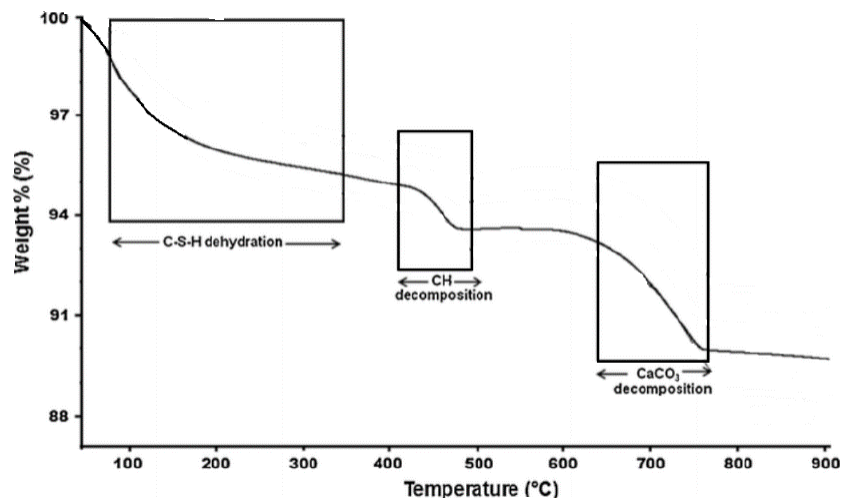


Figure 3.15 General TGA curve for hydrated cement (Singh et al. 2015)

In this study, TGA was used to determine the reactivity potential of ground aggregates based on the residual portlandite measured following the pozzolanic reactions that occur in GAST and GAP tests, as discussed in Sections 3.3.3.3 and 3.3.3.4.

Sample Preparation and Operating Parameters

Specimens for TGA were dried at $45 \pm 2^\circ\text{C}$ in a vacuum oven for 72 hours and then ground with a mortar and pestle (for GAST samples) or in a ring mill for 2 mins (for paste samples) until the powders passed a $75 \mu\text{m}$ sieve. The finely ground powders were stored in tightly closed HDPE centrifuge tubes under vacuum to prevent carbonation until needed for TGA.

TGA in this work was completed using a Netzsch STA 449 F5 Jupiter thermal analyser coupled with GC-MS (Figure 3.16). Approximately 25 ± 1 mg of the finely ground powders were weighed into an alumina crucible using an analytical scale

and analysed in a helium environment at a flow rate of 60 mL/min. Specimens were analysed at a heated rate of 10°C/min over a temperature range of 40°C to 1000°C. Conversely, the temperature range of 450°C to 500°C (Figures 6.28 to 6.30) was considered the dehydroxylation temperature range of portlandite.

The thermogravimetric (TG) data measured was differentiated to the 1st order to obtain differential thermogravimetric (DTG) results for determining the mass loss of portlandite in the systems (Lothenbach, Durdzinski & De Weerd 2016). All the DTG data obtained was smoothed with Savtzyk-Golay method B to reduce the background 'noise' in the data and enable better resolution for evaluating the respective mass losses. The portlandite mass loss was determined using the tangential method (Kim & Olek 2012).



Figure 3.16 Thermal analyser used for TGA in this study

3.3.5 Microwave Plasma Atomic Emission Spectroscopy (MP-AES)

MP-AES was also included in the array of characterization techniques adopted in this study to investigate the elemental composition of solutions.

Principle of Technique

AES follows a series of steps summarized as: atomization, excitation, and detection. In MP-AES, a nebulizer converts the liquid sample into an aerosol. This aerosol passes through a magnetically generated nitrogen plasma, where the atoms are excited to a higher energy state. As the energized particles return to their low energy state, they emit a spectrum of light with distinct wavelengths for specific elements (Kamala et al. 2014). A detector collects this emission spectrum and consequently provides information on the number and amount of elements in the liquid specimen. MP-AES provides precise and multi-element measurements and allows lower detection limits (Sajtos et al. 2019); thus making this analytical technique an essential tool in the study- to determine the concentration of respective ions that dissolved in alkaline solution during the ASTM C289 and the dissolution tests undertaken. MP-AES was also employed for the elemental analysis of pore solution of pastes containing GRAFs.

Sample Preparation

All specimens for MP-AES analysis were digested and diluted with 1% nitric acid prepared by diluting 67% (reagent grade) nitric acid supplied by Baseline Seaster chemicals with Milli-Q water. Acidifying the specimens dissolves precipitated ions

and allows for an accurate determination of the elements. Two different dilution ratios of 1:20 and 1:1000 were set to obtain ion concentration ranges within the equipment's capability and set range. Each specimen for MP-AES analysis was tested twice; however, the desired elements were determined in 1 single measurement. Thus the results reported in the present study is the mean concentration of the elements.

Operating Procedure

The Agilent 4200 instrument, shown in Figure 3.17, was used for the MP-AES analysis in this study. During the analysis, the elements that were selected to be of interest are Ca, Si, K, Na, and Al. The working wavelengths for these elements were selected to give a large linear dynamic range that fulfills the detection limit requirements while limiting spectral interferences. The selected wavelengths used for the MP-AES measurements carried out are presented in Table 3.7. Prior to the specimen analysis, each element of interest was calibrated to the concentration range of 0.05 ppm to 20 ppm by a 5 point calibration method using a combined standard reference diluted with 1% nitric acid. The resulting calibration curves for all the elements were linear, with a correlation coefficient ≥ 0.996 .



Figure 3.17 4200 Agilent Technologies MP-AES instrument with an autosampler

Table 3.7 Selected wavelengths of the desired elements for MP-AES analysis

Elements	Wavelength (nm)
Calcium	393.366
Sodium	588.995
Silica	251.611
Potassium	766.491
Aluminium	396.152

During measurements, the automatic background correction application was selected to correct the background for every sample and every wavelength automatically, thus reducing user interaction for improved accuracy. Further, the plasma gas from the nitrogen generator was supplied continuously throughout the measurement. The MP-AES instrument was fitted with an autosampler (Figure 3.17); therefore, the samples were measured automatically. The autosampler was rinsed for 30 s in 1% nitric acid prepared between each specimen measurement.

3.3.6 Laser Diffraction Particle Size Analysis

Principle of Technique

Particle size analysis was carried on powders using a laser diffraction technique. This technique utilizes light scattering to investigate particle sizes by measuring the diffraction of an incident laser beam as it interferes with the particles. The size of the particle is determined as the inverse of the diffraction angle observed. Conversely, the volume of particles in a specific size, characterized by the relative cross-sectional area at specific angles, is indicated by the intensity of the diffracted beam at that angle(Eshel et al. 2004).



Figure 3.18 Malvern MasterSizer 3000 laser diffraction particle size analyser

Sample Preparation and Operating Parameters

Particle size analysis by the laser diffraction technique was carried out on cement, fly ash, and ground aggregate fines using the Malvern MasterSizer (Figure 3.18) with

a broad particle size range of 0.01 μm to 3500 μm . The particle size distribution of the ground aggregate fines was analysed by continuous ultrasonic dispersion in a beaker filled with Milli-Q water for 90 s. For cement and fly ash, the powders were dispersed in absolute ethanol to avoid hydration. Additionally, the laser diffraction disc was removed and wiped clean after every measurement to remove debris that may interfere with the diffraction angle and thus the particle size distribution.

3.3.7 Compressive and Flexural Strength Tests

The compressive strength test following AS 1012.9 (Standards Australia 2014c) and flexural strength test as per AS 1012.11 (Standards Australia 2014d) were performed on concrete specimens containing GRAFs to determine the effect of GRAFs on the mechanical properties of concrete.

Concrete cylinders of diameter 100 mm and height 200 mm, and prisms of dimensions 100 mm \times 100 mm \times 300 mm were cast and cured in 90 \pm 5 % relative humidity and 23 \pm 2 $^{\circ}$ C temperature controlled chamber for 28 days before testing compressive and modulus of rupture. The 28-day compressive strength test was selected to assess the possibility of classifying GRAFs as natural pozzolans as per ASTM C 618 (ASTM 2019). Compressive strength tests were carried out using the UTEST automatic compression testing machine. Conversely, the modulus of rupture of the concretes was determined after 28 days with a universal testing machine fitted with a 3-point loading rig. Three concrete cylinders and two beams were tested for each concrete mix studied.

Chapter Summary

In this chapter, the various methods that were used in this work to investigate the reactivity of the aggregates and the potential ASR occurrence have been discussed. These methods were categorized as physical tests, chemical tests, and characterization techniques. Under physical tests, the standard expansion test methods used were identified as accelerated mortar bar tests and concrete prism tests in accordance with AS 1141.60.1 and AS 1141.60.2, respectively. The accelerated version of the concrete prism test (ACPT) and a modified Rilem AAR-3.2 method were also employed to determine aggregates' reactivity and alkali threshold limits accordingly. Additionally, ground aggregate slurry test (GAST) and ground aggregate paste (GAP) tests were the chemical tests adopted to provide quick information on the reactivity and pozzolanic behaviour of the aggregates under investigation.

Furthermore, a suite of characterization techniques, including SEM-EDS, XRD, petrography, TGA, MP-AES, XRF, and laser diffraction, were selected for the analytical investigations required to achieve the objectives of this work. The principles guiding these techniques, the sample preparation, and operating parameters as employed in this work have also been described. Finally, the AS 1012.9 and AS 1012.11 mechanical test methods were also mentioned as the standards used to investigate the compressive strength and flexural strength properties of some concrete mixes studied in this work.

CHAPTER 4. Investigating Alkali Limits and Aggregate Blends For Mitigating Deleterious ASR in Concretes

4.1 Overview

A well-recognized approach for mitigating the effects of ASR is limiting the alkali contents in cement and concrete (Leming & Nguyen 2000). For example, the allowable alkali limits for concretes are fixed as 2.5 kg/m^3 and $2.8 \text{ kg/m}^3 \text{ Na}_2\text{O}_e$ in New Zealand and Australia, respectively (CCANZ 2012; Standards Australia 2015). To comply with the set alkali limits in concrete, cement with alkali content not exceeding $0.6\% \text{ Na}_2\text{O}_e$ is permissible for use in concrete (CCANZ 2012; Standards Australia 2015; Standards New Zealand 2009b; Thomas et al. 2006). These limits are set conservatively to reduce the amount of alkali that is available to react with susceptible silica minerals in reactive aggregates to form ASR in concrete. However, implementing these strict alkali limits may not guarantee that ASR will not occur. Literature reports of instances where concretes containing low alkali cement still experienced ASR attack (Bérubé et al. 2000; Olague, Wenglas & Castro 2003; Stark & Bhatti 1986).

Typically, the alkali content that will initiate ASR is largely dependent on the mineralogical composition of the aggregate used in the concrete (Thomas et al. 2006). Meanwhile, the current set alkali limits are generalized for all aggregates regardless of the mineralogical composition of aggregate and its reactivity classification. Based on these limits, a preferential selection of non-reactive

aggregates has occurred over the years. This has caused a depletion in acceptable aggregates sources, as aggregates that are classified as potentially reactive have generally been rejected for use in concrete. Additionally, the emerging need for special concretes with high early age strength (also requiring the use of additives) has become challenging for concrete producers; to keep within the alkali limits set. Meanwhile, low alkali content cements are also expensive to manufacture due to specified clinker manufacturing processes that lead to the dumping of kiln dust in order to maintain the required alkali (Worrell 2008).

The work done in this chapter investigates individual alkali limits for different aggregates sources with distinct mineralogical compositions and reactivity classifications, using the petrography, chemical, and expansion test methods described in Sections 3.2.1, 3.2.3, and 3.2.4.1. The premise of the work carried out in this chapter will allow the concrete industry to adopt alkali limits for marginal aggregate supplies. This work will also provide evidence that will form part of the framework for future investigations on the potential use of cement with alkali limits higher than 0.6% Na_2O_e , particularly in Australia and New Zealand, thus relating to the revision of the current alkali limits for concretes.

4.2 Experimental Plan

4.2.1 Materials

Aggregates

Five aggregates of different mineralogical classifications and two fine aggregate blends (sand blends), given in Table 4.1, were chosen for this part of the study. A collection of natural aggregates, manufactured aggregates, and sand blends were selected to provide a comprehensive overview of different alkali limits applied to different systems.

Table 4.1 Aggregates and sand blends selected for investigating alkali limits

Aggregates	Symbol	Description	Reactivity Classification
Waikato	WT	River sand	Reactive ^α
Greywacke	GW	GW _C Manufactured Coarse Aggregate	Slowly reactive ^β
		GW _F Manufactured fine aggregate	
Rangitikei	RT	River sand	Reactive
Andesite	AS	Manufactured fine aggregate	Reactive
Peats Ridge	PR _C	Manufactured coarse aggregate	Non-reactive
	PR _F	Manufactured fine aggregate	
Sand Blend 1	WT ¹	60% WT + 40% PR _F	Unknown
Sand Blend 2	WT ²	60% WT + 40% GW _F	Unknown

Reactivity classification as per α= in-situ behaviour; β=petrographic analysis; γ= reports in literature and δ=AMBT and CPT expansion tests.

The supposed reactivity classification of the aggregates obtained from previous studies is also given in Table 4.1. However, it is acknowledged that changes in mineralogical composition and, thus, the reactivity of aggregates may occur over

time due to natural causes. Additionally, a variation in the reactivity of the same aggregate at different batching sites is plausible. Therefore, the reactivity classification given in Table 4.1 was primarily employed as a guide for aggregate selection in this study. Further testing to ascertain the actual reactivity of the as-received samples used was carried out.

The sand blends studied were based on the potentially reactive aggregate WT, which is well known and abundant in the Auckland region of New Zealand. Due to the depletion of so-called non-reactive aggregates, there is a rising demand for the use of aggregate WT for concretes. The sand blends were introduced in this study to evaluate their potential in reducing the ASR risk of WT. Further, the 60/40 proportion of the sand blends studied was selected in support of a broader test program by Concrete New Zealand. Thus, for the non-reactive aggregate portion of the sand blends (PR_F), any aggregate of similar chemical and physical properties may be substituted as it is unlikely to contribute to the reaction. For Easy interpretation of results, the sand blends are considered as single aggregates in this study.

Cement and Reagent

GP cement with alkali content of 0.58%, conforming to the current alkali limits set for cement in Australia and New Zealand, was used. The chemical composition and particle size distribution of the cement are presented in Table 3.2 and Figure 6.1, respectively. High purity grade NaOH (Section 3.1.3) was also used to prepare the storage solutions for AMBT and to boost the alkali content of the concrete prism curing expansion tests.

4.2.2 Methods

A comprehensive test schedule comprising of the combination of the test methods recommended by SA HB 79 (Section 2.7) was designed to achieve the set objective of characterizing the ASR reactivity of the aggregates and identifying appropriate alkali limits. A summary of the test schedule employed in this study is shown in Table 4.2. The test methods listed in Table 4.2 were carried out according to the procedures described in Section 3.3.

Although the test scheme used in this study follows the ASR assessment guideline provided by the Australian SA HB 79 (Standards Australia 2015), the approach used in this study is much similar to the RILEM recommended test protocol for assessing the risk of ASR (Nixon & Sims 2016b) in that it includes ACPT as an alternative short term test for ASR assessment. Indeed, the test schedule presented in Table 4.2 was designed more comprehensively to incorporate chemical methods (ASTM C289 and GAST), which are not included in both the SA HB 79 and RILEM recommendations. Further, post-expansion characterization of the mortar bars and concrete prisms was carried out to ascertain the occurrence of ASR as the leading cause of the expansion observed, evident by the presence of ASR gel. This step in assessing ASR is also absent from both the SA HB 79 and the RILEM Technical Committee 219-ACS testing protocols. Petrographic assessment of expanded specimens was also carried out to identify the reactive minerals that initiated ASR.

Table 4.2 Summary of the test program showing the different test methods used, the sample description and test conditions

Test Methods		Sample ID	Description	Test Condition
Petrographic assessment of aggregates (AS 1141.65)		All aggregates were assessed.		
Chemical tests	Dissolution test (ASTM C289)	WT	Ground aggregate	1M NaOH; 80°C; 24 hours
	GAST	RT	Ground aggregates + Ca(OH) ₂	1M NaOH; 80°C; 28 days
		GW		
		AS		
Accelerated mortar bar test (AS 1141.60.1)		WT	100% WT	0.6M, 0.8M 1.0M NaOH 28 days
		WT ¹	60% WT + 40% PR _F	
		WT ²	60% WT + 40% GW _F	
		GW _F	100% GW _F	
Concrete prism test at 38°C (CPT) Concrete Prism Test at 60°C (ACPT) (AS 1141.60.2)		WT ¹	WT ¹ + PR _C	2.5, 3.0, 3.5, 4.0 and 5.25 kg/m ³ Na ₂ O _e 24 months (CPT) 6 months (ACPT)
		WT ²	WT ² + GW _C	
		RT	RT + PR _C	
		GW	GW _F + GW _C	
		AS	AS + GW _C	

Accelerated Mortar Bar Test (AMBT)

In this study, AMBT was carried out at three alkali content levels of 0.6, 0.8, and 1.0 M NaOH. These alkali levels were selected to evaluate the potential of using AMBT to assess alkali limits of aggregates. In addition to this, the capability of AMBT to detect the pessimum effect in the sand blends was also considered. During testing, the AS 1141.60.1 standard expansion limits of 0.1% at 10 days (0.15% for natural sands) and 0.3% at 21 days (Standards Australia 2014b) were applied for all AMBT

mixes, including those mixes aged at the modified AMBT test conditions of 0.6 M and 0.8 M NaOH, to assess the reactivity of the mortar bars. In addition to the samples identified in Table 4.2, AMBT was also carried out on aggregates AS and RT at the standard test condition of 1.0 M NaOH storage solution. These aggregates were assessed in CPT and ACPT; therefore, AMBT was done to screen the reactivity of the aggregates prior to concrete tests and to establish a correlation between AMBT and the CPT test method.

Concrete Prism Test at 38°C (CPT) and 60°C (ACPT)

For CPT and ACPT, the tests were conducted as per AS 1141.60.2, described in Section 3.2.1.2. However, the alkali content was varied at 2.5, 3.0, 3.5, 4.0 kg/m³ Na₂O_e to following the RILEM AAR-3.2 recommended approach for determining alkali limits (Section 3.2.2). The additional alkali content of 5.25 kg/m³ Na₂O_e accounts for the 1.25% Na₂O_e alkali content requirement of the AS 1141.60.2 CPT method. Concrete prisms investigated for the alkali limit studies were monitored for 24 months, whereas ACPT was carried out for 8 months. However, expansion results of 6 months ACPT have been discussed in this thesis.

Post-Expansion Characterization

Upon completing the expansion tests, petrographic assessment was carried out on the selected samples listed in Table 4.3. The rationality for the samples selected for petrographic analysis is also detailed in Table 4.3. Petrographic assessments of the expanded bars and prisms were performed as described in Section 3.3.4.1.

Table 4.3 Mortar bars and concrete prisms selected for post-expansion petrographic assessment

Sample ID	Test Method	Alkali content*	Rationale for sample selection
WT ¹	AMBT	1.0 M NaOH	Mortar bars are tested at the standard alkali conditions. Therefore, observed expansions represent the aggregates' reactivity based on benchmarked performance tests.
WT ²			
GW			
WT			
WT ¹	CPT	5.25 kg/m ³ Na ₂ O _e	Investigating the effect of temperature on the mechanism of ASR expansion.
	ACPT		
WT ²	CPT	2.5; 3.5, and 5.25 kg/m ³ Na ₂ O _e	(i) Investigate the effect of alkali on expansion. (ii) Examine the mitigation potential of the sand blend

4.3 Results and Discussion

4.3.1 Petrographic Assessment of Aggregates

The mineral constituents of the aggregates under investigation, obtained within a count of 100 widely spaced points during petrographic assessments, are tabulated in Table 4.4a and 4.5b. The specific mineral components in the aggregates that are perceived to have the potential for alkali-silica reaction (containing reactive forms of silica) in concrete are *italics and underlined* in the table.

In this study, particular interest was placed on the mineralogical makeup of aggregates WT and GW, which have been used in a sand blend, to understand the potential expansion behaviour of the sand blends and establish reactive minerals that initiate a pessimum effect.

Table 4.4 Mineralogical composition and reactivity classification of aggregates selected for investigating alkali limits, as determined by petrography

Aggregate WT: Quartzo-feldspathic		Aggregate GW: Fine meta-greywacke	
Mineral Constituents	Vol. %	Mineral Constituents	Vol. %
<i>Moderately strained free quartz grains, tridymite, and volcanic glass</i>	11	Feldspar as silt, sand, and finely crystalline grains	30.8
Feldspar grains (plagioclase and orthoclase)	42.8	Quartz as silt, sand, and finely crystalline grains; <i>10% is moderately strained</i>	18.8
Lithic clasts of acid volcanic rock	8.8	Finely microcrystalline feldspars and <i>quartz in acid volcanic clasts (estimated to contain 2.9% microcrystalline quartz in lithic greywacke clasts)</i>	8.3
Lithic clasts of intermediate volcanic rock	6.5	Finely microcrystalline feldspars in intermediate volcanic clasts	11.3
<i>Vesicular pumice and glassy fragments</i>	18.8	epidote	11.2
Smectite-illite altered clasts (liberated clays)	2.5	Other minerals (pyroxene, hornblende, opaque oxide, calcite, sphene/leucoxene	7.2
Other mineral grains (pyroxene, opaque oxide, hornblende, epidote fragments, and a trace of free biotite	8.8	Weak (clayey), possibly deleterious components (sericite, chlorite, biotite, limonite/goethite	11.6
Free silica	33	Free silica	22
ASR classification: Reactive		ASR classification: Slowly (mildly) reactive	

Table 4-4 continued...

Aggregate RT: Lithic sand		Aggregate PR: Olivine basalt	
Mineral Constituents	Vol %	Mineral Constituents	Vol %
Quartz as unstrained or mildly strained free grains	6.2	Pristine random to faintly aligned laths of plagioclase	42
<i>Moderately strained quartz as free grains</i>	5.2	Pyroxene (Pristine tubular crystals)	30
<i>Vein quartz fragments (heavily-strained quartz)</i>	2.0	Olivine (euhedral phenocrysts)	14
Feldspar grains (plagioclase and subordinate orthoclase)	14.3	Magnetite/ilmenite	9
Lithic clasts of indurated greywacke and siltstone	57.5	Iddingsite (alteration product of olivine)	2
Lithic clasts of acid volcanic rock (<i>finely microcrystalline quartz</i> and quartz phenocrysts)	5.5	Smectite/chlorite	2
<i>Lithic clasts of intermediate volcanic rock</i>	2.7	Iron Oxide (ferruginous staining associated with pre-existing rock features and trivial weathering)	1
Other mineral grains (biotite, each of opaque oxides, epidote and hornblende, and dolomite pyroxene)	6.6	Pyrite and voids	Trace
Free silica	28.4	Free silica	Nil
ASR classification: Slowly (mildly) reactive		ASR classification: Non-reactive	

Aggregate WT

The reactive mineral components of aggregate WT were identified by petrography as glassy fragments within the pumice fraction of the aggregate and mildly strained high-temperature beta-quartz in the form of tridymite and cristoballite. Although reactive glassy shards are contained within the pumice clasts, pumice is a relatively

soft volcanic rock. Therefore it can easily be dissolved in an alkaline solution, making the glassy shards available for ASR (Hasanah et al.). Tridymite and cristobalite are usually well-defined forms of silica that may be stable at normal temperatures. However, these quartz minerals have the potential to form ASR when disordered intergrowths occur, and have been described as opal (Diamond 1976), thus are capable of and creating deleterious ASR (Mitchell, Beaudoin & Grattan-Bellew 2004). From Table 4.4a, it can be estimated that approximately 16% of the sample was identified as lithic clasts comprising of acid volcanic rock of finely crystalline feldspar and quartz of glassy and spherulitic variants, all of which are known to show reactivity to alkali (Lu et al. 2006). Ultimately, the free silica content of aggregate WT was estimated at 33%. That said, a high free silica amount does not affirm the reactivity of an aggregate as the dissolution rate of the silica, which can be determined through chemical tests, is an essential factor in the formation of ASR. It is also worth noting that aggregate WT also showed high feldspar content, consisting of free feldspar grains of fresh zoned and finely twinned plagioclase and fresh orthoclase to 42.8%. The potential release of alkali from feldspar (Na-plagioclase) has been documented (Gillott & Rogers 1994; Stark & Bhatta 1986; Van Aardt & Visser 1977). In one study, it was suggested that aggregates could contribute up to $12.7 \text{ kg/m}^3 \text{ Na}_2\text{O}_e$ of alkali in concrete over a long period, and up to 0.7M alkali could be released in 18 months (Bérubé et al. 2002). The plane polarised transmitted light images of the aggregates WT and GW are shown in Figure 4.1.

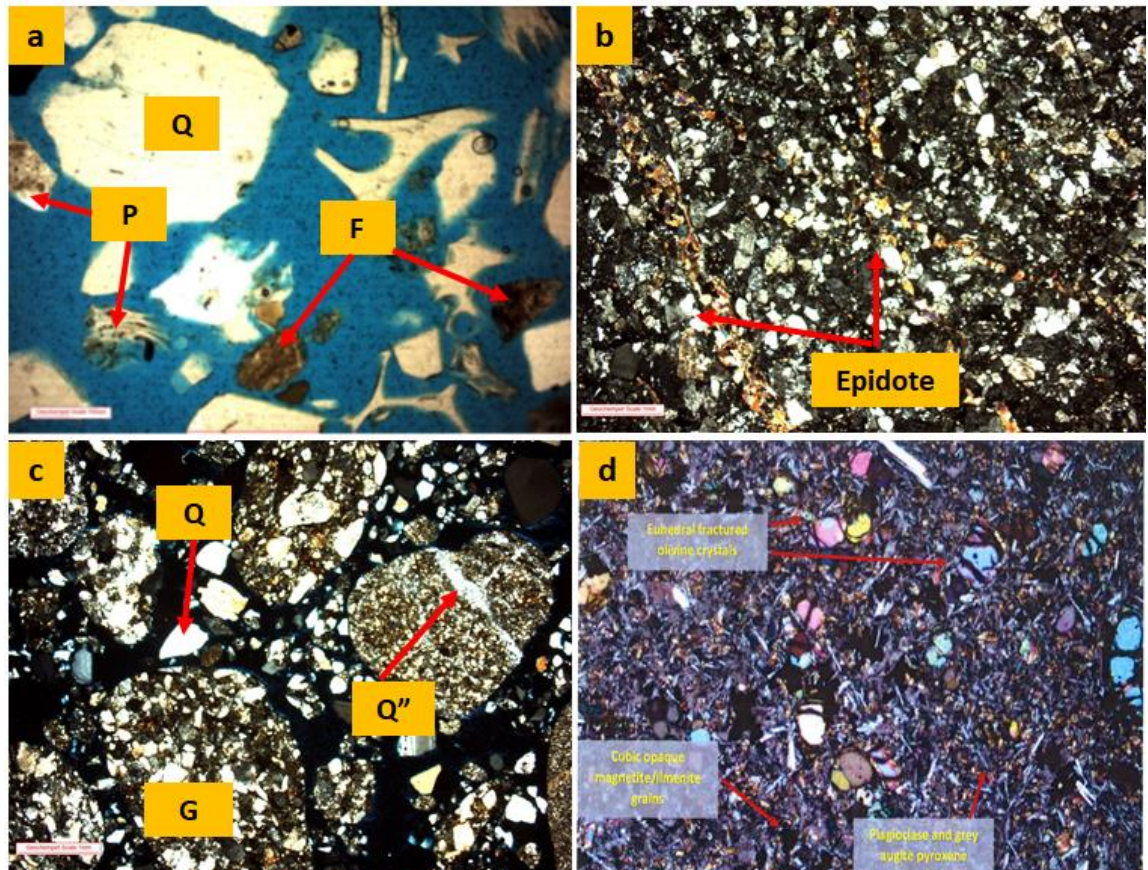


Figure 4.1 Plane polarised petrographic images of aggregate (a) aggregate WT, (b) GW, (c) RT, and (d) PR. Note: Q= Quartz; Q''= Quartz veining through aggregate particle; F= Feldspar; G= Indurated greywacke in aggregate RT (notice the resemblance to aggregate GW); P= Pumice, and epidote vein cutting across the meta-greywacke fragment of aggregate GW

Aggregate GW

The petrographic features of the aggregate GW were typical of a lithic fine-greywacke type rock, crushed from an indurated meta-greywacke parent rock. The lithic fragments in aggregate GW were composed of intermediate volcanic rock of partly epidotized and chloritized andesite, showing the presence of epidote veins (12-16%) cutting across through the aggregate clasts. This observation is usually common in metamorphic rocks (Fernandes et al. 2013). Mild to moderately strained quartz and sericitized acid volcanics that have devitrified into fine microcrystalline

feldspars and quartz were present. These minerals all indicate the potential ASR of aggregate GW, as shown in Table 2.4. However, the recurrence of these mineral phases was relatively low. From the estimated 22% free silica, 10% was found to be moderately strained finely crystalline, and 3% microcrystalline quartz was recognized. This is almost comparable to the amounts found in the reactive aggregate WT. A similar observation was also made for the amount of feldspar in these two aggregates (Table 4.4a). However, the reactive silica forms in GW were found to be within the greywacke clasts and thus may not be readily available to take part in ASR. Furthermore, the reactivity potential of the reactive mineral tridymite in aggregate WT is considered to be similar to opal thus can cause greater deleterious ASR than GW. For this reason, Aggregate GW can be characterized as slowly reactive.

4.3.2 Chemical Tests

Dissolution Test

The results from the dissolution test are presented in Figure 4.2. Under the reactivity classification by ASTM C289, aggregates WT and RT are concluded to be deleterious, releasing 124.9 mmol/L and 146.2 mmol/L of dissolved silica in solution, respectively. The amount of silica dissolved in solution from aggregate GW was found to be 29.1 mmol/L. This places aggregate GW in the category of aggregates considered innocuous.

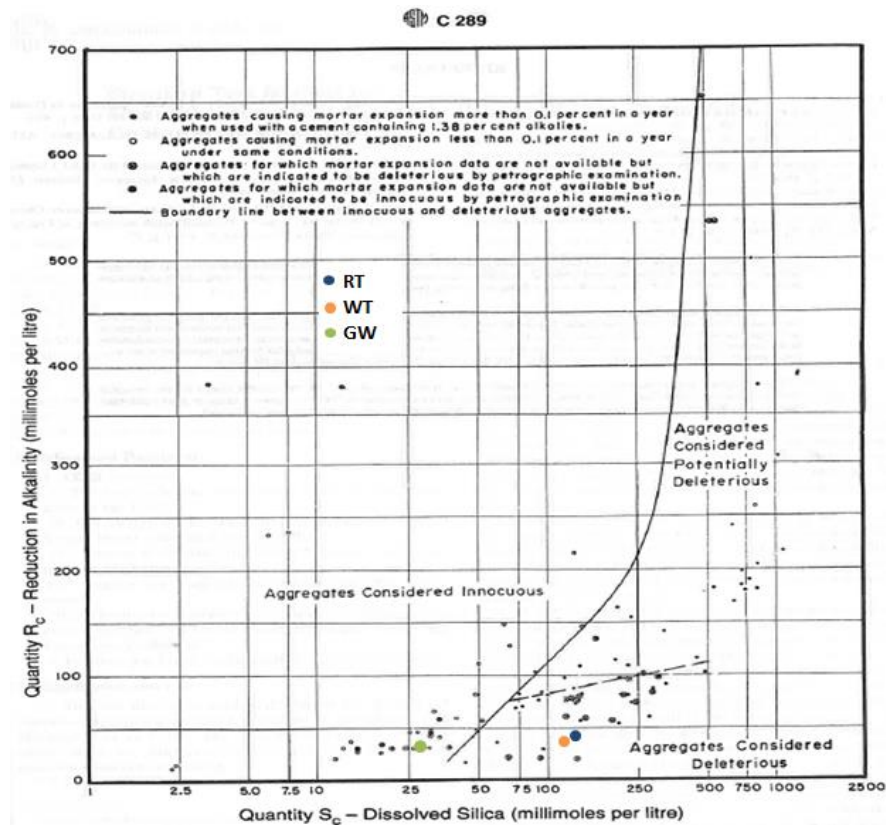


Figure 4.2 Classification of aggregates according to the dissolution test (as per ASTM C289)

Additionally, the amount of alkali bound in the silica grains indicated as a reduction in alkalinity of the solution was also measured. Aggregates WT and RT showed similar amounts of bound alkali, resulting in a 40.1 and 44.1 mmol/L alkali reduction, respectively. These results are consistent as both aggregates released comparable amounts of silica in solution. However, aggregate GW; which showed a much lower amount of silica dissolved into solution, consumed a similar amount of alkali, indicating 40.1 mmol/L of alkali reduction. From literature, it has been reported that this method is unreliable in identifying the reactivity of aggregates that contain alkali minerals because the evaluation of alkali fixation being inaccurate (Chatterji 2005). From the petrographic result discussed in Section 4.3.1, aggregates WT and

GW contain similar percentages of feldspar; 43.2% and 47.9%, respectively, in the form of plagioclase (Na-feldspar) and orthoclase (K-feldspar). Assuming this alkali is also released into solution during the test, an incorrect indication of the alkali reduction by the aggregates could result. Additionally, other ions such as calcium and magnesium that are released into the test solution from the aggregate could provide an incorrect indication of dissolved silica and, more often, the solution's alkalinity (Owsiak 2007). For this reason, a reactivity limit for the amount of silica of 100 mmol/L has been suggested (Bérubé & Fournier 1993).

For aggregate AS, the results from the dissolution test have been taken from literature. Black (Black 2009) reported the dissolution tests on three different rock types, including aggregate AS used in this study (Freitag 2003). Various samples of the same aggregate collected from different locations were tested to establish reproducibility in the test results as well as consistency in the reactivity classification. The results of the different samples for aggregate AS are illustrated in Figure 4.3.

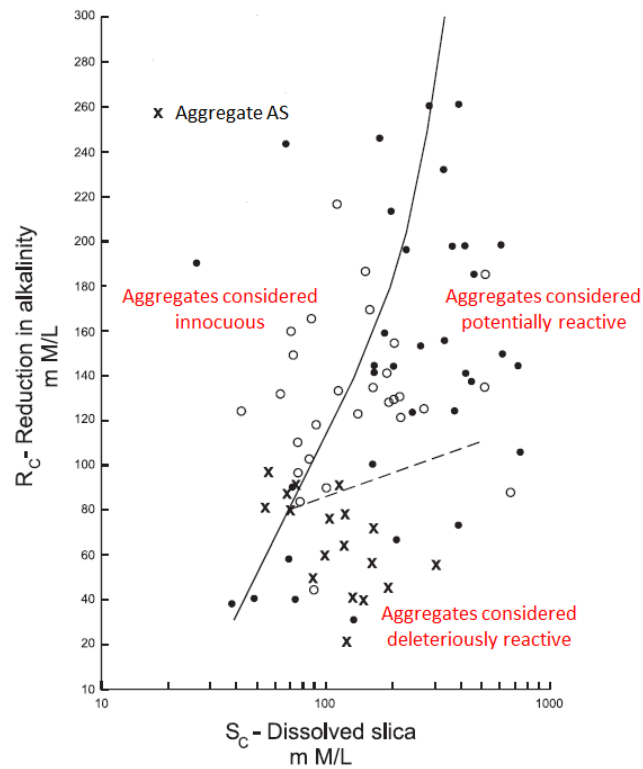


Figure 4.3 Compiled dissolution test from (Freitag 2003) for aggregate AS (x). Modified from (Black 2009)

Aggregate AS (represented by 'x') is observed to fall under the category of aggregates considered deleteriously reactive. A consistent reproducibility of the aggregates' reactivity was observed, as illustrated by the cluster of points in the designated region. It is worth noting that some samples tested in the innocuous region of the graph. Aggregate AS has been described as a volcanic andesite type rock bearing large amounts of glass as the principal constituent in this aggregate (Mackechnie 2003). The glass in the aggregate serves as a reservoir for Na; thus, high amounts of Na are usually bound within the amorphous regions of these aggregates. Therefore, as the silica is dissolved into the test solution, sodium is also released. This could cause an increase in the solution's alkalinity, consequently

affecting the alkali fixation in the aggregate grains and, in turn, the overall reduction in alkalinity recorded.

Ground Aggregate Slurry Test

Following the GAST chemical method described in Section 3.3.3.3, TGA analysis was conducted on the solids to provide information on the aggregates' reactivity based on the pozzolanic behaviour exhibited. Figure 4.4 shows the TG-DTG curve for the aggregates studied after 28 days of GAST.

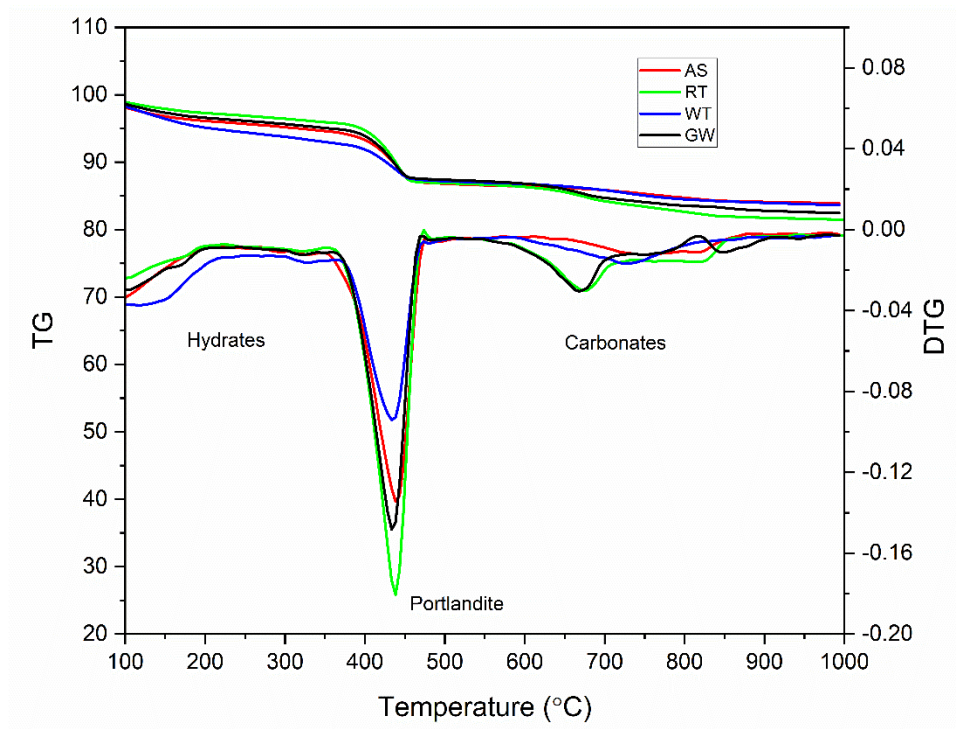


Figure 4.4 TG-DTG results of 28 days GAST test on aggregates

The samples were measured twice to produce the results presented in Figure 4.4. Considering the portlandite decomposition curve from 350 to 480°C, the amount of residual portlandite in the respective samples can be determined by evaluating the

area under the portlandite curve. Consequently, from Figure 4.4, it can be seen that the aggregate WT exhibited the highest pozzolanic behaviour by consuming the most portlandite. This infers that of the aggregates studied, aggregate WT is the most reactive. Conversely, the reactivity of the remaining aggregates can be ranked based on the amount of portlandite consumed as; AS>GW>RT. These results are inconsistent with the ASTM C 289 test results and may be due to a number of reasons, including the stabilization of calcium phases at the high testing temperature, thus reducing the availability of calcium to react in the pozzolanic reaction. Additionally, the potential release of other ions such as Al can inter with the results obtained. As the GAST is still an emerging technique, several tests need to be carried out to benchmark this method and overcome the limitations of its use. Nonetheless, the consistency in the two measurement results suggests that this test method has appreciable reproducibility and may yet present a promising approach for rapid testing of potential reactivity in aggregates

4.3.3 Expansion Tests

The AMBT, CPT, and ACPT expansion measurements shown in Section 4.3.3 are tabulated in Appendix B: Tables B0, B2, and B3.

4.3.3.1 Accelerated Mortar Bar Test (AMBT)

The AMBT expansion results as a function of age up to 28 days at the three alkali test environments are shown in Figure 4.5. By applying the standard AMBT expansion

limit of 0.1% (0.15% for natural sand) at 10 days and 0.3% at 21 days (Standards Australia 2014b) for all alkali environments, the following observations were made.

Aggregate WT and its subsequent sand blends, WT¹ and WT², showed expansion exceeding the prescribed expansion limits for all alkali environments studied. On this basis, aggregate WT, WT¹, and WT² can be classified as reactive at 0.6, 0.8, and 1.0M NaOH alkali concentrations. It is also evident that the reactivity of the sand blends is dominated by the reactivity of aggregate WT, resulting in higher expansion observed.

The AMBT results also show that at 0.6M NaOH concentration, aggregate GW_F exhibited an expansion of 0.005% after 10 days. Subsequently, an expansion of 0.018% was measured for these mortar bars after 21 days. This expansion behaviour is indicative of a non-reactive aggregate as per AS 1141.60.1. However, the reactivity potential of GW_F was seen to increase with increasing alkali concentration. Such that the mortar bars expanded up to 0.105% in 0.8 M and 0.200% in 1.0 M NaOH, thus classifying GW_F as slowly reactive. This increase in expansion with increasing alkali was not observed for the rest of the aggregates tested. In particular, although the expansion limits at 10 and 21 days were exceeded, mortar bars containing aggregate WT showed relatively lower expansions of 0.368% after 21 at 0.8M NaOH relative to the 0.520% recorded at 0.6M NaOH.

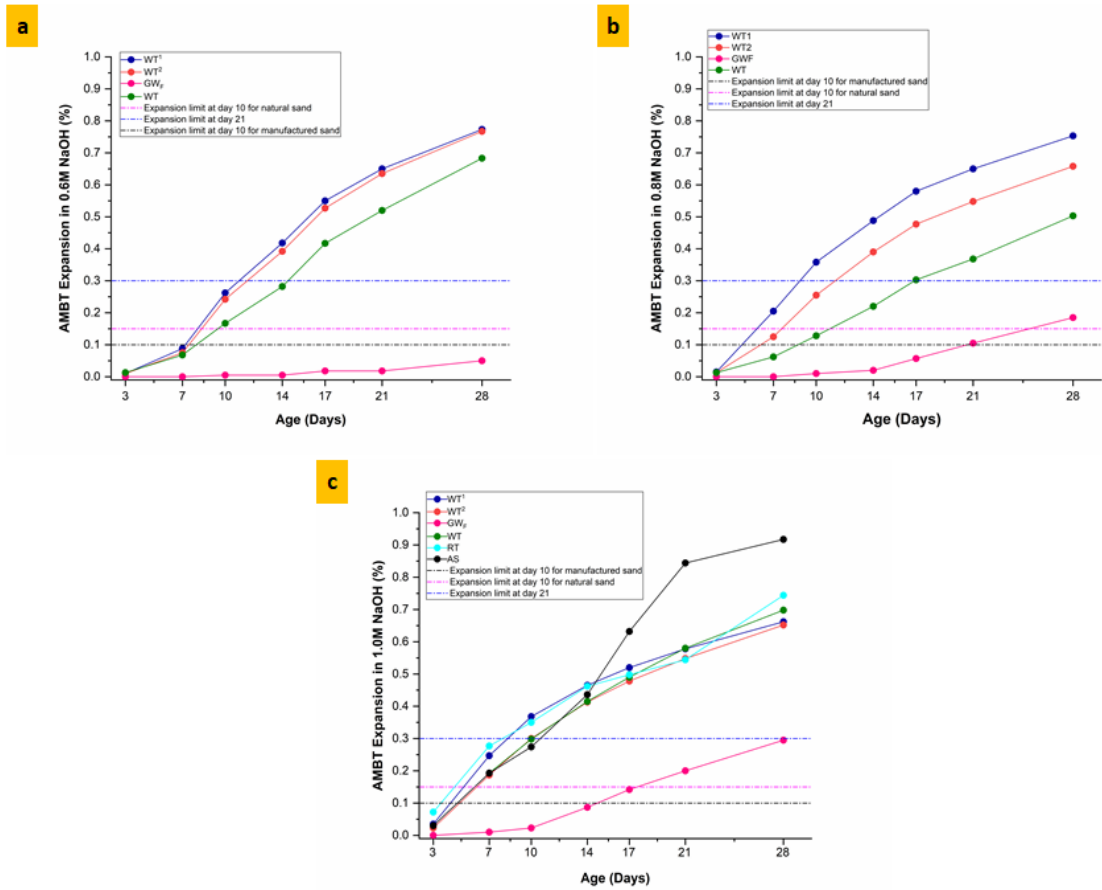


Figure 4.5 AMBT expansion results for aggregates at (a) 0.6 M, (b) 0.8 M and (c) 1.0 M NaOH alkali concentration

Furthermore, mortar bars containing WT show similar expansion behaviours at 1.0 M NaOH and 0.6M NaOH, with an expansion of 0.580 % recorded at 1.0 M concentration. This finding suggests that as a function of increasing alkali concentration, although the AMBT method can differentiate reactive from non-reactive aggregates (reactivity potential), this method appears to be limited in appropriately identifying the reactivity levels of aggregates. This is likely the consequence of the oversupply of temperature and alkali used in AMBT.

At the standard test condition of 1.0 M NaOH (Figure 4.4c), except for GW_F, all the aggregates expanded equally and above the 10 and 21-day expansion limits

classifying the aggregates as reactive. Particularly, aggregate RT showed an expansion of 0.35% after 10 days and 0.54% after 21 days. In contrast, GW_F classified as slowly reactive, exhibited expansion values of 0.02% and 0.2% after 10 and 21 days, respectively.

It is also clear from Figure 4.4c that AMBT successfully identified the slowly reactive aggregate GWF and the highly reactive aggregate AS. However, the test method showed expansion curves that implied that aggregates WT¹, WT², RT, and WT exhibit the same reactivity. This is a typical example of AMBT's limitation in identifying reactivity levels of aggregates. Thus this test method will be challenging to employ as the method for assessing alkali reactivity. It is also worth noting that at all the AMBT alkali concentrations studied, the reactivity of the sand blends was higher than the reactive sand WT.

Another aggregate classification index that is reliant on AMBT expansion measurements is ASTM C1778 (ASTM 2016). The ASTM C1778 guide categorizes aggregate reactivity into four classes based on the level of expansion recorded for the aggregates after 14 days of AMBT following ASTM C1260, similar to the AS 1141.60.1 test method used in this study. The limits set for determining the reactivity potential of aggregate by this standard are shown in Table 4.5. The ASTM 1778 reactivity classification index was introduced in this study as a complementary method to resolve any inconsistencies in the expansion results.

Table 4.5 ASTM C1778 Classification of Aggregate Reactivity

Aggregate Reactivity Class	Description of Aggregate Reactivity	1-Year Expansion in Test Method ASTM C1293 %	14-Day Expansion in Test Method ASTM C1260, %
R0	Non-reactive	<0.04	<0.10
R1	Moderately reactive	≥0.04, <0.12	≥0.10, <0.30
R2	Highly reactive	≥0.12, <0.24	≥0.30, <0.45
R3	Very highly reactive	≥0.24	≥0.45

From Figure 4.15c, the expansion recorded for WT, WT¹, WT², GW_F, AS and RT at 14 days was 0.415%, 0.465%, 0.413%, 0.087%, 0.438% and 0.462%, respectively. Based on ASTM C1778 reactivity classification, GW_F sand can be classified under the R0 class of non-reactive aggregates with an expansion of 0.087%. Aggregate WT and WT² showed expansion behaviour that is characteristic of the R2 class of highly reactive aggregates, while WT¹, RT, and AS exhibited expansion that exceeds the 0.45% limit for very highly reactive aggregates.

4.3.3.2 Concrete Prism Test (CPT)

The 12-month CPT expansion data captured for the aggregates assessed at the standard alkali concentration of 5.25 kg/m³ Na₂O_e is displayed in Figure 4.6.

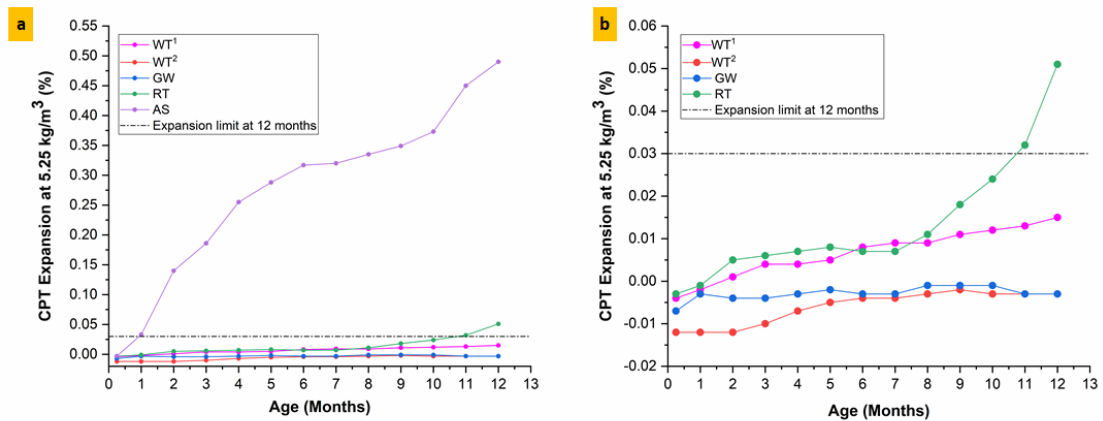


Figure 4.6 12 months CPT expansion results for the selected aggregates (a) including aggregate AS and (b) excluding aggregate AS at 38°C and 5.25 kg/m³ Na₂O_e alkali content. *Note: Initial expansion (Day 0/Month 0) is 0.00%. Graphs represent expansion measurements from Day 7 (Month 0.25)*

Sample AS (Figure 4.6a) showed significant expansion during CPT, such that the expansion limit of 0.03% was reached after one month of CPT. The graph in Figure 4.6b was plotted without aggregate AS to show a more apparent expansion behaviour of the aggregates. From Figure 4.6b, it can be seen that concrete prisms containing GW aggregates (WT² and GW) expanded similarly up to 12 months of testing. These prisms exhibited negligible expansion after 12 months of CPT and consequently can be designated as non-reactive. On the other hand, aggregates WT¹ and RT expanded equally up to 7 months. Thereafter, rapid increases in expansion were recorded for RT while WT¹ slowly expanded towards the end of the test. The similarity in the expansion behaviour of these aggregates was also observed during the 1.0 M NaOH AMBT test (Figure 4.5c). However, the CPT method identifies and distinguishes the extent of reaction of the aggregates. At the end of the 12-months test duration, aggregate WT¹, WT², and GW showed expansion that is categorized as

non-reactive under AS 1141.60.2. However, concrete prisms composed of RT expanded to 0.05%, thus informing that aggregate RT is potentially reactive. This outcome elucidates the reliability claim of CPT in suitably identifying the reactivity potential of aggregates and the reactivity levels (extent) of the aggregates.

Moreover, the findings from the CPT studies illuminate that the AMBT test may not be an effective method to investigate the effects of sand blends in mitigating ASR and further identifying potential pessimum effects that may occur in the use of sand blends. Additionally, the CPT test results propose that the potential exists to reduce the risk of ASR by incorporating sand blends. However, it is noted that in this study, the prospective sand blend WT² is partly composed of a slowly reactive aggregate. Indeed, the CPT method has been reported as unsuitable for testing slowly reactive aggregates due to the relatively low accelerated temperature test condition, unless the test duration is extended (Nixon & Sims 2016b). This recommendation was drawn from experiences where aggregates thought to have been non-reactive showed signs of deleterious ASR in field structures after some time (Owsiak 2007; Shayan & Morris 2000). As such, further testing up to 24 months has been carried out, and the outcomes will be discussed in Section 4.3.4.1.

Suppose the ASTM C1778 classification guide is considered (Table 4.5), AS with an expansion of 0.490% after 12 months is regarded as very highly reactive. In contrast, RT is categorized as highly reactive with an expansion of 0.05% after 12 months. In contrast, WT¹ showed a low expansion of 0.105%, and negligible expansions (-0.03%) were recorded for WT² and GW. Therefore classifying these aggregates as non-reactive.

4.3.3.3 Accelerated Concrete Prism Test (ACPT)

As discussed in Section 2.7.1.4, at present, there are different recommendations on the appropriate acceptance age and limit used for assessing aggregate reactivity and classification in ACPT. This knowledge gap will be explored in-depth in Chapter five. However, for this section of the study, The reactivity classification of the aggregates assessed under ACPT conditions was interpreted using the CPT expansion limit of 0.03% after 3 months of ACPT to correlate to the standard CPT at 12 months (Thomas et al. 2006). A similar recommendation has also been made by RILEM (Nixon & Sims 2016d). The expansion at 5 months of ACPT will also be considered to assess slowly reactive aggregates and to estimate reactivity prediction for the longer test CPT test at 24 months.

The ACPT expansion results up to 6 months of testing at $5.25 \text{ kg/m}^3 \text{ Na}_2\text{O}_e$ are presented in Figure 4.7. Generally, similar behaviour in expansion was observed in ACPT and CPT. It was observed that by applying the 0.03% CPT expansion limit after 3 months of ACPT, aggregates that were identified as non-reactive in CPT also satisfy the criteria in ACPT. Again, aggregate AS demonstrated an expansion of 0.359% above the limit at the early age of 7 days, whereas the other test aggregates expanded below 0.03% after 3 months of the ACPT test. However, at 4 months, the WT¹ and RT recorded a similar expansion measurement of 0.03%, equal to the expansion limit, thus exhibiting potentially reactive behaviour. Furthermore, for aggregate WT², which is a sand blend partly composed of the slowly reactive aggregate GW_F that showed a non-reactive behaviour in CPT, also measured an expansion of 0.013% when the CPT expansion limit was applied after 5 months of

ACPT (Lindgård et al. 2010). These results agree with the CPT finding and provide evidence to support the potential use of sand blends for ASR mitigation.

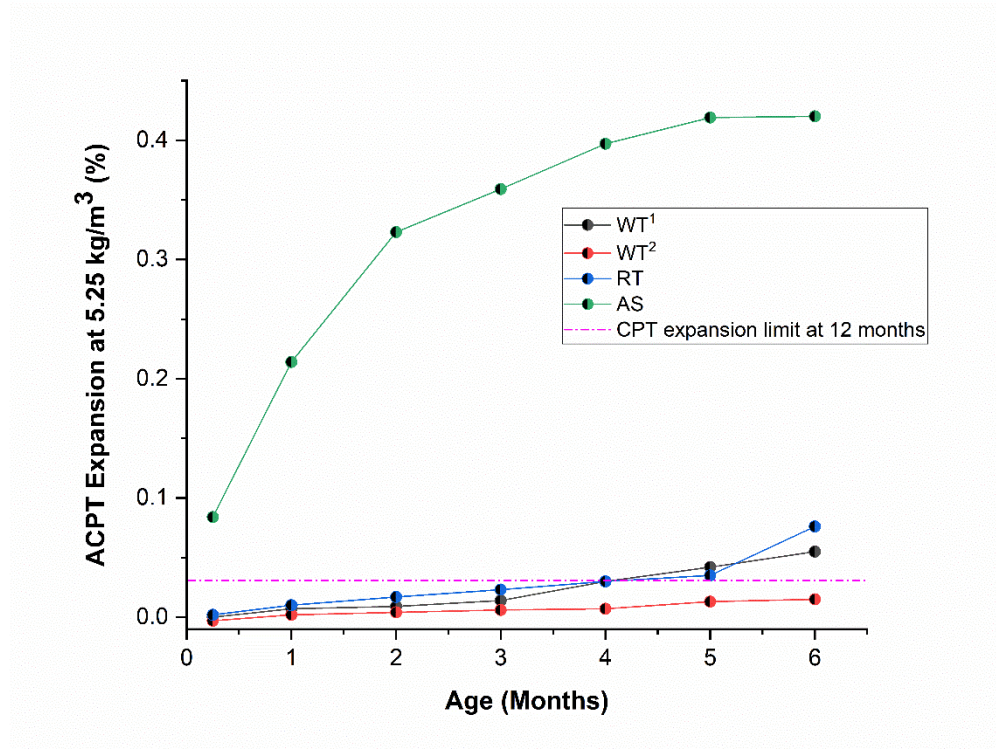


Figure 4.7 6 months ACPT expansion results for aggregates at 60°C and 5.25 kg/m³ Na₂O_e alkali content. *Note: Initial expansion (Day 0/Month 0) is 0.00%. Graphs represent expansion measurements from Day 7 (Month 0.25)*

4.3.3.4 Potential Correlation between Test Methods

The findings from this part of the study have shown a good correlation between the reactivity classification petrographic reactivity classification, the ASTM C289 (currently withdrawn), and the physical expansion tests. This observation will be scrutinized further in the subsequent chapter (Chapter five). In particular, apart from aggregate RT, which was identified as having the potential of mild to slow ASR in petrography yet showed expansion characterized as reactive in AMBT, the

reactivity classification of all other single aggregates via petrography and AMBT was consistent. Additionally, aggregate classification resulting from the dissolution test was comparable to the AMBT classification. For the expansion tests, a variation in the AMBT and concrete prism tests (at 38°C and 60°C) is observed. It is notable, though, that aggregates that passed the conservative AMBT test are non-reactive in CPT and ACPT. Additionally, although there seems to be a correlation between CPT and ACPT results, aligning the appropriate age at which ACPT compares with CPT is essential for corroborative reactivity classification. Ultimately, the outcome deduced from the various results establishes that the recommended practice of assessing the reactivity of aggregates using a suite of test methods (Nixon & Sims 2016b) is essential for the correct classification of aggregates' ASR potential.

4.3.4 Determination of Alkali Limits

The expansion measured after 12 months of CPT for the varying alkali concentrations studied has been assessed to identify the alkali limit, that is, the highest alkali content at which there is no deleterious expansion (Nixon & Sims 2016b). Other studies describe the alkali limit as the alkali content at which the initiation of expansion due to ASR may become evident (Hester, McNally & Richardson 2005; Lindgård et al. 2012). Both interpretations of alkali limits can be argued in the case that one considers the critical alkali limit (Nixon & Sims 2016b), whereas the other evaluates the expansions that are expected to become deleterious with age.

In Figure 4.8, the expansion results of the aggregates after 12 months of CPT, at the 5 alkali contents investigated, are shown. Again, the high reactivity behaviour of aggregate AS is observed with a 0.026% expansion recorded at 2.5 kg/m³ Na₂O_e alkali content. In considering the critical alkali limit of 0.03% at 12 months, AS measured an expansion of 0.044% at the alkali content of 3.0 kg/m³. Therefore, for this aggregate, the highest alkali content at which there is no deleterious expansion is 2.5 kg/m³ Na₂O_e. By applying the recommended safety margin of 1.0 kg/m³ Na₂O_e (Nixon & Sims 2016a), the alkali limit of 1.5 kg/m³ Na₂O_e can be suggested. This is lower than the current alkali limits set for concretes in New Zealand and Australia (2.5 and 2.8 kg/m³ Na₂O_e, respectively), relating to the 0.6% Na₂O_e alkali limit in cement. This outcome justifies the conservatively low alkali limit allowed in New Zealand and Australia and suggests that for concretes containing aggregate AS, the use of a lower alkali content cement and a selection of preventive measures to reduce ASR risk is essential (Freitag & Mackechnie 2018). It might also be worth considering the use of AS-based sand blends to minimize the ASR impact of aggregate AS, as this approach has shown some promising outcomes in this study.

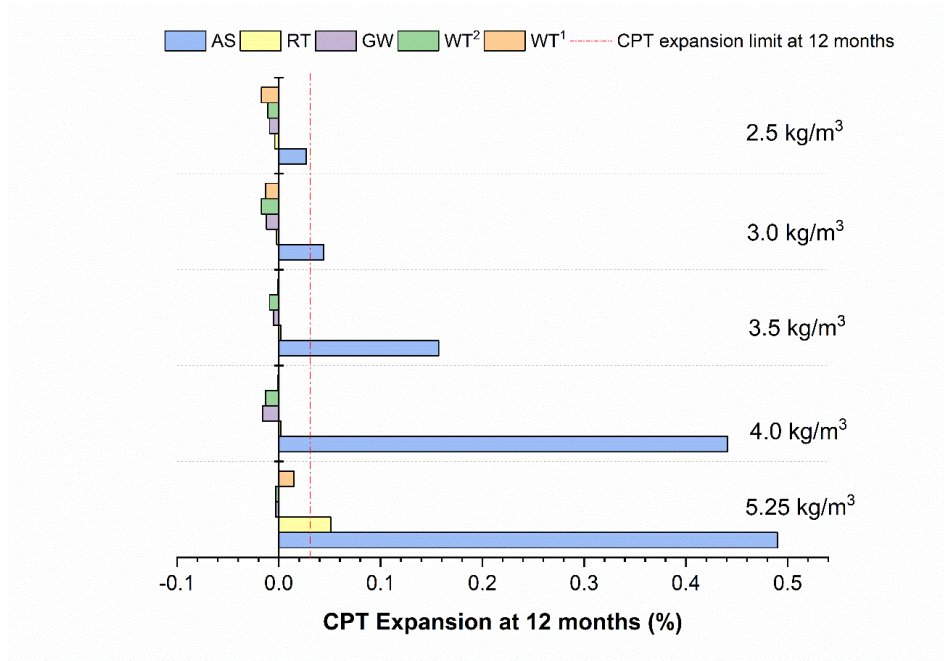


Figure 4.8 12-month CPT expansion of aggregates at varying alkali content (Na_2O_e)

Aggregates GW and WT² did not show any positive length change up to the alkali content of 5.25 kg/m³. For aggregates WT¹ and RT, the respective initial expansions of 0.015% and 0.051% were recorded at 5.25 kg/m³. This expansion measurement is considered critical for aggregate RT as it exceeds the CPT expansion limit of 0.03%. Thus, the alkali threshold for aggregate RT can be identified as 4.0 kg/m³. Consequently, a proposed alkali limit of 3.0 kg/m³ may be applied. From Figure 4.7, it can be visualized that assuming this new alkali limit (3.0 kg/m³) may yet be safe for all the aggregates studied, with the exception of aggregate AS, which appears to be a particular case.

4.3.4.1 Determination of Alkali Limits at 24 Months

The CPT test duration was extended to 24 months to accurately assess the reactivity of these aggregates- especially aggregate GW and WT², which exhibit a slowly reactive behaviour. In the case of WT², the 24-month expansion behaviour is particularly essential as the use of a sand blend is being assessed as a potential ASR mitigation approach. The 24-month CPT expansion results for the aggregates studied at varying alkali contents, except for aggregate AS whose expansion has already been classified, are illustrated in Figure 4.9.

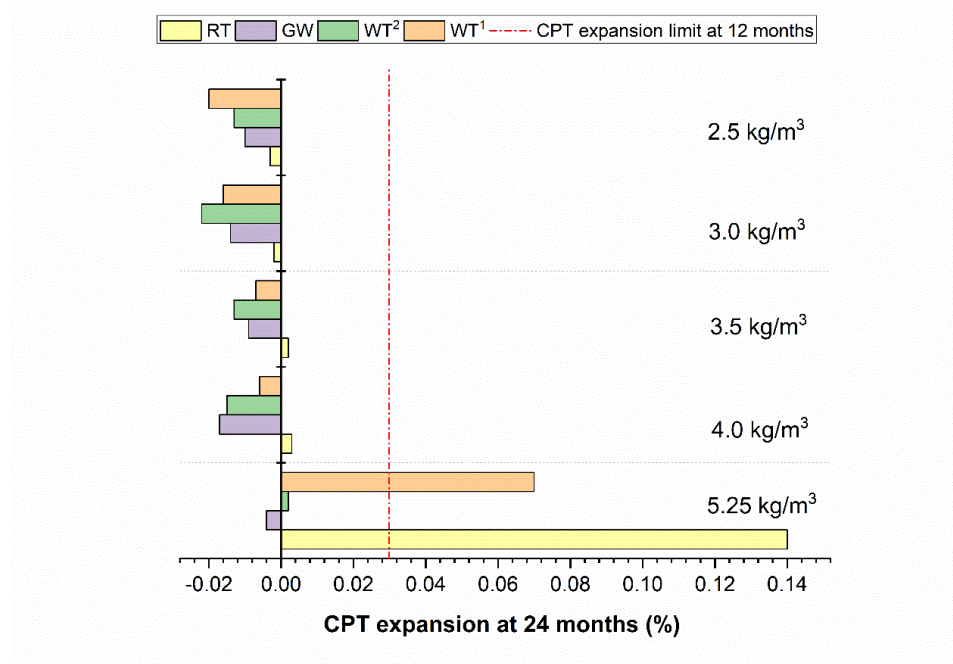


Figure 4.9 24-month CPT expansion of aggregates at varying alkali content (Na_2O_e)

After 24 months, aggregate RT showed an initial expansion of 0.002% at the alkali content of 3.5 kg/m³. After that, a consistent increase in expansion with alkali content was observed for aggregate RT up to 5.25 kg/m³, where a ‘deleterious’

expansion of 0.140% was measured. Similarly, aggregate WT¹ also exhibited an expansion of 0.07% at 5.25 kg/m³. Aggregates GW, WT¹, and WT² still did not measure any positive change in length after 24 months for all alkali contents up to and including 4.0 kg/m³. However, at 5.25 kg/m³, a minimal expansion of 0.002% was recorded of WT². It is also worth mentioning that after 24 months, there is still no critical expansion at 4.0 kg/m³ Na₂O_e for aggregates RT and WT¹. This supports that the proposed alkali limit of 3.0 kg/m³ Na₂O_e could be suitable for these aggregates.

The RILEM AAR-7.1 also recommends appropriate alkali limits for aggregates that have been classified as per the RILEM AAR-3.2 reactivity levels described in Table 3.6. The RILEM suggested alkali limits are expressed in Table 4.6 and agree with the alkali limits proposed for the aggregates in this work. However, where aggregate WT² is concerned, no expansion was observed for up to 24 months of CPT. Still, these aggregates showed high reactivity in AMBT, as they contain aggregate WT, which has been classified as having the potential for ASR in concrete (Section 4.3.1). Although the AMBT results of WT² can be attributed to the aggressive nature of the test compared to CPT, the long-term ASR potential of WT² (as a sand blend) in field structures is unknown. Therefore, although the RILEM AAR-3.2 categorization for this aggregate is low; thus requiring no alkali limit, an alkali limit is advisable. Therefore, based on the results obtained in this work, the alkali limit of 3.0-3.5 kg/m³ Na₂O_e is suggested for aggregates GW and WT².

Table 4.6 RILEM AAR-3.2 reactivity categories and recommended alkali limits as per RILEM AAR-7.1

Category	Description	Recommended Alkali Limit (kg/m ³ Na ₂ O _e)
Low	Aggregates that show no significant reaction from classification and expansion tests performed in accordance with petrographic assessment, AMBT, and CPT standards.	None required
Medium	Aggregates that show an alkali threshold higher than 4.0 kg/m ³ alkali content,	3.0 - 3.5
High	Aggregates with low alkali threshold, typically below 4.0 kg/m ³ alkali content.	2.5 - 3.0

Based on the results obtained and the reactivity classifications under AS 11 41.60.1, AS 1141.60.2, and RILEM AAR-3.2, a summary of the proposed alkali limits for the aggregates investigated are given in Table 4.7.

Table 4.7 Summary of aggregate reactivity classifications based on various expansion tests and suggested alkali limits

Aggregates	Reactivity Classification			
	AMBT (AS 1141.60.1)	12 months CPT (AS 1141.60.2)	RILEM AAR-3.2	Proposed alkali limit (based on RILEM AAR-7.1)
WT ¹	Reactive	Non-reactive	Medium	3.0-3.5
WT ²	Reactive	Non-reactive	Medium	3.0-3.5
AS	N/A	Reactive	High	2.5-3.0
R	Reactive	Reactive	Medium	3.0-3.5
GW	Slowly-reactive	Non-reactive	Low	3.0-3.5

4.3.4.2 Minimizing the risk of ASR using sand blends (WT¹ and WT²)

From the CPT expansion results at 12 months (Figure 4.5) and considering the expansion data after 24 months at the alkali content of 5.25 kg/m³ (Figure 4.8), it can be observed that aggregate WT² which did not show any positive length change after 12 months expanded marginally at 0.002% after 24 months. Contrarily, WT¹, which showed an expansion of 0.015% after 12 months, continued to expand until a percentage length change of 0.07% was measured after 24 months. This outcome clarifies the recommendation for extending the CPT test method to capture the longer-term effect of concrete mixes for ASR mitigation purposes. But more relatedly, the results support that an appropriate combination of aggregates to form sand blends can be an effective mitigation strategy against ASR.

4.3.5 Petrographic Analysis of Mortar and Concrete Samples

The expanded mortar bars and concrete prisms for petrographic analysis were selected for the reasons described in Table 4.3. Petrographic analysis was carried out after 12 months of CPT and 8 months of ACPT.

4.3.5.1 Mortar Bars

The polished and dyed cut-off block of mortar bars showed the presence of fine porosity and micro-cracks thought to have resulted from ASR gel expansion. Generally, all mortar bars displayed the presence of an isotropic hydrated gel, similar to the chemistry of ASR gel. The cement pastes also showed open micro-fractures, which appear to have once been filled by ASR gel that was removed during

thin section preparation of the specimens. The reactive components that were identified to have cause ASR in the mortar bars are listed in Table 4.7.

In particular, mortar bars WT showed internal cracking in quartz and feldspar grains. These cracks were found to emanate from or pass through affected minerals, identified as glassy shards from pumice fragments, acid volcanics, and beta form quartz (tridymite and cristobalite). The evidence of reactivity seen for tridymite indeed suggests that the forms of tridymite present in aggregate WT are disordered forms; thought to be potential opal fragments(Diamond 1976), thus making them highly susceptible to ASR.

Table 4.8 ASR causative minerals in the respective aggregates and their mortar bars

WT		GW _F	
Minerals in aggregate suspected to cause ASR	Mineral perceived to have caused ASR in the mortar	Minerals in aggregate suspected to cause ASR	Mineral perceived to have caused ASR in the mortar
Moderately strained free quartz grains; tridymite volcanic glass; vesicular pumice; glassy fragments	Acid volcanics; Glassy shards	Moderately strained quartz; quartz in acid volcanic clasts; microcrystalline quartz in lithic greywacke clasts	Acid volcanics; Greywacke clasts
WT ¹		WT ²	
Minerals in aggregate suspected to cause ASR	Mineral perceived to have caused ASR in the mortar	Minerals in aggregate suspected to cause ASR	Mineral perceived to have caused ASR in the mortar
Moderately strained free quartz grains; tridymite volcanic glass; vesicular pumice; glassy fragments	Acid volcanics; Glassy shards	Moderately strained quartz; quartz in acid volcanic clasts; microcrystalline quartz in lithic greywacke clasts; tridymite; volcanic glass; vesicular pumice; glassy fragments	Glassy shards; acid volcanics; Greywacke clasts

From the petrographic assessment, the aggregate components that are perceived to have caused ASR in WT are glassy chards and acid volcanics. These causative minerals can be seen in Figure 4.10 to show internal cracking and porosity resulting

from the depletion of silica. This observation is common for reactive silica and confirms that silica is released from aggregates into the pore solution to form part of the ASR gel (Leemann et al. 2016).

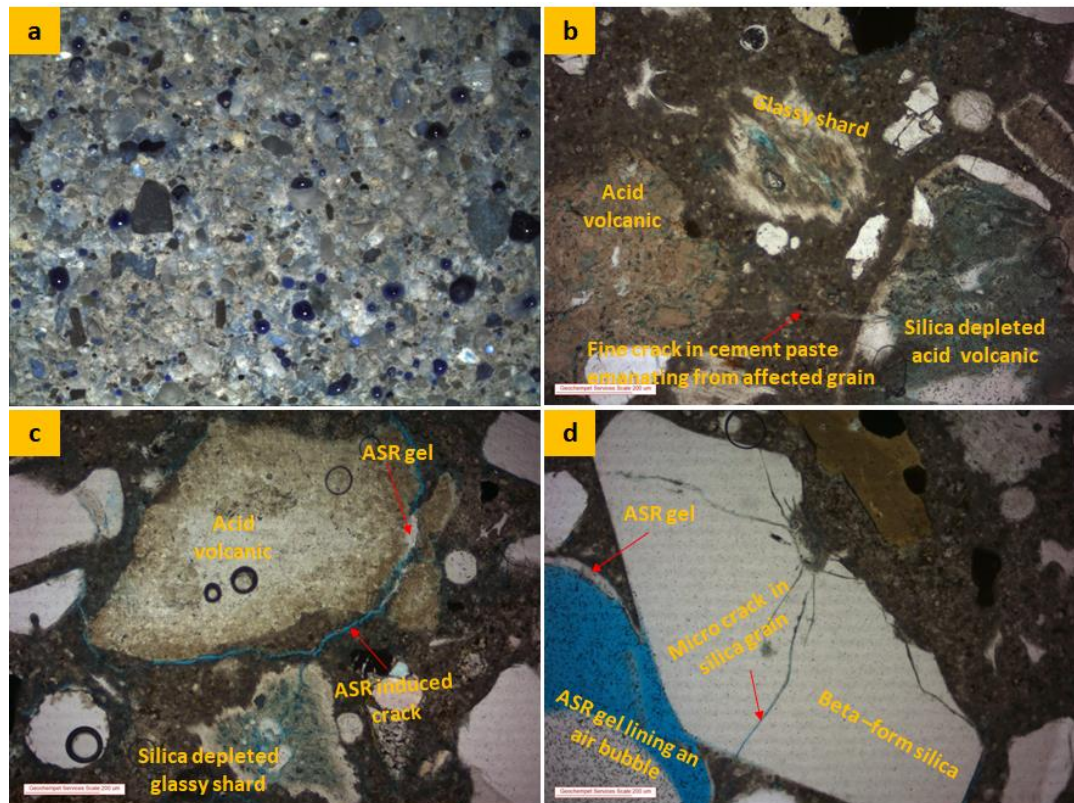


Figure 4.10 Petrographic images of mortar bar WT showing (a) photograph of cut-off dyed block surface (*image width= approx. 20mm*), (b) fine crack joining two acid volcanic fragments and showing porosity in a glassy shard and acid volcanics, (c) ASR induced open crack passing through an acid volcanic and porous depleted glassy shard, as well as through quartz grains and (d) ASR gel lining an air bubble leading from micro-cracks within a beta-form quartz grain (*Note: SCALE= 200 μ m*)

Whereas the initial assessment of aggregate WT predicted the potential for substantial ASR and subsequent AMBT showed expansion characteristics of a reactive aggregate, the feature observed here shows a relatively mild degree of ASR. Usually, aggregates containing reactive silica such as tridymite and cristobalite show a threshold effect. Thus, the ASR performance of such aggregates is dependent on the equilibrium being reached between the alkali concentration of a pore solution and the reactivity of the aggregate (Kawabata & Yamada 2017). At the threshold proportion, the ratio of silica to alkali concentration is optimized to achieve the highest expansion. This balance is reported as a mole ratio of 6 for most reactive siliceous aggregates that exhibit a threshold behaviour (Rajabipour et al. 2015). For aggregate WT, the degree of ASR is likely to increase when the amount of reactive silica constituents decreases towards a threshold value of approximately 2% (Forster et al. 1998b).

For mortar bars GW_F , The minerals perceived to be responsible for the expansions measured were identified as the greywacke clasts and deformed quartz in the acid volcanic fragments. Figure 4.11 shows the petrographic images of the GW_F mortar bars. Conspicuous cracks (circled in Figure 4.11(a)) were observed in the dye cut-off block, mostly in and around greywacke sand particles. However, the quartz particles also showed some evidence of micro-cracking and porosity from silica deletion.

Finely divided micro-cracks (empty cracks) that pass through and around the greywacke clasts, and intersect voids inside the cement paste, were observed. In some cases, observed the pores were lined with ASR gel. Generally, the mortar bar samples showed few cracks and gel presence, indicating the existence of mild ASR,

as was expected for these aggregates, which were classified as slowly reactive from AMBT results discussed in Section 4.3.3.1.

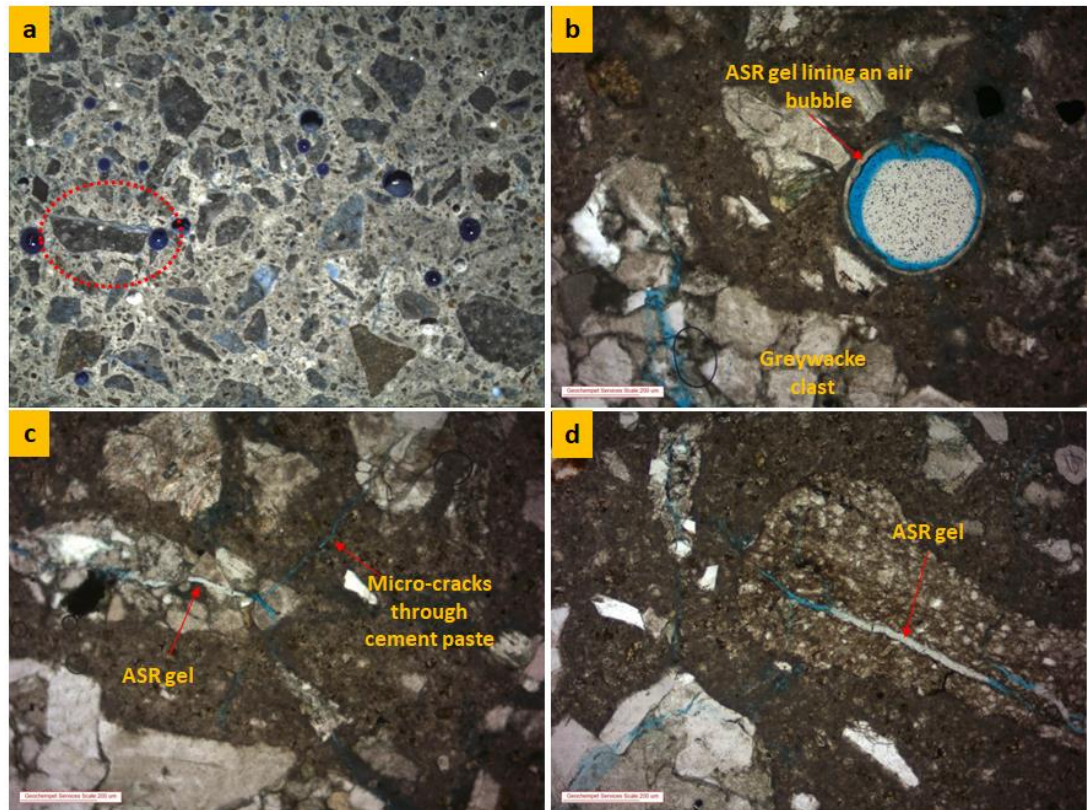


Figure 4.11 Petrographic images of mortar bar GW_F showing (a) polished and dyed cut-off blocks from the mortar bars (*image width= approx. 20mm*), (b) ASR gel lining air bubbles and open micro-cracking in greywacke clast, (c) micro-cracks pass through and connecting greywacke clasts and, (d) an ASR-filled crack passing through a greywacke fragment (*Note: SCALE= 200 μ m*)

Remnants of ASR gel were observed in internal cracks of greywacke clast, suggesting that these constituents caused ASR. A similar observation has also been reported for greywacke in field structures (Thomas 1996a). Typically, the reactivity of greywacke has been found to be deleterious in some cases (Le, Siewert & Ludwig 2015; Thomas 1996a), whereas in other instances, greywacke has been identified as

slowly reactive (Binal 2008) or inert (Mackechnie 2006). Generally, greywacke is usually found with argillite (Hodder & Hetherington 1991), consisting of quartz, feldspar, and mica. Gilliot et al. demonstrated in their work that the reactivity of greywacke is also related to the amount of mica porphyroblast found in these rocks. These clayey materials also exfoliate in alkali, releasing additional K^+ and Na^+ ions that favour the formation of ASR gel and expansion (Gillott 1986). The initial petrographic assessment of aggregate GW_F (Table 4.4) revealed mica (biotite) presence alongside other weak clayey minerals that are potentially deleterious. Although the volume percentage of such minerals may be considered low (a portion of 11%), it is plausible that biotite in the greywacke clasts also contributed to the ASR behaviour observed.

Similar conclusions can be drawn from the petrographic assessment of mortar bars WT^1 and WT^2 ; the sand blends composed of reactive aggregate WT and non-reactive PR_F , and GW_F . Typically, the ASR causative minerals in these mortars were identified as the reactive minerals found in the respective sands used in the sand blend, as shown in Figures 4.12 and 4.13. That is, for WT^1 , where a non-reactive aggregate was used, the minerals perceived to have caused ASR were only the acid volcanics and glassy shards from WT , given in Table 4.4. However, in both mortar systems, the vol% of the reactive minerals within a count of 100 widely spaced points was found to have decreased from that of WT . This is potentially the mechanism by which the sand blends minimize ASR. However, since the AMBT expansions of these mortars were similar to that of WT due to the conservative nature of the AMBT test, this conclusion can only be speculated at this time.

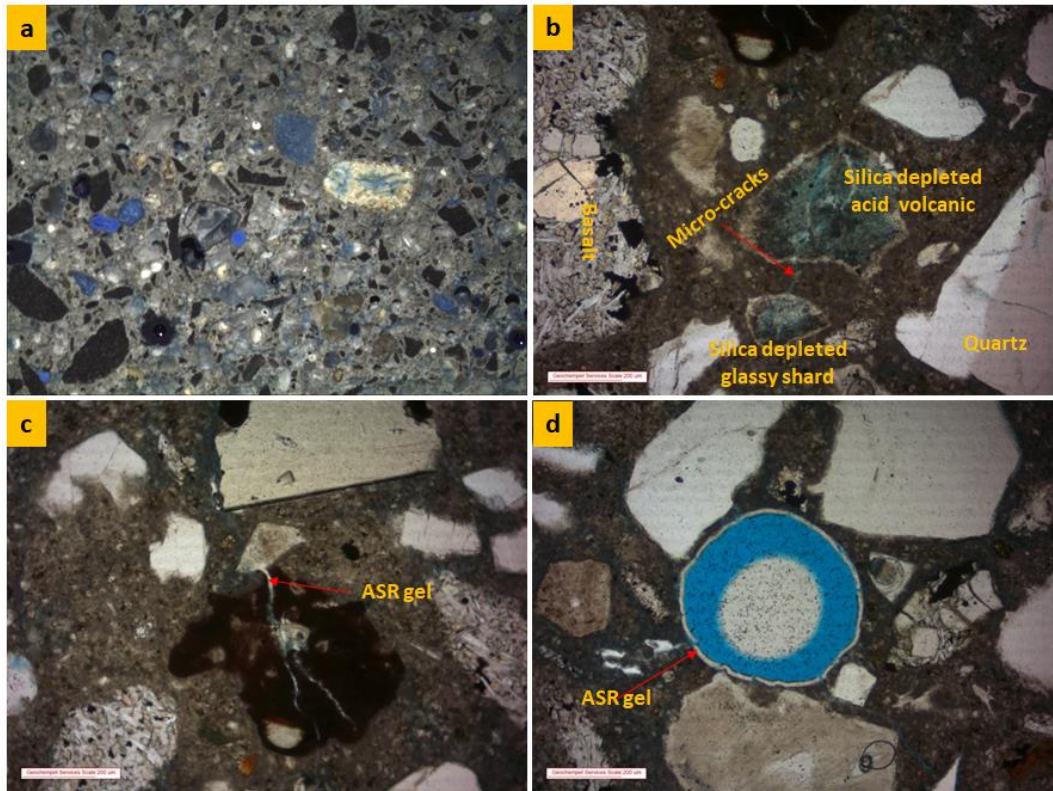


Figure 4.12 Petrographic images of mortar bars containing aggregate WT¹ showing (a) cut-off block from the mortar bar with fine porosity and micro-cracks occurring in and around WT grains and in the cement matrix (*image width= approx. 20mm*), (b) micro-cracks passing through silica depleted (porous) acid volcanic and glassy shard fragments (c) a crack passing through acid volcanic fragment. *Note the remnants of ASR gel in the cracks* and, (d) ASR gel lining an air bubble and, many micro-cracks emanating from the edge of the air bubble into the cement matrix (*Note: SCALE= 200µm*)

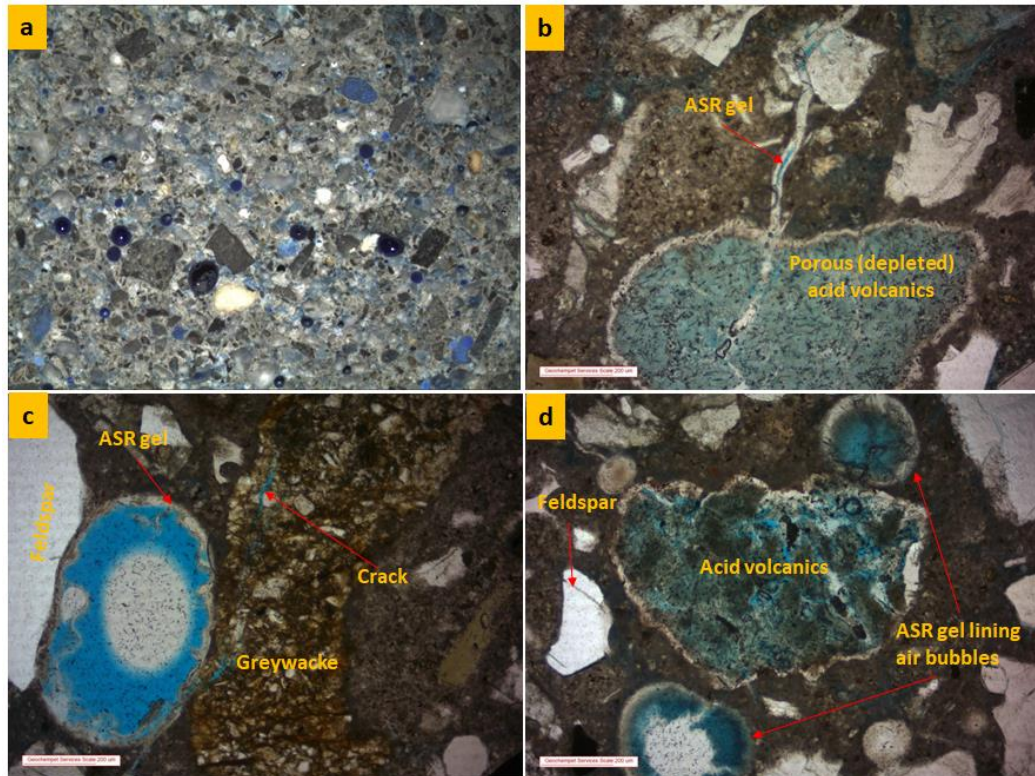


Figure 4.13 Petrographic images of the mortar bars containing aggregate WT² showing (a) dyed cut-off mortar blocks (*image width= approx. 20mm*), (b) conspicuous ASR-filled crack passing through an acid volcanic fragment and a silica-depleted (porous) acid volcanic fragment, (c) a micro-crack through a greywacke fragment and along an ovoid air bubble lined with ASR gel and (d) ASR gel lining air bubbles with associated micro-cracks passing into cement matrix. *Note the internal cracking and depletion-induced porosity in a glassy acid volcanic clast (Note: SCALE= 200 μ m)*

4.3.5.2 Concrete Prisms

As identified in Table 4.3, the concrete samples selected for petrographic analysis were chosen based on assessing the effect of temperature (38°C and 60°C) and alkali (2.5, 3.5, and 5.25 kg/m³) on the mechanism of ASR expansion. The sand blend aggregates; WT¹ and WT², have been selected in the hopes of establishing the mitigation effect exhibited in CPT.

At the end of the CPT and ACPT test, whitish streaks of is assumed to be leached alkali were observed on the surfaces of some of the prisms, especially those tested at 60°C (ACPT). The issue of alkali leaching is essential in determining the effect of alkali on ASR expansion, and will be discussed in detail in Section 5.2.3.

Effect of Temperature on ASR Expansion in Concrete Prisms

As established from the petrographic assessment of WT¹ mortar bars (Section 4.3.5.1), glassy shards and acid volcanics from the pumice fragments of WT were also observed as the ASR causative minerals in the WT¹ concrete prisms. This was verified by the presence of micro-cracks emanating from acid volcanic fragments, as presented in Figures 4.14a1 and 4.14a2.

At 38°C (CPT), fine (thin) ASR gels within micro-cracks of reacted grains were observed (Figures 4.13a1 and 4.13a2). Additionally, ettringite products due to secondary ettringite formation were seen as lining in some pores within the concrete. Indeed, in some cases, ettringite-lined pores that appeared to have once been filled by ASR gel were observed. A typical example of this is presented in Figures 4.14b1 and 4.14b2. This observation agrees well with the discussion that ASR and ettringite formation (delayed or secondary ettringite) usually occur in the same structure (Bauer et al. 2006; Bouzabata et al. 2012). Ettringite has been found to occur when concrete is exposed to a moist environment at a temperature below 70°C (Stark & Bollmann 2000). Usually, the crystallization of ettringite is known to induce stresses that lead to expansion and micro-cracking in the concrete (Czarnecki & Eng 2016). However, the frequency (presence) of ettringite crystals

observed during the petrographic assessment of the concrete samples was minimal to ASR gel, to suggest that expansion measured was driven by ettringite.

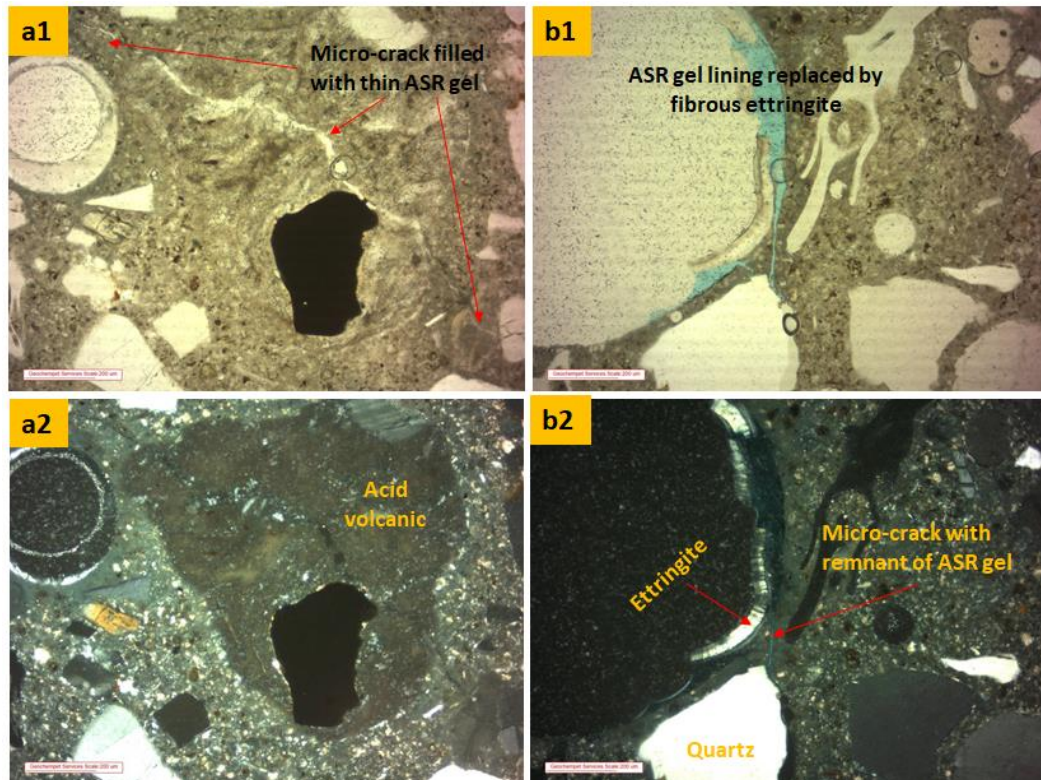


Figure 4.14 Plane and cross-polarized transmission light images of WT¹ CPT prism showing (a) ASR gel lining an air bubble (inner rim), outlined by fibrous ettringite (outer rim) and micro-crack passing through glassy acid volcanic clasts and, (b) ASR gel lining an air bubble replaced by fibrous ettringite. Note micro-cracks passing through cement matrix and alongside a quartz grain into the gel-lined air bubble. (Note: SCALE= 200 μ m)

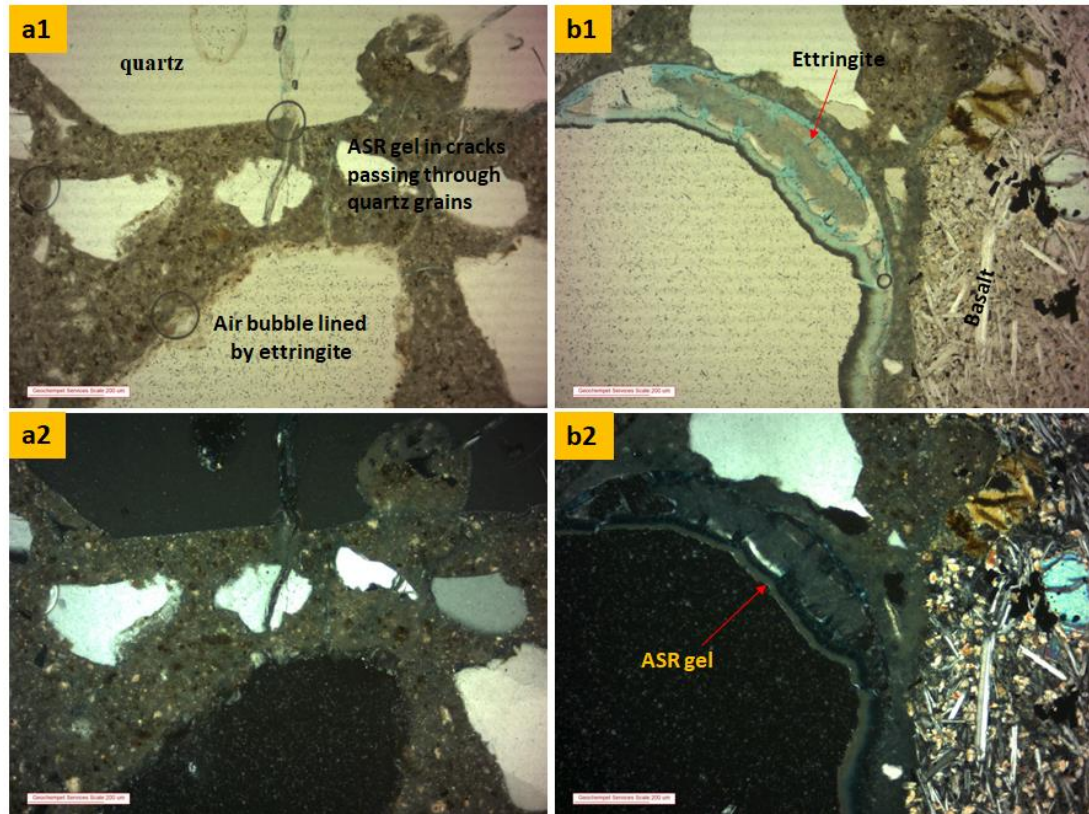


Figure 4.15 Plane and cross-polarized transmission light images of WT¹ ACPT prism showing (a) an air bubble lined with fibrous ettringite and ASR gel in micro-cracks passing through cement paste and quartz grain and (b) ASR gel lining an air bubble that is thinly outlined by low birefringent ettringite. Basaltic PR_C can also be seen (*Note: SCALE= 200μm*)

At 60°C (ACPT prisms) (Figure 4.15), a similar observation of acid volcanics and glassy shards reacting to form ASR gel. However, the width of the ASR gels formed in ACPT prisms was larger and more defined compared to that of the gels found in the CPT prisms. This can be seen from the petrographic images of WT¹ ACPT prisms presented in Figures 4.15a1 and 4.15a2. Thus it can be concluded that the formation of ASR is encouraged by the higher temperature test conditions. The expansion of the larger ASR gels at 60°C will have a significant impact on the concrete's overall expansion, as was observed in the expansion measurements of these prisms (Figures 4.6 and 4.7). At the end of 12 months, WT¹ CPT prisms showed an

expansion of 0.015%; however, an expansion of 0.055% was measured after 6 months of ACPT.

Additionally, the increased presence of ettringite in ACPT samples was also observed (Figures 4.15b1 and 4.15b2), indicating the movement of moisture in the concrete specimen. This indirectly infers the favouring ASR activity as moisture is the necessary ingredient for ASR gel expansion. Accordingly, no apparent cracks were observed around ettringite crystals (Figures 4.15b1 and 4.15b2), proposing no relevant expansion occurred by ettringite precipitation.

Effect of Alkali on ASR Expansion in Concrete Prisms

The effect of alkali content on the ASR in concretes was studied using concrete prism WT². These prisms contain GW_c as the coarse aggregate and GW_F (40%) as part of the fine aggregate blend. Thus the reactive mineral constituents identified in petrography were acid volcanics, glassy shards from the 60% WT fraction of the fine aggregate blend, and reactive silica minerals within the greywacke fragments of aggregate GW_c and GW_F. At all the alkali contents studied, WT² concrete prisms showed minimal expansion. This was evident by the relatively few micro-cracks identified in the thin section analysis of the specimen, suggesting the occurrence of mild ASR.

At the alkali content of 2.5 kg/m³ (Figure 4.16a), the presence of ASR gel was not identified. However, cracks were found in the cement paste along the rims of meta-greywacke particles, as shown in Figure 4.16a. These cracks are suspected to have formed due to water bleeding (Mohammed et al. 2002; Soylev & François 2003)

since there is no evidence that the particles had been affected by ASR. In some cases, the 'bleeding gaps' along the meta-greywacke were filled with a calcium variant that could be relatively coarse calcium hydroxide or calcium carbonate, probably derived from the finely crushed limestone blended with the GP cement.

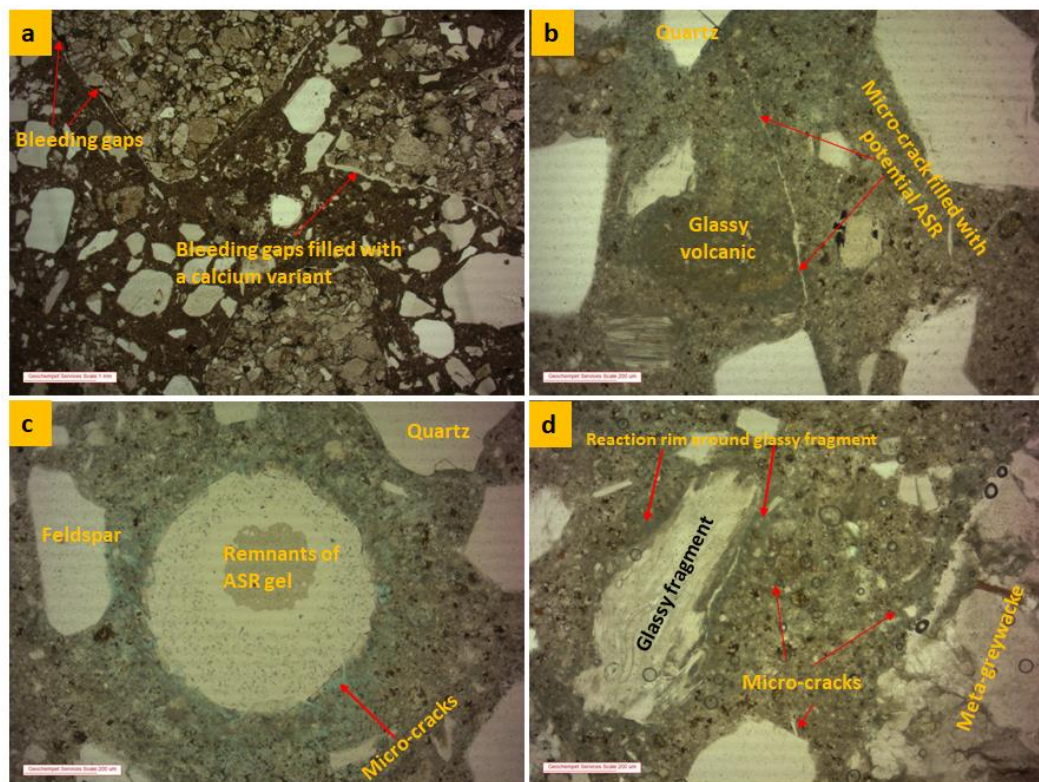


Figure 4.16 Plane and cross-polarized transmission light images of WT² CPT prism showing (a) fine cracking running alongside meta-greywacke fragments suspected to be bleeding gaps, (b) micro-crack joining two quartz grains and running alongside a glassy volcanic clast (c) an air void (pore) lined by remnants of a clear ASR gel and associated micro cracks around the air bubble and, (d) a micro-crack joining a glassy fragment and a meta-greywacke fragment (*Note: SCALE= 200µm*)

At the alkali content of 3.5 kg/m³, the petrographic analyses revealed the presence of micro-cracks passing through glassy acid volcanics and connecting quartz grains

in the concrete (Figure 4.16b). Additionally, some pores within the concrete were observed to be partially lined with ASR gel (Figure 4.16c). In some instances, those pores also exhibited signs of micro-cracking emanating from the edge of the pores, as seen in Figure 4.16b. These features indicate mild ASR has occurred; however, the amount of ASR gels or micro-cracks identified within the concrete was minimal. Subsequently, when the alkali content of the prism was boosted to 5.25 kg/m³, an increase in the number of reacted silica minerals was observed in the concrete, leading to the formation of several fine ASR-induced cracks at different reaction sites within the concrete. Some reactive silica minerals also showed darkened reaction rims around the particle (Figure 4.16d), suggesting that the particle has undergone or is still undergoing ASR

4.3.6.3 The Mechanism of ASR Expansion as a Function of Temperature and Alkali Content

Certainly, numerous reports in literature discuss that increasing the alkali content and temperature of concrete prisms increases the reactivity and, thus, expansion observed for aggregates under investigation (Kawabata et al. 2019; Ranc & Debray 1992; Saha et al. 2018). It is on this premise that the concrete prism test at 60°C (ACPT) has been developed and is accepted by many researchers globally as being arguably reliable for assessing the ASR of aggregates when early results are required (Thomas et al. 2006). While this may be true, the effects of increasing alkali and temperature on the expansion mechanism of ASR as pertained to the ASR gel formed are not well documented.

Therefore, based on the petrographic assessments of the concrete prisms studied in this work, a distinguishing observation was made for the prisms tested at the different temperatures, as well as those tested at varying alkali contents. The results show that when alkali content is high, a larger volume of ASR susceptible components in the aggregates are affected due to the abundance of alkali in the pore solution. This results in the increased number of relatively smaller ASR gels that form throughout the concrete. Therefore, multiple expansions occur that lead to the overall expansion of the prism that is recorded with increasing alkali content. On the other hand, temperature acts as a catalyst to increase the kinetics of the chemical reaction leading to ASR (Ulm et al. 2000). Therefore, when the temperature is increased, ASR susceptible components in the aggregates that are exposed to alkali react rapidly to form ASR gel. However, the gel formed has been observed in this work to be larger. This suggests that the ASR gel at higher temperatures is capable of exhibiting enough expansion in a relatively short time to provide results on the ASR potential of the aggregate. Then, it is worth mentioning that the determination of the reactivity potential of aggregates by increasing temperature is dependent on the amount and accessibility of reactive silica components in the aggregates to interact with available alkali to form ASR in the relatively short time the test requires.

Chapter Summary

In chapter 4, the effect of increasing alkali concentration on the reactivity of four aggregates identified as WT, GW, RT, and AS, as well as two sand blends; WT¹ and WT², have been studied to determine their alkali limits. Petrographic assessments on the aggregates were carried out to determine their mineralogical composition and to identify the potentially reactive component in the individual aggregates, prior to chemical and expansion tests.

Chemical tests described as dissolution test and GAST were then carried out on ground aggregate samples and slurries, respectively. The chemical test results were discussed to provide further information on the aggregates reactivity based on the amount of silica released by the aggregate, as well as the pozzolanicity of the released silica in Ca (OH)₂-rich slurries.

This chapter also discussed the determination of alkali limits using AMBT and CPT (at 38°C and 60°C (ACPT)) in the procedure recommended by AS 1141.60.1 and a combined AS 1141.60.2 and RILEM AAR-3.2/7.1 accordingly, as described in Sections 3.2.1 and 3.2.2 of Chapter Three. AMBT was carried out at 0.6M, 0.8M, and 1.0M NaOH alkali concentrations, whereas CPT and ACPT were done by varying the alkali content from 2.5-5.25 kg/m³ Na₂O_e. At the end of the expansion tests, petrographic assessments of the mortar bars tested at 1M NaOH, and selected concrete prisms were conducted. The findings from the work discussed in this chapter can be summarised as follows;

1. Except for aggregate RT, a consistent reactivity classification was inferred for all aggregates during the initial petrographic assessment, chemical tests, and standard AMBT expansion tests at 1.0 M NaOH alkali concentration.
2. During AMBT, the reactivity classification of the aggregates as per AS 1141.60.1 was the same at each alkali concentration investigated. However, the reactivity level of aggregates was inconsistent in increasing alkali content. Aggregate GW showed expansion that increased with increasing alkali, while for WT¹ and WT², the highest expansion was recorded at 0.6 M NaOH concentration. Therefore, for the purpose of alkali threshold determination, AMBT is inept at detecting reactivity levels of aggregates. It is, however, practical as a rapid screening tool for non-reactive aggregates.
3. At the alkali content of 5.25 kg/m³ Na₂O_e, aggregates RT and AS were found to be potentially reactive during CPT and ACPT tests, whereas the other aggregates were found to be non-reactive. The expansion results from the ACPT and CPT at varying alkali showed that except for aggregate AS, all other aggregates did not show deleterious expansion up to and including 4.0 kg/m³ Na₂O_e. This suggests the possibility of using these aggregates in concrete with slightly higher alkali limits than the current 2.5 and 2.8 kg/m³ Na₂O_e limits set in New Zealand and Australia, respectively. From the results obtained, a revised alkali limit of 3.0-3.5 kg/m³ Na₂O_e was proposed for the aggregates tested, except for aggregate AS, which showed higher expansions at 2.5 kg/m³ Na₂O_e. For AS, it was suggested that a low alkali content cement together with preventive measures such as the use of SCM would be required.
4. A good correlation between CPT and ACPT was detected. However, the appropriate ACPT age that correlates to CPT at 12 months is not apparent.

5. Post-expansion petrographic assessment of the mortar bars and concrete prisms showed evidence of ASR. Both mortar bars and concrete prisms showed the presence of micro-cracks and ASR gel passing through and around reactive constituents of the aggregates. For concrete prisms, ettringite crystals were also identified in some samples. However, it was discussed that the amount of ettringite was not sufficient to drive the expansion exhibited by the concrete prisms.
6. Although increasing temperature and alkali increase ASR expansion, the mechanism of the specimen expansion may differ. Petrographic assessment of selected concrete prisms showed that at high temperature, thicker and more defined ASR gels are formed; thus, the gels are capable of creating sufficient stresses within the sample to produce noticeable length within a short period of time. It was speculated that this could be the justification for the ACPT method. In contrast, when alkali is increased, a higher amount (number) of reactive constituents are affected. This leads to the increased formation of ASR gels at different sites within the concrete that expand to cause several micro-cracks throughout the sample, leading to the overall expansion observed.

CHAPTER 5. Correlations between ASR Test

Methods Used for Assessing Potential Reactivity of Aggregates

5.1 Overview

At present, the recognised laboratory test methods for assessing ASR are mainly expansion tests conducted on mortar bars (AMBT) at 80°C and concrete prisms (CPT) at 38 and 60 °C (ACPT). As discussed in Section 2.7.2, these expansion test methods have limitations that can affect the validity of the results obtained. Nonetheless, there is significant data in literature that suggests that CPT carried out at 38°C for up to 12 months provides results that are comparable to field performance and thus gives the most reliable prediction of an aggregate's reactivity (Sirivivatnanon, Mohammadi & South 2016). Although, the relatively long test period for CPT at 38°C is still an issue for the fast-paced industry where early results are desired.

Three main methods, namely, petrography, chemical tests, and expansion tests (AMBT, CPT, and ACPT), have been employed in this study to classify the reactivity of the aggregates. In this chapter, the correlation between aggregate classifications based on the different methods will be discussed. Furthermore, the relationship between CPT and ACPT will be studied using statistical methods to establish the correlation between the two test methods and determine the appropriate age at which ACPT results are comparable to 12-month CPT results, thus providing

evidence to support the potential use of ACPT as an accelerated test method for assessing ASR. This chapter will also address the issue of alkali leaching during concrete prism tests (CPT and ACPT) and the key parameters that are likely to affect the rate and degree of ASR and, consequently, the accuracy of the test methods.

5.2 Experimental Plan

5.2.1 Statistical Analysis

A detailed evaluation of the chemical and expansion data reported in Chapters three and six has been carried out to investigate the reliability and consistency of the current test methods used to identify the reactivity potential of aggregates to ASR. Additionally, the expansion measurements reported for CPT after 12 months were assessed against ACPT data after ages 1 - 6 months to determine the appropriate age at which ACPT is most comparable to the standard CPT method. All data analyses were carried out using OriginPro8 software. The correlation between CPT and ACPT was achieved by using Pearson's correlation coefficient method available in the data analysis tool pack of the software.

5.2.1.1 Pearson's Correlation Coefficient Method

Pearson's correlation coefficient method (PCC) is one of the most widely used statistical approaches that measure the linear dependence between two random variables (Emerson 2015; Hauke & Kossowski 2011). This coefficient of correlation is calculated using Equation 5.1 (Lee Rodgers & Nicewander 1988):

$$r_{x,y} = \frac{\sum (x_i - \bar{x})(y_i - \bar{y})}{\sqrt{\sum (x_i - \bar{x})^2 \sum (y_i - \bar{y})^2}} \dots\dots\dots \text{Eqn. 5.1}$$

Where x and y represent the values of the two random variables and their respective mean values symbolised as \bar{x} and \bar{y} . The symbol r denotes the coefficient of correlation, which typically varies from -1 to 1. Thus, the value of r defines the degree of correlation between the variables such that when r=0, there is no relationship between the variables. The closer the r value is to +1, the more related the variable is. In this way, a negative value of r suggests a relationship between the variables in which an increase in one variable causes a decrease in the other variable.

5.2.1.2 Factorial Analysis

Factorial analysis using a similar approach to the principal component analysis (PCA) and analysis of variance (ANOVA) was also applied to the expansion data to identify common underlying factors (components) that influence expansion, their significance, as well as their interaction with each other (Jolliffe & Morgan 1992; Zwanenburg et al. 2011). Figure 5.1 summarises the variables selected for the PCA and ANOVA studies. The three primary variables that have been selected for this study include alkali content, temperature, and age. These variables are known to affect the accelerated test conditions used to evaluate an aggregate's potential for ASR.

PCA is one of the oldest and most used factorial analysis techniques (Jolliffe & Cadima 2016). This technique potentially reduces the attributes in a data set in a way that preserves the variation and statistical information. This is achieved by

extracting factors referred to as principal components and allocating eigenvalues that signify the relevance of the extracted components (Friedman & Weisberg 1981). Similarly, ANOVA identifies the significance of components on the perceived outcome and the likely interaction between them that affect the outcome. The conclusions from ANOVA are usually drawn from the probability value (p-value) (Cuevas, Febrero & Fraiman 2004) based on a null hypothesis (H_0).

The PCA and ANOVA approaches used in this study were tailored to suit the available data set. ANOVA was carried out at a 95% confidence level with a p-value of 0.05, under the H_0 that- the effect of the identified components and their interaction is not significant. Thus, if the p-value is <0.05 , the null hypothesis may be rejected.

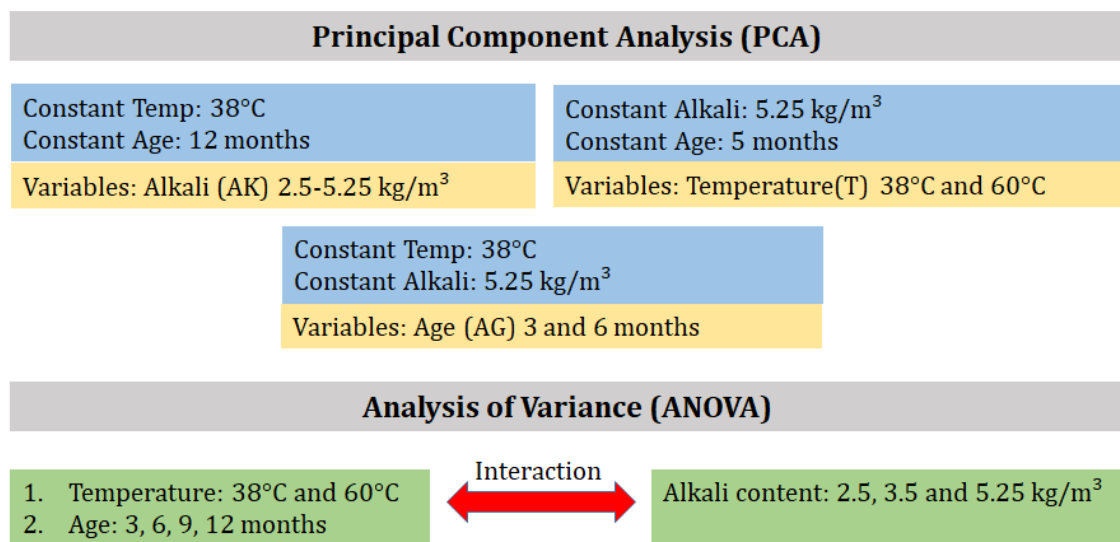


Figure 5.1 Selected variables for factorial analysis

5.2.2 Leachate Assessment of CPT Expansion Tests

To make a reasonable correlation between the CPT and ACPT expansion data, it is essential to consider the extent of alkali leaching that occurs during each test. As previously discussed in Section 2.7.2, alkali loss through leaching is a major challenge with CPT and ACPT test methods. It plays a significant role in the expansion observed by aggregates during testing. Additionally, ascertaining the amount of alkali that is lost during the test enables a safe prediction of the appropriate alkali threshold limits for the tested aggregates. Leachate assessment in CPT and ACPT test was carried out by considering the total alkali content that was present in the prisms at the start of the test as the control comparative.

Sample Collection

During prism curing at CPT and ACPT conditions, approximately 1500 ml of deionised water (storage water) was used to maintain a humidity of >95% in the storage pails (Figure 3.3). As the test progressed, an aliquot of 5 ± 0.5 ml of the storage water was collected at the time of expansion measurements at ages 1, 3, 6, and 12 months for CPT, and each month for ACPT until 6 months. Three concrete mixes from the test series discussed in Chapter six, namely, OPC, 25W_G, and 25GW_G, were selected for investigating the effect of temperature on alkali leaching. Concrete prisms 25W_G and 25GW_G were prepared with 25% cement replacement using ground reactive aggregate fines as a substitute for cement in the studies carried out in Chapter six. The effect of alkali content on leaching was also studied by analysing the storage water for concrete prisms containing varying alkali content, as discussed in Chapter four.

Sample Preparation and Analysis

The storage water samples were filtered through a 0.45 µm micro filter and diluted at a ratio of 1:1000 with 1% nitric acid prepared with Milli Q water (Figure 5.2). Approximately 13 ml of the diluted sample was pipetted into tightly closed HDPE tubes and sealed with parafilm. The tubes were kept refrigerated at 5°C no more than 24 hours prior to MP-AES analysis as per the parameters described in Section 3.5.6.

Post MP-AES analysis, the proportion of leached alkali in the storage water was calculated as the total sodium equivalent (Na_2O_e) using Equation 5.2 (The New Zealand Ready Mixed Concrete Association 2004):

$$\text{Na}_2\text{O}_e = (\text{Na} \times 1.35) + (0.658 \times \text{K} \times 1.02) \dots\dots\dots \text{Eqn. 5.2}$$

The Na_2O_e equation in Eqn. 5.2 represents the ion contents of Na and K in mg/L and may be converted to a percentage by dividing the right-hand side of the equation by 10,000. The correction factors; 1.35 and 1.20, account for the relative difference between the atomic weights of Na and K and their respective oxides, and the correction factor of 0.658 is applied to reflect the relative difference in formula weight between Na_2O and K_2O .



Figure 5.2 (a) Filtration and (b) dilution of sampled CPT and ACPT storage water for MP-AES analysis

5.3 Results and Discussion

5.3.1 Reliability of Existing Test Methods for Aggregate Reactivity

Determination

Table 5.1 presents a summary of the reactivity classification of the aggregates that have been studied using the various test methods discussed. The numerical data for the classification summary presented in the table is given in the Appendices. Although it is noted that each of these test methods measures a different entity (silica content, $\text{Ca}(\text{OH})_2$ content and expansion) as an indication of reactivity (or ASR), it is anticipated that the results provide corroborative information on the aggregates likelihood to react to form ASR. From Table 5.1, it can be observed that a reasonably consistent outcome of reactivity classification was achieved from the different test methods.

Table 5.1 Comparison of reactivity classification by various test methods

Aggregates	Petrography	Chemical Tests		Expansion Tests	
		Dissolution ASTM C289	GAST at 28 days (reactivity rank)	AMBT at 21 days AS1141.60.1	CPT at 12 months AS1141.60.2
WT	Substantially reactive	Considered Deleterious	1	Reactive	Potentially Reactive
RT	Mild - slowly reactive	Considered deleterious	4	Reactive	Potentially reactive
GW	Mild - slowly reactive	Considered Innocuous	3	Slowly reactive	Non-reactive
AS	Reactive	Considered Deleterious	2	Reactive	Potentially reactive

Typically, the basis for an ASR test method is (i) to determine the potential of an aggregate to alkali-silica reactivity in a reasonably short time and (ii) to assess and establish an acceptance limit of reactive constituents or response, which is comparable to the long-term behaviour of the aggregate in field structures. Assuming these pre-requisites, petrography, although recognised as a reliable tool (Castro, Sorensen & Broekmans 2012; Jóźwiak-Niedźwiedzka, Gibas & Glinicki ; Ramos et al. 2016) for identifying potentially reactive mineral constituents and their respective quantities in aggregates, may not provide conclusive information on the standard acceptance limits for known minerals for ASR preventative purposes. Indeed, guidelines have been established for predicting the ASR potential of aggregates by this technique (CCANZ 2012; Fernandes et al. 2016; Standards Australia 2008). Yet, aggregate reactivity classification by petrography and acceptable amounts of the respective reactive constituents (or minerals) depend strongly on the expertise of the petrographer as well as documented field evidence

of the aggregate (Nixon & Sims 2016b; Schouenborg, Åkesson & Liedberg 2008), which could typically vary from one location to another (local or national) and, thus, affect the precision and reproducibility of the petrographic technique (Sims; Nixon 2003). Nevertheless, in this study, with the exception of aggregate RT, a consistent outcome and corroboration was observed in the reactivity classification of the aggregates by petrography, the chemical and expansion test methods, in particular AMBT.

At present, the GAST method does not provide a pass-fail limit for aggregate reactivity as it has not been benchmarked against an array of aggregate performances. As such, it cannot be used to categorise aggregates into reactivity classes. It is, however, useful for classifying aggregates into reactivity levels based on their residual portlandite content after undergoing a $\text{Ca}(\text{OH})_2$ -aggregate reaction in a high alkali environment. By applying a ranking system from 1-4, in order of decreasing reactivity, the reactivity potentials for the aggregates can be set as $\text{WT} > \text{AS} > \text{GW} > \text{RT}$. Although there is no acceptance limit for this test method, considering the free silica content measured for the aggregates (Section 4.3.1), the GAST method correctly identifies the reactivity ranks for aggregates, except for RT and GW, whose reactivity predictions by GAST does not agree with the reactivity classification by the other test methods. This could be associated with several factors, including the similarity in the mineral constituents (meta-greywacke) of aggregate GW and RT as detailed in Section 4.3.1, or the likely formation of other reaction products. However, after 56 days (Figure 5.3), it was observed that a higher amount of Portlandite consumed was detected for aggregate RT.

In Figures 5.3 and 5.4, aggregate AS, which has been identified to show very high reactivity, has been omitted in the correlation studies as including such values could influence the reliability of the correlation results.

When the Portlandite consumption potential of the aggregates after 56 days was plotted against their respective CPT expansion data measured after 12 months, a low correlation of $r = 0.36$ was observed between GAST and CPT, as illustrated in Figure 5.3.

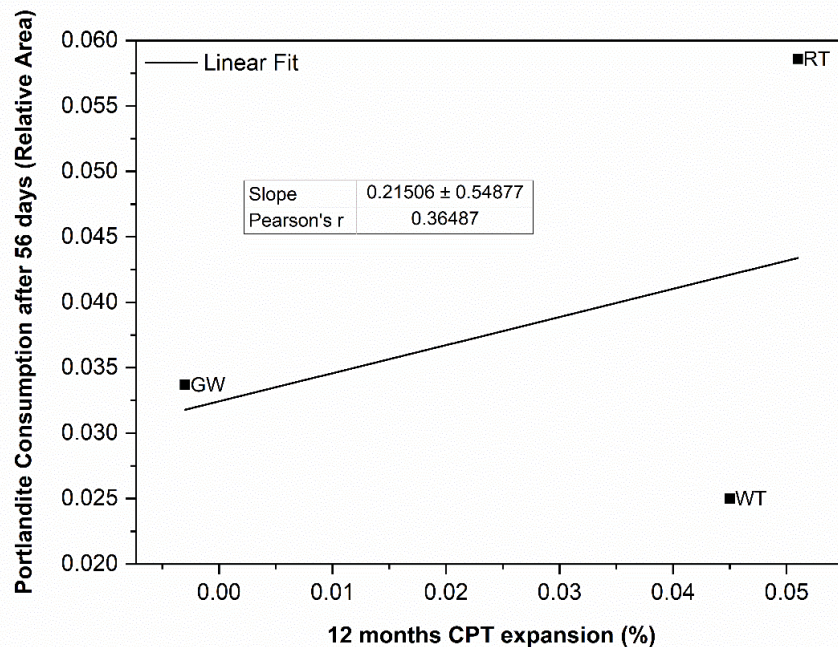


Figure 5.3 Relationship between GAST after 56 days and 12 months CPT expansion test

On the other hand, when the aggregates were evaluated in a state that accounts for the full range of their particle size distribution (expansion tests), aggregate RT showed higher reactivity than aggregate GW for both AMBT (Figure 4.5c) and CPT (Figure 4.6) methods. Conversely, except for aggregate GW, which was classified as

non-reactive at 12 months of AS 1141.60.2 CPT, there is a consistency in the prediction of the reactivity of the aggregates. In a previous study on the reliability of the AS 1141.60.1 AMBT method to correctly identify the reactivity potential of aggregates against their known field performance (Sirivivatnanon, Mohammadi & South 2016), it was found that although AS 1141.60.1 is more efficient than the ASTM version (ASTM 1260) in identifying reactive aggregates, it falsely classified 12% of the aggregates as slowly reactive; however, these aggregates exhibited no signs of ASR in field structures. This observation may be associated with the extended 21-day test period used in the AS 1141.60.1 AMBT method; thus, allowing non-reactive aggregates containing even minimal amounts of susceptible silica to show some level of expansion in the high temperature-alkali test environment resulting in a false positive indication of reactivity. This further endorses the recommendation to carry out CPT on all aggregates that show expansion exceeding the 10-day expansion limit of 0.1% (for AS 111.60.1) in AMBT.

5.3.2 Correlation between Expansion Test Methods

5.3.2.1 Accelerated Mortar Bar Test (AMBT) and Concrete Prism Test (CPT)

The AMBT test method, in general, is the most widely used accelerated (rapid) screening method for assessing ASR, whereas CPT is recognised as the most reliable test procedure (Lu, Fournier & Grattan-Bellew 2006). Due to this relationship, there have been several studies to determine a correlation between these two test methods to fine-tune AMBT test conditions and establish its applicability for assessing ASR globally (DeMerchant, Fournier & Strang 2000; Fournier & Bérubé

2000; Lu, Fournier & Grattan-Bellew 2006). Nonetheless, the majority of these correlation studies are based on the comparison between the 14- day limit of the ASTM 1260 AMBT method. In Section 5.3.1, it was identified that the AS 1141.60.1 AMBT test method was 88% accurate in correctly predicting the reactivity of aggregates and arguably more effective than ASTM 1260.

A graphical representation of the correlation between the AS 1141.60.1 AMBT after 21 days and the CPT (AS 1141.60.2) for nine different mix formulations studied in this work is given in Figure 5.4. Three mixes are seen to exceed both the limits for AMBT and CPT, suggesting confirmatory results for both tests and indicates the potential reactivity of those aggregates in field structures. Similarly, three non-reactive mixes were also congruently identified by both test methods. However, at the 21-day limit, AS 1141.60.1 incorrectly identified two non-reactive aggregates (WT¹ and WT²) as reactive. This outcome calculates as 78% reliability for the AS 1141.60.1 test method in correctly detecting the potential reactivity of aggregates.

Furthermore, a correlation coefficient of 0.50% was achieved for AS 1141.60.1 and AS 1141.60.2 test methods at the stipulated expansion limits and ages. This depicts a corroboration between the outcomes of both expansion test methods as previously reported (Rocker et al. 2015; Sirivivatnanon, Mohammadi & South 2016). It is also worth noting that the aggregates that were found to be reactive in AMBT and non-reactive in CPT may actually exhibit a slowly reactive behaviour (Shayan 2001). Therefore, this study recommends that the test duration for CPT be extended to 24 months for slowly reactive aggregates to capture the long-term reactivity behaviour of such aggregates. Consequently, by considering the 0.03% expansion

limit at 24 months of CPT, a stronger relationship between the two test methods may be achieved.

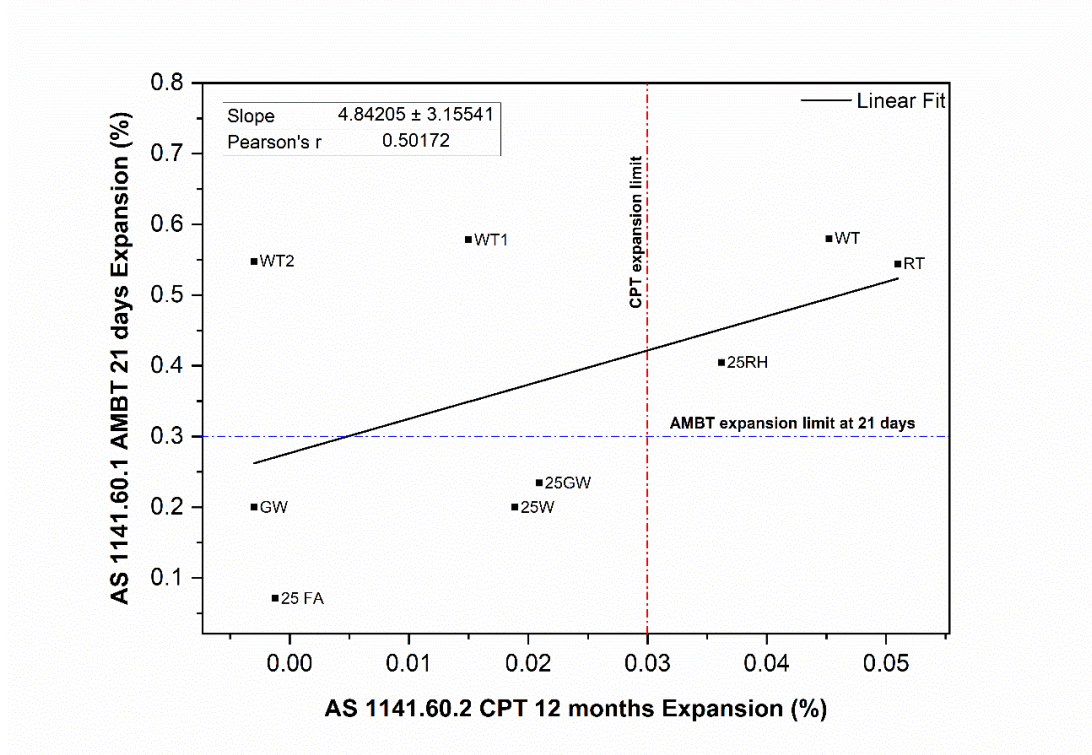


Figure 5.4 Relationship between AS 1141.60.1 AMBT and AS 1141.60.2 CPT test methods

Shayan et al. reported on similar results obtained from a study conducted on a variety of aggregates from various projects. In their work, they compared the AMBT 10-day limit of 0.1% (0.15% for natural sands) after 21 days for aggregates assessed using either version of AMBT, to the CPT limit of 0.03% after 12 months (Shayan, Xu & Andrews-Phaedonos 2003). They demonstrated that regardless of the AMBT method used, a good correlation still exists between AMBT and CPT methods, as seen in Figure 5.5.

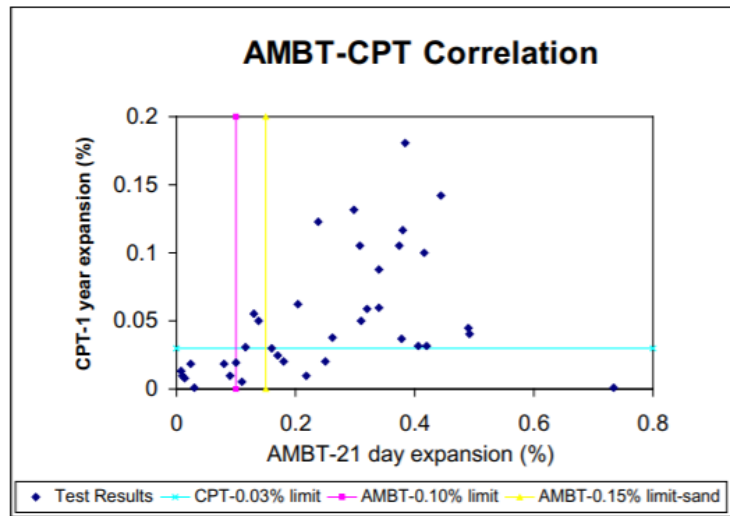


Figure 5.5 Related studies on the comparison of AMBT and CPT results for several aggregates from various projects

The authors also reported that for certain cases, the AMBT test method proved to be more effective in identifying aggregates such as granophyres- that have been reported to exhibit slow reactivity in field performance. These aggregates usually require high alkalinity and an extended test period (typically 3 years) in large structures to show signs of reactivity. In that case, the 0.1% expansion limit after 21 days of AMBT, which tests at abundant alkali supply, was recommended to be used, instead of the CPT limit at 12 months (Shayan 2001). The use of this approach has also been advised by the Roads and Maritime Services (RMS), Australia (RMS 2001).

Further inclusion of data from other projects (Rocker et al. 2015) on the correlation between AMBT after 21 days and CPT after 12 months for tests carried out in accordance with the AS 1141.60.1 and AS 1141.60.2 methods is presented in Figure 5.6.

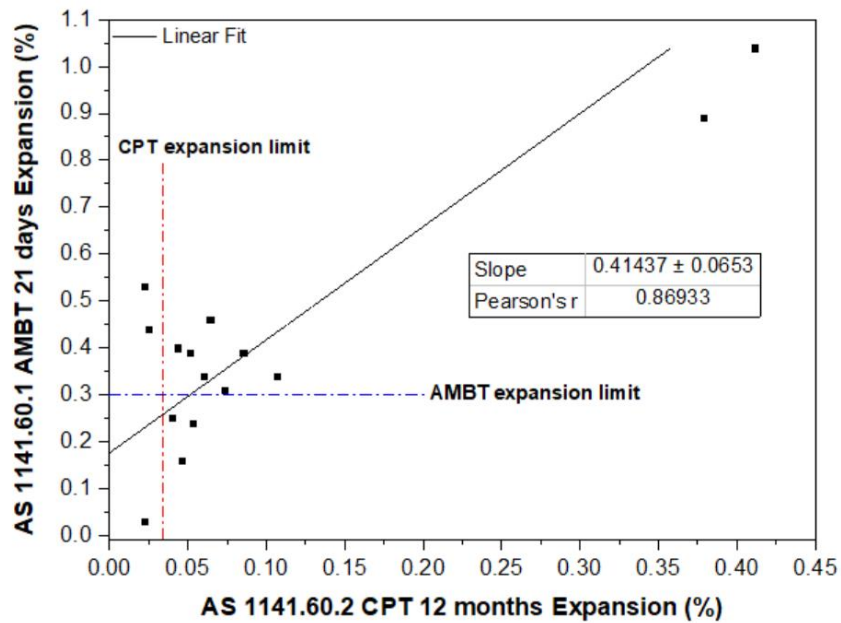


Figure 5.6 Correlation between AMBT and CPT for different aggregates assessed under AS 1141.60.1 and AS 1141.60.2 test methods

From Figure 5.6, it can be seen that the non-reactive aggregate in the group of aggregates assessed was correctly identified by both AMBT and CPT. However, AMBT provided false-positive results for two aggregates and classified another three as slowly reactive (expansion within 0.1% and 0.3%), whereas these aggregates were found to be reactive in CPT. Nonetheless, a strong correlation of $r = 0.87$ was observed between AMBT and CPT.

5.3.2.2 Concrete Prism Tests at 38°C (CPT) and 60°C (ACPT)

To determine the potential of standardising the ACPT method as an alternative short-term test to predict the potential reactivity behaviour of aggregates as accurately as the standard CPT test, a comparison of the expansion data obtained

for CPT at 38°C for 12 months and ACPT at ages 1-6 months for all concrete mixes assessed in this study was carried out. At present, work carried out on the correlation of ACPT and CPT expansion data indicates that expansion results taken at 3 months of ACPT is congruent to expansion results taken at 12 months of CPT for most siliceous aggregates (Fournier et al. 2004; Thomas et al. 2006). For aggregates that exhibit slow reactivity in AMBT or field conditions, the ACPT age of 5 months has been found to optimally correlate to 12 months of CPT. In this study, the correlation between the CPT at 12 months and the respective ages of ACPT for a total of 26 concrete mixes were investigated. The results obtained from this statistical study are presented in Table 5.2.

Table 5.2 Correlation between 12 months CPT results and ACPT results at different ages

ACPT Age (Months)	False-negative results in ACPT (%)	False-positive results in ACPT (%)	Pearson's correlation Coefficient (r)
1	23%	---	0.74
2	15%	---	0.87
3	8%	---	0.89
4	8%	4%	0.89
5	8%	4%	0.90
6	4%	4%	0.89

Correlation coefficient reported to 2 decimal places

Overall, a positive correlation was calculated at all ACPT ages. A similar Pearson's correlation coefficient of approximately 0.9 was found between 12 months CPT and ACPT from ages 3 - 6 months. Table 5.2 shows that the percentage accuracy of ACPT reduces with increasing age with the lowest percentage of false-negative results obtained after 6 months of ACPT. However, at 6 months, the results also showed a 4% likelihood of obtaining false-positive results in ACPT. Considering the proposed

ages of 3 months and 5 months, the correlation coefficients are statistically equal at both ages as aforementioned. Nonetheless, at 5 months, the reliability of ACPT in accurately predicting the reactivity of aggregates is lower, as ACPT may also provide false-positive results. From the work done in this study, the results demonstrate that the best correlation between CPT and ACPT was achieved at 3 months of ACPT. This outcome is also represented in the correlation plot shown in Figure 5.7.

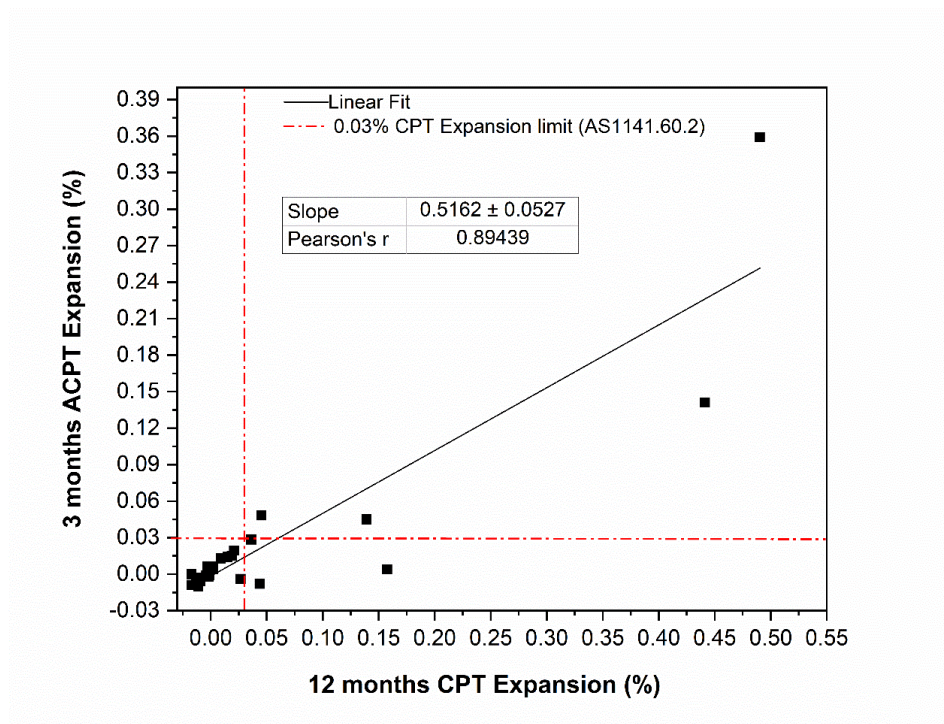


Figure 5.7 Correlation between 12 months CPT and 3 months ACPT expansion tests.

Figure 5.7 indicates the well-correlated linear relationship between CPT at 38°C and ACPT at 3 months. That is, by applying the 0.03% acceptance limit for AS 1141.60.2 to ACPT at 3 months, a reliable indication of an aggregates reactivity (expansion) at 12 months of CPT can be made. Furthermore, out of the 26 concrete mixes studied, the two concrete mixes that were incorrectly identified by the ACPT method can be observed. It has been reported that concrete prisms tested under ACPT conditions

may exhibit lower expansions than prisms tested under CPT conditions (Ideker et al. 2010). This may be attributed to the higher alkali leaching that occurs over the test duration, which will be discussed in Section 5.3.3. In that case, the identified mixes may otherwise have shown expansion exceeding the 0.03% limit at 3 months of ACPT. Consequently, some studies suggest that due to alkali leaching and considering that the ACPT method is an accelerated version of an already accelerated test method (CPT), a lower acceptance limit for ACPT may be appropriate when considering this test method as a short-term alternative to CPT, for assessing ASR of aggregates (Fournier et al. 2004; Ranc & Debray 1992).

5.3.3 Leachate Assessment for Concrete Prism Expansion Tests

The amount of alkalis leached into the storage water at the bottom of storage pails during CPT and ACPT as determined using MP-AES is presented in Figures 5.8 to 5.11. The graphs represent the approximate leachate amount for a single prism average, that is, the measured value divided by three (three prisms in a pail). The volume of each concrete prism ($75 \text{ mm} \times 75 \text{ mm} \times 285 \text{ mm}$) is approximately 0.0017 m^3 , with 8.9 g of alkali (Na_2O_e).

The results show that a significant amount of alkali leaching occurred. Generally, an increase in alkali leaching was observed with increasing age and temperature (38°C and 60°C). These specific observations are highlighted in Figures 5.8 and 5.9, and Table 5.3. Nonetheless, the relative difference in the leachate amount (amount of leached alkali relative to the previous age measured) decreased towards the end of the 12 months and 6 months for CPT and ACPT, respectively (Table 5.3), although an increase in expansion was recorded for these prisms (Section 6.3). The continued

expansion observed for the concrete prisms is likely because the amount of alkali leached was not enough to reduce the overall alkali content of the concrete below the alkali threshold of the aggregates (Costa, Mangialardi & Paolini 2017).

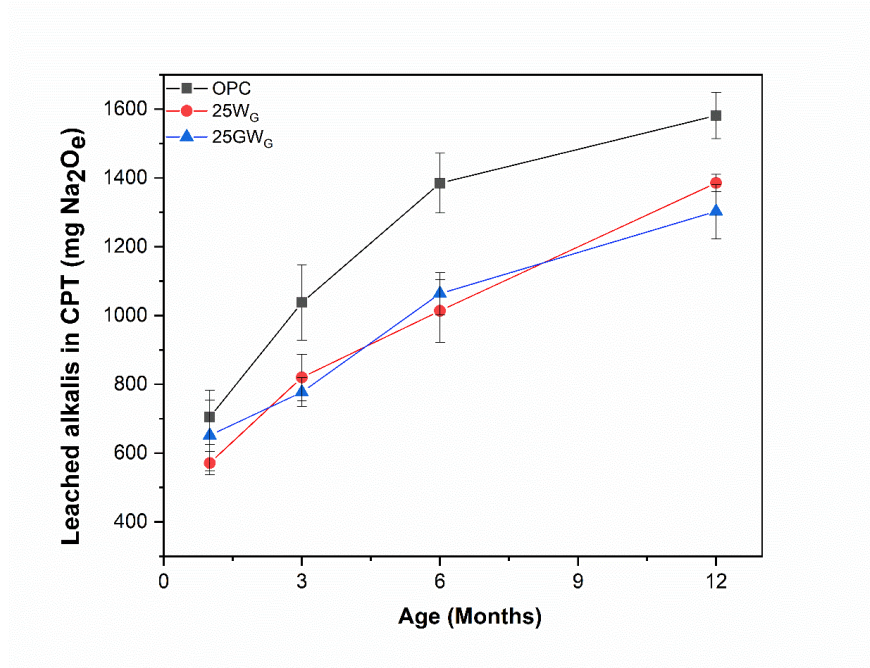


Figure 5.8 Alkali leaching from prisms tested under CPT condition (38°C). *Note: All concrete prisms have initial alkali content of 5.25 kg/m³ Na₂O_e*

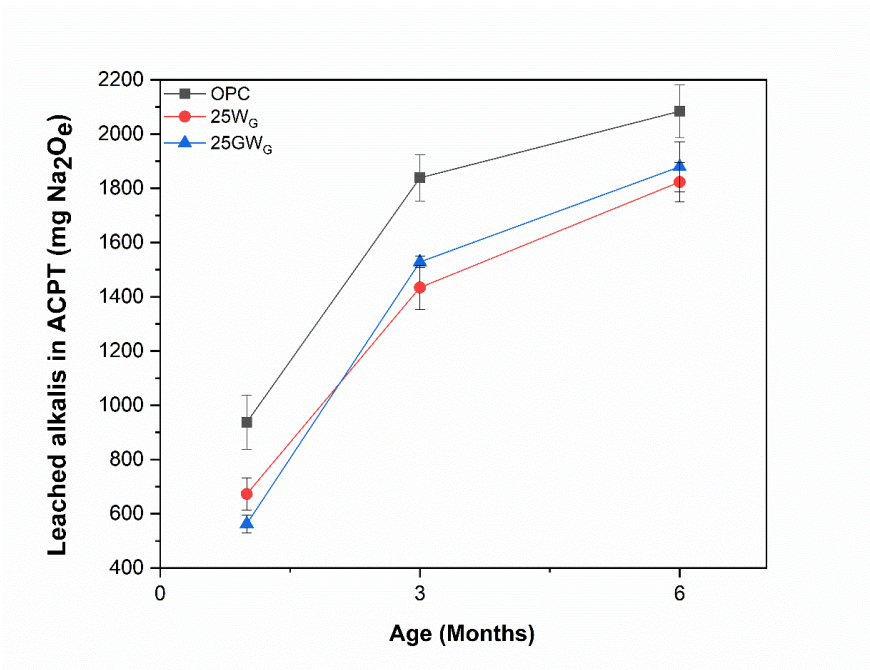


Figure 5.9 Alkali leaching from prisms tested under ACPT condition (60°C). *Note: All concrete prisms have initial alkali content of 5.25 kg/m³ Na₂O_e*

The proportion of alkalis leached, expressed as a percentage of the total alkali of 5.25 kg/m³ Na₂O_e (alkali content in cement + NaOH in mix water) supplied, is presented in Table 5.3. The values in the table represent the average of the three different prisms shown in Figures 5.8 and 5.9 at the corresponding ages.

Table 5.3 Alkali leaching (Na₂O_e) for three concrete mixes, during CPT and ACPT expansion tests

<i>Assumptions</i>	Test Method	Cumulative Percentage of leached alkali (%)			
		1 month	3 months	6 months	12 months
<i>Prism volume: 0.0017 m³</i> <i>Total Alkali: 5.25 kg/m³</i> <i>Alkali per prism: 8.86 g</i>					
	CPT	7	10	13	16
	ACPT	9	18	22	-

The proportion of leached alkalis measured in this study was lower than the typical 25 to 40% level reported in literature for the CPT test method (Lindgård et al. 2013; Rivard et al. 2007; Thomas et al. 2006). This could be debated as being due to the 25% replacement of cement to form a binary binder blend for prisms 25W_G and 25GW_G. Yet, for concrete prisms containing only cement (OPC), the recorded leachate amount (Figure 5.10) is relatively lower than what is usually reported for the CPT test method.

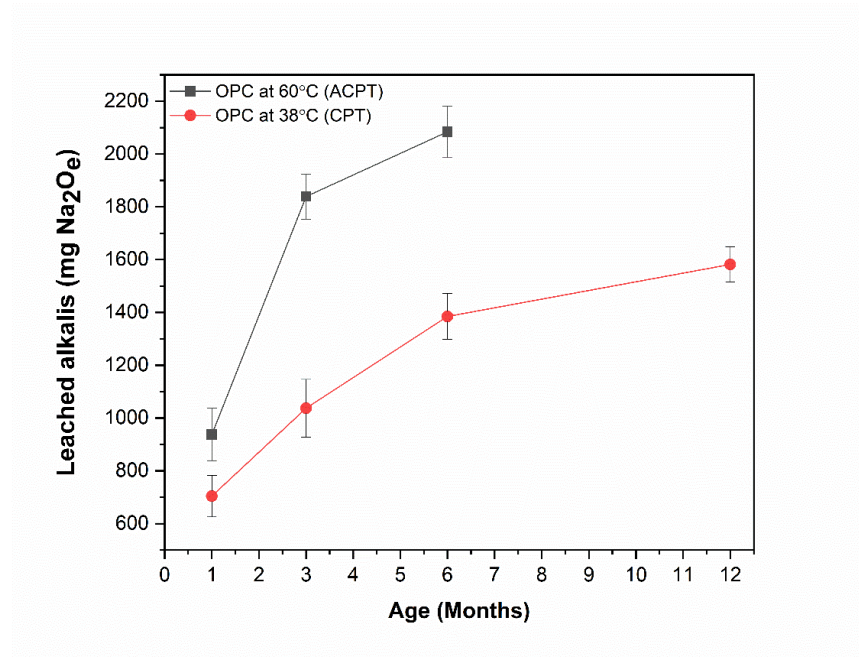


Figure 5.10 Alkali leaching from prisms containing only cement, tested under CPT and ACPT. *Note: All concrete prisms have initial alkali content of 5.25 kg/m³ Na₂O_e*

The differences in the percentage of alkali leaching reported in literature and this work are probably associated with the reactivity level of the aggregate used in the concrete mix. Considering that a proportion of the total alkalis available in the concrete, thought to be about 51% (Duchesne & Be 1995; Taylor 1991), is potentially bound in hydrates and ASR reaction products, and therefore cannot be leached, it can be concluded that the reactivity of the aggregate plays a vital role in the amount of alkalis leached from the concrete prisms. Potentially high reactive aggregates that form more ASR products consume more alkalis, thus reducing the amount of alkalis available to be leached. This alkali leaching behaviour was also observed by Bavasso et al. (Bavasso et al. 2020). Additionally, the lower alkali leachate concentration measured for concrete prisms containing 25% cement replacement levels can be attributed to the presence of the fine particles of the

ground aggregate fines that act as a pozzolanic material to bind the alkalis (Einarsdottir & Hooton 2018), as discussed in Section 6.3.1.

The storage water for concrete prisms composed of aggregate AS at different alkali content; which was studied for the determination of alkali threshold (Section 4.3.4), was also analysed to investigate the effect of alkali content on alkali leaching and, therefore, the reliability of the alkali threshold determined using the RILEM AAR-3.2 CPT test method. The chemical analysis of the storage water for concrete prisms containing varying amounts of alkalis is given in Table 5.4 and Figure 5.11.

Table 5.4 Effect of alkali content on alkali leaching during CPT per prism (total alkali measured divided by three)

Alkali Content Na ₂ O _e (kg/m ³)	Alkali content in one prism Na ₂ O _e (g)	Na ⁺ leached (mg)	Na ₂ O (mg)	K ⁺ leached (mg)	K ₂ O (mg)	Total leached alkali Na ₂ O _e (mg)	Leached alkali for one prism Na ₂ O _e (mg)
1 month							
2.5	4.22	221	297	716	863	866	288
3.0	5.06	247	333	944	1137	1082	360
3.5	5.91	278	375	961	1158	1138	379
4	6.75	345	465	969	1168	1233	411
5.25	8.86	421	568	986	1188	1350	450
3 months							
2.5	4.22	1339	1805	816	984	2453	817
3.0	5.06	1063	1433	944	1137	2181	727
3.5	5.91	924	1246	961	1158	2009	669
4	6.75	1288	1737	869	1047	2426	808
5.25	8.86	1623	2188	996	1200	2978	992
6 months							
2.5	4.22	1778	2397	717	864	2965	988
3.0	5.06	1630	2197	870	1048	2887	962
3.5	5.91	1421	1916	997	1201	2707	902
4	6.75	1920	2588	986	1188	3370	1123
5.25	8.86	2836	3823	129	156	3925	1308
12 months							
2.5	4.22	1931	2603	913	1100	3327	1109
3.0	5.06	1965	2649	975	1175	3423	1141
3.5	5.91	2082	2807	165	199	2938	979
4	6.75	2602	3507	135	163	3615	1205
5.25	8.86	3184	4292	162	195	4421	1473

From this data, except for prisms containing 3.5 kg/m³ Na₂O_e, which showed the least amount of alkali leached, an increase in alkali leaching can be observed as the alkali content of the concrete increased. This is usually the case for alkali boosted concretes (Costa, Mangialardi & Paolini 2017; Rivard et al. 2003). Figure 5.11 illustrates the average total leached alkali measured per AS prism for up to 12 months of CPT. It can be visualised that prisms containing 5.25 kg/m³ Na₂O_e continuously leached relatively higher amounts of alkali. Conversely, for prisms containing 3.5 kg/m³ Na₂O_e, leaching was consistently observed to be lower at all tested ages.

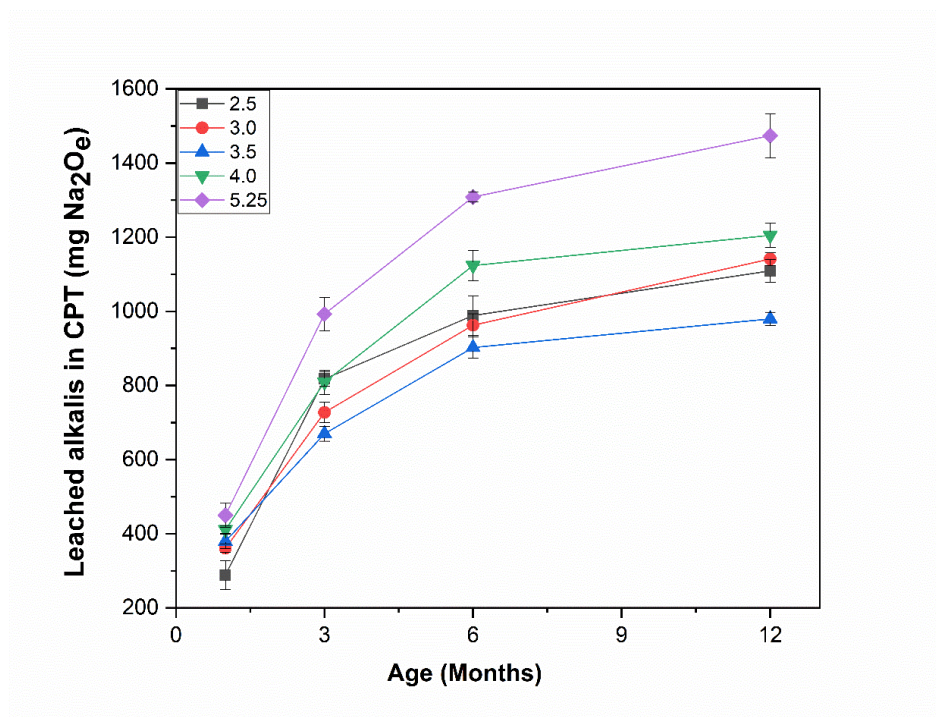


Figure 5.11 Alkali leaching for one prism tested under standard CPT condition at varying alkali contents (total alkali measured divided by three)

The work done on the determination of alkali threshold limits for the different aggregates and sand blends showed that except for prisms composed of aggregate

AS, no significant expansion exceeding the 0.03% expansion limit was measured for all prisms up to and including 4.0 kg/m³ Na₂O_e (Figure 4.8). Assumptions that:

1. Approximately the same amount of alkalis represented in Figure 5.11 (as well as Table 5.4) will be leached out at the end of 12 months for concrete prisms at their respective alkali contents.
2. The alkali safety margin (Section 3.3.3) of 1 kg/m³ Na₂O_e is equivalent to 25% of the 4.0 kg/m³ Na₂O_e alkali content in the concrete.

From Table 5.4, it is apparent that approximately 1205 mg (Na₂O_e) per prism of the total alkali can be leached out at 12 months of CPT testing for prisms containing 4.0 kg/m³ Na₂O_e. This amount can be expressed as 18% of the alkali content per concrete prism, as estimated in Table 5.5.

Table 5.5 Percentage of alkali in safety margin and leached alkali per prism at alkali content of 4.0 kg/m³ Na₂O_e

<p>Assumptions:</p> <ol style="list-style-type: none"> 1. Total alkali content: 4.0 kg/m³ Na₂O_e 2. Volume per prism: 0.0017m³ 3. Alkali content per prism: 6.8 g 4. Safety margin: 1.0 kg/m³ Na₂O_e 	<p>Alkali content of safety margin for 4.0 kg/m³ Na₂O_e</p> <p>= 1.0 kg/m³ × 0.0017m³ = 0.0017 kg = 1.7 g</p>
	<p>Amount of alkali in safety margin as a percentage of total alkali content</p> <p>= $\frac{1.7 \text{ g}}{6.8 \text{ g}} \times 100$ = 25%</p>
	<p>Amount of alkali leached after 12 months of CPT at 4.0 kg/m³ Na₂O_e</p> <p>= $\frac{1.205 \text{ g (1205 mg)}}{6.8 \text{ g}} \times 100$ = 17.7 % ~ 18%</p>

Therefore, it can be inferred that this loss is accounted for as part of the safety margin (25%) allowance; thus, the implementation of the 1 to 1.5 kg/m³ Na₂O_e safety margin in the determination of alkali threshold as suggested by RILEM AAR-7.1 is reasonable. Furthermore, it can be concluded that the proposed alkali limits shown in Table 4.7 that have been derived from RILEM AAR-3.2 and AAR-7.1, may prove to be beneficial for reducing the risk of ASR in the aggregates and sand blends that have been assessed in this study. Implementing the proposed limits, which are lower than 4.0 kg/m³ Na₂O_e, could result in lower alkali leaching, therefore, giving a higher allowance for other unknown uncertainties accounted for by the safety margin.

5.3.4 Assessment of Factors that Affect ASR Expansion

5.3.4.1 Principal Component Analysis (PCA)

The results of PCA on the expansion datasets for determining the significance of the three known principal components (PC): alkali content, temperature, and age, that influence ASR expansion are shown in Figures 5.12 and 5.13 and presented in Appendix A: Table A1. These PCs with their respective eigenvalues are graphically represented as a scree plot in Figure 5.12. From Figure 5.12, it can be seen that PC 1, representing alkali content, has the highest eigenvalue of 8.98105. This result indicates that alkali content is likely to have the largest influence on the outcome of expansion data.

Upon the evaluation of the secondary components of each PC (Appendix A: Tables A2), it can be seen that the constitutional factors affecting PC 1 are not clearly defined. This is evident from the secondary components showing equivalent

eigenvalues of 0.33 to 0.35. In the case of secondary components relating to PC 2, it was revealed that the alkali content followed by temperature has the most influence. A similar observation was made for PC 3, with alkali content and temperature being the most influential factors.

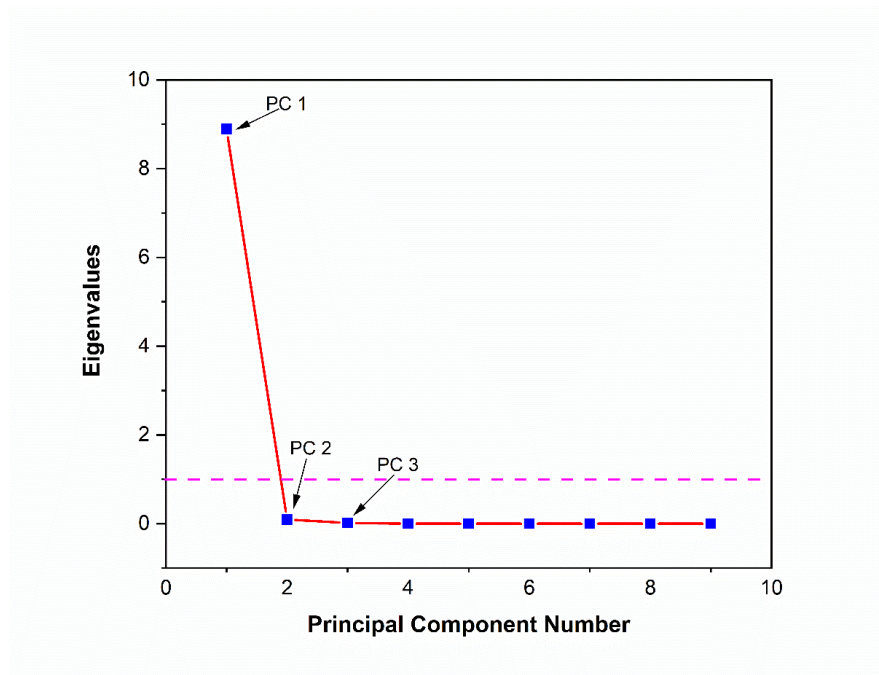


Figure 5.12 Scree plot of extracted principal components and related eigenvalues

The overall outcome of the PCA indicates that the main components of alkali content (PC 1) and temperature (PC 2) are likely the most influential on expansion. The loading plot shown in Figure 5.13 confirms this interpretation. From Figure 5.13, it can be seen the loading representing alkali (AK) is dominant, followed by temperature (T). The component representing alkali content (AK 5.25, AK 3.5, and AK 4.0) is seen to align closely to PC 1 (x-axis) representative of alkali content, which also constitutes 98.7% of the dataset. Conversely, temperature (T 38 and T 60) is centred between the two axes, showing that temperature is relevant to PC 2 and likely related to alkali (PC 1). Age (AG 3 and AG 6) is also observed to align closely

with alkali (PC 1), suggesting that the two components are also likely related. The results from the loading plot agree with the observations made in literature and the empirical studies undertaken in this work; that expansion as a function of age is dependent on the alkali content present. As presented in Table 5.3, alkali leaching increases with age and temperature, and a decrease in alkali can influence ASR expansion. The correlation shown in Figure 5.13 is similar to the observation made in Appendix A: Table A2.

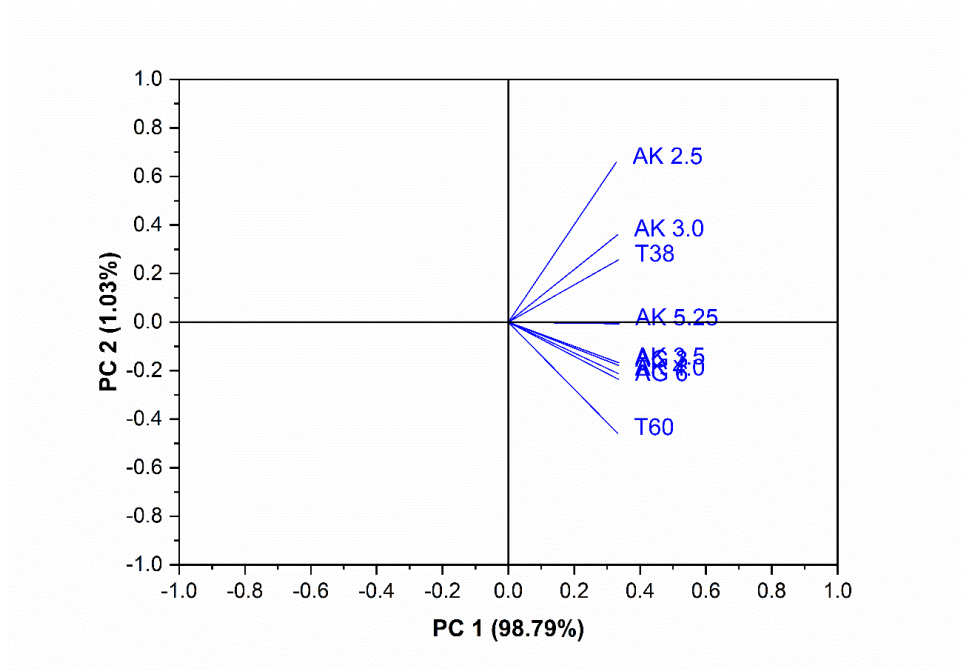


Figure 5.13 Loading plot for variables in principal component analysis

5.3.4.2 Analysis of Variance

The results of the ANOVA studies of the components are shown in Appendix A: Tables A3 and A4. For a confidence level of 95%, the alkali content has a significant effect on the response (expansion), as demonstrated by the p-value of 0.037 (Table A3) and 0.045 (Table A4). However, the analysis showed that temperature and age,

as well as their interaction with alkali content, have no significance on the ASR expansion. The p-values for temperature and its interaction with alkali content were found to be 0.55 and 0.85, respectively, inferring that the null hypothesis is correct. Similarly, the p-value for age was found to be 0.78, and the interaction between age and alkali content showed a p-value of 1.0. These outcomes infer that temperature and age have no effect on the expansion data, and a change in either one of the three respective components is not dependent on the other (Box, Hunter & Hunter 2008). However, this is not the case for age and alkali since a change in alkali is likely dependent on age, as observed in Table 5.3. Nonetheless, in this study, the amount of alkali lost due to alkali leaching was below the alkali threshold of the respective aggregates. Consequently, a decrease in expansion was not observed; thus, this phenomenon did not reflect in the expansion data used for the ANOVA analysis.

Likewise, despite the results obtained from the factorial analysis, a plot of alkali content versus temperature for two selected aggregates, RT and AS (Figure 5.14), confirms that although increasing the alkali content has no interaction with the outcome of temperature, an increase in temperature does affect the response by showing a decrease in expansion. This effect, which is exacerbated by higher alkali leaching occurring with the increase in temperature, was not detected in the factorial analysis. Evidently, the perceived inconsistency in the results from the statistical analysis in this study is likely due to the small set of variables that were considered in the dataset for the analysis (Boivin & Ng 2006). Notwithstanding, the factorial analysis approach used identified the components and showed that the effect of alkali content ($p < 0.05$) is the most influential factor on ASR expansion.

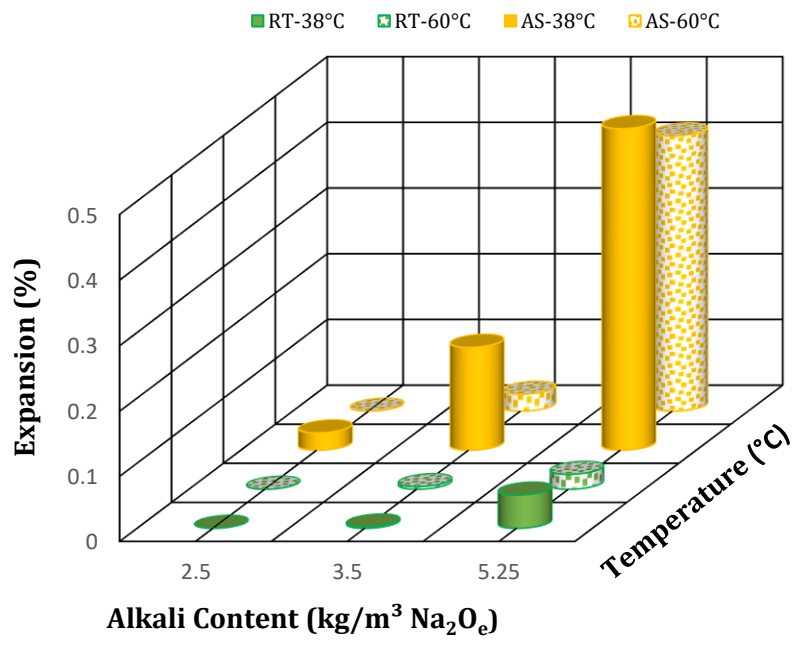


Figure 5.14 Effect of varying alkali and temperature on measured expansion.

Chapter Summary

In this chapter, the reliability of the recognised ASR assessment methods was investigated. A statistical approach was employed to analyse the test results for chemical (GAST) and expansion tests carried out at 80°C (AMBT), 38°C (CPT), and 60°C (ACPT) to determine relationships and interactions amongst the different test methods. In particular, Pearson's correlation coefficient method and a factorial analysis approach using principal component analysis (PCA) and analysis of variance (ANOVA) have been used to explain the variations and commonalities in the ASR expansion data measured by these methods. ANOVA has also been used to identify the significance of the principal components that influence ASR expansion and their interaction significance. Additionally, the effect of temperature and alkali content on leaching, which occurs during CPT and ACPT testing, have been studied to understand their impact on the overall expansion data for aggregates studied under the test conditions and the trustworthiness of the data obtained.

The outcome of these studies showed there is consistency in the reactivity classification of aggregates by the different test methods. In particular, a positive correlation ($r = 0.36$) was established for GAST at 56 days and the standard CPT at 12 months. Likewise, AMBT at 21 days was observed to correlate well ($r = 0.50$) with CPT at 12 months. The results also showed that ACPT expansion from 3 to 6 months is comparable to the CPT expansion at 12 months, with a correlation coefficient (r) of 0.89. However, using MP-AES analysis, the extent of alkali leaching was found to increase with age, temperature, and alkali content. Such that, 16% of alkali leaching was measured after 12 months of CPT and 22% after 6 months of ACPT. Conversely, 18 % alkali leaching at 3 months of ACPT was measured, similar to the 16% alkali

leaching that occurs after 12 months of CPT. Therefore, ACPT at 3 months showed a better correlation to CPT at 12 months. It was further suggested that a lower acceptance limit of expansion might be appropriate for ASR assessment of aggregates using ACPT. The concentration levels of alkali leaching in this study are lower than what is usually reported in literature. This outcome is likely related to the reactivity level of the aggregates used in this study and the possible influence of finely ground aggregate fines in the cement binder that potentially contributes to pozzolanic activity and the formation of secondary C-S-H phases that further bind the alkali.

Furthermore, factorial analysis performed on the expansion data revealed that the two main factors that drive ASR and, thus, the reliability of physical test methods that measure expansion are alkali content and temperature. Nonetheless, ANOVA revealed that the effect of alkali content is significant ($p=0.038$) than that of temperature, which was confirmed by the resulting p-value of 0.55 at a 95% confidence level. Further evaluation also proved an increase in temperature resulted in a decrease in expansion associated with higher alkali leaching.

CHAPTER 6. Investigating the ASR Mitigation

Potential of Ground Reactive Aggregate Fines

6.1 Overview

The use of supplementary cementitious materials (SCMs) such as fly ash, granulated blast furnace slag, silica fume, and metakaolin in concrete is globally accepted as an effective approach to mitigate ASR (Lumley 1993; Shekarchi et al. 2010; Thomas 1996b). The ASR mitigation mechanism associated with the use of SCM has been discussed thoroughly in Section 2.7.3.3. Having been used as a partial replacement of cement in concrete for several decades, many of the benefits of using SCMs are well-documented and understood (Khatri, Sirivivatnanon & Gross 1995; Lothenbach, Scrivener & Hooton 2011; Snellings 2016). Typically, SCMs are sourced as industrial by-products or waste materials from industrial processes. For instance, fly ash is generated as waste from coal combustion in thermal plants, and silica fume is derived as a by-product of manufacturing silicon and ferrosilicon alloys. Consequently, with the world moving towards greener technologies in the pursuit of conserving the environment, the obtainability of SCMs for ASR mitigation in the future is expected to decrease. This is mainly due to changes in materials processing technologies and the impending shutdown of coal power plants. Moreover, for countries like New Zealand, the option of adding SCMs to concrete is expensive, as these materials are not readily available (Chandra Paul et al. 2019; Durant, Bigley & Milestone 2013). This realisation has inspired a series of researches targeted at exploring the possibility of utilising available resources, including mining, agricultural, consumer, and recycled construction waste, as alternative SCMs for

ASR mitigation (Kazmi et al. 2017; Sousa et al. 2011). One material that has often been considered as an alternative SCM to traditional SCMs is cullet glass (Afshinnia & Rangaraju 2015a; Rashidian-Dezfouli, Afshinnia & Rangaraju 2018; Zheng 2016). This is mainly because, similar to traditional SCMs, ground cullet glass contains a large quantity of amorphous silica and has been reported to not react with alkali to form deleterious ASR below the particle size of 300 μm (Meyer & Xi 1999; Shi et al. 2004). In this manner, ground reactive aggregates may also be considered a feasible option for alternative SCMs. Aggregates are an abundant resource that can be readily obtained in developing countries. However, limited studies have focused on the efficacy and mechanism of using ground reactive aggregate fines in concretes for mitigating ASR.

In this chapter, the work done on the addition of ground reactive aggregate fines (GRAFs) to pastes, mortars, and concretes as potential additives for mitigating ASR will be discussed. The experimental program used for this study follows the RILEM recommended test protocol for assessing ASR (Section 2.7) with the inclusion of chemical dissolution tests and post-expansion characterisation. The results of this study will elucidate the effect of dosage and the mechanism by which GRAFs mitigate ASR through analytical techniques and chemical and physical expansion tests that have been carried out on pastes, mortar, and concrete specimens. Further, the effect of GRAFs on basic mechanical properties, the pore solution chemistry, and ASR gel composition will also be presented.

6.2 Experimental Plan

6.2.1 Materials

6.2.1.1 Ground Reactive Aggregate Fines (GRAFs)

As listed in Table 6.1, three different types of aggregates were studied for their potential in mitigating ASR when finely ground. Table 6.1 also presents the amount of free silica in the aggregates as determined by petrography. GRAFs were prepared by grinding the as-received aggregates in a ring mill for 10 min. A typical example of the GRAFs produced and the particle size distribution of the GRAFs as determined by laser diffraction is shown in Figure 6.1 and Table 6.3. Due to the capacity of the grinding equipment available, it was challenging to achieve fineness equivalent to fly ash (FA) and cement. Additionally, although the GRAFs were grinded for the same period of time, it can be observed that their particle size distribution differs. This could be attributed to the relative hardness of the minerals in the respective aggregates; thus, some aggregates requiring a longer grinding time to achieve the same fineness as the other GRAFs.

Similarly, the chemical composition of the GRAFs determined by XRF is presented in Table 6.2. To compare the effectiveness of GRAFs to traditional SCMs, conventional fly ash (FA) was also used in this study. The chemical composition and particle size of the FA used are also given in Table 6.2 and Figure 6.1, respectively. Table 6.2 shows the total silica phase in the chemical composition of the materials, including free silica and silica bound in other compounds such as aluminosilicates. The percentage sodium equivalent (Na_2O_e) of the FA was found via XRF to be 0.85%, higher than the percentage measured in the cement used.

Table 6.1 Details of the ground reactive aggregates used in this study determined by petrography

Ground Reactive Aggregate Fines (GRAFs)	Symbol	Type of aggregate	Amount of free silica (%)	Reactivity as per petrography
Waikato	WT _G	Natural river sand	33	Reactive
Greywacke	GW _G	Manufactured sand	21	Mild-slowly reactive
Rhyolite	RH _G	Manufactured sand	45	Reactive

Table 6.2 Chemical composition of GRAFs, FA, and cement determined by XRF

Oxides (%)	WT _G	GW _G	RH _G	FA	Cement
Na ₂ O	4.31	4.79	5.65	0.3	0.25
MgO	1.43	2.45	1.57	1.1	0.95
Al ₂ O ₃	14.21	15.79	15.44	26.3	3.8
SiO ₂	62.93	60.73	61.93	58.0	20.79
P ₂ O ₅	0.04	0.21	0.18	0.48	0.18
SO ₃	<0.01	0.13	0.07	0.3	2.25
K ₂ O	1.09	2.70	2.89	0.84	0.50
CaO	3.46	3.64	2.30	3.6	64.55
TiO ₂	0.55	0.80	0.81	1.4	0.28
Mn ₃ O ₄	0.09	0.10	0.10	0.10	0.08
Fe ₂ O ₃	4.45	5.98	5.75	7.2	2.52
LOI	7.08	2.96	4.09	0.9	3.20

Cement

Cement with a total alkali content of 0.58% (Section 3.2.2) was used for the preparation of paste, mortar, and concrete specimens. Details of the particle size and chemical composition of the cement are given in Figure 6.1 and Table 6.2, respectively. The particle size analysis shows that a high volume of the cement and FA particles were found in the range of 10 to 70 μm , whereas the GRAFs had almost an equal volume of particles ranging from 1 to 110 μm . The particle size distribution of the GRAFs, FA and cement is also given in Table 6.3.

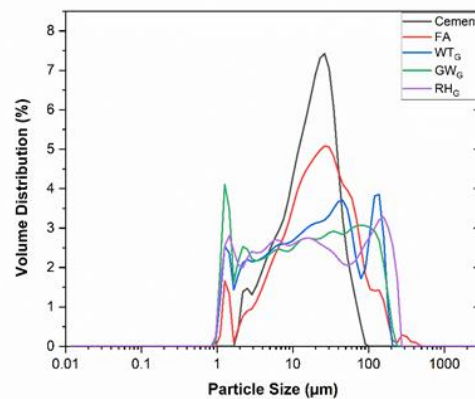


Figure 6.1 A typical example of GRAFs used and the particle size distribution of cement, GRAFs, and FA

Table 6.3 Particle Size distribution of GRAFs, cement, and FA

Sample ID	$d_{0.1}$ (μm)	$d_{0.5}$ (μm)	$d_{0.9}$ (μm)
WT _G	1.973	17.543	110.409
GW _G	1.475	15.150	101.898
RH _G	1.706	15.618	141.417
Cement	3.608	14.060	36.834
FA	4.133	20.422	74.418

6.2.1.2 Reference Aggregates

For this work, two reactive fine aggregates: Waikato (WT) and Rangitikei (RT) river sands, were selected as the aggregates for testing the mitigation efficacy of GRAFs. The reactivity classification of the fine aggregates according to petrography, chemical, and physical expansion tests is presented in Table 5.1. A non-reactive coarse aggregate: Peats Ridge (PR), was used as the reference aggregate with aggregate WT for the concrete prism expansion tests.

6.2.2 Methods

Table 6.4 presents a summary of the test program for the study carried out in the GRAFs investigation.

Table 6.4 Summary of the test program for investigating the ASR mitigation potential of GRAFs

Test Schedule	Description		Materials
1	Chemical Test <i>Solution: 1M NaOH</i> <i>Temp: 80°C</i> <i>Test duration: up to 28 days</i>		WT _G , GW _G , RH _G , and FA
2	Paste studies	Pore solution analysis <i>Temp: 23°C, 38°C, and 60°C</i> <i>Test duration: 28, 90, and 180 days</i>	WT, GRAFs, and FA GRAFs dosage: 25%
		Thermogravimetric analysis <i>Temp: 80°C</i> <i>Test duration: 7, 14, 21, and 28 days</i>	WT, GRAFs, and FA GRAFs dosage : 0, 10, 25, 40 %
3	Expansion Tests	Accelerated mortar bar test at 80°C (AS 1141.60.1)	Fine aggregates: WT and RT Binder system: Cement, GRAFs, and FA GRAFs dosage : 0, 10, 25, 40%
		Concrete prism test at 60°C (modified AS 1141.60.2)	Fine aggregate: WT Coarse aggregate: Inert PRc
		Concrete prism test at 38°C (AS 1141.60.2)	Binder system: Cement, GRAFs, and FA GRAFs dosage: 25%
4	Compression and flexural strength tests <i>Curing: 23°C; >90% humidity; 28 days</i>		Fine aggregate: WT Coarse aggregate: Inert PRc Binder system: Cement, GRAFs, and FA GRAFs dosage: 25%

6.2.3 Chemical Tests

6.2.3.1 Dissolution of Silicon and Aluminium from GRAF in Alkaline

Solution

The amount of silicon (Si) and aluminium (Al) released from the respective GRAFs and FA in alkaline solution was investigated. 5 ± 0.1 g of each material was reacted with 1M NaOH at 80°C in a solute-to-solvent mass ratio of 1:2. Four slurries (for the respective ages) were prepared for each material in HDPE centrifuge tubes. The concentration of the released Si and Al in the solution was measured using MP-AES at ages 7, 14, 21, and 28 days following the procedure described in Section 3.5.6.

At each age, 5 ml of the supernatant liquid was siphoned for MP-AES. The solid residue was filtered out with a vacuum funnel and dried in a vacuum oven at 45°C for three days. At the end of 28 days, microstructural changes and phase development on the solid residue of the reacted samples were investigated using SEM and XRD, respectively.

6.2.3.2 Paste Studies

Pore Solution Chemistry

The concentration of ions in the pore solution is essential to understand the progression of ASR in concretes. Pore solution studies may be carried out on mortar and concrete specimens; however, aggregates from the mortar can affect the pore solution's alkalinity and composition (Drolet, Duchesne & Fournier 2017). Moreover, in this work, where GRAFs are being studied for their influence on the pore solution chemistry and ASR mitigative effect, the involvement of additional

aggregates could interfere with the results obtained. Therefore in this study, pore solution analysis was carried out on paste specimens.

Sample Preparation

Paste specimens containing 25% GRAFs cement replacement were prepared in a Hobart mixer with a water to cement ratio of 0.5. Mixing was carried out for 90 s with a 60 s wait, followed by additional mixing for 60 s. This procedure successfully achieved a homogenous dispersal of GRAFs (Figure 6.2), which is essential for the effective performance of additives in the concretes (Mehdipour & Khayat 2016).

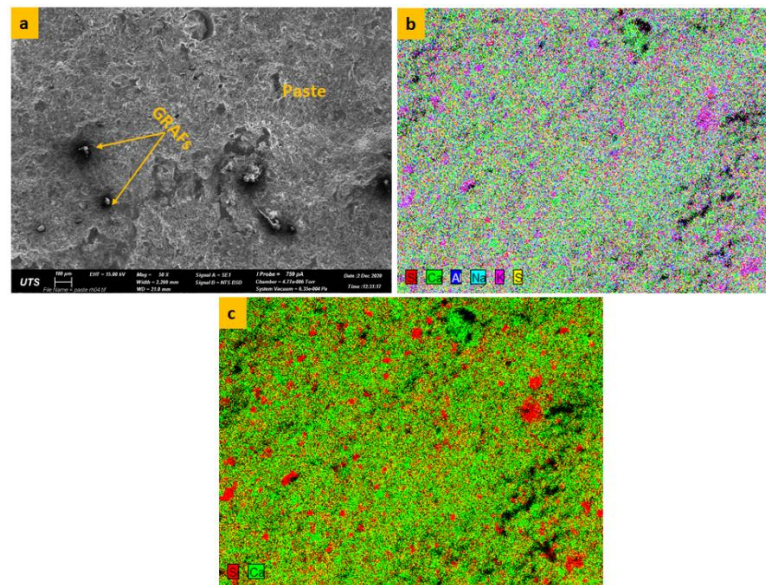


Figure 6.2 SEM micrograph and elemental mapping of fractured hardened paste surface showing (a) GRAFs in cement paste and (b-c) well-dispersed GRAFs (Si) in paste (*Note: Paste contains 25% RH_G*)

A total of ten cylindrical test specimens were prepared for each mix studied. The paste mixes were cured in cylindrical moulds of dimensions (\varnothing) 50 mm \times 100 mm for 24 hours. The cylindrical moulds were covered with plastic wrap during this

period to reduce carbonation and retain moisture. After 24 hours, the cylindrical specimens were demoulded and wrapped thoroughly in cling film to avoid potential alkali leaching and moisture loss that may occur during curing at the respective temperatures. Specimens were stored above deionized water in a sealed container to ensure high humidity (Figure 6.3b). Curing was achieved at 23°C, 38°C, and 60°C for 28 days. Additional specimens were cured at 38°C for 90 and 180 days.



Figure 6.3 Photographs of paste specimens during curing phase for pore solution analysis

Pore Solution Extraction and Analysis

Pore solutions were extracted from hardened paste under high compressive load (800 kN) using a mechanical pore extraction device (Barneyback Jr & Diamond 1981; Longuet, Burglen & Zelwer 1973). A schematic of the pore extraction device and the set-up used to extract the pore solution in this work is shown in Figure 6.4.

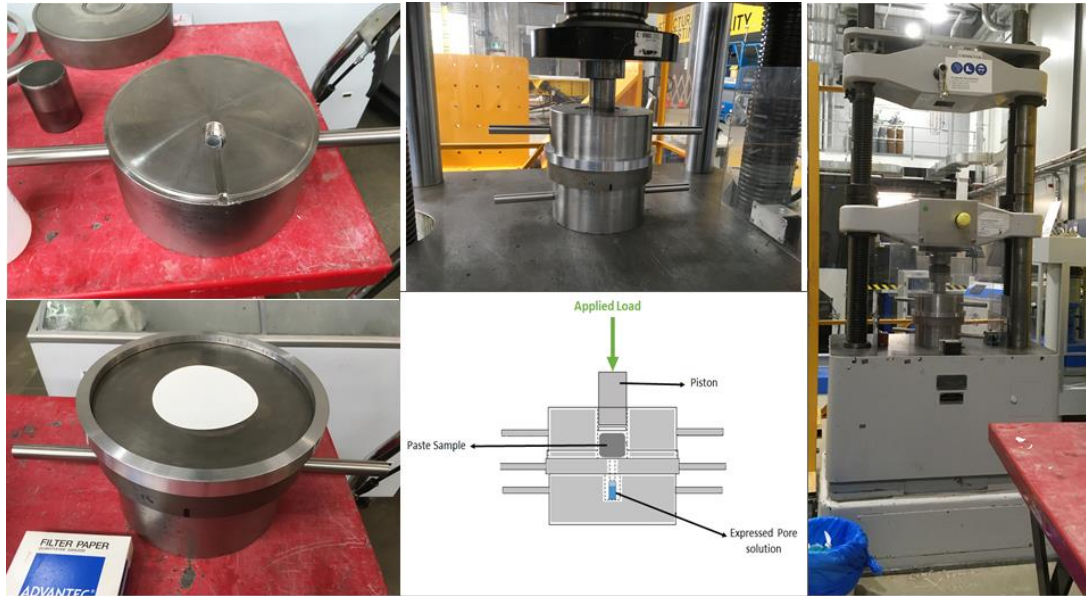


Figure 6.4 Illustration of pore solution extraction device

Before pore solution extraction, specimens cured at 38°C and 60°C were conditioned to room temperature. A continuous load was applied on the piston at 2000 N/s until a maximum load of 800 kN was reached. The load was maintained at 800 kN for 5 minutes to extract pore solution into a polyethylene vial. For paste specimens cured at 38°C for 90 and 180 days, a holding time of 10 minutes was employed. Approximately 5 ml of pore solution was obtained from each cylindrical paste specimen. The collected pore solutions were immediately filtered through a 0.45 µm micro filter to remove any cement residue that may continue to hydrate. Likewise, the pore solution's pH was determined within 2 hours of extraction using a Thermo Scientific temperature-PH meter at 23 ± 0.02 °C. The pH of each sample was measured twice, and the average value was calculated. During pH measurements, the probe was rinsed in deionized water after each reading. Similarly, the pH meter was calibrated before and mid measurements, with buffer solutions of pH 4.0 and 10.0.

1 ml of each pore solution was subsequently diluted with 1% nitric acid for MP-AES analysis within 48 hours of extraction. Two dilution ratios of 1:1000 for the determination of Na⁺ and K⁺ ion concentrations and 1:20 for Ca²⁺, Si²⁺, and Al³⁺ ion concentrations were used. To check reproducibility and equipment error, two MP-AES samples were prepared from each sample for MP-AES analysis. The remaining pore solutions were acidified with 69% nitric acid to prevent precipitation of alkali ions and sealed with parafilm as backup solutions. Both diluted and backup specimens were stored at 5°C until the time of testing.

Thermogravimetric Analysis

Pastes containing 0, 10, 25, and 40% GRAFs were prepared using deionized water, with a water-to-cement ratio of 0.5 in HDPE tubes. The pastes were tested at 80°C for 28 days. After 28 days, the hardened pastes were pulverised in a ring mill for 2 minutes. Thermogravimetric analysis was then carried out on the powdered pastes to determine the residual portlandite amount present in the paste. Additionally, pastes containing 25% GRAFs cured at 38°C and 60°C for 28 days were also studied using thermogravimetric analysis.

6.2.4 Expansion Tests

6.2.4.1 Accelerated Mortar Bar Test (AMBT)

AMBT tests as per AS 1141.60.1 were carried out on mortar bars containing 0, 10, 25, and 40% GRAFs for an extended period of 56 days. Mortar bars with 25% FA were also studied. During AMBT, two reactive sands, WT and RT, were selected as

the test sands for investigating the effectiveness of GRAFs in mitigating expansion due to ASR.

6.2.4.2 Concrete Prism Tests (CPT) and Accelerated Concrete Prism Tests (ACPT)

The concrete mix design indicating the proportion of fine and coarse aggregates used for producing the concrete and the fresh properties of the concrete studied in this investigation are given in Appendix B: Table B6. Concrete prism tests were carried out as per AS 1141.60.2 at 38°C (CPT) and 60°C (ACPT) for prisms composed of reactive fine sand WT and non-reactive coarse aggregate PR_c, at a cement replacement level of 25%. This replacement level was chosen to meet workability, strength, and durability requirements that are often prescribed in commercial-grade concrete mixes and to alleviate higher GRAFs dosage, potentially impacting 28-day requirements. This dosage also allows a direct comparison of the performance of GRAFs against FA, which is mostly used at a recommended dosage of 25% (Standards Australia 2015). Expansion for CPT prisms was monitored for 12 months (to be extended to 24 months), whereas ACPT prisms were monitored for an extended test period of 8 months.

For Each 30 litre concrete mix produced, six prisms of dimensions 75 mm x 75 mm x 285 mm (C1), two prisms of dimensions 100 mm x 100 mm x 300 mm (C2), and three cylinders with dimensions 100 mm (∅) x 200 mm (C3) were cast as shown in Figure 6.5. Sample set C1 was tested under CPT and ACPT conditions, whereas C2 and C3 were cured at >90% relative humidity for 28 days to determine the effect of

GRAFs on the flexural and compressive strength of the hardened concrete in the procedure described in Section 3.5.8.

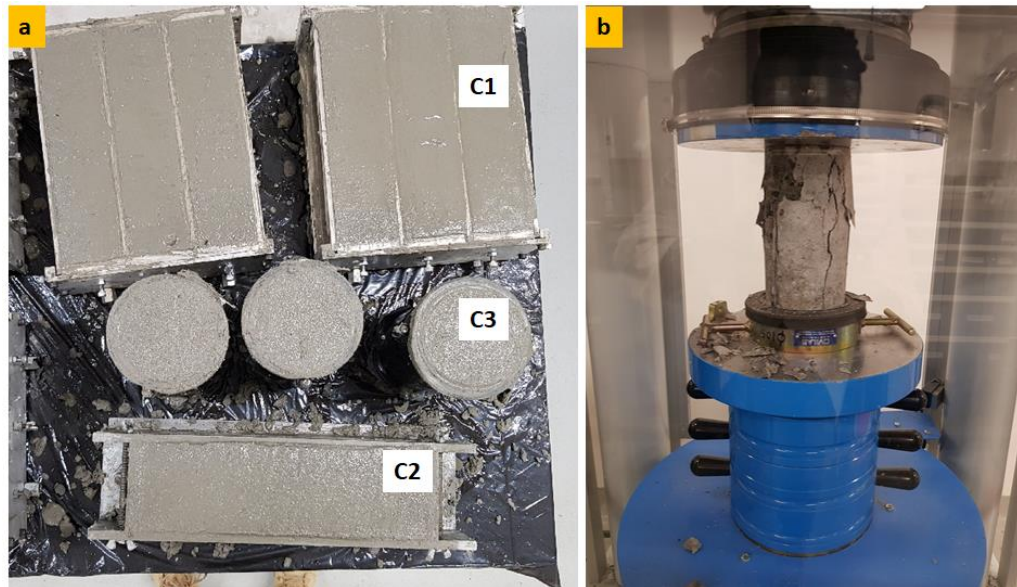


Figure 6.5 Photograph of (a) concrete specimens cast for the various tests and (b) concrete cylinder during 28 days compressive strength testing

6.3 Results and Discussion

6.3.1 Determination of Silicon and Aluminium released from Ground Reactive Aggregate Fines (GRAFs) in Alkali solution

Figures 6.6 and 6.7 show the concentration of silicon (Si) and aluminium (Al) ions released by the GRAFs and FA in alkali solution at 80°C. From Figure 6.6, it can be seen that the amount of Si dissolved into solution increases with time for all the materials tested. The highest amount of released Si was measured for FA samples.

This result is expected as FA generally contains a high amount of reactive silica that readily dissolves into solution (Skibsted & Snellings 2019). For the GRAFs, although the petrographic assessment of the aggregates showed that RH contained the highest percentage of silica, the order of the amount of Si released was found to be $WT_G > RH_G > GW_G$. This suggests that the amount of soluble silica in aggregate RH is lower compared to WT. Additionally, the dissolution rate of the reactive silica minerals in RH may be slower than that of WT. Aggregate WT has been found to contain very reactive forms of silica such as tridymite, cristobalite, and volcanic glass (Section 4.3.1). This could have influenced a higher dissolution of silica in alkaline solution, resulting in the observation obtained. It is also noticeable that at the end of the 28-day test GW_G recorded a slightly higher amount of Si than RH_G ; however, the difference between the amount of Si released by GW_G and RH_G is minimal.

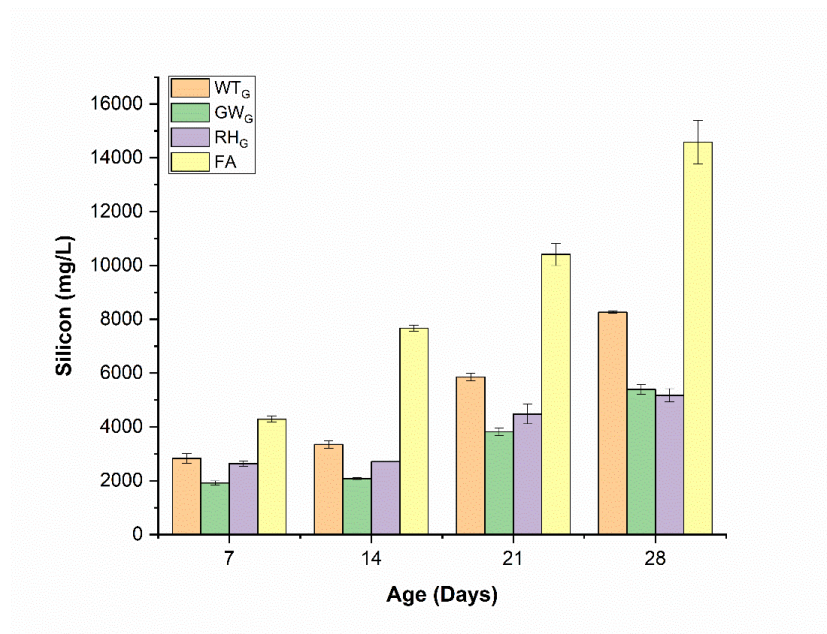


Figure 6.6 Concentration of silicon released by GRAFs and FA in 1M NaOH at 80°C

Similarly, the reference SCM, FA, showed a higher release of Al compared to the GRAFs in the column graph presented in Figure 6.7. In particular, WT_G measured a higher Al concentration followed by GW_G and then RH_G . Contrary to Si, the amount concentration of Al was observed to reduce with age for all the samples tested. This may be associated with the precipitation of Al through the development of new aluminosilicate phases (Duxson et al. 2007; Fernández-Jiménez, Palomo & Criado 2005) as observed in the XRD diffraction patterns of the reacted materials (Figure 6.13). Thus, the amount of Al (and Si) measured is essentially the remainder in solution post the formation of new phases.

The presence of reactive Al has been reported to increase the effectiveness of SCMs by encouraging the formation of aluminosilicate phases that potentially form a layer on the aggregates' surface, which prevents further dilution of the silica. Furthermore, the reaction to form these phases consumes dissolved silica, and the aluminosilicates formed tend to bind alkali from solution. As a result, the amount of silica and alkali available in the pore solution to form ASR products is reduced (Chappex & Scrivener 2012; Hüniger 2007). Thus, it can be hypothesized that the efficacy of GRAFs in mitigating ASR may fall in the order $WT_G > GW_G > RH_G$.

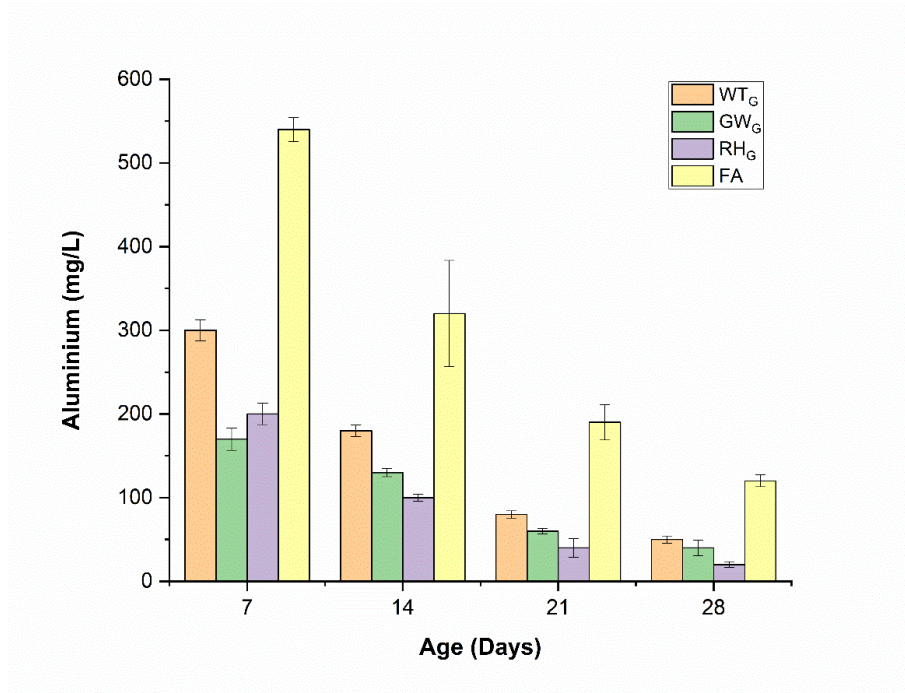


Figure 6.7 Concentration of aluminium released by GRAFs and FA in 1M NaOH at 80°C

6.3.1.1 Characterisation of reaction products

Figure 6.8 shows the change in the morphology and phase development of FA reacted at 80°C in alkali solution for 28 days. To prevent potential damage to the microstructure, dried reacted products were not ground prior to SEM analysis. This is reflected by the agglomeration (increase in particle size) of the particles observed in the micrographs for FA as well as all the GRAFs studied.

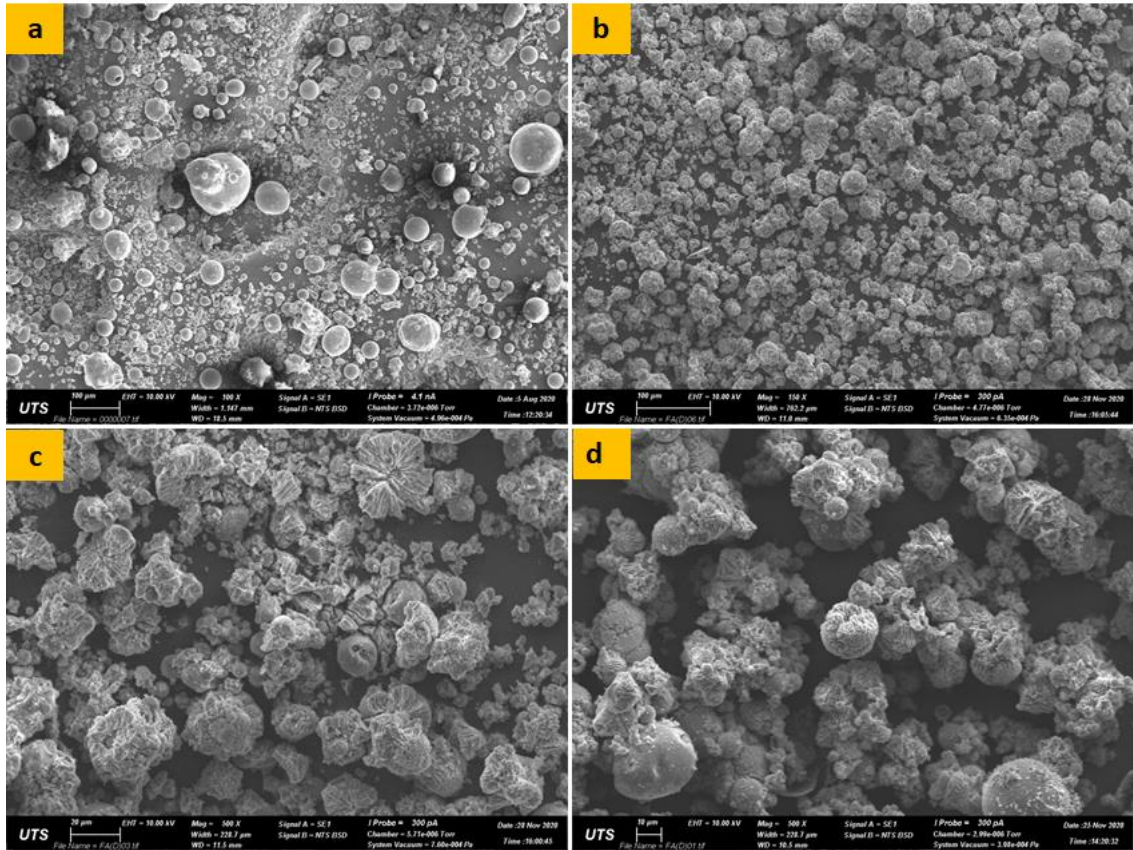


Figure 6.8 Microstructure of (a) unreacted FA and (b-d) FA treated in 1M NaOH alkali solution at 80°C after 28 days

Figure 6.8a shows that the unreacted FA particles are spherical in shape with a reasonably smooth surface texture. This is typical of air-borne materials (Jordanidis et al. 2008). At the end of 28 days test in 1M NaOH, the microstructure of the FA particles appears to have reformed into a fleurette structure characteristic of zeolite. Some FA particles also showed a less defined microstructure representative of sodium aluminium silicate hydrate (N-A-S-H) (Alehyen, Achouri & Taibi 2017; Palomo et al. 2015), whereas some unreacted FA particles were also observed (Figure 6.8d).

The alkali activation of FA ensues in a process that is best described as zeolitisation (Ojha, Pradhan & Samanta 2004). Zeolitization occurs in three distinct steps identified as: (i) dissolution of Si and Al from FA; (ii) condensation of silicate and aluminate ions in alkali solution to form aluminosilicate hydrogel; and (iii) crystallization of the gel to form zeolite. This process is summarised in the schematic provided in Figure 6.9.

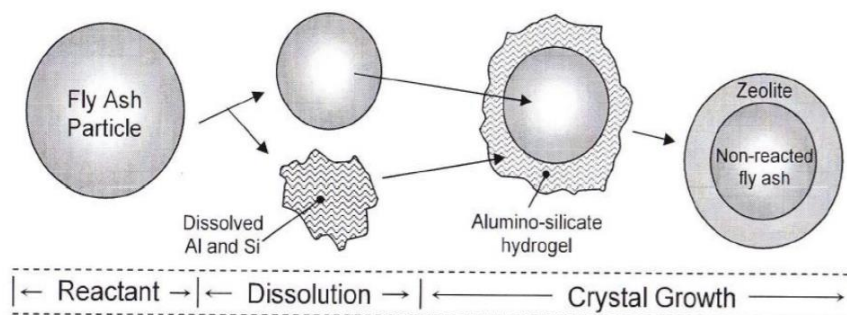


Figure 6.9 Schematic showing the zeolitisation process of FA (Fansuri, Pritchard & Zhang 2008)

The supposed layering of aluminosilicate hydrogel and zeolite can be clearly seen on GRAFs surfaces, as shown in the SEM images in Figures 6.10b to Figure 6.10d.

The microstructural changes of WT_G particles are presented in Figure 6.10. Before the dissolution test, the particle shape of WT_G is observed to be angular in shape, with a few particles exceeding 100 μm in size (Figure 6.1). A similar observation in particle size distribution can be made for all unreacted GRAFs. At the end of the dissolution test, the microstructure of some of the WT_G particles was seen to be porous, indicating a depletion of silica, whereas other particles appeared unreacted. In Figures 6.10c to 6.10d, a clear indication of the above-mentioned aluminium-

silicate layering on the aggregate particles can be seen. At a higher magnification level of 500x (Figure 6.10d), the reacted particles' microstructure showed a homogenous product consisting of clusters of nearly uniformly sized spherical and cubical particles. This feature is characteristic of the formation of analcime zeolite (N-A-S-H phase with low Si/Al ratio) (Azizi, Alavi Daghigh & Abrishamkar 2013; Chen et al. 2017; Novotna et al. 2003).

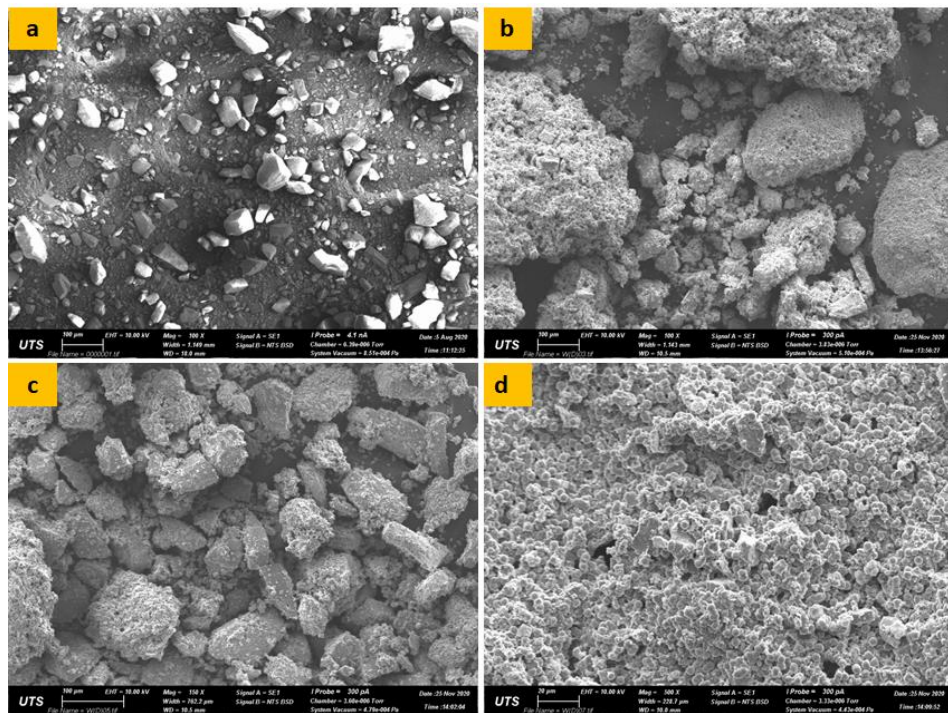


Figure 6.10 Microstructure of (a) unreacted WT_G and (b-d) WT_G treated in 1M NaOH alkali solution at 80°C after 28 days

GW_G and RH_G (Figures 6.11 and 6.12) showed relatively less evidence of reactivity (silica depletion induced porosity) and precipitation of reaction products as compared to WT_G. This is consistent with the lower levels of the respective Si and Al ion concentrations recorded for these materials (Figures 6.6 and 6.7). Nonetheless,

the microstructure of the reacted GW_G and RH_G particles showed the presence of analcime zeolite (identified by XRD in Figure 6.13) and a less defined microstructure identified by some researchers as the metastable zeolite-p phase (Azizi & Ehsani Tilami 2009). Zeolite-p is usually present in materials that exhibit a slow dissolution rate in NaOH solution (Chen et al., 2017). Overall, it can be gathered from the SEM micrographs that a relatively high amount of GW_G particles were unreacted compared to RH_G . This is corroborative to the lower Si concentration measured in the dissolution test.

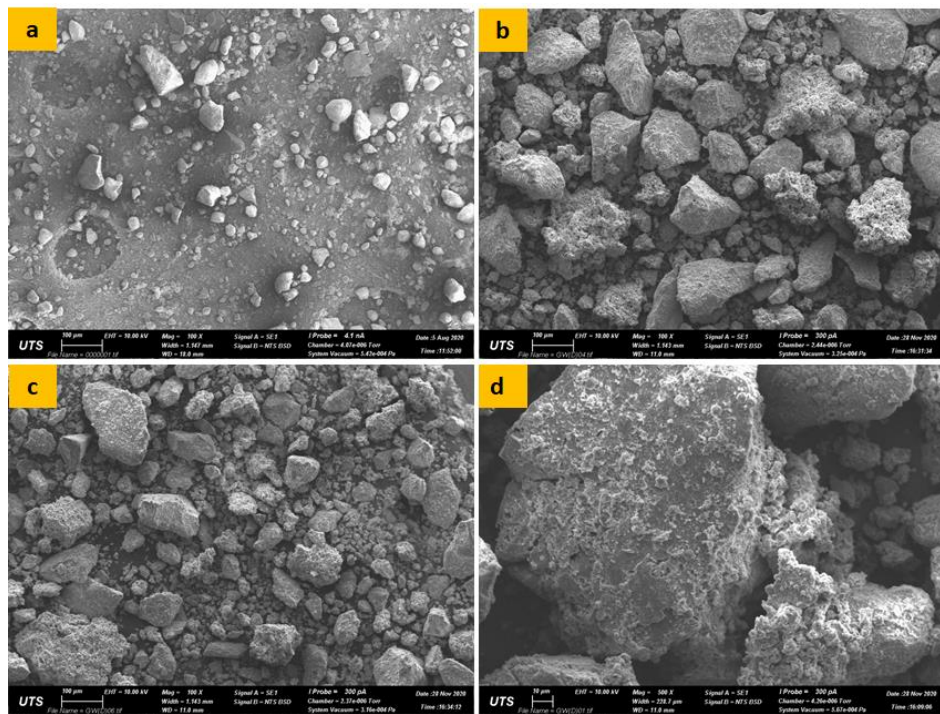


Figure 6.11 Microstructure of (a) unreacted GW_G and (b-d) GW_G treated in 1M NaOH alkali solution at 80°C after 28 days

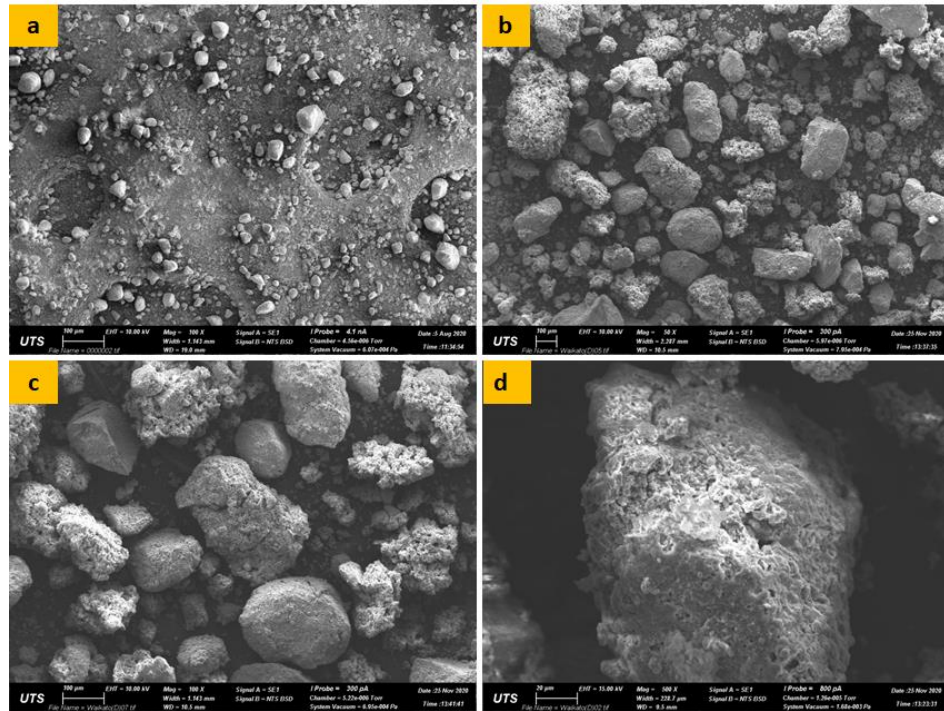
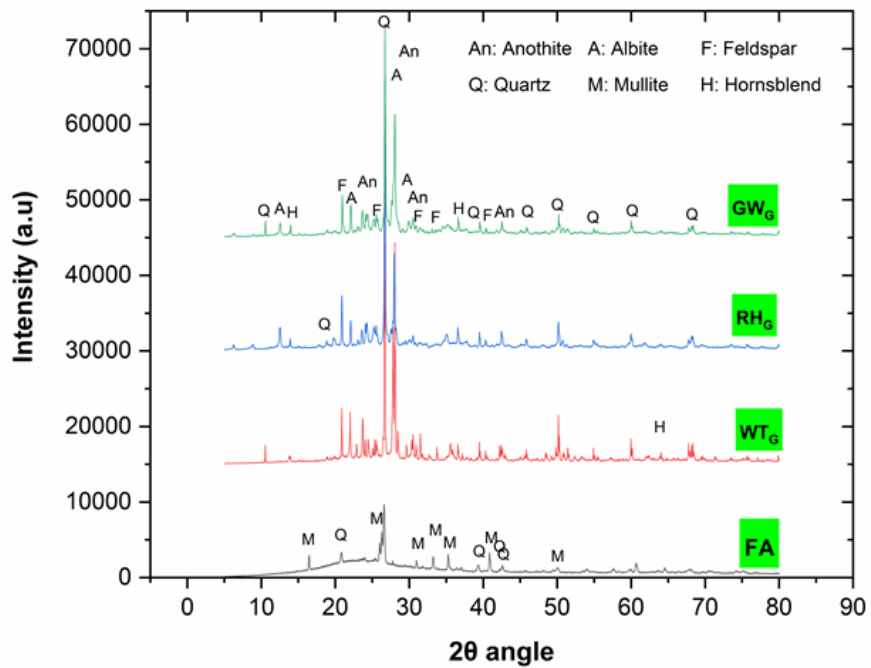


Figure 6.12 Microstructure of (a) unreacted RH_G and (b-d) RH_G treated in 1M NaOH alkali solution at 80°C after 28 days

The reaction products from the WT_G, GW_G, and RH_G studies were further characterised with XRD to qualify the phase changes in the aggregate. The XRD patterns of the GRAFs and FA before and after the dissolution test are shown in Figure 6.13. FA showed the presence of mullite and quartz as the main phases in the material. A large 'halo' under the quartz peak at 22° (2θ) is also evident, signifying the presence of amorphous silica in the FA. Conversely, GRAFs were found to be mainly composed of phases identified as quartz, albite, anorthite, and feldspar. At 38° (2θ) and 64° (2θ) (for WT_G), peaks representing hornblende were also identified.

a



b

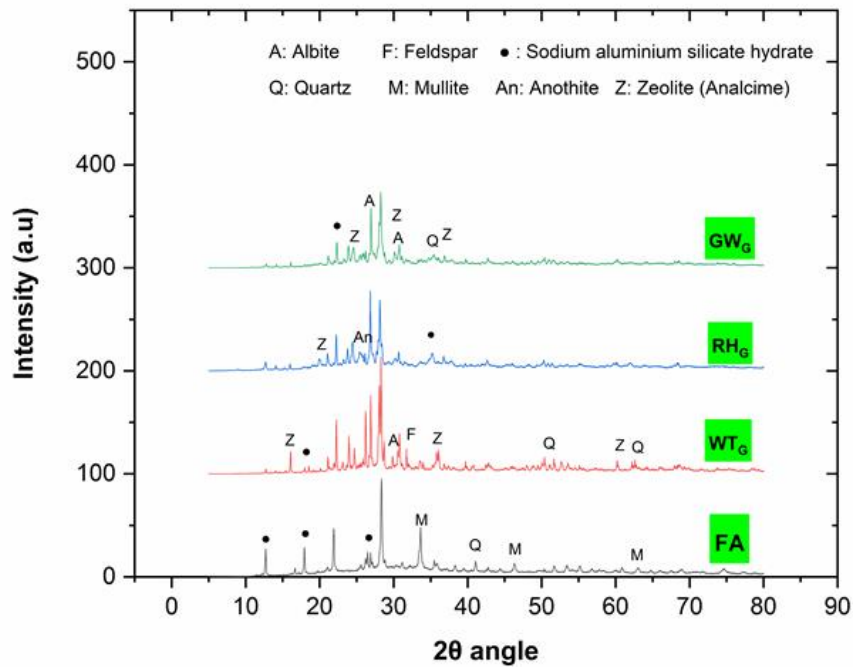


Figure 6.13 XRD diffraction patterns of GRAFs and FA (a) untreated and (b) treated in 1M NaOH at 80°C after 28 days

After 28 days of dissolution test in alkaline solution (Figure 6.13b), FA samples showed a reduction in the amorphous silica 'halo', suggesting the depletion of reactive silica in the formation of the aluminosilicate phases. Furthermore, FA samples showed some disappearance of mullite peaks in place of precursor sodium aluminium silicate hydrate (N-A-S-H) and zeolite phases. This is consistent with other studies and confirms the microstructural features observed (Criado et al. 2007). The XRD analysis of the GRAFs also showed evidence of silica depletion evident by the diminishing, with reference to the ratio of the quartz peak at $28^\circ(2\theta)$ and albite peak at $29^\circ(2\theta)$. The presence of zeolite, resulting from the reaction of silica with feldspar and albite, was also detected. This observation is consistent for all the GRAFs studied. The XRD analysis also showed the presence of some albite, anorthite, and feldspar phases, supporting that some of the particles are either partially reacted or unreacted.

6.3.2 Influence of Ground Reactive Aggregate Fines (GRAFs) on the Pore Solution Chemistry of Pastes

6.3.2.1 Alkalinity (pH) of Pore Solutions

The measured pH values of the pore solution of pastes cured at 23°C , 38°C , and 60°C for 28 days are shown in Figure 6.14. Generally, the pH for all the paste samples was seen to decrease with an increase in temperature. This result may arise from the higher rate of dissociation of water as temperature increases, thus affecting the hydrogen ion concentration (Thomas et al. 2003). The pH range recorded in this study was between 12.7 and 13.4. This is consistent with the values reported in

other studies carried out on pozzolanic cement systems containing ASR mitigating additives (Alonso, Garcia & Walker 2012; Andersson et al. 1989; Coleman & Page 1997; Vollpracht et al. 2016).

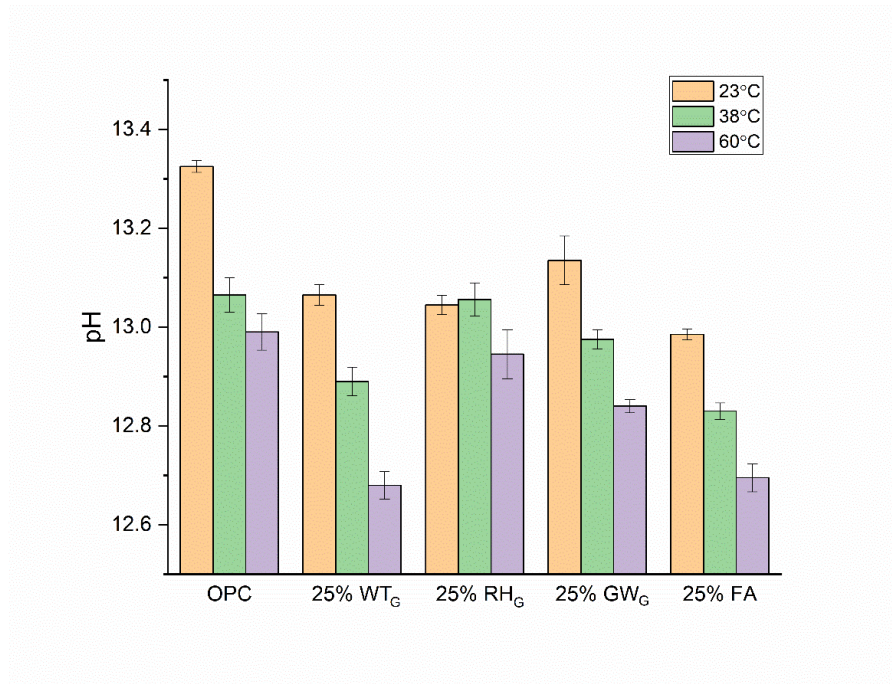


Figure 6.14 Effect of temperature on the measured pH of pore solutions of pastes containing GRAFs after 28 days

At any given temperature, the pH of pastes containing 100% cement (OPC) is higher than pastes containing 25% GRAFs. Although it can be argued that the replacement of part of the cement certainly reduces the alkali content present in the system, it can also be appreciated that the pH value (alkalinity) of the pore solution is influenced by the type of GRAFs present. In particular, pastes with 25% WT_G were found to reduce the alkalinity of the pore solution more, followed by GW_G and then RH_G. This trend was found to be more apparent at a higher test temperature (60°C) and is associated with the pozzolanic reaction of GRAFs resulting in alkali binding through the formation of reaction products.

Considering the effect of the GRAFs at 38°C at 28, 90, and 180 days (Figure 6.15), it is perceived that after 90 days, the alkalinity of the pore solution was higher regardless of the composition of the paste.

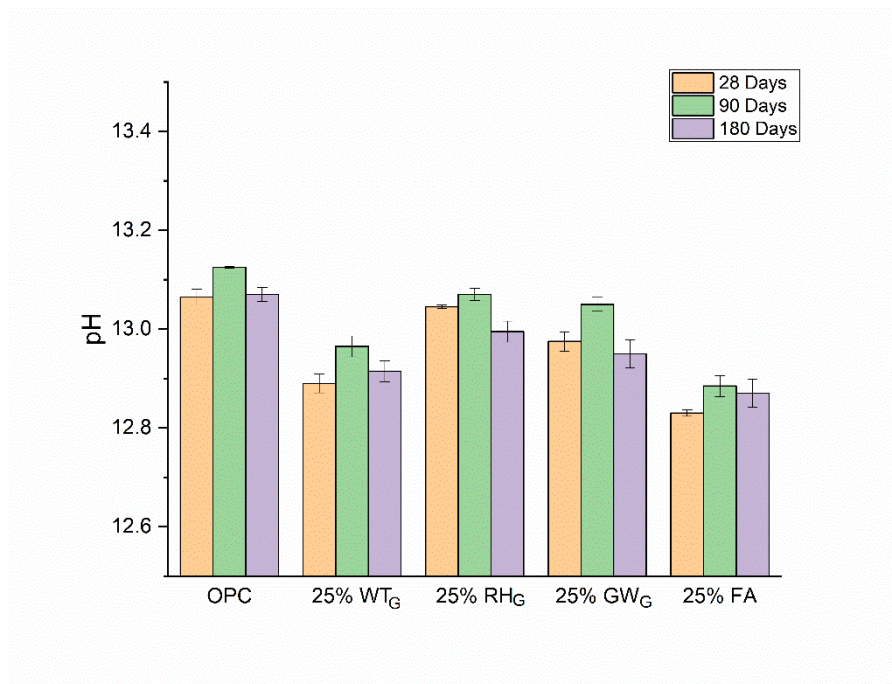


Figure 6.15 Effect of age on the measured pH of pore solutions of pastes containing GRAFs at 38°C

One reason for the increase in alkalinity noted after 90 days could be due to the progression of hydration reactions resulting with age, thus consuming water thus concentrating the ore solution, as well as releasing more alkali from the belite hydration reaction in the pore solution. At the later age of 180 days, lower pH measurements were recorded for the samples. This is attributed to the consumption of alkali in the formation of other reaction products through the pozzolanic reaction, particularly for paste compositions containing GRAFs and FA. Again, it is seen that among the GRAFs studied, pastes with 25% WT_G showed a lower pH measurement at all ages, followed by GW_G and then RH_G. Pastes

containing 25% FA showed the lowest pH level with increasing temperature or age.

6.3.2.2 Ion Concentration of Pore Solutions

It is well known that the alkalinity of cement pore solution is mainly composed of alkali cations (Na^+ and K^+) and hydroxyl ions. Although pH measurements give a fair indication of the pore solution alkalinity, the OH^- ion concentration is affected by other ions in the solution, such as calcium, silicate, and sulphate. For this reason, changes in pore solution are mostly evaluated by analysing the alkali cation (Na^+ and K^+) concentrations, especially for systems assessing the performance of cementitious materials or additives (Lawrencphe 1966; Rothstein et al. 2002).

In Figure 6.16, the total alkali ion concentration ($\text{Na}+\text{K}$) in the pore solution after 28 days at the temperatures studied is presented. From the plotted data, a decrease in ion concentration with increasing temperature was observed for all pastes, including pastes composed of 100% ordinary Portland cement (OPC). Whereas this is consistent with the pH measurements obtained in the previous sub-section, a different study reported that temperature had no significant influence on the alkalinity of ordinary Portland cement samples after 28 days (Thomas et al. 2003).

The data from Figure 6.16 is also presented in Table 6.5. The total alkali detected for pastes containing 25% FA at 23°C was unexpectedly high at 9.7×10^3 mg/L, comparable to the 10.2×10^3 mg/L measured for pastes containing 25% WT_G . It is speculated that the cause of this may be the release of alkali from the FA, which apparently can occur at lower temperatures (Diamond & Lopez-Flores 1981).

However, as temperature increases, a significant reduction in the total alkali concentration of these samples was observed.

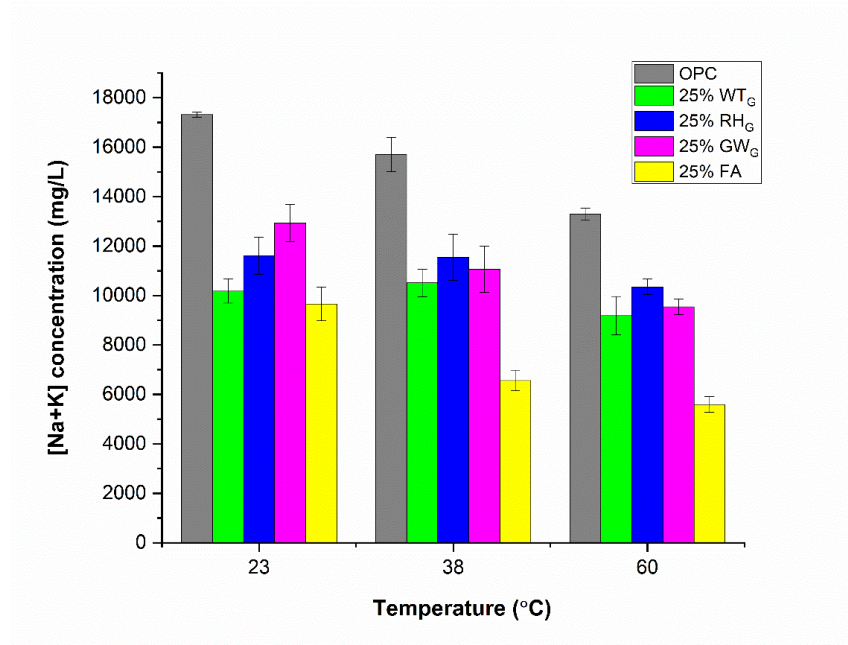


Figure 6.16 Total alkali concentration of the pore solution after 28 days and varying temperatures

Figure 6.16 also illustrates that the addition of GRAFs reduces the total alkali concentration in the pore solution. These reductions in alkali concentrations are consistent with the widely established mechanism of ASR mitigation by SCMs, in which alkali ions (Na^+ and K^+) combine with available silica ions in the solution and precipitate C-S-H among other hydrates, thereby removing alkali from the solution (Duchesne & Bérubé 1994; Shafaatian et al. 2013; Thomas 2011).

Table 6.5 Sodium and potassium ion concentration in the pore solution of pastes after 28 days as a function of temperature

Sample	Temperature	[Na ⁺]/10 ³ (mg/L)	[K ⁺]/10 ³ (mg/L)	[Na ⁺ +K ⁺]/10 ³ (mg/L)
OPC	23°C	6.83	10.48	17.32
25% WT _G		3.26	6.92	10.18
25% RH _G		3.60	8.00	11.61
25% GW _G		5.35	7.58	12.93
25% FA		2.04	7.62	9.66
OPC	38°C	4.94	10.77	15.70
25% WT _G		3.36	7.15	10.51
25% RH _G		4.17	7.38	11.55
25% GW _G		4.50	6.57	11.07
25% FA		2.31	4.25	6.56
OPC	60°C	4.51	8.79	13.29
25% WT _G		5.16	4.02	9.18
25% RH _G		4.45	5.90	10.35
25% GW _G		4.40	5.14	9.54
25% FA		2.16	3.43	5.59

Specifically, pastes with 25% WT_G showed a higher reduction in alkalinity, followed by GW_G and then RH_G. A similar observation can be made after 180 days at 38°C (Figure 6.17). As shown in Figure 6.17, the total alkali concentration for pastes composed of only cement (OPC) showed a marginal decrease over time. This suggests that except for the minimal alkali that was likely consumed by the reaction between the soluble amount of silica in the cement (Table 6.1) and available alkali, most of the alkalis from the cement remained in the pore solution. Thus will be available to react with reactive silica, if present, to form ASR. Conversely, a consistent reduction in alkali concentration was measured for all pore solutions with GRAFs even after 180 days.

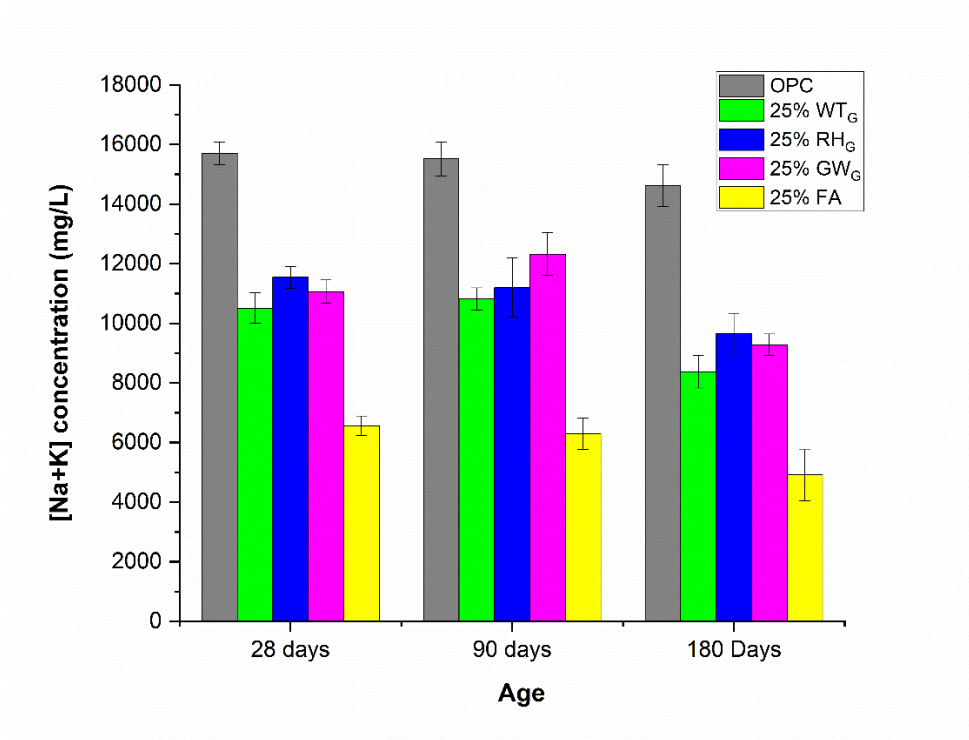


Figure 6.17 Total alkali concentration of the pore solution at 38°C and varying ages

In addition to the alkali ions, the concentration of Al, Si, and Ca ions were also determined. The results obtained are presented in Figures 6.18 and 6.19 and Table 6.6. In all scenarios, the concentration of these ions was found to be much lower (less than 20 mg/L) in the pore solution compared with Na and K ions. Similar observations are made in other works (Li, Thomas & Ideker 2018; Vollpracht et al. 2016).

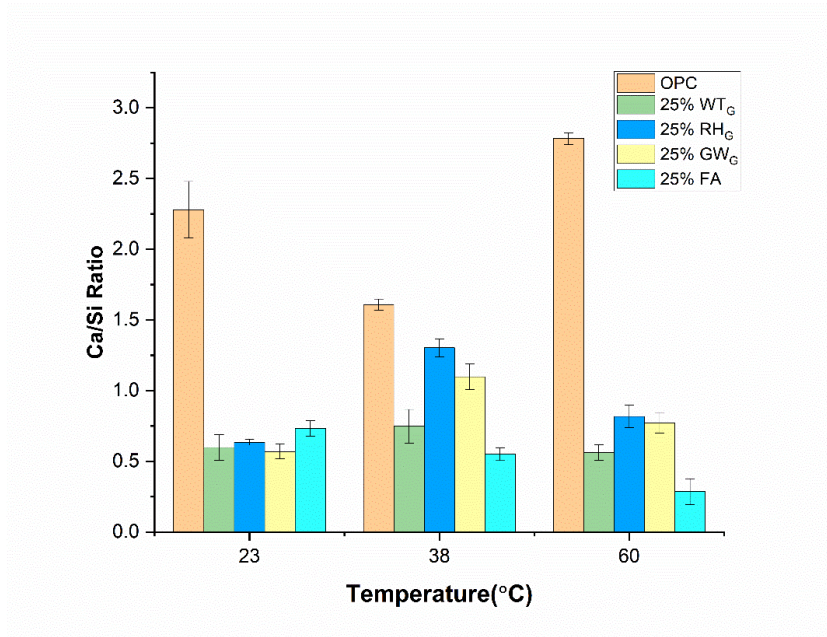


Figure 6.18 Ca/Si ratio of the pore solution of pastes after 28 days and varying temperatures

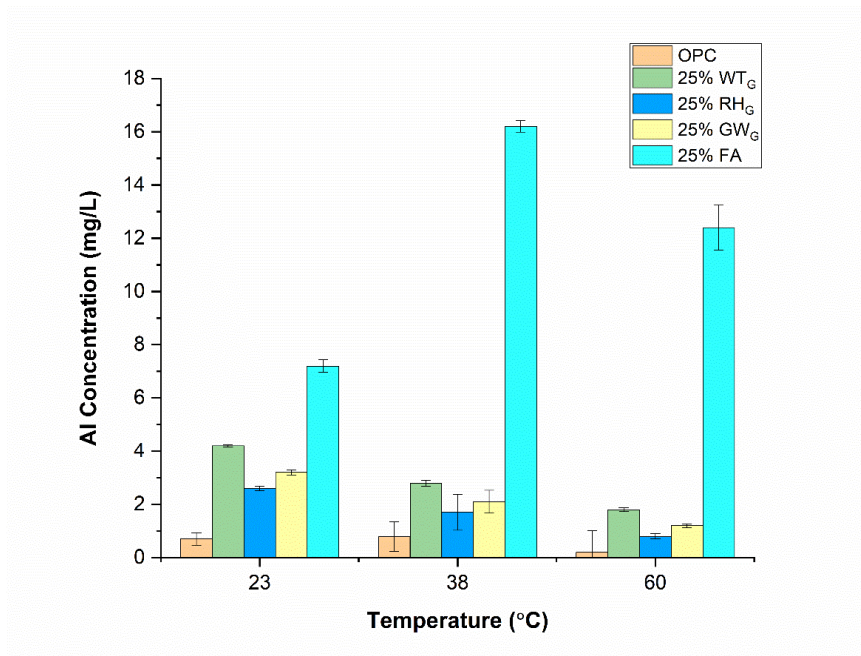


Figure 6.19 Concentration of Al in the pore solution of pastes after 28 days and varying temperatures

The Ca/Si ratio of the pore solution after 28 days is presented in Figure 6.18. Typically, a lower Ca/Si ratio has been known to attract Al, forming less expansive calcium aluminium silicate hydrate (C-A-S-H) phases. The formation of less expansive C-A-S-H fosters alkali binding (Bach et al. 2013; Hooton, Thomas & Ramlochan 2010), thus reducing the alkalis (alkalinity) in the pore solution. After 28 days, a decreasing trend in Al concentration was observed (Figure 6.19), while the Ca/Si ratio was observed to decrease as a function of increasing temperature. This result is consistent with the decrease in pH measurements, and alkali concentration noted with increasing temperature. As aforementioned, Ca, Si, and Al in the pore solution are used up in the formation and precipitation of C-A-S-H, which further binds alkali from solution. This trend also agrees with the mechanisms of cement hydration and reactions reported in literature (Lothenbach et al. 2007; Thomas et al. 2003). Indeed the decrease in Al concentration observed with decreasing alkali concentration and Ca/Si ratio corroborates this theory.

For the GRAFs studied, the results of Figures 6.18 and 6.19 show that paste pore solutions with WT_G had a lower Ca/Si ratio, indicating a higher potential to mitigate ASR. Additionally, WT_G showed a higher amount of Al in the pore solution. As discussed in Section 6.3.1, the presence of Al encourages the formation of aluminosilicate phases that potentially layers available silica particles, thus preventing further dissolution of silica and minimising the risk of ASR. The results obtained for pore solutions of pastes incorporating GW_G and RH_G are similar and consistent with the trend in results observed so far, with GW_G samples exhibiting a lower Ca/Si ratio and more Al ion concentration than RH_G samples. It is also worth mentioning that pastes with FA showed significantly lower Ca/Si and higher Al concentrations as expected.

The MP-AES pore solutions analysis of the paste samples studied at 38°C after 28, 90, and 180 days are presented in Table 6.6. From these results, the continuous impact of age on altering the pore solution chemistry of the systems investigated was not observed. The concentration of Si and Al appear to decrease from 28 days to 90 days, after which higher concentrations of these ions were found. This trend is also reflected in the overall Ca/Si ratio calculated for the samples and may be due to partial decalcification of the formed C-S-H phase (He et al. 2011; Sun, Liu & Du 2019). However, such a conclusion may be premature to draw at this stage of the investigation as further thermodynamic and characterisation studies are required to verify this information. That said, at the individual ages studied, paste samples containing GRAFs and FA showed a lower Ca/Si ratio and higher Al ion concentration than the OPC. Although the concentration of Al and Si ions measured was relatively low, a well-defined trend in the order of decreasing Ca/Si ratio and increasing Al concentration for the GRAFs samples follows as: $WT_G > GW_G > RH_G$.

Table 6.6 MP-AES results of pore solution of pastes containing GRAFs and FA at different ages

Samples	Age (Days)	[Ca ²⁺] (mg/L)	[Si ²⁺] (mg/L)	[Al ³⁺] (mg/L)	Ca/Si
OPC	28	15 ±0.090	9.3 ±0.021	1.8 ±0.041	1.6
	90	14.6 ±0.073	3.7 ±0.393	1.8 ±0.065	3.9
	180	15.3 ±0.031	3.9 ±0.12	3.4 ±0.081	3.9
25% WT _G	28	9.3 ±0.11	12.4 ±0.06	5.8 ±0.05	0.75
	90	9.9 ±0.093	7.5 ±0.09	1.8 ±0.071	1.32
	180	11.1 ±0.019	9.8 ±0.02	7.2 ±0.063	1.13
25% RH _G	28	13.2 ±0.023	10.1 ±0.052	3.7 ±0.092	1.31
	90	13.8 ±0.035	8.6 ±0.033	0.7 ±0.059	1.60
	180	13.3 ±0.06	9.9 ±0.086	4.5 ±0.1	1.34
25% GW _G	28	11.9 ±0.083	10.8 ±0.089	7.4 ±0.073	1.10
	90	12.2 ±0.069	8.2 ±0.012	0.9 ±0.062	1.49
	180	12.1 ±0.071	8.6 ±0.04	9.8 ±0.083	1.41
25% FA	28	12 ±0.031	21.7 ±0.205	23.2 ±0.402	0.55
	90	11.8 ±0.087	11 ±0.092	2.9 ±0.038	1.07
	180	12.5 ±0.043	10.9 ±0.035	13.1 ±0.079	1.15

6.3.3 Expansion Test Results

The expansion measurements at standard ages for AMBT mortar bars and CPT and ACPT concrete prisms are tabulated in Appendix B: Table B4, B7, and B8. The mix design for the concrete prisms studied is also presented in Appendix B: Table B6

6.3.3.1 Effect of Ground Reactive Aggregate Fines on ASR Expansion of Mortar Bars

Figure 6.20 shows the 28-day expansion behaviour of the selected aggregates before their use as ground aggregate fines.

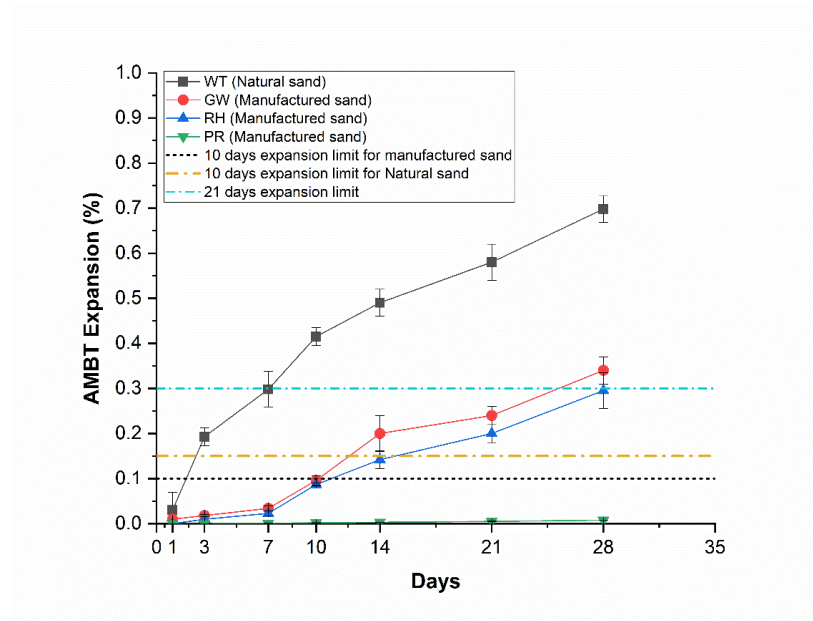


Figure 6.20 AMBT expansion results of aggregates used as GRAFs

The 10-day expansion limit of 0.15% is applied for aggregate WT (natural sand). Among the aggregates studied, WT showed the highest reactivity, reaching the 21-day limit after 7 days. Aggregates GW and RH (manufactured sands) showed similar expansion until the 10-day limit of 0.1%. Subsequently, an increase in expansion was recorded for aggregate GW. However, both aggregates did not exceed the 0.3% limit after 21 days and can be classified as slowly reactive according to the AS1141.60.1 AMBT test method. This expansion behaviour relates with the amount of soluble silica available in the aggregates, as confirmed in the dissolution test, where GW_G measured a relatively higher Si concentration

after 28 days. Negligible expansion was recorded for aggregate PR (manufactured sand) after 28 days, indicating no reactivity.

In Figure 6.21, a comparison of the effectiveness of the three types of GRAFs in reducing the expansion of mortar bars prepared with the two reactive aggregates is shown. A consistent decrease in expansion was observed with increasing GRAFs addition for both aggregate WT and RT systems. However, all the mortar bars studied in this work exceeded the nominated expansion limit of 0.3% by the end of the 56 days test period.

At the standard test duration of 21 days, up to 89% expansion reduction was achieved by 40% GRAFs cement replacement for mortar bars containing aggregate WT (Figure 6.21a-c), while 83% expansion reduction was obtained when aggregate RT was used (Figure 6.21d-f). The expansion results that have been measured are noted to be influenced by the reactivity of the reference aggregate as well as the performance of the GRAFs used. It can be seen that for all the replacement levels studied, WT_G showed the highest effect in reducing ASR expansion, followed by GW_G and then RH_G . This trend in expansion reduction of the GRAFs is coherent with the results obtained from the other analytical studies carried out in this study.

Notably (from Table 6.2), the GRAFs, particularly RH_G , have relatively higher sodium (Na) and potassium (K) amounts than FA, which may be bound in stable phases or encapsulated in metastable silica. According to literature, the rate of ASR is preferential to potassium than sodium (Hou, Struble & Kirkpatrick 2004). The assumption can then be made that other than the relative reactivity of the silica present (as discussed in Section 6.3.1), another cause for the lower performance

exhibited by RH_G is as a consequence of its high potassium content. From the AMBT results, except for aggregates containing WT_G, all mortar bars showed expansion characteristic of slowly reactive and reactive aggregates, even at 40% cement replacement level. Generally, to obtain the same level of mitigation as 25% WT_G at both 10 and 21 days, 40% cement replacement of GW_G and RH_G was required. This is evident from both mix sets using reactive test aggregates WT and RT.

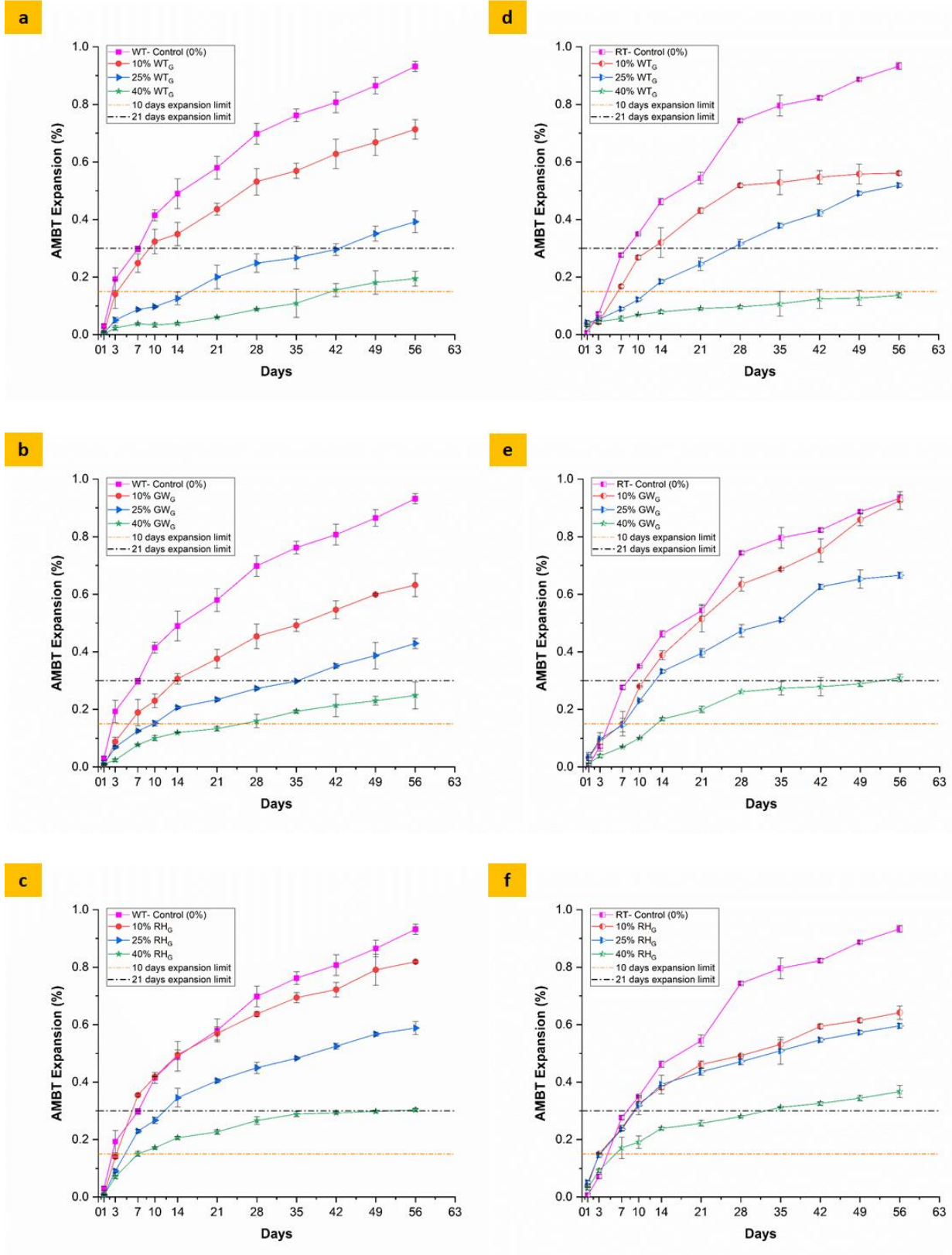


Figure 6.21 Effect of GRAFs on AMBT expansion of mortar bars with reactive test aggregates WT (a-c) and RT (d-f)

The performance of mortar bars with 25% GRAFs was matched with FA at the same replacement level. Expansion data for both the WT and RT aggregate systems are presented in Figure 6.22. From the GRAFs and FA evaluated, RH_G provided the least level of mitigation. At the 10-day limit of 0.15%, an expansion of 0.05% was recorded for mortar bars containing reactive test aggregate WT and FA (Figure 6.22a). Conversely, mortar bars containing WT_G, GW_G, and RH_G showed expansions of 0.12%, 0.23%, and 0.32%, respectively. Likewise, after 21 days, mortar bars with FA expanded below the 10-day limit, while bars containing WT_G, GW_G, and RH_G expanded to 0.20%, 0.23%, and 0.41%, respectively. A similar response in expansion was seen for the RT mortar bars, except that slightly higher expansion values were recorded for the samples due to the difference in the reactivity behaviour of the test aggregate RT (also see Figure 4.15c).

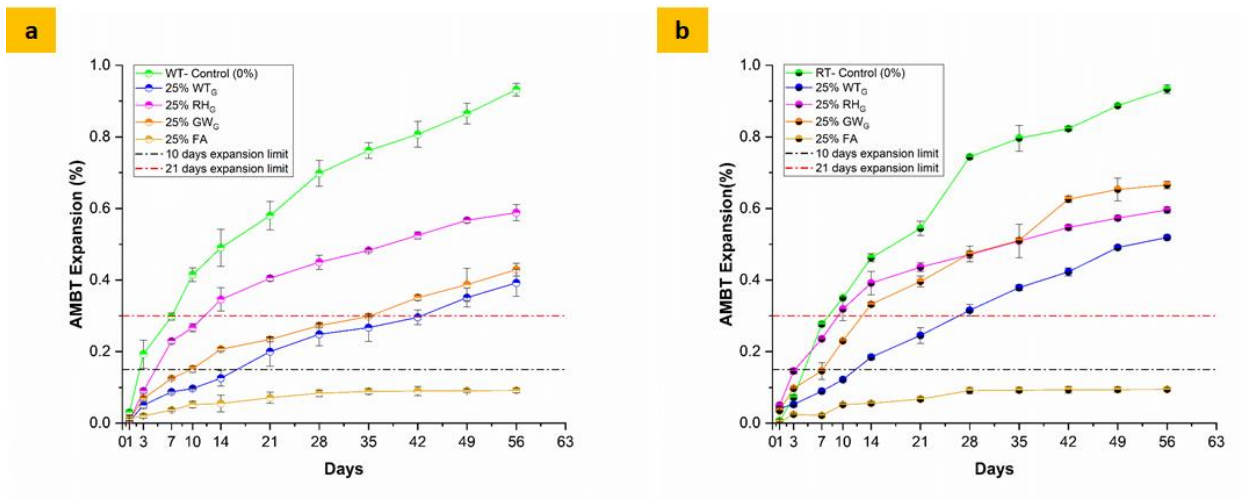


Figure 6.22 AMBT results of mortar bars containing GRAFs and FA at 25% cement replacement level

Furthermore, at the end of the 56-day test period, mortar bars with FA appear to reach a reaction state where ASR is not progressing. Contrarily, a continuous increase in expansion was noted for samples containing GRAFs, signifying the reaction is still ongoing. Overall, the AMBT results obtained indicate that by the expansion thresholds stipulated in AS1141.60.1, 25% cement replacement of WT_G and GW_G can reduce the ASR potential of mixes from reactive to slowly reactive. However, from this study, the performance of GRAFs is lower in comparison to fly ash.

Additional AMBT tests were carried out on samples containing the reactive test aggregate WT and ground non-reactive aggregate PR_G (Figure 6.23). This test was carried out to investigate the influence of cement dilution on the AMBT results obtained. The plot in Figure 6.23 shows that the reactivity of the mortar bars was not significantly affected by PR_G cement replacement regardless of the percentage of PR_G added.

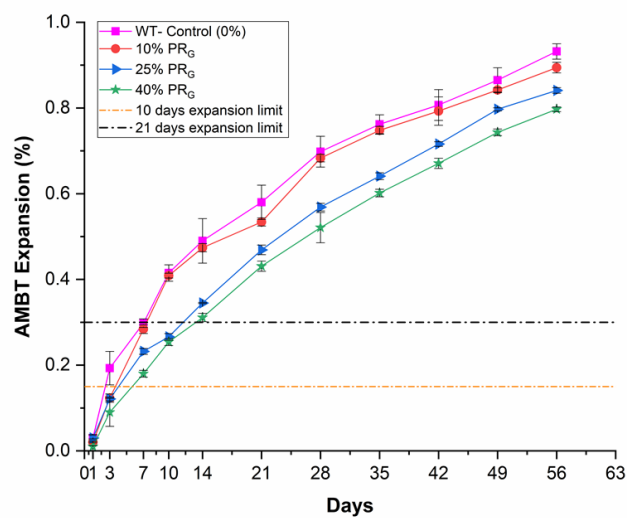


Figure 6.23 AMBT expansion results for mortar bars containing reference aggregate WT and ground non-reactive aggregate PR (PR_G)

All mortar bars were found to expand over the 10, and 21-day limits and thus can be classified as reactive. This implies that the effect of cement dilution is minimal in the AMBT due to the oversupply of alkali from the test solution. The result of this part of the study also agrees well with the results obtained in previous works (Islam et al. 2016; Lindgård et al. 2012). An AMBT study conducted on mortar bars prepared with cements of different alkali contents reported a similar negligible effect on the outcome of ASR expansion (Figure 6.24). The outcome of the aforementioned literature study is consistent with the results obtained in this present study.

In the petrographic assessment of PR, the aggregate was identified to be composed of olivine basalt, absent of any free silica (Section 4.3.1). Therefore, the AMBT results in Figure 6.23 also emphasise the role of silica in the mitigation potential of ground aggregates. That is, the higher the amount of soluble silica in the aggregate, the greater its potential for mitigating ASR when used as fines.

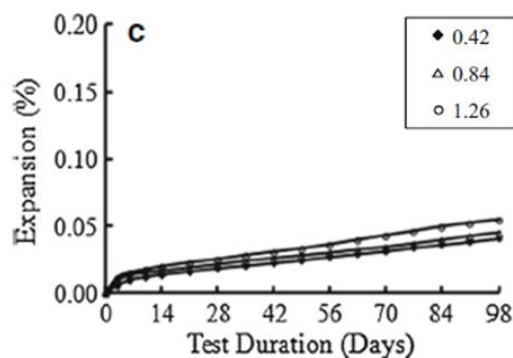


Figure 6.24 Mortar bar expansions as related to three cement alkali contents in 1M NaOH 80°C test solution (Islam et al. 2016)

6.3.3.2 Effect of Ground Reactive Aggregate Fines on ASR Expansion of Concrete Prisms

Concrete Prism Test (CPT)

The results obtained for WT concrete prisms containing 25% addition of GRAFs and FA for the replacement cement after 12 months of testing are shown in Figure 6.25.

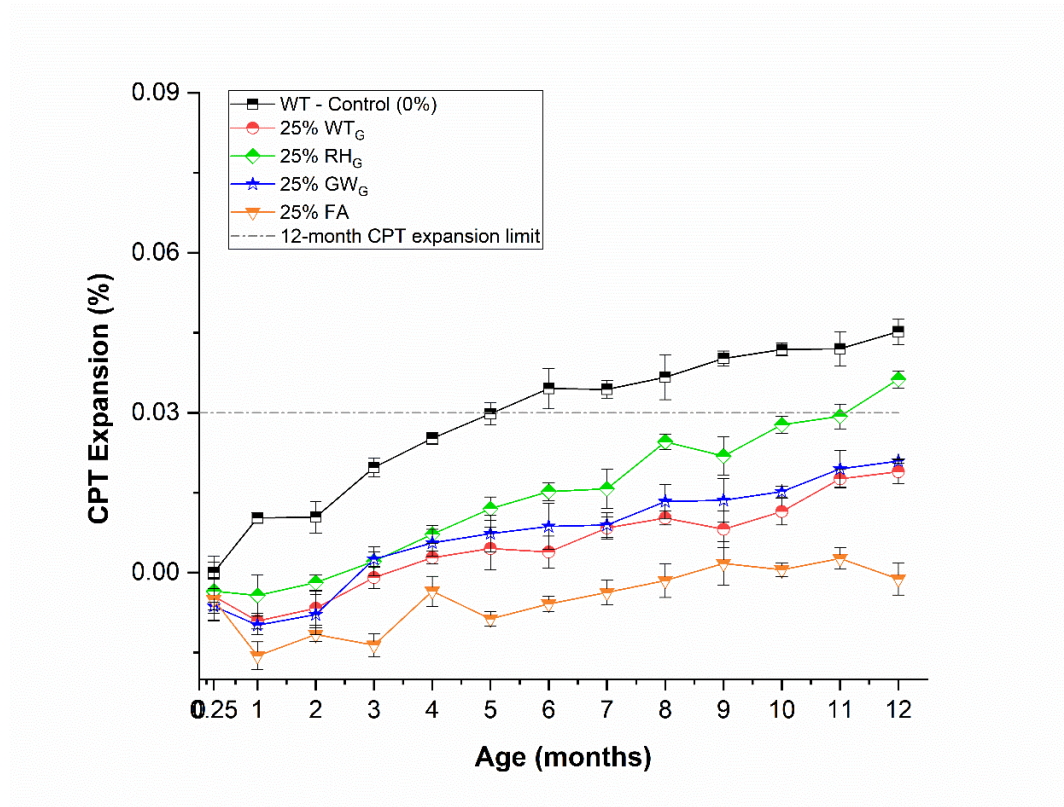


Figure 6.25 Expansion results of 12 months CPT at 38°C for concrete prisms containing GRAFs and FA. *Note: Initial expansion (Day 0/Month 0) is 0.00%. Graphs represent expansion measurements from Day 7 (Month 0.25)*

After the 12 months test duration, concrete prisms having 25% FA did not show any relevant expansion. Except for mixes containing RH_G, which showed an expansion of 0.036% after 12 months, all concrete prisms showed a significant reduction in expansion compared to WT-control. In fact, the concrete prisms with

WT_G and GW_G showed expansions of 0.018% and 0.021%, respectively, below the expansion limit of 0.03%. From Figure 6.25, it can further be seen that all concrete prisms showed an increasing gradient in expansion after 12 months of CPT, indicating that ASR is still ongoing. As such, continuous monitoring of expansions up to 24 months duration is essential (and currently ongoing) to better assess the performance of GRAFs in mitigating ASR in commercial concretes. Nevertheless, from the current results of this study, it can be concluded that WT_G and GW_G offer efficient mitigation to ASR for the aggregate fines studied.

Accelerated Concrete Prim Test (ACPT)

A similar trend in expansion to CPT (Figure 6.25) was observed for ACPT prisms containing GRAFs and FA. Figure 6.26 shows the ACPT expansion results of WT concrete prisms containing 25% cement replacement of GRAFs and FA. Considering the correlation between ACPT expansion data after 3 months to be comparable to CPT expansion data after 12 months as discussed in Sections 5.3.2.2 and 5.3.3, the expansion limit of 0.03% was applied to assess the performance of GRAFs. Concrete prisms containing 100% cement (WT-control) showed an expansion of 0.048% after 3 months of ACPT. Of the three GRAFs evaluated, WT_G was the most effective in reducing the expansion after 3 months, showing an expansion of 0.015%. Concrete prisms with GW_G exhibited a similar expansion of 0.019%. These two mixes can thus be classified as non-reactive as per the AS 1141.60.2 test method reactivity classification index. However, for concrete prisms with RH_G, an expansion of 0.028%, almost reaching the expansion threshold of 0.03%, was noted. Allowing for the standard deviation of error and

considering the gradient of the expansion curve, the RH_G samples are considered reactive. This is more obvious after 4 months, where the concrete prisms containing RH_G showed an expansion of 0.033%, exceeding the expansion limit of 0.03%.

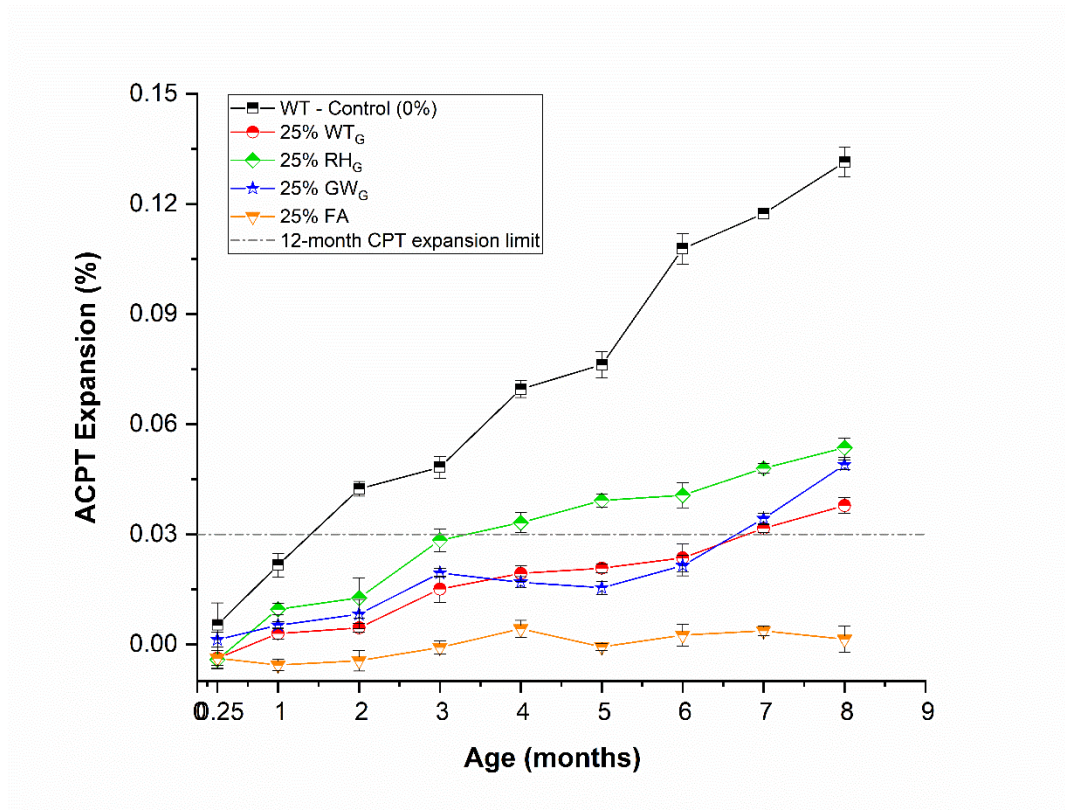


Figure 6.26 Expansion results of ACPT (CPT at 60°C) for concrete prisms containing GRAFs and FA. *Note: Initial expansion (Day 0/Month 0) is 0.00%. Graphs represent expansion measurements from Day 7 (Month 0.25)*

6.3.4 Thermogravimetric Analysis (TGA) of Pastes containing GRAFs

To understand the mitigation effect of the GRAFs observed in the expansion tests, TGA analysis was carried out on 28 days paste samples containing 0, 10, 25, and 40% GRAFs tested at 80°C (similar to AMBT conditions) and at 38° and 60°C (similar to CPT and ACPT conditions, respectively) for pastes containing 25% GRAFs and FA. A typical example of the microstructure of the fractured paste samples cured at 60°C after 28 days is presented in Figure 6.27. The presence of ettringite (Ett), Portlandite (CH), calcium silicate hydrate (C-S-H), calcium aluminium silicate hydrate (C-A-S-H), and aluminate ferrite monosulfate (AF_m), identified by their distinctive microstructural characteristic features can be seen (Demir et al. 2017; Kunal et al. 2016). The presence of C-A-S-H in the microstructure of the pastes supports the pore solution results obtained in Section 6.3.2.

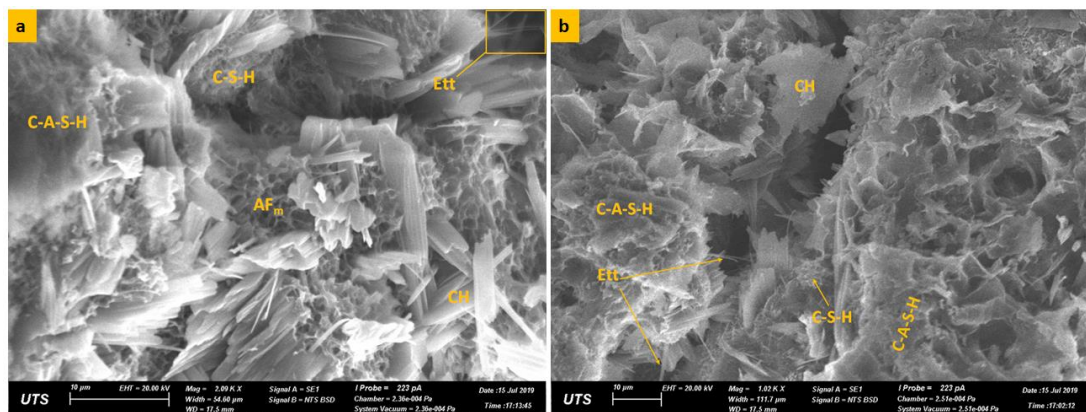


Figure 6.27 Microstructure of fractured paste samples containing (a) FA (2000x) and GRAFs (WT_G) (1000x) cured at 60°C after 28 days (Note the presence of ettringite (Ett), portlandite (CH), calcium silicate hydrate (C-S-H), calcium aluminium silicate hydrate (C-A-S-H), and aluminate ferrite monosulfate (AF_m)).

The TGA results on the amount of portlandite present in paste samples (represented as a percentage) at different curing conditions after 28 days is illustrated in Figures 6.28 -6.30. Usually, for a binder composed of 100% cement, the amount of portlandite formed after curing for 28 days is approximately 20 wt.% of the hydration products (Bignozzi et al. 2015). The results presented in Figure 6.28 have been normalized to the percentage mass loss of portlandite measured in the control sample (100% OPC) between a temperature range of 350-500°C, which represents the de-hydroxylation region of calcium hydroxide (CH).

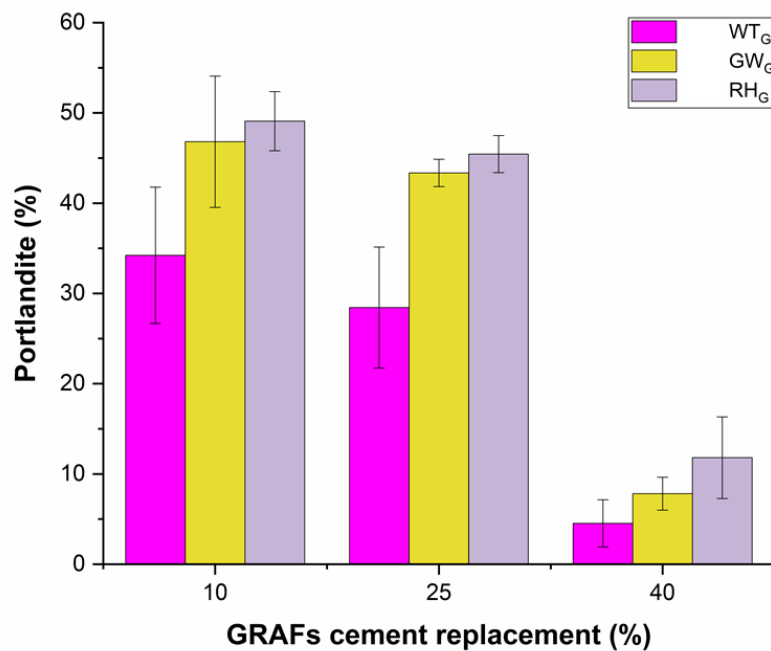


Figure 6.28 Portlandite content in pastes containing GRAFs at different dosages after 28 days curing at 80°C

The amount of portlandite in the pastes is observed to decrease rapidly on the addition of GRAFs, reaching the lowest value of 4.3% at 40% WT_G. The decrease in portlandite does not appear to be linearly proportional to the cement replacement

level of the respective GRAFs, suggesting that the results obtained are not influenced by the dilution effect of replacing OPC with GRAFs. As shown in Figure 6.28, the amount of portlandite in the paste decreased with an increase in GRAFs addition. The portlandite consumption potential of the GRAFs is consistent with the pore solution results obtained in Section 6.3.2. The order of pozzolanicity for the GRAFs can be seen as $WT_G > GW_G > RH_G$.

The chemical analysis of the GRAFs (Table 6.2) showed that the percentage of silica in WT_G is highest at 62.93%, while GW_G and RH_G contain 60.75% and 61.93%, respectively. These values are considerably higher than the 58.0% recorded for fly ash (FA). However, not all the silica phases are soluble, as determined from the dissolution test results at 28 days (Figure 6.6). The dissolution test results showed that of the GRAFs, the amount of soluble silica is highest for WT_G . Soluble silica in GW_G was observed to be slightly higher than in RH_G after the 28-day test period. By way of the pozzolanic reaction (defined in Eqn. 3.3), SCMs with high soluble Si content are more pozzolanic and react to form hydrates with lower Ca/Si ratio and higher alkali binding, as the pore solution analysis of this study has also shown.

Under CPT and ACPT temperature test conditions at 25% cement replacement level (Figures 6.29 and 6.30), a similar order of increasing portlandite consumption of $WT_G > GW_G > RH_G$ was observed at both 38°C and 60°C. It is worth noting that so far in this study, the reaction behaviour of GW_G and RH_G is comparable. As the pozzolanic reaction progresses, the available Ca in the solution is depleted. This also encourages a lower Ca/Si ratio, as shown in Figure 6.18, thus corroborating the TGA results presented in Figures 6.29 and 6.30.

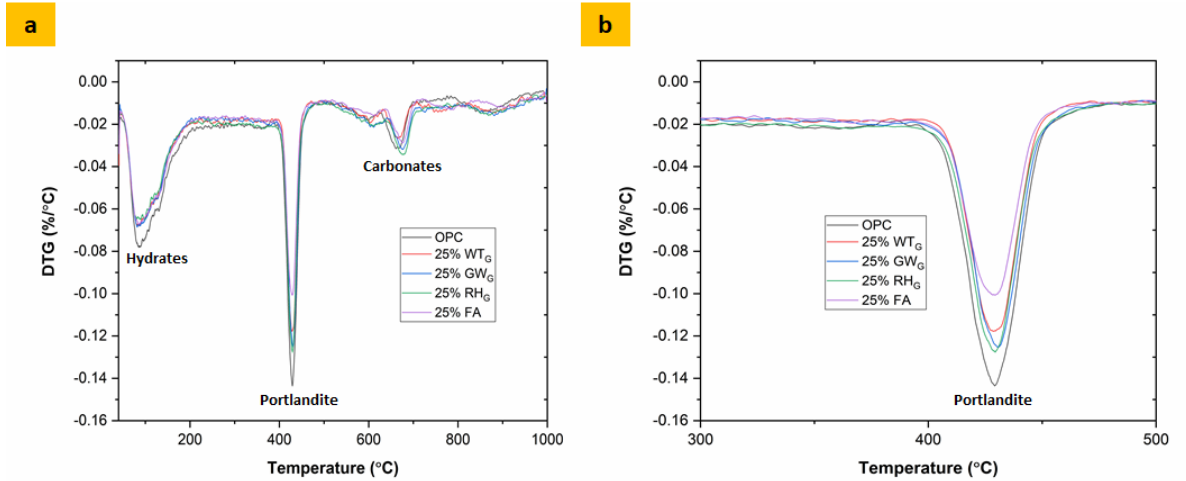


Figure 6.29 (a) Full range DTG curves and (b) partial range DTG curves showing portlandite content in pastes with 25% cement replacement after 28 days at CPT temperature (38°C) *Note: Area under portlandite curve represents the amount of portlandite present in the system*

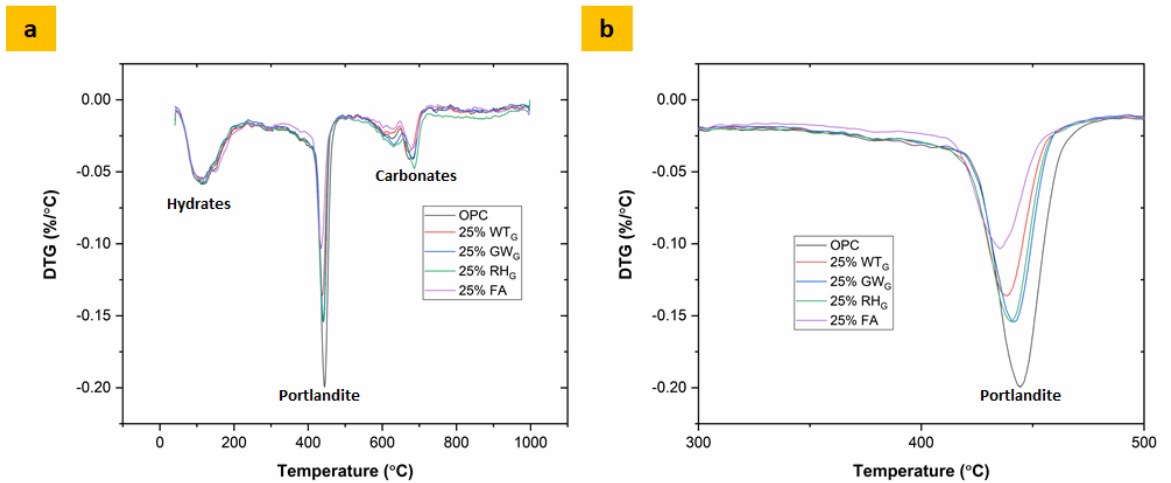


Figure 6.30 (a) Full range DTG curves and (b) partial range DTG curves showing portlandite content in pastes with 25% cement replacement after 28 days at ACPT temperature (60°C) *Note: Area under portlandite curve represents the amount of portlandite present in the system*

6.3.5 Influence of Ground Reactive Aggregates on Mechanical Properties of Concrete

The analysis and discussion of the test results of concrete samples subjected to compressive and flexural strength (modulus of rupture) tests are presented in this section. The variations in the compressive strength of WT-control samples and the prisms containing GRAFs and FA are given in Figure 6.31. After curing for 28 days, WT-control samples showed a compressive strength of 47.9 MPa. This strength result is consistent with the compressive strength usually reported for concretes cured in a moist environment (Shariq, Prasad & Masood 2010). Conversely, the compressive strength of the concrete prisms containing GRAFs was observed to be lower, between 34-37 MPa, as shown in Figure 6.31. The strengths obtained for the three GRAFs mixes represent approximately 76% of the strength of the WT-control samples after 28 days. The ASTM C618-19 describes the chemical and physical requirements for the classification of natural pozzolans for cement replacement (ASTM 2019; Pourkhorshidi et al. 2010). In accordance with the ASTM C618-19 specification, for a material to be classified as a natural pozzolan, it must be siliceous or aluminous and be able to react with lime in the presence of moisture to form compounds with pozzolanic properties when used as a partial replacement of cement. Additionally, the 7-day and 28-day strength index requirement for natural pozzolans is set as 75% of the control (concrete or mortar). Thus with 76% of the concrete strength retained, the GRAFs investigated in this study satisfy these specifications and

may yet be qualified as natural pozzolans following further characterization tests as required by the ASTM C618-19 method.

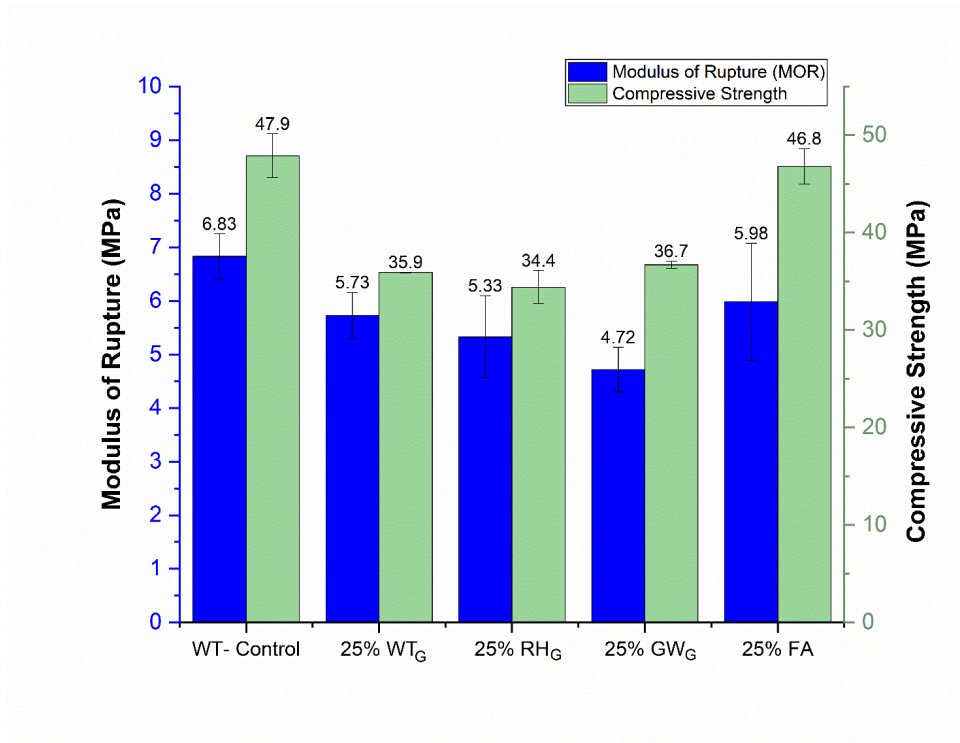


Figure 6.31 Effect of GRAFs and FA on the compressive and flexural strengths of concrete after 28 days

Conversely, FA samples maintained 97% of the initial concrete strength with a compressive strength of 46.8 MPa. The higher strength values noted for the FA samples could be explained by several factors, including the formation of strong cementitious products through the pozzolanic reaction and the refinement of pore structure in the concrete by the finer size of FA particles (Chindaprasirt, Jaturapitakkul & Sinsiri 2005) compared to cement and GRAFs as shown in Figure 6.1. The relatively high fineness of FA particles increases the surface area for

pozzolanic reaction to occur; thus, an increase in the formation of cementing C-S-H phases resulting in the higher compressive strength obtained (Pereira-de-Oliveira, Castro-Gomes & Santos 2012; Shayan & Xu 2006). Consequently, a reduced pozzolanic reaction owed to the increase in particle size is likely the main reason for the lower strengths measured for concretes with GRAFs. Additionally, a lower pore-filling effect by the relatively larger particle size of GRAFs compared to FA may have also contributed to higher porosity in the concrete that can reduce the concrete density and compressive strength. The air content results presented in Appendix B: Table B6 for these concrete mixes confirm this by showing a higher air content for concretes containing GRAFs relative to those prepared using FA. In fact, the lower pore filling effect exhibited by the GRAFs could have further contributed to the lower ASR mitigatory effect (higher expansions) observed for the GRAFs concretes compared to the FA concretes (Oh, Jun & Jeong 2014; Thomas 2011). A high volume of pores in the hardened concrete increases the probability of connecting pores, which allows the permeation of moisture and ASR gel through the concrete, leading to higher ASR expansion.

Similarly, the modulus of rupture (MOR) of concrete prisms was found to decrease with the addition of GRAFs, though prisms containing WT_G exhibited a relatively higher MOR of 5.73 MPa. GW_G prisms, which showed the highest compressive strength for the three GRAFs studied, showed the lowest MOR of 4.72 MPa. This result is representative of concrete mixes incorporating lower amounts of supplementary cementitious materials (Song & Hwang 2004; Tasdemir et al. 1996). Similar to the compressive strength findings, FA prisms maintained a high MoR of 5.98 MPa compared to the 6.83 MPa measured for WT-control.

It has been reported that the workability of concrete mixes influences the mechanical properties of the hardened concrete (Kumar, Srikanth & Rao 2012; Sim & Yang 2012). At the same water to cement ratio used in the concrete mix, mixes with GRAFs showed less workability than fly ash, evident by the concrete slump shown in Appendix B: Table B6. This is possibly due to an increase in the surface area and porosity of GRAFs particles, thus requiring more water as per the absorption capacity requirement of the aggregate used. Other researchers have found similar results using ground glass as an alternative pozzolanic material proposed. In these studies, researchers reported that the decrease in workability could also be due to the higher water requirement of the angular shape of the crushed particles (Shekhawat & Aggarwal 2014). This is also plausible in the case of this study, as the particles of the GRAFs were mostly sub-angular and angular in shape (Figure 6.8, and 6.10 - 6.12). Further, angular-shaped particles may reduce the compaction level and overall density of the concrete for better mechanical properties.

6.3.6 Evaluating ASR Mitigation Mechanism of Ground Reactive Aggregates through Post-Expansion Characterisation of Concrete Prisms

After 8 months of ACPT, a visual inspection of the concrete prisms was undertaken (Figure 6.32). The presence of whitish efflorescence streaks found in all the concrete prisms indicates the occurrence of alkali leaching (Barger & Hansen 1998; Nijland & Larbi 2010). Images of the control samples in Figure 6.32 also showed the presence of visible map cracking on the surface of the concrete prisms.

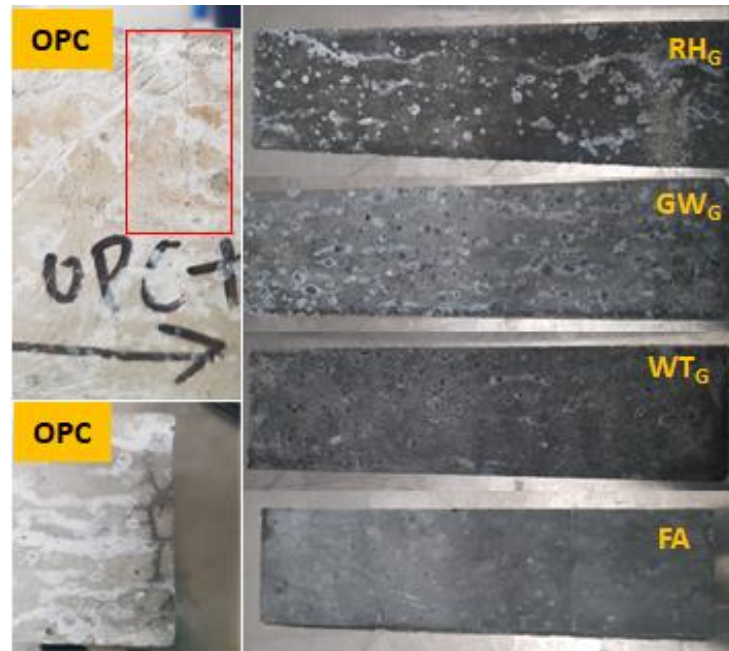


Figure 6.32 Appearance of concrete prisms after 8 months ACPT (*Note micro-cracks (within red squares) and map cracking on the surface of control samples (OPC)*)

The microstructure of polished sections of concrete prisms subjected to ACPT was further analysed to identify the presence, location, and chemical composition of the ASR gel. Sampling for microstructural analysis was carried out by sectioning the concrete prisms approximately 1 inch (25 mm) away from the studded end to avoid portions that had experienced the largest effect of alkali leaching from the most contact with moisture.

Except for prisms containing FA, all concrete prisms showed the presence of ASR after 8 months. This observation is expected as the concrete prisms eventually expanded over the 0.03% limit. However, the degree of ASR distress was generally found to be lower for concrete prisms containing WT_G. The microstructural analyses of the expanded concrete prisms are presented in Figures 6.33- 6.37. The SEM analyses showed the presence of micro-cracks through and around aggregate particles. Some cracks were filled with ASR gel, while other empty cracks showed

remnants of the gel, indicating that they were once filled with ASR gel. These observations were made for all the concrete samples analysed.

The characterisation of various ASR gels from different studies in literature suggests that the gel's composition is dominated by the presence of Na, K, Si, and Ca with traces of Al and Mg (Monteiro et al. 1997; Thomas 2001). However, the proportions of these elements in the gel vary significantly, depending on several factors such as the age and the distance the gel is sampled from the reaction site (Diamond 2000; Knudsen & Thaulow 1975).

In particular, the control samples showed dense ASR gel presence within the cracks of the aggregate particles, as shown in the SEM-BSE image in Figure 6.33. The composition of the gel identified, taken from the average of at least 15 EDS point scans across the surface of two sighted ASR gels, is also presented in Table 6.7.

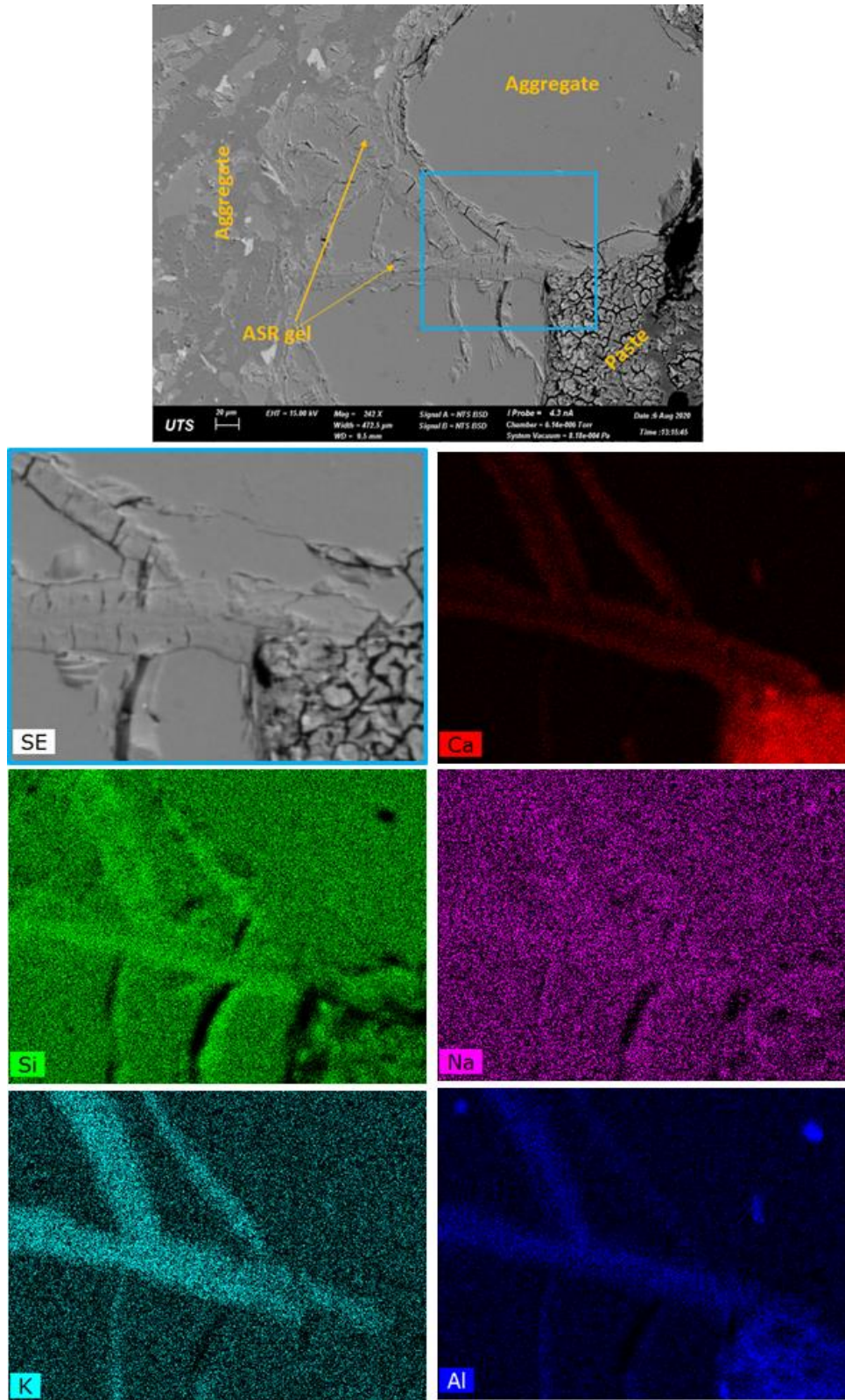


Figure 6.33 SEM-BSE micrograph and elemental mapping of ASR gel found in the control sample (WT- control) after 8 months (242x) (*Note: aggregate has higher Na alkali content*)

Thomas et al. reported that ASR gels found in and around aggregates are rich in alkali with less Ca concentration (Thomas 2001). This is consistent with the observations made in this study. From the EDS analysis (Table 6.6), the Ca/Si ratio of the gel was found to be 0.14. This Ca/Si ratio is consistent with the ratio reported for ASR in field structures by other researchers (Hou et al. 2005). It is well acknowledged that ASR gel does not form when Ca is absent (Struble & Diamond 1981a; Thomas 2001). However, the role of Ca in the formation of expansive ASR is controversial. In a study investigating the effect of the Ca/Si ratio on ASR gel's expansive capability (Gholizadeh-Vayghan & Rajabipour 2017), the authors found a threshold Ca/Si ratio of 0.05-0.5. At the lower boundary limit of $\text{Ca/Si} < 0.05$, ASR gel was found to flow through the pore structure without causing damage (Gholizadeh-Vayghan & Rajabipour 2017; Kawamura & Iwahori 2004). Whereas when the ratio reached $\text{Ca/Si} > 0.18$, the expansive nature of the gel becomes dependent on the Ca content such that an increase in Ca content reduces the degree of freedom of the gel, making it rigid and thus less expansive (Gholizadeh-Vayghan & Rajabipour 2017; Powers & Steinour 1955). In this aforementioned study, the researchers established that the threshold Ca/Si ratio for expansion was 0.1-0.18. In this range, the ASR gel formed has a considerable swelling capacity, as well as the viscosity to move through the pores in the concrete and cause damage. To that end, the ASR gel identified in the control sample (OPC) in this study has a Ca/Si ratio (0.14) that suggests the possibility of highly expansive ASR, as observed in the ACPT expansion results discussed in Section 6.3.3.2.

It was also noted that the gel formed in the control prisms contained Al, accounting for 1.2% of the gel's overall composition. Al in that proportion can influence the crystallisation of the C-S-H phase to form ASR gel with morphology (structure)

typical of tobermorite (Nelson & Kalousek 1977; Nocuò-Wczelik 1999). This crystalline ASR gel is characterised by a platy morphology (Leemann et al. 2016; Shi et al. 2019). The tobermorite microstructure associated with the ASR gel found covering the aggregate surface on a fractured piece of the control sample is shown in Figure 6.34.

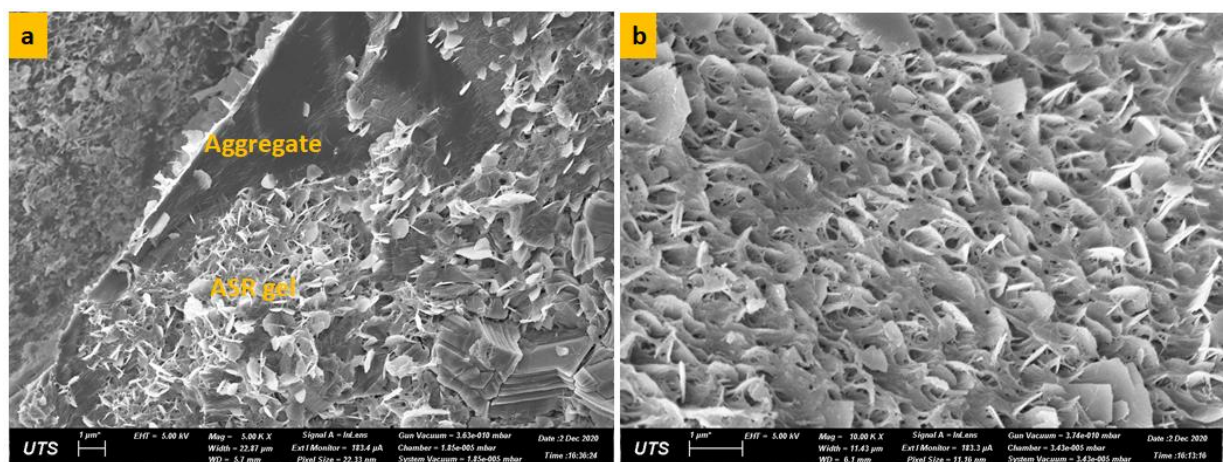


Figure 6.34 Morphology of crystalline ASR gel after 8 months (a) forming on the surface of the aggregate particle in the control prisms (5000x) (b) ASR gel at a higher magnification (10000x)

For concrete prisms containing GRAFs, the microstructural analysis showed the presence of several micro-cracks within the paste regions of the concrete. Due to challenges with achieving well-polished surfaces for image analysis, there were a few instances where actual ground aggregate particles ($<100 \mu\text{m}$) were found during SEM analysis contrary to reports made by similar studies that incorporated ground glass or fine expanded clay additives (Afshinnia & Poursaei 2015; Bignozzi et al. 2015; Li, Thomas & Ideker 2018). However, it is plausible that the micro-cracks in the paste resulted from the ASR of the GRAFs.

In Figure 6.35, the typical microstructural analysis of concrete prisms containing 25% WT_G is shown.

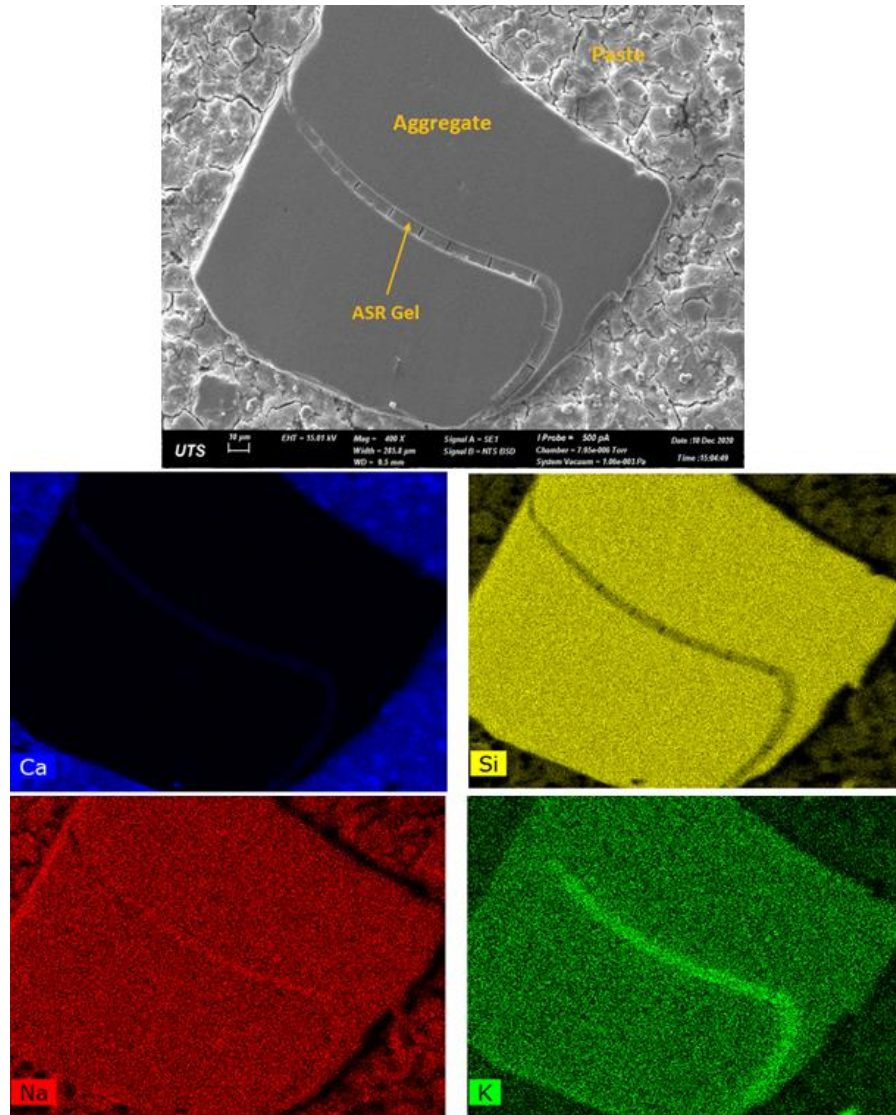


Figure 6.35 SEM-SEI micrograph and elemental mapping of ASR gel found in concrete prism containing 25% WT_G after 8 months (400x)

Generally, the ASR gels formed in concretes containing GRAFs had higher K than Na contents. The Ca/Si ratio of the ASR gels identified in concretes containing WT was 0.10. This is lower than the Ca/Si ratio found in the control samples (0.14) and falls within the threshold category previously discussed. However, the ASR gels found in

these prisms were relatively thinner (width < 5 μ m) compared to the gels found in the control samples. Additionally, the ASR gels were also found to have a higher Al content. A reasonable assumption can be made that the ASR gels found in concretes containing GRAFs are narrower because they originate from the smaller (finer-sizes) aggregate particles in the paste. The high Al presence in the ASR gels of prisms containing WT_G suggests the formation of C-A-S-H gels, which are apparently less expansive and reduce the pore solution pH through alkali binding (Hong & Glasser 2002). The relatively higher Na/Si ratio noted in the ASR gel (Table 6.7) confirms this hypothesis.

Table 6.7 EDS Analysis of ASR gels in concrete prisms after eight months (Atomic weight percentages have been normalized relative to oxygen)

Sample	ASR Gel	Location	Elemental composition (atomic weight %)							
			Ca	Si	Al	K	Na	Ca/Si	[Na+K]/Si	Al/Si
WT- Control	1	Aggregate	4.98	36.13	1.20	3.42	1.82	0.14	0.13	0.06
	2	Aggregate	3.48	24.94	1.23	0.91	1.98	0.15	0.14	0.05
	Average		4.23	30.535	1.215	2.165	1.9	0.145	0.135	0.06
25% WT _G	1	Aggregate	1.77	23.91	5.09	2.40	2.80	0.08	0.22	0.21
	2	Aggregate	3.14	21.40	4.80	2.58	3.36	0.15	0.28	0.22
	Average		2.455	22.655	4.945	2.49	3.08	0.115	0.25	0.22
25% GW _G	1	Paste	9.12	6.24	2.74	1.51	0.26	1.48	0.29	0.24
	2	Paste	15.37	15.61	2.18	0.09	0.67	1.18	0.06	0.17
	Average		12.25	10.925	2.46	0.8	0.465	1.33	0.175	0.21
25% RH _G	1	Aggregate	8.58	28.46	2.08	0.36	2.06	0.31	0.09	0.08
	2	Aggregate	9.17	32.74	1.48	0.35	2.06	0.30	0.07	0.04
	Average		8.875	30.6	1.78	0.355	2.06	0.305	0.08	0.06

The SEM analysis also showed the presence of small air voids within the paste that were filled with ettringite. This was seen in all the concrete prisms studied. However, in every instance, no cracks were observed emanating from the ettringite-filled air voids, suggesting that the expansions observed are not significantly influenced by delayed or secondary ettringite formation.

In Figure 6.36, a typical example of ASR gels found in concrete prisms containing GW_G is shown. The ASR gels in these prisms were primarily located in the paste regions and along the aggregate-paste interface. The gel located in these regions exhibited a Ca/Si ratio of 1.34.

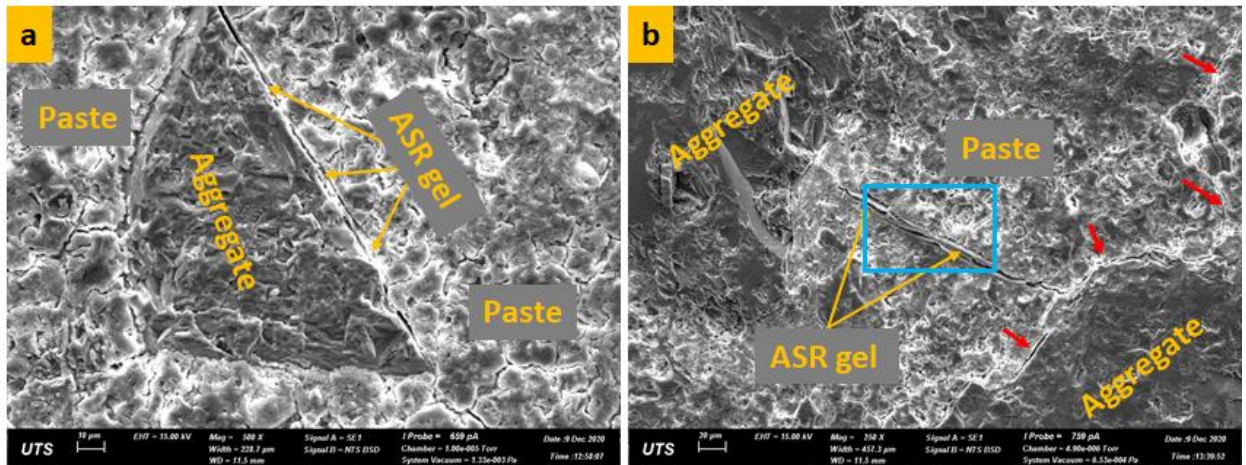


Figure 6.36 SEM-SEI micrographs of the concrete prisms containing 25% GW_G showing ASR gel in cracks after 8 months (a) along the aggregate-paste interface (500x) and (b) within the paste (250x)

ASR gels found within the paste regions were generally noted to be higher in Ca amount, as seen from the elemental mapping in Figure 6.37. It is well known that ASR gels tend to undergo an ion exchange process where the Na ions in the gels are replaced by Ca ions that dissolve from portlandite in the cement paste. This occurrence is referred to as alkali- recycling (Rajabipour et al. 2015; Thomas 2001) and has been found to initiate at $Ca/Si > 0.18$ (Gholizadeh-Vayghan & Rajabipour 2017), usually in portions of the gel that are in close proximity to the cement paste.

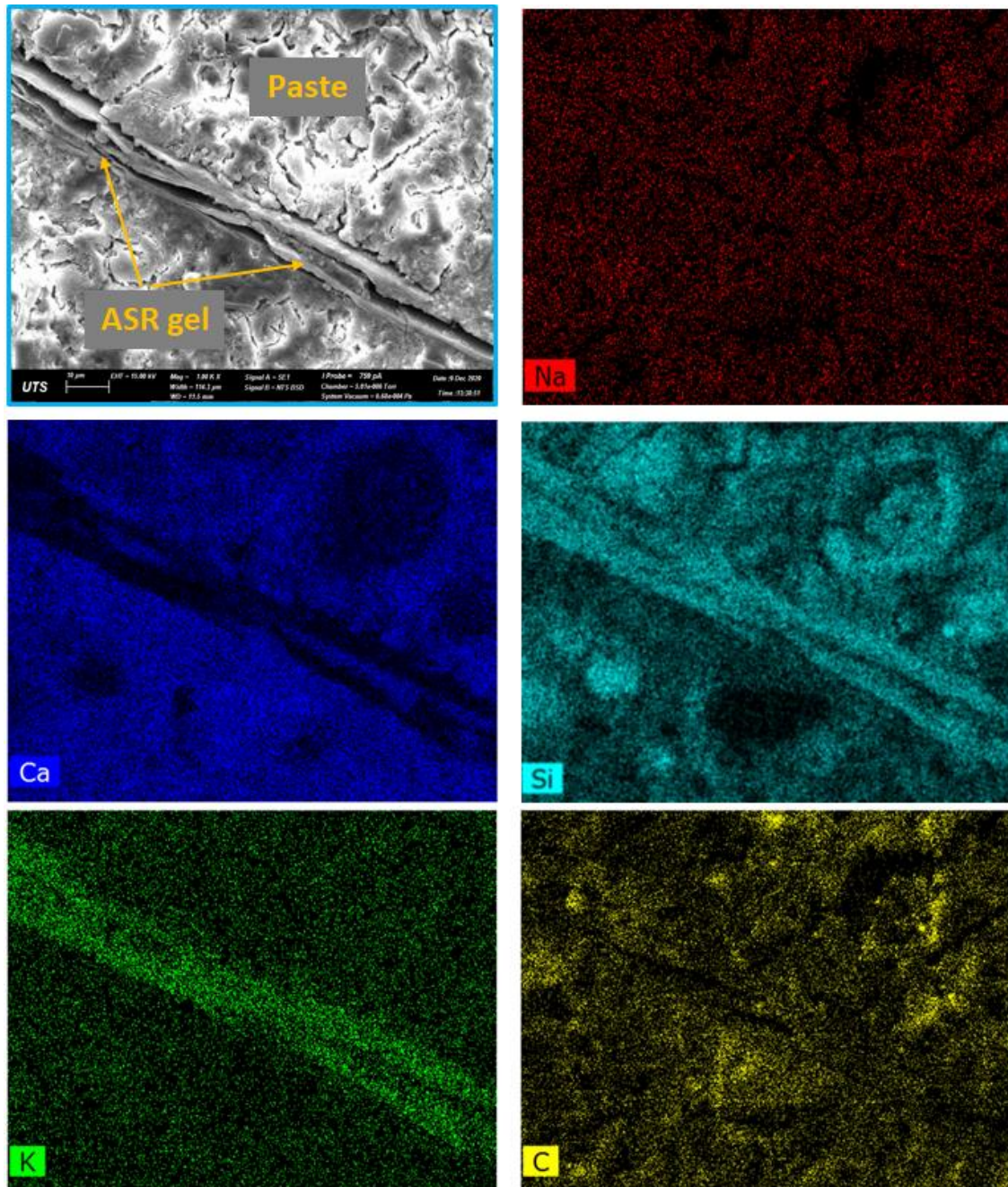


Figure 6.37 SEM-SEI micrograph and elemental mapping of ASR gel found in concrete prism containing 25% GW_G after 8 months (1000x)

The occurrence of alkali recycling contributes to higher Ca amounts detected in the gel. Therefore, the results obtained in this study support this conclusion. It is worth noting that alkali recycling releases alkali ions back into the pore solution, causing a

rise in pH and, in most cases, the likelihood for further ASR occurrence. Thus, gels with high Ca content tend to have a lower Na/Si ratio, as observed from Table 6.6. However, the gels detected in the concrete prisms containing GW_G also showed Al/Si ratios that are comparable to the values measured in concrete prisms having WT_G . This finding proposes that C-A-S-H phases may also be present. Nonetheless, the amount of C-A-S-H in GW_G prisms is possibly lower than in WT_G prisms, indicated by the less alkali binding was observed for gels found in prisms containing GW_G . In fact, ASR gels with such high Ca content as recorded in this work are thought to approach the composition and properties of pozzolanic C-S-H and thus can have high stiffness and low expansion properties (Monteiro et al. 1997; Powers & Steinour 1955). This is likely the driving mechanism for the mitigation observed during the expansion test for concrete prisms containing GW_G .

For concrete prisms prepared with 25% RH_G , the SEM analysis (Figure 6.38) showed the presence of extensive cracking occurring throughout the prism, explaining the relatively higher expansion recorded for these materials among the GRAFs studied. From Figure 6.38a, it can be identified that some proportion of the RH_G GRAFs (circled in yellow) reacted with the alkali to generate micro-cracks emanating from the aggregate particles. This is evident by the reaction rim found around these RH_G particles. Meanwhile, other areas of the microstructure (circled in blue) showed unreacted RH_G particles. Consequently, sufficient alkali was available in the pore solution to react with the test aggregate WT to form ASR, resulting in the extensive cracking of the larger aggregate particles, as shown in Figure 6.38. Typically, the cracks were observed to emanate from within the larger aggregate particles or successively along the rim of the aggregates (Figure 6.38c), where the reaction

begins. Furthermore, ASR-filled cracks running across the large aggregate particles and into the cement paste were also observed (Figure 6.38b-c).

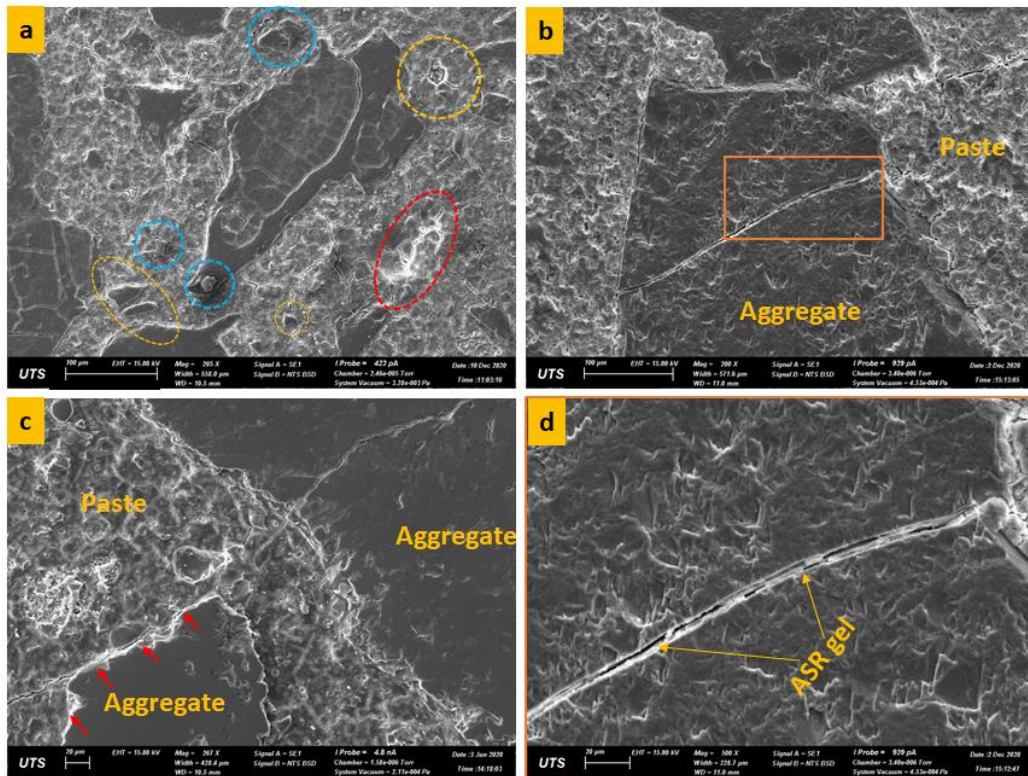


Figure 6.38 SEM-SEI micrographs of concrete prisms containing 25% RH_G at (a) 200x (b) 200x (c) 250x and (d) 500x, showing extensive cracking and presence of ASR gel after 8 months (*Note red arrows in (c) indicate the reaction rim of aggregate*)

The composition of the ASR gels identified in RH_G systems was higher in Ca content, with a Ca/Si ratio value of 0.3 identified. Conversely, a significantly lower Na/Si ratio (0.08) was found. This comparison is made with reference to the composition of the ASR gels in concrete prisms containing WT_G, as both ASR gels were located within the aggregate and not inside the paste. The ASR gels in RH_G prisms appear to exhibit a typical example of alkali recycling. From the dissolution test results presented in Figures 6.6-6.7, it was found that at 60°C, RH_G released the highest amount of alkalis

and Ca, compared to the other two GRAFs studied. Additionally, the alkali concentration in the pore solution of the paste containing these aggregates decreased from 28 days to 90 days, after which time the alkali concentration in the pore solution began to increase. These observations agree with the composition of the gels, as shown in Table 6.6, as well as the related expansions observed. Certainly, the composition of the ASR gels identified satisfies the presumed conditions for the initiation of alkali recycling (Gholizadeh-Vayghan & Rajabipour 2017). As a consequence of alkali recycling, significant alkali remains in the pore solution to react with the larger aggregate particle forming more expansive ASR gel and resulting in the cracks and the level of expansions observed. That said, the high Ca/Si ratio of the gel reduces the swelling capacity of the gel, yet providing some level of mitigation over the gels found in the control concrete prisms. Additionally, although the ASR gels in the control and RH_G concrete prisms have comparable Al/Si ratios, the Na/Si ratio in the RH_G concrete prisms is significantly lower than in the control sample, proposing that the composition of the gel in the former is closer to pozzolanic C-S-H (Monteiro et al. 1997; Powers & Steinour 1955).

Chapter Summary

The work discussed in this chapter evaluates the potential of using ground reactive aggregate fines (GRAFs) as alternative additives to conventional supplementary cementitious materials to reduce the likelihood of deleterious ASR. The efficacy of GRAFs was assessed using chemical dissolution tests, pore solution analysis and determination of residual portlandite in pastes, and physical expansion tests conducted on mortar bars and concrete prisms.

Three GRAFs, WT_G, RH_G, and GW_G, of different reactivity potentials, have been studied. Overall, the results elucidate that the addition of GRAFs to mortar and concrete test specimens significantly reduces the expansion due to ASR and thus provides a promising cost-effective technique for mitigating ASR in commercial concrete. In particular, GRAFs with high soluble silica and Al reacts with alkali in the pore solution through a pozzolanic reaction to form C-S-H and C-A-S-H phases that further bind alkali; thus, reducing the availability of alkali for larger reactive aggregates to form expansive ASR. This reaction also reduces the amount of portlandite in the cement systems, limiting the Ca required for the precipitation of ASR.

All mortar and concrete specimens saw a reduction in expansion upon the addition of GRAFs. However, of the three GRAFs studied, WT_G showed the best ASR mitigatory performance in chemical and physical expansion tests. Characterisation of the concrete prisms after 8 months of ACPT expansion test showed the presence of micro-cracks in the cement pastes as well the presence of narrow (width) ASR gel bands in the aggregate. The composition of the ASR gels suggests ionic exchange in the pore solution driven by the GRAFs, resulting in the formation of less expansive

C-S-H gels and non-expansive C-A-S-H gels that also bind alkali, compared to the expansive (Na, K)-C-S-H gels seen in the control samples. However, when the performance GRAFs was compared to fly ash (FA) as a reference SCM, GRAFs showed a lower mitigation effect relative to FA. This feature was attributed to the particle sizes of GRAFs being larger ($<100\mu\text{m}$) than the particle size of fly ash ($<75\ \mu\text{m}$). The larger particle size of the GRAFs reduced their pozzolanicity and potential pore structure refinement relative to FA. As a consequence, a decrease in the mechanical properties of concrete containing GRAFs was noted. Nonetheless, concretes with GRAFs still retained approximately 76% of the initial concrete strength, thus satisfying the ASTM C618-19 requirements for natural pozzolans

CHAPTER 7. Conclusion

7.1 Overview

In this study, alternative techniques to mitigate against the potential for ASR in mortars and concretes were evaluated using new and recognised test methods. Subsequently, studies on the correlation between these test methods and the factors influencing the occurrence of ASR and, as well as the reliability of the respective test methods were carried out. The key findings from this study are discussed in Chapters four, five, and six. Conversely, the objectives and test programs undertaken in this study are summarized in Sections 7.1, 7.2, and 7.3. Considering the range of materials and variables investigated, this chapter presents the following conclusions.

7.2 Investigation of Alkali Limits and Aggregate Blends for Mitigating Deleterious ASR in Concretes (Chapter Four)

The objectives in this part of the study were aimed:

- I. To identify separate alkali threshold limits for aggregates in concrete, based on their mineralogical composition and reactivity classification rather than the generalised alkali limit of 2.5-2.8 kg/m³ Na₂O_e imposed on all aggregates.
- II. To assess the possibility of reducing the risk of ASR by incorporating sand blends in concrete.

Four reactive aggregates and two sand blends composed of (i) reactive and non-reactive sands and (ii) reactive aggregate and slowly reactive sand were investigated. The aggregates were assessed using a suite of test methods, including petrography and chemical tests, to ascertain the presence of ASR reactive components and the amount of soluble silica in the aggregates. Accelerated mortar bar test (AMBT), concrete prism test (CPT), and accelerated concrete prism test (ACPT) were carried out in accordance with the AS 1141.60.1 and AS 1141.60.2 test method requirements as specified by Standards Australia, to determine the extent of expansion. The alkali content for AMBT was varied from 0.6 M to 1M NaOH and 2.5-5.25 kg/m³ Na₂O_e for CPT and ACPT, following RILEM AAR-3.2 test method requirements. The alkali limits for the aggregates and sand blends were obtained using the RILEM AAR 7.1 specification procedure.

The results demonstrate that the current alkali limits set for concretes are conservatively low and could be adjusted to permit the use of available aggregate and cement sources. This will reduce economic impacts and promote the conservation of natural resources. The outcomes also suggest that the use of sand blends in concretes to mitigate ASR is likely. However, the type and amount of reactive mineral constituents in the reactive sand, as well as the proportions of different sands in the fine aggregate blend, play a crucial role in the success of this technique.

From the key findings in Chapter four, it can be concluded that:

1. The ASR of aggregates is dependent on the mineralogical composition, crystal structure, and amount of reactive constituents present in the aggregate.

2. Aggregates containing volcanic fragments such as glassy shards and acid volcanics have a high susceptibility to ASR. Furthermore, volcanic rocks such as andesites are highly reactive because they contain large amounts of devitrified glass that tend to accommodate alkali in the form of Na-plagioclase. This alkali is released as the metastable silica dissolves and reacts with silica to form deleterious ASR.
3. Argillaceous aggregates such as greywackes that have quartz veins in their structure are usually slowly reactive and have the potential to cause mild ASR.
4. Aggregates containing alkali bearing minerals such as feldspar can influence the outcomes of the dissolution test as per ASTM C289. The test method evaluates the reactivity of aggregate based on the amount of silicon released into alkaline solution, as well as the reduction in the alkalinity of the solution. For this reason, aggregates that release alkali may provide a false indication of the amount of alkalis, thus affecting the prediction of the aggregate's reactivity. Accordingly, if such aggregates are used in concretes, the slow release of alkali could lead to ASR at a later age.
5. AMBT is a practical test method for screening aggregates into reactive and non-reactive categories. However, it is limited in accurately identifying aggregates' reactivity levels due to the extreme alkali and temperature test conditions. As such, it is an unreliable test method for evaluating the alkali limit of aggregates. It was noted that, although the expansion of mortar bars was influenced by the alkali concentration of the AMBT test solution over

time, the reactivity behaviour of the aggregates was not consistent with increasing alkali concentration. For the slowly reactive aggregate, an increase in mortar bar expansion was seen with increasing alkali content. However, the potentially reactive aggregate showed the lowest expansion at 0.8M NaOH, while the mortar bars composed of the sand blends indicated comparable expansion levels at 0.6M and 1.0M NaOH. Although the expansion behaviour of the sand blends could be due to the interaction of varying alkali contents with a pessimum proportion of the reactive minerals in the sand blends, a more consistent response was observed with increasing alkali in ACPT and CPT.

6. Contrary to AMBT, ACPT is a less conservative accelerated test method that is considered reliable in determining the alkali threshold and limits of aggregates in concrete.
7. The current low alkali limit of 2.5-2.8 kg/m³ Na₂O_e set in concrete is indeed unfitting for some aggregates. In contrast, applying the limits for some aggregates may be effective for reducing the likelihood of ASR. Of the aggregates tested, except for the andesitic rock, which potentially releases additional alkali into the pore solution, all other aggregates showed negligible expansion in ACPT and CPT, up to 4.0 kg/m³ Na₂O_e. This affirms the significance of setting alkali limits for aggregate groups based on their mineralogical composition and reactivity classification. Thus the results provide a framework for reconsidering the generalised and conservative current alkali limits set in concretes to allow the use of cements with slightly higher alkali contents.

8. The mechanism of ASR gel expansion differs with increasing temperature and alkali content. Petrographic assessments of concrete specimens studied at 38°C and 60°C showed that dense ASR gels are formed at a high temperature. Dense ASR gels have a potentially high swelling capability and can cause significant concrete expansion in a short time. Conversely, at higher alkali content, specimens showed micro-cracks at several reaction sites, proposing that more metastable silica particles have been affected. This suggests an increase in the concentration of ASR gels leading to a build-up of expansion throughout the concrete. This usually results in a much higher effect on the overall ASR expansion of the concrete as compared to an increase in temperature. The effect of temperature and alkali was further investigated in Chapter five.

9. Due to the severe test conditions for AMBT, expansions exceeding the 0.3% AMBT limit were recorded for mortars containing the sand blends studied. Generally, the AMBT results showed that the reactivity of the sand blends was dominated by the reactivity of the reactive sand. However, in CPT and ACPT, concrete prisms composed of these sand blends showed expansion below the CPT limit of 0.03% after 12 months and 8 months, respectively. After 24 months of CPT, the sand blend composed of reactive aggregate and slowly reactive aggregate did not expand above the 0.03% limit, indicating that it is non-reactive. This demonstrates that it is possible to reduce the risk of ASR by using sand blends.

7.3 Correlation between Test Methods for Assessing Potential ASR of Aggregates (Chapter Five)

The objectives in this part of the study were aimed at:

- I. Evaluating the reliability of the recognised laboratory test methods for assessing ASR by establishing a relationship between the aggregate reactivity classifications as per the different test methods.
- II. Investigating the correlation between CPT and ACPT to determine the potential and viability of using ACPT as an accelerated test method to determine the ASR potential of aggregates; thus, providing an alternative for obtaining an accurate prediction of aggregates' ASR potential for early decision making.
- III. Identifying the influence of temperature, alkali, and age on ASR and related expansions measured in the respective test methods, as well as the effect of alkali leaching on the accuracy of results obtained in concrete prism tests.

These aims were achieved by employing a statistical approach to analyse the results from the dissolution test, ground aggregate slurry test (GAST), and expansion tests conducted in this work. Correlation studies were carried out using Pearson's coefficient of correlation method. Principal component analysis and ANOVA factorial analysis were also performed on the ACPT and CPT results obtained in Chapters four and six to identify variations and commonalities in the two concrete prism test methods. The effect of temperature and alkali on ASR was also discussed.

Furthermore, the amount of alkali leached during concrete prisms tests was evaluated by performing MP-AES on the water solution in storage pails containing ACPT and CPT specimens.

The results showed a good correlation between the different test methods. By comparing the expansion results of ACPT at varying ages to 12 months CPT, a strong correlation with a Pearson's coefficient (r) of 0.9 was obtained, suggesting that ACPT could be used in place of CPT in time-constrained scenarios. From the analysis of the CPT and ACPT storage solutions, it was realised that about 16% of the total alkali in concrete prisms is leached out after 12 months of CPT. Conversely, 22% alkali leaching occurs after 6 months of ACPT. However, the amount of alkalis leached in both cases are lower than $1.0 \text{ kg/m}^3 \text{ Na}_2\text{O}_e$ of the initial alkali content in the concrete.

From the key findings discussed in Chapter five, the following conclusions can be drawn:

1. Owing to the limitations of the individual test methods, adopting a protocol consisting of a set of test methods is essential to obtain the true indication of the reactivity of aggregates.
2. Generally, there is a consistency in the reactivity prediction of aggregates by the different test methods. However, the reactivity classification of aggregates by petrography vary slightly from the results obtained in CPT. This is because the accuracy of petrography strongly relies on the skill of the petrographer and available information on the aggregates' field performance, which can vary with location.

3. The GAST chemical test carried out after 56 days is a promising rapid test method that produces results comparable to CPT after 12 months.
4. A positive correlation exists between AMBT after 21 days and CPT after 12 months. However, due to the severe test conditions in AMBT, certain non-reactive aggregates may be incorrectly identified as slowly reactive aggregates. This emphasizes the need to employ other complementary test methods for aggregates that fail the 10-day expansion limit of 0.1% in AMBT.
5. Alkali leaching occurring in concrete prism tests is noteworthy. However, the amount of alkali leached is not high enough to reduce the alkali content of prisms below the alkali threshold of the respective aggregate. Therefore, the expansion results obtained for aggregates after 12 months of CPT and 3 months are not significantly influenced by the loss of alkali through alkali leaching and hence provide a reliable indication of the aggregates' reactivity
6. The extent of alkali leaching in concrete prism tests is intensified with increasing temperature and alkali content. However, alkali leaching reduces with age. This is attributed to the continued consumption of alkali in the formation of hydration products resulting with age; thus, reducing the amount of alkali in the pore solution that could be leached out.
7. There is a strong positive correlation between CPT after 12 months and ACPT from 3-6 months. However, due to the effect of temperature on continued alkali leaching, ACPT after 3 months is more suitable for correlating and predicting aggregates' reactivity potential after 12 months of CPT. Additionally, the percentage of alkali leaching after 3 months of ACPT

is comparable (18%) to the alkali leached out after 12 months of CPT (16%), supporting the correlation of the ACPT to CPT after 3 months.

8. From the factorial analysis, the two main factors that influence ASR and the reliability of expansion test methods are alkali content and temperature, with alkali content having a more significant effect on the degree of expansion than temperature. An increase in alkali content causes a notable increase in the degree of expansion. However, for higher temperature systems, a decrease in expansion was measured. This is associated with the increased alkali leaching that occurs at higher temperatures. Nonetheless, the aggregates' reactivity potential depends on the mineralogical composition and crystal structure of the aggregate and, therefore, remains unchanged by the effects of temperature and alkali.
9. Although alkali content and temperature affect the rate of ASR occurrence, indicated by the expansion of mortar bars and concrete prisms, there is no interaction between these two factors. That is, a change in alkali content is not dependent on temperature and vice versa.

7.4 Investigating the ASR Mitigating Potential of Ground Reactive Aggregate Fines (Chapter Six)

In Chapter six, the objectives addressed in this part of the study were to determine the efficacy of ground reactive aggregate fines (GRAFs) as alternative additives for mitigating ASR in the absence of conventional supplementary cementitious materials (SCMs).

Three aggregates of different mineralogical compositions, classified by petrography as substantially reactive, reactive, and mild-slow reactive, were ground to approximately 100 µm particle size and used as GRAFs. The potential of GRAFs for mitigating ASR was evaluated by investigating their ability to release silicon and aluminium, and their pozzolanicity in the presence of calcium. The effect of GRAFs on the alkalinity of the pore solution and the expansion behaviour of mortar bars and concrete prisms were also determined. The microstructural changes and composition of the ASR gel formed were correlated with the expansions observed to understand the mechanism of ASR occurrence exhibited by the GRAFs. The effect of GRAFs on the compressive and flexural strengths of concrete specimens was also studied. Furthermore, the performance of the GRAFs was compared to fly ash performance at a 25% replacement level of cement.

Overall, all the GRAFs showed the prospective for mitigating ASR in a similar technique to ASR mitigation mechanism by conventional SCMs such as fly ash. Among the three GRAFs studied, the aggregate classified as substantially reactive in petrography, which also showed the highest expansions in AMBT and concrete prisms tests, exhibited better performance in mitigating ASR. A reduction in the

mechanical properties of the concrete was measured after 28 days when GRAFs were used. However, the compressive and flexural strength measurements obtained in this study were approximately 75%, which complies with the strength activity index limit requirement in the ASTM C618-19. Thus GRAFs can be classified as pozzolanic.

Based on the findings discussed in Chapter six, the main conclusions from this part of the study are as follows:

1. GRAFs that contain high amounts of soluble silica exhibit greater potential for mitigating ASR. The dissolved silica rapidly reacts with available calcium (Ca) in a pozzolanic reaction to form calcium silicate hydrate (C-S-H) phases that are either non-expansive or have low swelling capacity.
2. The presence of aluminium (Al) increases the effectiveness of GRAFs in ASR mitigation. Al reduces silica in the pore solution in a reaction to form sodium aluminium silicate hydrates (N-A-S-H). N-A-S-H usually precipitates on the surface of potentially reactive aggregates, thus preventing further dissolution of silica and in turn hindering ASR progression.
3. GRAFs that release Al in the pore solution also influence the formation of calcium aluminium silicate hydrate (C-A-S-H) gels in place of ASR gels. C-A-S-H gels are non-expansive and exhibit high alkali binding properties
4. The total alkali concentration of the pore solution decreased with the addition of GRAFs. A reduction in the pore solution's alkalinity implies a decrease in the dissolution of silica for ASR. The reaction between Al and silicon (Si) released by GRAFs, and alkali and calcium from the cement, lead

to the precipitation of C-S-H and other alkali binding phases, thus removing alkalis from the pore solution. The extent of reduction in alkalinity of the pore solution is dependent on the amount of Si and Al released by the GRAFs.

5. The addition of GRAFs reduced the Ca/Si ratio of the pore solution by consuming Portlandite in a pozzolanic reaction to form secondary non-expansive C-S-H phases. Additionally, a low Ca/Si ratio attracts Al and precipitates C-A-S-H that potentially binds alkali, reducing alkali availability in the pore solution for ASR.
6. A significant decrease in Portlandite occurred with increasing GRAFs content. Approximately 85% of the Portlandite in the systems containing 100% cement was consumed by the addition of 40% GRAFs through a pozzolanic reaction with the Si released by GRAFs. The depletion of Portlandite reduces Ca, which is essential for the formation of ASR products.
7. GRAFs effectively reduced ASR expansions of mortar bars and concrete prisms in AMBT, CPT, and ACPT. However, the performance of GRAFs was found to be less than the performance of fly ash. This is due to the smaller particle size of the fly ash and its higher surface area contributing to enhanced pozzolanicity better than GRAFs. In addition to releasing silica, consuming portlandite, and reducing alkali content in the pore solution, SCMs also mitigate ASR by refining the pore structure. Pore refinement restricts the ingress of moisture and ASR gel through the concrete and in turn, reduces ASR expansion.

8. The reduction in compressive and flexural strength of the concrete upon addition of GRAFs is due to the lower pore refinement of the concrete structure as a result of the larger particle size of GRAFs ($\leq 100 \mu\text{m}$) compared to cement and conventional SCMs ($\leq 75 \mu\text{m}$). Furthermore, the relatively larger particle size of GRAFs resulted in a reduction in pozzolanicity available after 28 days of curing; therefore, less secondary C-S-H phases, which also contributes to the filling of pores in the concrete, was formed.
9. ASR gels formed in concretes containing GRAFs have varying compositions depending on the reactivity of the GRAFs present and the location of the gel. For GRAFs capable of releasing high amounts of Si and Al, the gels formed within the aggregate particles have a low Ca/Si ratio. The $[\text{Na}+\text{K}]/\text{Si}$ and Al/Si ratios of these gels tend to be high, thus nearing the composition of non-expansive C-A-S-H gels. When the ASR gel is located within the paste, the Ca/Si ratio is high, usually >1 . With a high Ca/Si ratio, the $[\text{Na}+\text{K}]/\text{Si}$ ratio in the gel is low as Ca typically replaces alkalis in the gel structure. The high amount of Ca in the gel improves the crosslinking of the silicate structure. Consequently, a more rigid ASR gel with low expansion capability, termed as pozzolanic C-S-H, is formed. The mechanisms of ASR mitigation identified for GRAFs is similar to the mechanism exhibited by SCMs.

CHAPTER 8. Recommendation for Future Studies

The present study has taken positive steps towards developing techniques to maximise the utilisation of available aggregate and cement sources, while reducing the likelihood of ASR occurrence in concrete. The parameters studied are some of the essential factors that govern the ASR behaviour of aggregates and influence the validity of ASR assessment methods. However, further research outside the scope of this study is recommended to explore a deeper understanding of the outcomes and preventive measures achieved in this work. Consequently, the following future studies are suggested:

1. It has been found that the conservatively low current alkali limit of 2.5-2.8 kg/m³ Na₂O_e set in concrete is unreasonably generalised for all aggregates and may be adjusted to suit aggregates based on their mineralogical composition and reactivity classification. However, in this work, a few selected aggregates were studied. To form a strong basis for this argument, further studies on the respective alkali limit of an extensive collection of aggregates from different sources classified under the various reactivity classification groups, such as described in AMBT, will be beneficial. This will provide a database that can be used to revise the current alkali limits as per the aggregate's reactivity classification.
2. The CPT alkali threshold studies carried out in this study varied alkali content by adding NaOH to the water used in the concrete mix. It will be interesting to reproduce the results obtained by incorporating cements of alkali content similar to the amounts achieved with the addition of NaOH and

extending the test duration up to 24 months. This will give a reliable indication of the aggregates' behaviour in field structures containing cement of the respective alkali contents for better decision-making.

3. The findings from this study have shown a strong positive correlation between the ASR test methods used, that is, petrography, GAST, AMBT, CPT, and ACPT. However, the number of aggregates studied was limited to New Zealand and Australia. In order to establish a general correlation index that will be globally accepted and applied, further testing on a wide selection of aggregates is recommended to determine the correlation between the petrography of the aggregates and expansion test methods, as well as the petrography of post-expansion test specimens and their respective expansions measured. Consistency in these results will boost confidence in the reliability of the various test methods, and may provide industry and researchers with reference to predict the ASR of aggregates in long-term tests based on the results obtained from short-term test methods. Additionally, future studies on this research topic could also investigate the influence of test the conditions such as alkali, age, and temperature, on the correlation between AMBT, CPT, and ACPT.

4. It will be beneficial to carry out studies on the use of ground reactive aggregate fines (GRAFs) of particle size $\leq 75 \mu\text{m}$. In this study, it was established that the addition of GRAFs reduced the mechanical properties of the concrete due to the lower pore refinement and the limited pozzolanicity exhibited by the $\leq 100 \mu\text{m}$ particle size. This could also be the reason for the

lower performance of GRAFs relative to fly ash. With the exception of pore refinement, GRAFs exhibited high ASR mitigation potential. By reducing the particle size to ranges similar to SCMs, the pore filling effect and pozzolanicity of GRAFs is also likely to improve, making these materials comparable to conventional SCMs. It is also recommended to increase the curing age of concrete prisms beyond 28 days to evaluate the influence of GRAFs on later age mechanical properties of concrete.

5. There are reports in literature that suggest that fine grinding can alter the crystal structure of minerals. In particular, one study stated that a longer grinding duration results in the reduction of crystallite size and an increase in lattice strain of silica (Sohor, Mustapha & Mamat 2017). This leads to some interesting hypothesis that the reactivity or pozzolanicity of GRAFs is not only due to the increase in surface area but also due to the transformation of some crystalline silica minerals into strained silica. Therefore, increasing their susceptibility to alkali. Accordingly, the assumption could be made that all aggregates containing silica, crystalline or otherwise, may possess ASR mitigating properties when used as GRAFs. Further studies to explore this hypothesis will be valuable in understanding the utilisation of available aggregate sources as potential GRAFs for ASR mitigation. Additionally, from this further testing recommendation, a database of the aggregate types that show high ASR mitigation when used as GRAFs may also be established.

References

- Afshinnia, K. & Poursaee, A. 2015, 'The potential of ground clay brick to mitigate Alkali–Silica Reaction in mortar prepared with highly reactive aggregate', *Construction and Building Materials*, vol. 95, pp. 164-70.
- Afshinnia, K. & Rangaraju, P.R. 2015a, 'Efficiency of ternary blends containing fine glass powder in mitigating alkali–silica reaction', *Construction and Building Materials*, vol. 100, pp. 234-45.
- Afshinnia, K. & Rangaraju, P.R. 2015b, 'Mitigating Alkali–Silica Reaction in Concrete: Effectiveness of Ground Glass Powder from Recycled Glass', *Transportation Research Record*, vol. 2508, no. 1, pp. 65-72.
- Aldred, J.M., Holland, T.C., Morgan, D.R., Roy, D.M., Bury, M.A., Hooton, R.D., Olek, J., Scali, M.J., Detwiler, R.J. & Jaber, T.M. 2006, 'Guide for the use of silica fume in concrete', *ACI–American Concrete Institute–Committee: Farmington Hills, MI, USA*, vol. 234.
- Alehyen, S., Achouri, M. & Taibi, M. 2017, 'Characterization, microstructure and properties of fly ash-based geopolymer', *J. Mater. Environ. Sci*, vol. 8, no. 5, pp. 1783-96.
- Alison Pryor 2020, 'TVA slicing into Chickamauga Dam, water to spray out temporarily', *WRCBTv*.
- Alonso, M., Garcia, C. & Walker, C. 2012, *Development of an accurate pH measurement methodology for the pore fluids of low pH cementitious materials*, Swedish Nuclear Fuel and Waste Management Co.

- Andersson, K., Allard, B., Bengtsson, M. & Magnusson, B. 1989, 'Chemical composition of cement pore solutions', *Cement and Concrete Research*, vol. 19, no. 3, pp. 327-32.
- Ashley Walsh 2011, 'Bay Bridge Building', *ABC News*.
- ASTM 2003, 'ASTM C295/03: Standard Guide for Petrographic Examination of Aggregates for Concrete', *ASTM International*.
- ASTM 2007, 'ASTM C289 - 07 Standard Test Method for Potential Alkali - Silica Reactivity of Aggregates (Chemical Method)'.
- ASTM 2016, 'ASTM C1778 - Standard Guide for Reducing the Risk of Deleterious Alkali-Aggregate Reaction in Concrete.', *American Society for Testing and Materials.*, vol. 4.
- ASTM 2019, *ASTM C 618, -19 Standard Specification for Coal Fly Ash and Raw or Calcined Natural Pozzolan for Use in Concrete.*, ASTM International, West Conshohocken, PA.
- ASTM C856 2018, *Standard Practice for Petrographic Examination of Hardened Concrete*, ASTM International, West Conshohocken, PA.
- ASTM, C. 2008, '1293', *Standard Test Method for Concrete Aggregates by Determination of Length Change of Concrete Due to Alkali Silica Reaction*.
- Azizi, S.N., Alavi Daghigh, A. & Abrishamkar, M. 2013, 'Phase transformation of zeolite P to Y and analcime zeolites due to changing the time and temperature', *Journal of Spectroscopy*, vol. 2013.
- Azizi, S.N. & Ehsani Tilami, S. 2009, 'Recrystallization of Zeolite Y to Analcime and Zeolite P with d - Methionine as Structure - Directing Agent (SDA)', *Zeitschrift für anorganische und allgemeine Chemie*, vol. 635, no. 15, pp. 2660-4.

- Bach, T., Chabas, E., Pochard, I., Coumes, C.C.D., Haas, J., Frizon, F. & Nonat, A. 2013, 'Retention of alkali ions by hydrated low-pH cements: Mechanism and Na⁺/K⁺ selectivity', *Cement and Concrete Research*, vol. 51, pp. 14-21.
- Barger, G.S. & Hansen, E.R. 1998, 'Cementitious systems and methods of making the same', Google Patents.
- Barneyback Jr, R. & Diamond, S. 1981, 'Expression and analysis of pore fluids from hardened cement pastes and mortars', *Cement and Concrete Research*, vol. 11, no. 2, pp. 279-85.
- Bauer, S., Cornell, B., Figurski, D., Ley, T., Miralles, J. & Folliard, K. 2006, 'Alkali-silica reaction and delayed ettringite formation in concrete: A literature review'.
- Bavasso, I., Costa, U., Mangialardi, T. & Paolini, A.E. 2020, 'Assessment of Alkali-Silica Reactivity of Aggregates by Concrete Expansion Tests in Alkaline Solutions at 38° C', *Materials*, vol. 13, no. 2, p. 288.
- Bektas, F., Turanli, L. & Monteiro, P. 2005, 'Use of perlite powder to suppress the alkali-silica reaction', *Cement and Concrete Research*, vol. 35, no. 10, pp. 2014-7.
- Bentur, A., Berger, R.L., Kung, J.H., Milestone, N. & Young, J. 1979, 'Structural properties of calcium silicate pastes: II, effect of curing temperature', *Journal of the American Ceramic Society*, vol. 62, no. 7 - 8, pp. 362-6.
- Berke, N., Hicks, M. & Folliard, K. 1997, 'Systems Approach to Concrete Durability', *Special Publication*, vol. 170, pp. 1293-316.
- Bérubé, M.-A. 2004, 'Alkali releasable by aggregates in concrete-significance and test methods', *Proceedings of 12th Inter. Conf. on Alkali-Aggregate Reaction in Concrete, 2004*, vol. 1, pp. 17-30.
- Bérubé, M.-A., Duchesne, J., Dorion, J. & Rivest, M. 2002, 'Laboratory assessment of alkali contribution by aggregates to concrete and application to concrete structures

- affected by alkali–silica reactivity', *Cement and Concrete research*, vol. 32, no. 8, pp. 1215-27.
- Bérubé, M.-A., Durand, B., Vézina, D. & Fournier, B. 2000, 'Alkali-aggregate reactivity in Quebec (Canada)', *Canadian Journal of Civil Engineering*, vol. 27, no. 2, pp. 226-45.
- Bérubé, M.-A. & Fournier, B. 1993, 'Canadian experience with testing for alkali-aggregate reactivity in concrete', *Cement and Concrete Composites*, vol. 15, no. 1-2, pp. 27-47.
- Bérubé, M. & Fournier, B. 1992, 'Accelerated test methods for alkali-aggregate reactivity', *Advances in Concrete Technology*, pp. 583-627.
- Bignozzi, M., Sacconi, A., Barbieri, L. & Lancellotti, I. 2015, 'Glass waste as supplementary cementing materials: The effects of glass chemical composition', *Cement and Concrete Composites*, vol. 55, pp. 45-52.
- Binal, A. 2008, 'The determination of gel swelling pressure of reactive aggregates by ASGPM device and a new reactive-innocuous aggregate decision chart', *Construction and Building Materials*, vol. 22, no. 1, pp. 1-13.
- Black, P. 2009, 'Andesites as resources for roading and concrete industries, North Island of New Zealand', *Department of Geology, University of Auckland*, vol. 328, p. 332.
- Blaikie, N., Bowling, A. & Carse, A. 1996, 'The assessment and management of alkali-silica reaction in the gordon river power development intake tower', *Proc. 10th Inter. Conf. on Alkali-aggregate Reaction in Concrete*, pp. 500-7.
- Bleszynski, R.F. & Thomas, M.D. 1998, 'Microstructural studies of alkali-silica reaction in fly ash concrete immersed in alkaline solutions', *Advanced Cement Based Materials*, vol. 7, no. 2, pp. 66-78.

- Blight, G., McIver, J., Schutte, W. & Rimmer, R. 1981, 'The effects of alkali–aggregate reaction on reinforced concrete structures made with Witwatersrand quartzite aggregate, 5th ICAAR—International Conference on Alkali–Aggregate Reaction in Concrete', *Cape Town, South Africa*, pp. 733-9.
- Boivin, J. & Ng, S. 2006, 'Are more data always better for factor analysis?', *Journal of Econometrics*, vol. 132, no. 1, pp. 169-94.
- Bollotte, B. 1992, 'Development of an accelerated performance test on concrete for evaluating its resistance to AAR', *Proc. 9th Int. Conf. on AAR in Concrete, London*, pp. 110-6.
- Bouzabata, H., Multon, S., Sellier, A. & Houari, H. 2012, 'Swellings due to alkali-silica reaction and delayed ettringite formation: Characterisation of expansion isotropy and effect of moisture conditions', *Cement and Concrete Composites*, vol. 34, no. 3, pp. 349-56.
- Box, G.E., Hunter, J.S. & Hunter, W.G. 2008, *Statistics for experimenters: design, innovation, and discovery. Estadística para investigadores: diseño, innovación y descubrimiento*, 8429150447.
- Boyd-Weetman, B. & Thomas, P. 2020, 'Assessment of the ground aggregate paste (GAP) test for aggregate alkali–silica reactivity screening', *JOURNAL OF THERMAL ANALYSIS AND CALORIMETRY*.
- Broekmans, M.A. 2004, 'Structural properties of quartz and their potential role for ASR', *Materials characterization*, vol. 53, no. 2-4, pp. 129-40.
- Brown, h.L.H.L., Eugene; Bursten, Bruce E. ;Catherine Murphy, Patrick Woodward, Steven Langford, Dalius Sagatys, Adrian Georg 2012, 'Chemistry: The Central Science', vol. 3rd Edition.

- Bukhari, S.K. 2019, 'Potential alkali silica reactivity of aggregates from different sources of Kashmir and mitigation measures thereof', *Asian Journal of Civil Engineering*, vol. 20, no. 3, pp. 437-42.
- Callister, W.D.J. & Rethwisch, D.G. 2014, *Materials Science and Engineering- An Introduction*, 9E edn, John Wiley & Sons, United States of America.
- Canadian Standards Association 2000, *CSA A23.2-27A*, Canadian Standards Association, Mississauga, Ontario, Canada.
- Castro, N., Sorensen, B.E. & Broekmans, M.A. 2012, 'Quantitative assessment of alkali-reactive aggregate mineral content through XRD using polished sections as a supplementary tool to RILEM AAR-1 (petrographic method)', *Cement and concrete research*, vol. 42, no. 11, pp. 1428-37.
- CCANZ 2012, ' Alkali Silica Reaction. Minimising the risk of damage to concrete. Guidance notes and recommended practice. Technical Report 3, 2nd ed, incl Amendment 1. ', *Cement and Concrete Association of New Zealand*.
- Chandra Paul, S., Mbewe, P.B., Kong, S.Y. & Šavija, B. 2019, 'Agricultural solid waste as source of supplementary cementitious materials in developing countries', *Materials*, vol. 12, no. 7, p. 1112.
- Chappex, T. & Scrivener, K. 2012, 'Controlling alkali silica reaction by understanding the contribution of aluminium provided by supplementary cementitious materials', *14th International Conference on Alkali–Aggregate Reactions in concrete, Austin, Texas*.
- Chatterji, S. 2005, 'Chemistry of alkali–silica reaction and testing of aggregates', *Cement and Concrete Composites*, vol. 27, no. 7-8, pp. 788-95.

- Chatterji, S., Jensen, A., Thaulow, N. & Christensen, P. 1986, 'Studies of alkali-silica reaction. Part 3. Mechanisms by which NaCl and Ca (OH) 2 affect the reaction', *Cement and Concrete Research*, vol. 16, no. 2, pp. 246-54.
- Chatterji, S. & Kawamura, M. 1992, 'Electrical double layer, ion transport and reactions in hardened cement paste', *Cement and Concrete Research*, vol. 22, no. 5, pp. 774-82.
- Chen, H., Soles, J. & Malhotra, V. 1993, 'Investigations of supplementary cementing materials for reducing alkali-aggregate reactions', *Cement and Concrete Composites*, vol. 15, no. 1-2, pp. 75-84.
- Chen, J., Ma, H., Liu, C. & Yuan, J. 2017, 'Synthesis of analcime crystals and simultaneous potassium extraction from natrolite syenite', *Advances in Materials Science and Engineering*, vol. 2017.
- Chindaprasirt, P., Jaturapitakkul, C. & Sinsiri, T. 2005, 'Effect of fly ash fineness on compressive strength and pore size of blended cement paste', *Cement and Concrete Composites*, vol. 27, no. 4, pp. 425-8.
- Cline, J., Mendenhall, M., Black, D., Windover, D. & Henins, A. 2019, 'The instrument profile function'.
- Coleman, N. & Page, C. 1997, 'Aspects of the pore solution chemistry of hydrated cement pastes containing metakaolin', *Cement and concrete research*, vol. 27, no. 1, pp. 147-54.
- Costa, U., Mangialardi, T. & Paolini, A. 2017, 'Minimizing alkali leaching in the concrete prism expansion test at 38° C', *Construction and Building Materials*, vol. 146, pp. 547-54.

- Criado, M., Fernández-Jiménez, A., De La Torre, A., Aranda, M. & Palomo, A. 2007, 'An XRD study of the effect of the SiO₂/Na₂O ratio on the alkali activation of fly ash', *Cement and concrete research*, vol. 37, no. 5, pp. 671-9.
- Cuevas, A., Febrero, M. & Fraiman, R. 2004, 'An anova test for functional data', *Computational statistics & data analysis*, vol. 47, no. 1, pp. 111-22.
- Czarnecki, B. & Eng, P. 2016, 'Delayed Ettringite Formation (DEF) in Precast Concrete Fear, Facts and Risks', *Annual Conference of Transportation Association of Canada*.
- Deboucha, W., Leklou, N., Khelidj, A. & Oudjit, M.N. 2017, 'Hydration development of mineral additives blended cement using thermogravimetric analysis (TGA): Methodology of calculating the degree of hydration', *Construction and Building Materials*, vol. 146, pp. 687-701.
- DeGrosbois, M. & Fontaine, E. 2000, 'Performance of the 60 C-accelerated concrete prism test for the evaluation of potential alkali-reactivity of concrete aggregates', *The*, vol. 1, pp. 277-86.
- DeMerchant, D., Fournier, B. & Strang, F. 2000, 'Alkali-aggregate research in New Brunswick', *Canadian Journal of Civil Engineering*, vol. 27, no. 2, pp. 212-25.
- Demir, İ., Güzelkçük, S., Sevim, Ö., Filazi, A. & Şengül, Ç.G. 2017, 'Examination of Microstructure of Fly Ash in Cement Mortar', *Conference: International Conference on Engineering and Natural Science (ICENS), At Lisbon, Portugal*.
- Diamond, S. 1975, 'A review of alkali-silica reaction and expansion mechanisms 1. Alkalies in cements and in concrete pore solutions', *Cement and Concrete research*, vol. 5, no. 4, pp. 329-45.
- Diamond, S. 1976, 'A review of alkali-silica reaction and expansion mechanisms 2. Reactive aggregates', *Cement and Concrete Research*, vol. 6, no. 4, pp. 549-60.

- Diamond, S. 1989, 'ASR-another look at mechanisms', *Proc. 8th Intl. Conf. on Alkali-Aggregate Reaction*, pp. 115-9.
- Diamond, S. 1997, 'Alkali silica reactions—some paradoxes', *Cement and Concrete Composites*, vol. 19, no. 5-6, pp. 391-401.
- Diamond, S. 2000, 'Chemistry and Other Characteristics of ASR Gels', *Proc. of the 11th International Conference on Alkali-Aggregate Reaction in Concrete*, pp. 31-40.
- Diamond, S. & Lopez-Flores, F. 1981, 'Comparative studies of the effects of lignitic and bituminous fly ashes in hydrated cement systems', *Material Research Society. In: Effects of Fly Ash Incorporation in Cement and Concrete: Proc. Sympos. N Annual Meeting. (Diamond, S.(Ed.)). Boston*, pp. 112-23.
- Diamond, S. & Thaulow, N. 1974, 'A study of expansion due to alkali—silica reaction as conditioned by the grain size of the reactive aggregate', *Cement and Concrete Research*, vol. 4, no. 4, pp. 591-607.
- Dolar-Mantuani, L. 1983, 'Handbook of concrete aggregates: A petrographic and technological evaluation', *NOYES DATA CORP., MILL RD. AT GRAND AVE., PARK RIDGE, NJ 07656, USA, 1983, 345*.
- Drolet, C., Duchesne, J. & Fournier, B. 2017, 'Validation of the alkali contribution by aggregates to the concrete pore solution', *Cement and Concrete Research*, vol. 98, pp. 10-23.
- Duchesne, J. & Be, M. 1995, 'Effect of supplementary cementing materials on the composition of cement hydration products', *Advanced Cement Based Materials*, vol. 2, no. 2, pp. 43-52.
- Duchesne, J. & Bérubé, M.-A. 2001, 'Long-term effectiveness of supplementary cementing materials against alkali–silica reaction', *Cement and concrete research*, vol. 31, no. 7, pp. 1057-63.

- Duchesne, J. & Bérubé, M. 1994, 'The effectiveness of supplementary cementing materials in suppressing expansion due to ASR: another look at the reaction mechanisms part 2: pore solution chemistry', *Cement and Concrete Research*, vol. 24, no. 2, pp. 221-30.
- Durant, A., Bigley, C.H. & Milestone, N.B. 2013, 'Pozzolans and Admixtures – How Can We Use These to Our Best Advantage?', paper presented to the NZ Concrete Industry Conference 2013-Concrete Futures, Queenstown, New Zealand, 3-5 October 2013.
- Duxson, P., Fernández-Jiménez, A., Provis, J.L., Lukey, G.C., Palomo, A. & van Deventer, J.S. 2007, 'Geopolymer technology: the current state of the art', *Journal of materials science*, vol. 42, no. 9, pp. 2917-33.
- Einarsdottir, S.U. & Hooton, R.D. 2018, 'Modifications to ASTM C1293 that Allow Testing of Low Alkali Binder Systems', *ACI Materials Journal*, vol. 115, no. 5, pp. 739-47.
- Emerson, R.W. 2015, 'Causation and Pearson's correlation coefficient', *Journal of visual impairment & blindness*, vol. 109, no. 3, pp. 242-4.
- Eshel, G., Levy, G., Mingelgrin, U. & Singer, M. 2004, 'Critical evaluation of the use of laser diffraction for particle - size distribution analysis', *Soil Science Society of America Journal*, vol. 68, no. 3, pp. 736-43.
- Fanghui, H., Qiang, W. & Jingjing, F. 2015, 'The differences among the roles of ground fly ash in the paste, mortar and concrete', *Construction and Building Materials*, vol. 93, pp. 172-9.
- Fansuri, H., Pritchard, D. & Zhang, D.-K. 2008, 'Manufacture of Low-Grade Zeolites from Fly Ash for Fertiliser Applications'.

- Fernandes, I., dos Anjos Ribeiro, M., Broekmans, M.A. & Sims, I. 2016, *Petrographic atlas: characterisation of aggregates regarding potential reactivity to alkalis: RILEM TC 219-ACS recommended guidance AAR-1.2, for use with the RILEM AAR-1.1 petrographic examination method*, vol. 20, Springer.
- Fernandes, I., Silva, A.S., Gomes, J.P., de Castro, A.T., Noronha, F. & dos Anjos Ribeiro, M. 2013, 'Characterization of deleterious expansive reactions in fagilde dam', *Metallography, Microstructure, and Analysis*, vol. 2, no. 5, pp. 299-312.
- Fernández-Jiménez, A., Palomo, A. & Criado, M. 2005, 'Microstructure development of alkali-activated fly ash cement: a descriptive model', *Cement and concrete research*, vol. 35, no. 6, pp. 1204-9.
- Ferrara, L., Van Mullem, T., Alonso, M.C., Antonaci, P., Borg, R.P., Cuenca, E., Jefferson, A., Ng, P.-L., Peled, A. & Roig-Flores, M. 2018, 'Experimental characterization of the self-healing capacity of cement based materials and its effects on the material performance: A state of the art report by COST Action SARCOS WG2', *Construction and Building Materials*, vol. 167, pp. 115-42.
- Figg, J. 1987, 'ASR-Inside Phenomena and Outside Effects (Crack Origin and Pattern)', *Concrete Alkali-Aggregate Reactions, Proceedings of the 7th International Conference, edited by Grattan-Bellew, Patrick E., Noyes Publications, Park Ridge, New Jersey*, pp. 152-6.
- Folliard, K.J., Barborak, R., Drimalas, T., Du, L., Garber, S., Ideker, J., Ley, T., Williams, S., Juenger, M. & Thomas, M.D. 2006, 'Preventing Alkali-Silica Reaction and Delayed Ettringite Formation in New Concrete', *Project Summary report 0-4085, Center for Transportation Research, University of Texas, Austin*.
- Folliard, K.J., Ideker, J., Thomas, M.D. & Fournier, B. 2004, 'Assessing Aggregate Reactivity Using the Accelerated Concrete Prism Tests', *Aggregates: Asphalt*

Concrete, Portland Cement Concrete, Bases, and Fines. Twelfth Annual Symposium International Center for Aggregates Research (ICAR); University of Texas at Austin; Texas A&M University System; Aggregates Foundation for Technology, Research & Education (AFTRE); National Stone, Sand & Gravel Association (NSSGA); Florida Rock Industries.

Forster, S.W., Akers, D.J., Lee, M.K., Pergalsky, A., Arrand, C.D., Lewis, D.W., Pierce, J.S., Barger, G.S., MacDonald, D.R. & Pisaneschi, R.R. 1998a, 'Report on alkali-aggregate reactivity', *American Concrete Institute ACI*, vol. 221, no. 1.

Forster, S.W., Akers, D.J., Lee, M.K., Pergalsky, A., Arrand, C.D., Lewis, D.W., Pierce, J.S., Barger, G.S., MacDonald, D.R. & Pisaneschi, R.R. 1998b, 'State-of-the-art report on alkali-aggregate reactivity', *Am. Concr. Inst. ACI*, vol. 221, pp. 1-23.

Fournier, B. & Bérubé, M.-A. 2000, 'Alkali-aggregate reaction in concrete: a review of basic concepts and engineering implications', *Canadian Journal of Civil Engineering*, vol. 27, no. 2, pp. 167-91.

Fournier, B., Bérubé, M., Thomas, M. & Folliard, K. 2005, 'Mitigation of the effect of alkali-silica reaction in concrete structures: a review', *IBRACON Materials Journal*, vol. 1, no. 1.

Fournier, B., Chevrier, R., de Grosbois, M., Lisella, R., Folliard, K., Ideker, J., Shehata, M., Thomas, M. & Baxter, S. 2004, 'The accelerated concrete prism test (60 C): variability of the test method and proposed expansion limits', *Proc. of the 12th Int. Conf. on AAR in Concrete, Beijing (China)*, pp. 314-23.

Francisco, R. 2018, *XRF: X-Ray Fluorescence Spectroscopy | Hi Rel Parts*.

Freitag, S.A., Goguel, R. and Milestone, N.B. 2003, *Alkali silica reaction. Minimising the risk of damage to concrete. Guidance notes and recommended practice. Second Edition. Cement and concrete association*

of New Zealand Technical Report 3, 84 pp.

Freitag, S.A. & Mackechnie, J. 2018, 'ALKALI AGGREGATE REACTION IN NZ CONCRETE: MINIMISING DAMAGE IN NEW STRUCTURES', paper presented to the The Concrete NZ Conference 2018, Claudelands, Hamilton. New Zealand, 11-13 October 2018.

Friedman, S. & Weisberg, H.F. 1981, 'Interpreting the first eigenvalue of a correlation matrix', *Educational and Psychological Measurement*, vol. 41, no. 1, pp. 11-21.

Gholizadeh-Vayghan, A. & Rajabipour, F. 2017, 'The influence of alkali-silica reaction (ASR) gel composition on its hydrophilic properties and free swelling in contact with water vapor', *Cement and Concrete Research*, vol. 94, pp. 49-58.

Gillott, J. 1986, 'Alkali-reactivity problems with emphasis on Canadian aggregates', *Engineering Geology*, vol. 23, no. 1, pp. 29-43.

Gillott, J. & Asgeirsson, H. 1975, 'Practical implications of the mechanisms of alkali-aggregate reactions', *Alkali-Aggregate Reaction Preventative Measures, Symposium, Reykjavik*, pp. 213-30.

Gillott, J. & Rogers, C. 1994, 'Alkali-aggregate reaction and internal release of alkalis', *Magazine of Concrete Research*, vol. 46, no. 167, pp. 99-112.

Glasser, L.D. & Kataoka, N. 1981, 'The chemistry of 'alkali-aggregate' reaction', *Cement and concrete research*, vol. 11, no. 1, pp. 1-9.

Golmakani, F. 2013, 'Possible modifications to the accelerated mortar bar test (ASTM C1260)'.

Grattan-Bellew, P. 1995, 'Laboratory evaluation of alkali-silica reaction in concrete from Saunders Generating Station', *Materials Journal*, vol. 92, no. 2, pp. 126-34.

Grattan-Bellew, P. & Chan, G. 2013, 'Comparison of the morphology of alkali-silica gel formed in limestones in concrete affected by the so-called alkali-carbonate

- reaction (ACR) and alkali–silica reaction (ASR)', *Cement and concrete research*, vol. 47, pp. 51-4.
- Grattan-Bellew, P., Mitchell, L., Margeson, J. & Min, D. 2010, 'Is alkali–carbonate reaction just a variant of alkali–silica reaction ACR= ASR?', *Cement and Concrete Research*, vol. 40, no. 4, pp. 556-62.
- Gudmundsson, G. & Asgeirsson, H. 1975, 'Some Investigation on Alkali Aggregate Reaction, Cement and Concrete Research, Vol. 5', *New York*, pp. 211-20.
- Hasanah, F., Anwar, S., Hartono, A. & Sudadi, U., 'Potential Use of Alkaline-Activated Indonesian Pumice Powder as Lead Adsorbent in Solution System', *SAINS TANAH-Journal of Soil Science and Agroclimatology*, vol. 16, no. 2, pp. 203-15.
- Hauke, J. & Kossowski, T. 2011, 'Comparison of values of Pearson's and Spearman's correlation coefficients on the same sets of data', *Quaestiones geographicae*, vol. 30, no. 2, pp. 87-93.
- He, Z., Wang, L., Shao, Y. & Cai, X. 2011, 'Effect of decalcification on CSH gel microstructure in cement paste', *Journal of Building Materials*, vol. 14, no. 3, pp. 293-8.
- Helgeson, H.C., Murphy, W.M. & Aagaard, P. 1984, 'Thermodynamic and kinetic constraints on reaction rates among minerals and aqueous solutions. II. Rate constants, effective surface area, and the hydrolysis of feldspar', *Geochimica et Cosmochimica Acta*, vol. 48, no. 12, pp. 2405-32.
- Helmuth, R., Stark, D., Diamond, S. & Moranville-Regourd, M. 1993, 'Alkali-silica reactivity: an overview of research', *Contract*, vol. 100, p. 202.
- Hester, D., McNally, C. & Richardson, M. 2005, 'A study of the influence of slag alkali level on the alkali–silica reactivity of slag concrete', *Construction and Building Materials*, vol. 19, no. 9, pp. 661-5.

- Hobbs, D. 1982, 'Influence of pulverized–fuel ash and granulated blastfurnace slag upon expansion caused by the alkali–silica reaction', *Magazine of concrete Research*, vol. 34, no. 119, pp. 83-94.
- Hobbs, D.W. 1988, 'Alkali-silica reaction in concrete'.
- Hodder, A. & Hetherington, J. 1991, 'A quantitative study of the weathering of greywacke', *Engineering Geology*, vol. 31, no. 3-4, pp. 353-68.
- Holdren Jr, G.R. & Berner, R.A. 1979, 'Mechanism of feldspar weathering—I. Experimental studies', *Geochimica et Cosmochimica Acta*, vol. 43, no. 8, pp. 1161-71.
- Hong, S.-Y. & Glasser, F.P. 2002, 'Alkali sorption by CSH and CASH gels: Part II. Role of alumina', *Cement and Concrete Research*, vol. 32, no. 7, pp. 1101-11.
- Hooton, R., Thomas, M. & Ramlochan, T. 2010, 'Use of pore solution analysis in design for concrete durability', *Advances in cement research*, vol. 22, no. 4, pp. 203-10.
- Hou, X., Kirkpatrick, R.J., Struble, L.J. & Monteiro, P.J. 2005, 'Structural investigations of alkali silicate gels', *Journal of the American Ceramic Society*, vol. 88, no. 4, pp. 943-9.
- Hou, X., Struble, L.J. & Kirkpatrick, R.J. 2004, 'Formation of ASR gel and the roles of CSH and portlandite', *Cement and Concrete Research*, vol. 34, no. 9, pp. 1683-96.
- Hu, C., Gautam, B.P. & Panesar, D.K. 2018, 'Nano-mechanical properties of alkali-silica reaction (ASR) products in concrete measured by nano-indentation', *Construction and Building Materials*, vol. 158, pp. 75-83.
- Hünger, K.-J. 2007, 'The contribution of quartz and the role of aluminum for understanding the AAR with greywacke', *Cement and concrete research*, vol. 37, no. 8, pp. 1193-205.

- Hünger, K.-J., Hübert, C. & Scholz, Y. 2016, 'On the Interactions of Aggregates with Supplementary Cementing Materials for Durable Concrete Structures'.
- Ichikawa, T. 2009, 'Alkali–silica reaction, pessimum effects and pozzolanic effect', *Cement and Concrete Research*, vol. 39, no. 8, pp. 716-26.
- Ideker, J.H., East, B.L., Folliard, K.J., Thomas, M.D. & Fournier, B. 2010, 'The current state of the accelerated concrete prism test', *Cement and Concrete Research*, vol. 40, no. 4, pp. 550-5.
- Iordanidis, A., Buckman, J., Triantafyllou, A. & Asvesta, A. 2008, 'Fly ash–airborne particles from Ptolemais–Kozani area, northern Greece, as determined by ESEM-EDX', *International Journal of Coal Geology*, vol. 73, no. 1, pp. 63-73.
- Islam, M.S. 2010, 'Performance of Nevada’s aggregates in alkali-aggregate reactivity of Portland cement concrete'.
- Islam, M.S. & Akhtar, S. 2013, 'A critical assessment to the performance of alkali-silica reaction (ASR) in concrete', *Canadian Chemical Transactions*, vol. 1, no. 4, pp. 253-66.
- Islam, M.S., Alam, M.S., Ghafoori, N. & Sadiq, R. 2016, 'Role of solution concentration, cement alkali and test duration on expansion of accelerated mortar bar test (AMBT)', *Materials and Structures*, vol. 49, no. 5, pp. 1955-65.
- Jolliffe, I. & Morgan, B. 1992, 'Principal component analysis and exploratory factor analysis', *Statistical methods in medical research*, vol. 1, no. 1, pp. 69-95.
- Jolliffe, I.T. & Cadima, J. 2016, 'Principal component analysis: a review and recent developments', *Philosophical Transactions of the Royal Society A: Mathematical, Physical and Engineering Sciences*, vol. 374, no. 2065, p. 20150202.
- Jóźwiak-Niedźwiedzka, D., Gibas, K. & Glinicki, M., 'Petrographic Evaluation of Reactive Minerals in Selected Crushed Aggregates in Poland'.

- Kamala, C., Balaram, V., Dharmendra, V., Satyanarayanan, M., Subramanyam, K. & Krishnaiah, A. 2014, 'Application of Microwave Plasma Atomic Emission Spectrometry (MP-AES) for environmental monitoring of industrially contaminated sites in Hyderabad City', *Environmental monitoring and assessment*, vol. 186, no. 11, pp. 7097-113.
- Katayama, T. 1992, 'A critical review of carbonate rock reactions—Is their reactivity useful or harmful', *Proceeding of the 9th International Alkali–Aggregate Reactions Conference, London, Concrete Society, Slough, Publ. CS-104*, pp. 508-18.
- Katayama, T. 2004, 'How to identify carbonate rock reactions in concrete', *Materials Characterization*, vol. 53, no. 2-4, pp. 85-104.
- Katayama, T. 2010, 'The so-called alkali-carbonate reaction (ACR)—Its mineralogical and geochemical details, with special reference to ASR', *Cement and Concrete Research*, vol. 40, no. 4, pp. 643-75.
- Katayama, T., Mauco, A., Kosec, T., Kopar, T. & Gartner, N. 2011, 'So-called alkali–carbonate reaction—petrographic details of field concretes in Ontario', *BOOK OF EXTENDED*, p. 38.
- Kawabata, Y., Dunant, C., Yamada, K. & Scrivener, K. 2019, 'Impact of temperature on expansive behavior of concrete with a highly reactive andesite due to the alkali–silica reaction', *Cement and Concrete Research*, vol. 125, p. 105888.
- Kawabata, Y. & Yamada, K. 2017, 'The mechanism of limited inhibition by fly ash on expansion due to alkali–silica reaction at the pessimum proportion', *Cement and Concrete Research*, vol. 92, pp. 1-15.
- Kawabata, Y., Yamada, K., Sagawa, Y. & Ogawa, S. 2018, 'Alkali-Wrapped Concrete Prism Test (AW-CPT)—New Testing Protocol Toward a Performance Test against

- Alkali-Silica Reaction-', *Journal of Advanced Concrete Technology*, vol. 16, no. 9, pp. 441-60.
- Kawamura, M. & Iwahori, K. 2004, 'ASR gel composition and expansive pressure in mortars under restraint', *Cement and concrete composites*, vol. 26, no. 1, pp. 47-56.
- Kazmi, S.M.S., Munir, M.J., Patnaikuni, I. & Wu, Y.-F. 2017, 'Pozzolanic reaction of sugarcane bagasse ash and its role in controlling alkali silica reaction', *Construction and Building Materials*, vol. 148, pp. 231-40.
- Khatri, R., Sirivivatnanon, V. & Gross, W. 1995, 'Effect of different supplementary cementitious materials on mechanical properties of high performance concrete', *Cement and Concrete Research*, vol. 25, no. 1, pp. 209-20.
- Kim, T. & Olek, J. 2012, 'Effects of sample preparation and interpretation of thermogravimetric curves on calcium hydroxide in hydrated pastes and mortars', *Transportation research record*, vol. 2290, no. 1, pp. 10-8.
- Knapen, E., Cizer, Ö., Van Balen, K. & Van Gemert, D. 2006, 'Comparison of solvent exchange and vacuum drying techniques to remove free water from early age cement-based materials', *Proceedings of 2nd International RILEM Symposium on Advances in Concrete through Science and Engineering, Quebec, Canada, September 11-13*, Rilem Publications SARL; France.
- Knudsen, T. 1987, 'A Continuous, Quick Chemical Method For The Characterization Of The Alkali-Silica Reactivity Of Aggregates--Proceedings Of The 7th International Conference On Concrete Alkali-Aggregate Reactions, Ottawa, Canada, 1986', *Publication Of: Noyes Publications*.
- Knudsen, T. & Thaulow, N. 1975, 'Quantitative microanalyses of alkali-silica gel in concrete', *Cement and Concrete Research*, vol. 5, no. 5, pp. 443-54.

- Kőrösy, G., Tomolya, K., Janovszky, D. & Sólyom, J. 2013, 'Evaluation of XRD analysis of amorphous alloys', *Materials Science Forum*, vol. 729, Trans Tech Publ, pp. 419-23.
- Kumar, M.J., Srikanth, M. & Rao, K.J. 2012, 'Strength characteristics of self-curing concrete', *Nature*, vol. 20, p. M40.
- Kunal, Siddique, R., Rajor, A. & Singh, M. 2016, 'Influence of bacterial-treated cement kiln dust on strength and permeability of concrete', *Journal of Materials in Civil Engineering*, vol. 28, no. 10, p. 04016088.
- Latifee, E.R. & Rangaraju, P.R. 2015, 'Miniature concrete prism test: rapid test method for evaluating alkali-silica reactivity of aggregates', *Journal of Materials in Civil Engineering*, vol. 27, no. 7, p. 04014215.
- Lawrence, C. 1966, 'Changes in composition of the aqueous phase during hydration of cement pastes and suspensions', *Highway Research Board Special Report*, no. 90.
- Le, H.T., Siewert, K. & Ludwig, H.-M. 2015, 'Alkali silica reaction in mortar formulated from self-compacting high performance concrete containing rice husk ash', *Construction and building materials*, vol. 88, pp. 10-9.
- Lee Rodgers, J. & Nicewander, W.A. 1988, 'Thirteen ways to look at the correlation coefficient', *The American Statistician*, vol. 42, no. 1, pp. 59-66.
- Leemann, A., Katayama, T., Fernandes, I. & Broekmans, M.A. 2016, 'Types of alkali–aggregate reactions and the products formed', *Proceedings of the Institution of Civil Engineers-Construction Materials*, vol. 169, no. 3, pp. 128-35.
- Leming, M., Mitchell, J., Johnson, J. & Ahmad, S. 1996, *Investigation of alkali-silica reactivity in North Carolina highway structures*.
- Leming, M.L. & Nguyen, B.Q. 2000, 'Limits on alkali content in cement—results from a field study', *Cement, Concrete and Aggregates*, vol. 22, no. 1, pp. 41-7.

- Li, C., Thomas, M.D. & Ideker, J.H. 2018, 'A mechanistic study on mitigation of alkali-silica reaction by fine lightweight aggregates', *Cement and Concrete Research*, vol. 104, pp. 13-24.
- Lindgård, J., Andiç-Çakır, Ö., Fernandes, I., Rønning, T.F. & Thomas, M.D. 2012, 'Alkali-silica reactions (ASR): Literature review on parameters influencing laboratory performance testing', *Cement and Concrete research*, vol. 42, no. 2, pp. 223-43.
- Lindgård, J., Nixon, P.J., Borchers, I., Schouenborg, B., Wigum, B.J., Haugen, M. & Åkesson, U. 2010, 'The EU “PARTNER” Project—European standard tests to prevent alkali reactions in aggregates: final results and recommendations', *Cement and concrete research*, vol. 40, no. 4, pp. 611-35.
- Lindgård, J., Thomas, M.D., Sellevold, E.J., Pedersen, B., Andiç-Çakır, Ö., Justnes, H. & Rønning, T.F. 2013, 'Alkali-silica reaction (ASR)—performance testing: influence of specimen pre-treatment, exposure conditions and prism size on alkali leaching and prism expansion', *Cement and Concrete Research*, vol. 53, pp. 68-90.
- Lloyd, G.E. 1987, 'Atomic number and crystallographic contrast images with the SEM: a review of backscattered electron techniques', *Mineralogical Magazine*, vol. 51, no. 359, pp. 3-19.
- Longuet, P., Burglen, L. & Zelwer, A. 1973, 'The liquid phase of hydrated cement', *Revue des Matériaux*, vol. 1, pp. 35-41.
- Lothenbach, B., Durdzinski, P. & De Weerd, K. 2016, 'Thermogravimetric analysis', *A practical guide to microstructural analysis of cementitious materials*, vol. 1, p. 178.

- Lothenbach, B., Scrivener, K. & Hooton, R. 2011, 'Supplementary cementitious materials', *Cement and concrete research*, vol. 41, no. 12, pp. 1244-56.
- Lothenbach, B., Winnefeld, F., Alder, C., Wieland, E. & Lunk, P. 2007, 'Effect of temperature on the pore solution, microstructure and hydration products of Portland cement pastes', *Cement and Concrete Research*, vol. 37, no. 4, pp. 483-91.
- Lu, D., Fournier, B. & Grattan-Bellew, P. 2006, 'Evaluation of accelerated test methods for determining alkali-silica reactivity of concrete aggregates', *Cement and Concrete Composites*, vol. 28, no. 6, pp. 546-54.
- Lu, D., Zhou, X., Xu, Z., Lan, X., Tang, M. & Fournier, B. 2006, 'Evaluation of laboratory test method for determining the potential alkali contribution from aggregate and the ASR safety of the Three-Gorges dam concrete', *Cement and concrete research*, vol. 36, no. 6, pp. 1157-65.
- Lumley, J. 1993, 'The ASR expansion of concrete prisms made from cements partially replaced by ground granulated blastfurnace slag', *Construction and Building Materials*, vol. 7, no. 2, pp. 95-9.
- Mackechnie, J. 2003, 'Properties of New Zealand Concrete Aggregates', *CCANZ*, vol. TR 11.
- Mackechnie, J. 2006, 'Shrinkage of concrete containing Greywacke sandstone aggregate', *ACI materials journal*, vol. 103, no. 5, p. 390.
- Mazer, J.J. & Walther, J.V. 1994, 'Dissolution kinetics of silica glass as a function of pH between 40 and 85 C', *Journal of non-crystalline solids*, vol. 170, no. 1, pp. 32-45.

- Mazumder, M., Ahmed, R., Ali, A.W. & Lee, S.-J. 2018, 'SEM and ESEM techniques used for analysis of asphalt binder and mixture: A state of the art review', *Construction and Building Materials*, vol. 186, pp. 313-29.
- Mehdipour, I. & Khayat, K.H. 2016, 'Effect of Supplementary Cementitious Material Content and Binder Dispersion on Packing Density and Compressive Strength of Sustainable Cement Paste', *ACI Materials Journal*, vol. 113, no. 3.
- Meyer, C. & Xi, Y. 1999, 'Use of recycled glass and fly ash for precast concrete', *Journal of materials in civil engineering*, vol. 11, no. 2.
- Mielenz, R. 1954, 'Petrographic examination of concrete aggregate', *PROCEEDINGS-AMERICAN SOCIETY FOR TESTING AND MATERIALS*, vol. 54, AMER SOC TESTING MATERIALS 100 BARR HARBOR DR, W CONSHOHOCKEN, PA 19428-2959, pp. 1188-218.
- Mitchell, L.D., Beaudoin, J.J. & Grattan-Bellew, P. 2004, 'The effects of lithium hydroxide solution on alkali silica reaction gels created with opal', *Cement and concrete research*, vol. 34, no. 4, pp. 641-9.
- Mo, K.H., Ling, T.-C., Tan, T.H., Leong, G.W., Yuen, C.W. & Shah, S.N. 2020, 'Alkali-silica reactivity of lightweight aggregate: A brief overview', *Construction and Building Materials*, p. 121444.
- Mohammed, T.U., Otsuki, N., Hamada, H. & Yamaji, T. 2002, 'Chloride-induced corrosion of steel bars in concrete with presence of gap at steel-concrete interface', *Materials Journal*, vol. 99, no. 2, pp. 149-56.
- Monteiro, P., Wang, K., Sposito, G., Dos Santos, M. & de Andrade, W.P. 1997, 'Influence of mineral admixtures on the alkali-aggregate reaction', *Cement and concrete research*, vol. 27, no. 12, pp. 1899-909.

- Mukhopadhyay, A. 2013, 'An effective approach to utilize recycled aggregates (RAs) from alkali-silica reaction (ASR) affected Portland cement concrete', *Handbook of Recycled Concrete and Demolition Waste*, Elsevier, pp. 555-68.
- Multon, S., Cyr, M., Sellier, A., Diederich, P. & Petit, L. 2010, 'Effects of aggregate size and alkali content on ASR expansion', *Cement and Concrete Research*, vol. 40, no. 4, pp. 508-16.
- Multon, S., Cyr, M., Sellier, A., Leklou, N. & Petit, L. 2008, 'Coupled effects of aggregate size and alkali content on ASR expansion', *Cement and Concrete Research*, vol. 38, no. 3, pp. 350-9.
- Muscato, C. 2017, '6th Street Bridge: Demolition & Replacement', <<https://study.com/academy/lesson/6th-street-bridge-demolition-replacement.html#lesson>>.
- Nelson, E.B. & Kalousek, G.L. 1977, 'Effects of Na₂O on calcium silicate hydrates at elevated temperatures', *Cement and Concrete Research*, vol. 7, no. 6, pp. 687-94.
- Nijland, T. & Larbi, J. 2010, 'Microscopic examination of deteriorated concrete', *Non-destructive Evaluation of Reinforced Concrete Structures*, Elsevier, pp. 137-79.
- Nixon, P., Canham, I., Page, C. & Bollinghaus, R. 1987, 'SODIUM CHLORIDE AND THE ALKALI-AGGREGATE REACTION--PROCEEDINGS OF THE 7TH INTERNATIONAL CONFERENCE ON CONCRETE ALKALI-AGGREGATE REACTIONS, OTTAWA, CANADA, 1986', *Publication of: NOYES PUBLICATIONS*.
- Nixon, P.J. & Sims, I. 2016a, 'RILEM Recommended Specification: AAR-7.1—International Specification to Minimise Damage from Alkali Reactions in Concrete—Part 1: Alkali-Silica Reaction', *RILEM Recommendations for the*

- Prevention of Damage by Alkali-Aggregate Reactions in New Concrete Structures*, Springer, pp. 131-45.
- Nixon, P.J. & Sims, I. 2016b, 'RILEM Recommended Test Method: AAR-0—Outline Guide to the Use of RILEM Methods in the Assessment of the Alkali-Reactivity Potential of Aggregates', *RILEM recommendations for the prevention of damage by alkali-aggregate reactions in new concrete structures*, Springer, pp. 5-34.
- Nixon, P.J. & Sims, I. 2016c, 'RILEM Recommended Test Method: AAR-3—Detection of Potential Alkali-Reactivity—38 C Test Method for Aggregate Combinations Using Concrete Prisms', *RILEM Recommendations for the Prevention of Damage by Alkali-Aggregate Reactions in New Concrete Structures*, Springer, pp. 79-97.
- Nixon, P.J. & Sims, I. 2016d, 'RILEM Recommended Test Method: AAR-4.1—Detection of Potential Alkali-Reactivity—60° C Test Method for Aggregate Combinations Using Concrete Prisms', *RILEM Recommendations for the Prevention of Damage by Alkali-Aggregate Reactions in New Concrete Structures*, Springer, pp. 99-116.
- NocuÒ-Wczelik, W. 1999, 'Effect of Na and Al on the phase composition and morphology of autoclaved calcium silicate hydrates', *Cement and Concrete Research*, vol. 29, no. 11, pp. 1759-67.
- Novotna, M., Satava, V., Maixner, J., Klouzkova, A., Kostka, P. & Ležal, D. 2003, 'Preparation and characterisation of analcime powders', *Journal of Optoelectronics and Advanced Materials*, vol. 5, no. 5, pp. 1405-9.
- Oberholster, R. & Davies, G. 1986, 'An accelerated method for testing the potential alkali reactivity of siliceous aggregates', *Cement and Concrete research*, vol. 16, no. 2, pp. 181-9.

- Oh, J.E., Jun, Y. & Jeong, Y. 2014, 'Characterization of geopolymers from compositionally and physically different Class F fly ashes', *Cement and Concrete Composites*, vol. 50, pp. 16-26.
- Ojha, K., Pradhan, N.C. & Samanta, A.N. 2004, 'Zeolite from fly ash: synthesis and characterization', *Bulletin of Materials Science*, vol. 27, no. 6, pp. 555-64.
- Olague, C., Wenglas, G. & Castro, P. 2003, 'Influence of alkalis from different sources than cement in the evolution of alkali-silica reaction', *Materiales de Construcción*, vol. 53, no. 271-272, pp. 189-98.
- Oldham, K.B. 2008, 'A Gouy–Chapman–Stern model of the double layer at a (metal)/(ionic liquid) interface', *Journal of Electroanalytical Chemistry*, vol. 613, no. 2, pp. 131-8.
- Owsiak, Z. 2007, 'Testing alkali - reactivity of selected concrete aggregates', *Journal of Civil Engineering and Management*, vol. 13, no. 3, pp. 201-7.
- Palomo, Á., Kavalerova, E., Fernández-Jiménez, A., Krivenko, P., García-Lodeiro, I. & Maltseva, O. 2015, 'A review on alkaline activation: new analytical perspectives'.
- Pereira-de-Oliveira, L.A., Castro-Gomes, J.P. & Santos, P.M. 2012, 'The potential pozzolanic activity of glass and red-clay ceramic waste as cement mortars components', *Construction and Building Materials*, vol. 31, pp. 197-203.
- Perenchio, W.F., Kaufman, I. & Krause, R.J. 1991, 'Concrete Repair in a Desert Environment', *Concrete International*, vol. 13, no. 2, pp. 23-6.
- Pignatelli, R., Comi, C. & Monteiro, P.J. 2013, 'A coupled mechanical and chemical damage model for concrete affected by alkali–silica reaction', *Cement and Concrete Research*, vol. 53, pp. 196-210.
- Pike, R.G. 1958, 'Pressures developed in cement pastes and mortars by the alkali-aggregate reaction', *Highway Research Board Bulletin*, no. 171.

- Poole, A.B. 1992, 'Introduction to alkali-aggregate reaction in concrete', *The alkali-silica reaction in concrete*, pp. 1-29.
- Pope, C.G. 1997, 'X-ray diffraction and the Bragg equation', *Journal of chemical education*, vol. 74, no. 1, p. 129.
- Pourkhorshidi, A., Najimi, M., Parhizkar, T., Jafarpour, F. & Hillemeier, B. 2010, 'Applicability of the standard specifications of ASTM C618 for evaluation of natural pozzolans', *Cement and Concrete Composites*, vol. 32, no. 10, pp. 794-800.
- Powers, T.C. & Steinour, H.H. 1955, 'An interpretation of some published researches on the alkali-aggregate reaction Part 1-The chemical reactions and mechanism of expansion', *Journal Proceedings*, vol. 51, pp. 497-516.
- Poyet, S., Sellier, A., Capra, B., Foray, G., Torrenti, J.-M., Cognon, H. & Bourdarot, E. 2007, 'Chemical modelling of alkali silica reaction: influence of the reactive aggregate size distribution', *Materials and structures*, vol. 40, no. 2, pp. 229-39.
- Putterill, K. & Oberholster, R. 1985, *Investigation of different variables that influence the expansion of concrete caused by alkali-aggregate reaction under natural environmental conditions*, National Building Research Institute, Council for Scientific and Industrial
- Rajabipour, F., Giannini, E., Dunant, C., Ideker, J.H. & Thomas, M.D. 2015, 'Alkali-silica reaction: current understanding of the reaction mechanisms and the knowledge gaps', *Cement and Concrete Research*, vol. 76, pp. 130-46.
- Ramos, V., Fernandes, I., Silva, A.S., Soares, D., Fournier, B., Leal, S. & Noronha, F. 2016, 'Assessment of the potential reactivity of granitic rocks—Petrography and expansion tests', *Cement and Concrete Research*, vol. 86, pp. 63-77.

- Ranc, R. & Debray, L. 1992, 'Reference test methods and a performance criterion for concrete structures', *The Ninth International Conference on Alkali-Aggregate Reaction in Concrete, July 1992, London, Volume 2*.
- Rashidian-Dezfouli, H., Afshinnia, K. & Rangaraju, P.R. 2018, 'Efficiency of Ground Glass Fiber as a cementitious material, in mitigation of alkali-silica reaction of glass aggregates in mortars and concrete', *Journal of Building Engineering*, vol. 15, pp. 171-80.
- Regourd-Moranville, M. 1989, 'Products of reaction and petrographic examination', *Proc. 8th International Conference on Alkali-Aggregate Reaction, Japan Society of Materials Science, Kyoto*, p. 445-456.
- Regourd, M., Hornain, H. & Poitevin, P. 1981, 'The alkali-aggregate reaction-concrete microstructure evolution'.
- Rivard, P., Bérubé, M.-A., Ollivier, J.-P. & Ballivy, G. 2003, 'Alkali mass balance during the accelerated concrete prism test for alkali-aggregate reactivity', *Cement and Concrete Research*, vol. 33, no. 8, pp. 1147-53.
- Rivard, P., Bérubé, M., Ollivier, J. & Ballivy, G. 2007, 'Decrease of pore solution alkalinity in concrete tested for alkali-silica reaction', *Materials and Structures*, vol. 40, no. 9, pp. 909-21.
- RMS 2001, T363, NSW.
- Rocker, P., Mohammadi, J., Sirivivatnanon, V. & South, W. 2015, 'Linking new Australian alkali silica reactivity tests to world-wide performance data', *Proceedings, 24th Biennial Conference of the Concrete Institute of Australia, Melbourne, Australia*.

- Rodrigues, F.A., Monteiro, P.J. & Sposito, G. 1999, 'The alkali-silica reaction: The surface charge density of silica and its effect on expansive pressure', *Cement and Concrete Research*, vol. 29, no. 4, pp. 527-30.
- Rothstein, D., Thomas, J.J., Christensen, B.J. & Jennings, H.M. 2002, 'Solubility behavior of Ca-, S-, Al-, and Si-bearing solid phases in Portland cement pore solutions as a function of hydration time', *Cement and Concrete Research*, vol. 32, no. 10, pp. 1663-71.
- Rowe, G. & Freitag, S. 1991, 'Alkali Aggregate Reaction in New Zealand', *Proceedings of the IPENZ Annual Conference 1991: Engineering, Choosing Our Future; Volume 1-General and Civil; Papers Prepared for the Conference Auckland, February 10-13*, Institution of Professional Engineers New Zealand, p. 77.
- Saha, A.K., Khan, M.N.N., Sarker, P.K., Shaikh, F.A. & Pramanik, A. 2018, 'The ASR mechanism of reactive aggregates in concrete and its mitigation by fly ash: A critical review', *Construction and Building Materials*, vol. 171, pp. 743-58.
- Sajtos, Z., Herman, P., Harangi, S. & Baranyai, E. 2019, 'Elemental analysis of Hungarian honey samples and bee products by MP-AES method', *Microchemical Journal*, vol. 149, p. 103968.
- Saouma, V. & Perotti, L. 2006, 'Constitutive model for alkali-aggregate reactions', *ACI materials journal*, vol. 103, no. 3, p. 194.
- Schouenborg, B., Åkesson, U. & Liedberg, L. 2008, 'Precision trials can improve test methods for alkali aggregate reaction (AAR)—part of the PARTNER project', *13th International Conference on Alkali-Aggregate Reactions in Concrete, Trondheim*, p. 9.

- Scrivener, K.L., Lothenbach, B., De Belie, N., Gruyaert, E., Skibsted, J., Snellings, R. & Vollpracht, A. 2015, 'TC 238-SCM: hydration and microstructure of concrete with SCMs', *Materials and Structures*, vol. 48, no. 4, pp. 835-62.
- Shafaatian, S.M., Akhavan, A., Maraghechi, H. & Rajabipour, F. 2013, 'How does fly ash mitigate alkali-silica reaction (ASR) in accelerated mortar bar test (ASTM C1567)?', *Cement and Concrete Composites*, vol. 37, pp. 143-53.
- Shariq, M., Prasad, J. & Masood, A. 2010, 'Effect of GGBFS on time dependent compressive strength of concrete', *Construction and Building Materials*, vol. 24, no. 8, pp. 1469-78.
- Shayan, A. 2001, 'Validity of Accelerated Mortar Bar Test Methods for Slowly Reactive Aggregates Comparison of Test Results with Field Evidence', *Concrete in Australia*, vol. 24, p. 26.
- Shayan, A. 2007, 'Field evidence for inability of ASTM C1260 limits to detect slowly reactive Australian aggregates', *Australian Journal of Civil Engineering*, vol. 3, no. 1, pp. 13-26.
- Shayan, A. & Morris, H. 2000, 'AVOIDING DELETERIOUS ALKALI-REACTIVE AGGREGATES IN CONCRETE FOR BRIDGES: A COMPARISON OF RTA T363 AND ASTM C1260 ACCELERATED MORTAR BAR TEST METHODS', *AUSTROADS BRIDGE CONFERENCE, 4TH, 2000, ADELAIDE, SOUTH AUSTRALIA*, vol. 3.
- Shayan, A. & Quick, G. 1989, 'Microstructure and composition of AAR products in conventional standard and new accelerated testing'.
- Shayan, A. & Xu, A. 2006, 'Performance of glass powder as a pozzolanic material in concrete: A field trial on concrete slabs', *Cement and concrete research*, vol. 36, no. 3, pp. 457-68.

- Shayan, A., Xu, A. & Andrews-Phaedonos, F. 2003, 'Development of a performance measure for durability of concrete bridges', *Proceedings 21 st Biennial Conference, Concrete Institute of Australia, Brisbane*, pp. 739-57.
- Shekarchi, M., Bonakdar, A., Bakhshi, M., Mirdamadi, A. & Mobasher, B. 2010, 'Transport properties in metakaolin blended concrete', *Construction and Building Materials*, vol. 24, no. 11, pp. 2217-23.
- Shekhawat, B.S. & Aggarwal, D.V. 2014, 'Utilisation of waste glass powder in concrete– A Literature Review', *Int. J. Innovative Res. Sci. Eng. Technol.(An ISO 3297: 2007 Certified Organization)*, vol. 3, no. 7.
- Shi, C., Wu, Y., Shao, Y. & Riefler, C. 2004, 'AAR expansion of mortar bars containing ground glass powder', *Proc. 12th IAARC, Beijing, China, October*, pp. 789-95.
- Shi, Z., Geng, G., Leemann, A. & Lothenbach, B. 2019, 'Synthesis, characterization, and water uptake property of alkali-silica reaction products', *Cement and Concrete Research*, vol. 121, pp. 58-71.
- Shi, Z. & Lothenbach, B. 2019, 'The role of calcium on the formation of alkali-silica reaction products', *Cement and Concrete Research*, vol. 126, p. 105898.
- Shi, Z., Shi, C., Zhang, J., Wan, S., Zhang, Z. & Ou, Z. 2018, 'Alkali-silica reaction in waterglass-activated slag mortars incorporating fly ash and metakaolin', *Cement and Concrete Research*, vol. 108, pp. 10-9.
- Shon, C.-S., Zollinger, D.G. & Sarkar, S.L. 2002, 'Evaluation of modified ASTM C 1260 accelerated mortar bar test for alkali–silica reactivity', *Cement and Concrete Research*, vol. 32, no. 12, pp. 1981-7.
- Sim, J.-I. & Yang, K.-H. 2012, 'Effect of the maximum aggregate size on the workability and mechanical properties of lightweight concrete', *Journal of the Architectural Institute of Korea Structure & Construction*, vol. 28, no. 5, pp. 61-8.

- Sims, I. & Poole, A.B. 2017, *Alkali-Aggregate Reaction in Concrete: A World Review*, CRC Press.
- Sims; Nixon 2003, '191-ARP:'Alkali-reactivity and prevention-Assessment, specification and diagnosis of alkali-reactivity', RILEM Recommended Test Method AAR-1: Detection of potential alkali-reactivity of aggregates-Petrographic method', *Mater. Struct*, vol. 36, pp. 472-9.
- Singh, L.P., Goel, A., Bhattacharyya, S.K., Ahalawat, S., Sharma, U. & Mishra, G. 2015, 'Effect of morphology and dispersibility of silica nanoparticles on the mechanical behaviour of cement mortar', *International Journal of Concrete Structures and Materials*, vol. 9, no. 2, pp. 207-17.
- Sirivivatnanon, V., Mohammadi, J. & South, W. 2016, 'Reliability of new Australian test methods in predicting alkali silica reaction of field concrete', *Construction and Building Materials*, vol. 126, pp. 868-74.
- Skibsted, J. & Snellings, R. 2019, 'Reactivity of supplementary cementitious materials (SCMs) in cement blends', *Cement and Concrete Research*, vol. 124, p. 105799.
- Smith, M.D., Hammack, A., Moser, R.D., Alexander, Q., Burnham, B. & Williams, S.L. 2017, *Concrete growth and fatigue analysis of Chickamauga Lock miter gate anchorages*, ENGINEER RESEARCH AND DEVELOPMENT CENTER VICKSBURG MS VICKSBURG.
- Snellings, R. 2016, 'Assessing, understanding and unlocking supplementary cementitious materials', *RILEM Technical Letters*, vol. 1, pp. 50-5.
- Sohor, M.A.H.M., Mustapha, M. & Mamat, O. 2017, 'The effect of milling duration on silicon dioxide characterization', *MATEC Web of Conferences*, vol. 131, EDP Sciences, p. 03007.

- Song, P. & Hwang, S. 2004, 'Mechanical properties of high-strength steel fiber-reinforced concrete', *Construction and Building Materials*, vol. 18, no. 9, pp. 669-73.
- Sousa, S., Silva, A.S., Velosa, A. & Rocha, F. 2011, 'Use of Tungsten Mine Sludge Waste in the Mitigation of Internal Expansive Reaction', *XII DBMC International Conference on Durability of Building Materials and Components, Porto, Portugal*.
- Soylev, T.A. & François, R. 2003, 'Quality of steel–concrete interface and corrosion of reinforcing steel', *Cement and Concrete Research*, vol. 33, no. 9, pp. 1407-15.
- Standards Australia 2008, *AS 1141.65-2008 Methods for sampling and testing aggregates Alkali aggregate reactivity-*.
- Standards Australia 2014a, *AS1012.2-Methods of testing concrete:* , SAI Global.
- Standards Australia 2014b, ' AS1141.60.1 Methods for sampling and testing aggregates-Potential alkali-silica reactivity', *SAI Global, Sydney, Australia*.
- Standards Australia 2014c, *AS 1012.9 Methods of testing: Compressive strength tests-Concrete, mortar and grout specimens*, SAI Global, Australia.
- Standards Australia 2014d, *AS 1012.11 Methods of testing-Concrete Determination of the modulus of rupture*
SAI Global, Australia.
- Standards Australia 2014e, *AS 1141.60.2 Methods for sampling and testing aggregates.* ,
Sydney.
- Standards Australia 2015, 'Alkali Aggregate Reaction - Guidelines on Minimising the risk of damage to concrete structures in Australia, SA HB 79,' *SAI Global, Sydney*.
- Standards Australia 2016, ' Alkali Aggregate Reaction – Guidelines on Minimising the Risk of Damage to Concrete Structures in Australia. Handbook SA HB 79:2015'.
- Standards New Zealand 2009a, 'NZS 3122, New Zealand'.

- Standards New Zealand 2009b, *Standard Specification for Protland and blended cement*.
NZS 3122, New Zealand.
- Stanton, T.E. 1940, 'Influence of cement and aggregate on concrete expansion',
Engineering News-Record.
- Stark, D. 1995, 'Effects of water-cement ratio on expansion due to ASR', *Concrete Technology Today*, pp. 3-5.
- Stark, D. & Bhatta, M.S. 1986, 'Alkali-silica reactivity: effect of alkali in aggregate on expansion', *Alkalies in concrete*, ASTM International.
- Stark, J. & Bollmann, K. 2000, 'Delayed ettringite formation in concrete', *NORDIC CONCRETE RESEARCH-PUBLICATIONS*-, vol. 23, pp. 4-28.
- Struble, L. & Diamond, S. 1981a, 'Unstable swelling behaviour of alkali silica gels',
Cement and concrete research, vol. 11, no. 4, pp. 611-7.
- Struble, L.J. & Diamond, S. 1981b, 'Swelling properties of synthetic alkali silica gels',
Journal of the American ceramic society, vol. 64, no. 11, pp. 652-5.
- Sun, C., Liu, L. & Du, Y. 2019, 'Analyses of decalcification process of calcium silicate hydrate (CSH) phase', *IOP Conference Series: Materials Science and Engineering*, vol. 490, IOP Publishing, p. 022050.
- Suraneni, P., Fu, T., Azad, V.J., Isgor, O.B. & Weiss, J. 2018, 'Pozzolanicity of finely ground lightweight aggregates', *Cement and Concrete Composites*, vol. 88, pp. 115-20.
- Swamy, R.N. 1991, *The alkali-silica reaction in concrete*, CRC Press.
- Tapas, M., Vessalas, K., Thomas, P., Sirivivatnanon, V. & Kidd, P. 2019, 'Mechanistic Role of Supplementary Cementitious Materials (SCMs) in Alkali-Silica Reaction (ASR) Mitigation', *Concrete in Practice-Progress Through Knowledge*.

- Tapas, M.J., Sofia, L., Vessalas, K., Thomas, P., Sirivivatnanon, V. & Scrivener, K. 2021, 'Efficacy of SCMs to mitigate ASR in systems with higher alkali contents assessed by pore solution method', *Cement and Concrete Research*, vol. 142, p. 106353.
- Tasdemir, C., Tasdemir, M.A., Lydon, F.D. & Barr, B.I. 1996, 'Effects of silica fume and aggregate size on the brittleness of concrete', *Cement and Concrete Research*, vol. 26, no. 1, pp. 63-8.
- Taylor, H.F. 1987, 'A method for predicting alkali ion concentrations in cement pore solutions', *Advances in Cement Research*, vol. 1, no. 1, pp. 5-17.
- Taylor, H.F.M. 1991 *Cement Chemistry*; , Academic: London.
- The New Zealand Ready Mixed Concrete Association 2004, 'Alkali Content of Concrete Mix Water and Aggregates', *The New Zealand Ready Mix Concrete Association Inc.*
- Thomas, J.J., Rothstein, D., Jennings, H.M. & Christensen, B.J. 2003, 'Effect of hydration temperature on the solubility behavior of Ca-, S-, Al-, and Si-bearing solid phases in Portland cement pastes', *Cement and Concrete Research*, vol. 33, no. 12, pp. 2037-47.
- Thomas, M. 1989, 'The suitability of solvent exchange techniques for studying the pore structure of hardened cement paste', *Advances in Cement Research*, vol. 2, no. 5, pp. 29-34.
- Thomas, M. 1996a, 'Field studies of fly ash concrete structures containing reactive aggregates', *Magazine of concrete research*, vol. 48, no. 177, pp. 265-79.
- Thomas, M. 1998, 'The role of calcium in alkali-silica reaction', *Materials Science of Concrete (Sidney Diamond Symposium)*, *The American Ceramic Society, Ohio, USA*, pp. 325-37.

- Thomas, M. 2001, 'The role of calcium hydroxide in alkali recycling in concrete', *Materials Science of Concrete Special*, pp. 225-36.
- Thomas, M. 2011, 'The effect of supplementary cementing materials on alkali-silica reaction: A review', *Cement and concrete research*, vol. 41, no. 12, pp. 1224-31.
- Thomas, M., Fournier, B., Folliard, K., Ideker, J. & Shehata, M. 2006, 'Test methods for evaluating preventive measures for controlling expansion due to alkali-silica reaction in concrete', *Cement and Concrete Research*, vol. 36, no. 10, pp. 1842-56.
- Thomas, M., Hooton, R.D. & Rogers, C. 1997, 'Prevention of damage due to alkali-aggregate reaction (AAR) in concrete construction—Canadian approach', *Cement, Concrete and Aggregates*, vol. 19, no. 1, pp. 26-30.
- Thomas, M.D. 1996b, 'Field studies of fly ash concrete structures containing reactive aggregates', *Magazine of concrete research*, vol. 48, no. 177, pp. 265-79.
- Thomas, M.D.A., Fournier, B. & Folliard, K.J. 2013, *Alkali-Aggregate Reactivity (AAR) Facts Book*, <http://www.fhwa.dot.gov/pavement/concrete/asr/pubs/hif13019.pdf>.
- Thomas, P., Ha Hau, V., Vessalas, K., Sirivivatnanon, V. & South, W. 2019, 'Assessment of Aggregate Reactivity Using Slurry Tests', *29th Biennial National Conference of the Concrete Institute of Australia*.
- Thomas, P., Roboredo, C., Boyd-Weetman, B., Vessalas, K., Farah, D. & Sirivivatnanon, V. 2019, 'Investigation of ASR Reactivity through Slurry Dissolution Tests', *29th Biennial National Conference of the Concrete Institute of Australia*.
- Touma, W., Fowler, D.W. & Carrasquillo, R.L. 2001, *Alkali-silica reaction in portland cement concrete: testing methods and mitigation alternatives*.

- Turanli, L., Shomglin, K., Ostertag, C. & Monteiro, P. 2001, 'Reduction in alkali–silica expansion due to steel microfibers', *Cement and concrete research*, vol. 31, no. 5, pp. 825-7.
- Turriziani, R. 1986, 'Internal degradation of concrete: alkali-aggregate reaction, reinforcement steel corrosion', *Proceedings of the 8th International Conference on Chemistry of Cement, Rio de Janeiro, Brazil*, pp. 388-437.
- Ulm, F.-J., Coussy, O., Kefei, L. & Larive, C. 2000, 'Thermo-chemo-mechanics of ASR expansion in concrete structures', *Journal of engineering mechanics*, vol. 126, no. 3, pp. 233-42.
- Van Aardt, J. & Visser, S. 1977, 'Calcium hydroxide attack on feldspars and clays: possible relevance to cement-aggregate reactions', *Cement and Concrete Research*, vol. 7, no. 6, pp. 643-8.
- Vayghan, A.G., Rajabipour, F. & Rosenberger, J.L. 2016, 'Composition–rheology relationships in alkali–silica reaction gels and the impact on the gel's deleterious behavior', *Cement and Concrete Research*, vol. 83, pp. 45-56.
- Vivian, H. 1981, 'The effect of drying on reactive aggregate and mortar expansions', *Proc., 5th Int. Conf. on Alkali Aggregate Reaction in Concrete*, pp. 252-28.
- Vogelsberger, W., Seidel, A. & Rudakoff, G. 1992, 'Solubility of silica gel in water', *Journal of the Chemical Society, Faraday Transactions*, vol. 88, no. 3, pp. 473-6.
- Vollpracht, A., Lothenbach, B., Snellings, R. & Haufe, J. 2016, 'The pore solution of blended cements: a review', *Materials and Structures*, vol. 49, no. 8, pp. 3341-67.
- Wakizaka, Y., Morita, S. & Kawano, H. 1987, 'Relationship between Mineral Assemblages of Rocks and Their Alkali Reactivities', *Cement Association of Japan Review*, p. 292295.

- Wallau, W., Pirskawetz, S., Volland, K. & Meng, B. 2018, 'Continuous expansion measurement in accelerated concrete prism testing for verifying ASR-expansion models', *Materials and Structures*, vol. 51, no. 3, p. 79.
- Walther, J.V. & Helgeson, H.C. 1977, 'Calculation of the thermodynamic properties of aqueous silica and the solubility of quartz and its polymorphs at high pressures and temperatures', *American Journal of Science*, vol. 277, no. 10, pp. 1315-51.
- Wang, H. & Gillott, J. 1991, 'Mechanism of alkali-silica reaction and the significance of calcium hydroxide', *Cement and Concrete Research*, vol. 21, no. 4, pp. 647-54.
- Wang, W. & Noguchi, T. 2020, 'Alkali-silica reaction (ASR) in the alkali-activated cement (AAC) system: A state-of-the-art review', *Construction and Building Materials*, vol. 252, p. 119105.
- Wigum, B.J. 2012, 'Assessment and development of performance tests for Alkali Aggregate Reaction in Iceland', *Proceedings of the 14th International Conference on Alkali-Aggregate Reactions in Concrete*.
- Wirth, G. & Gieskes, J. 1979, 'The initial kinetics of the dissolution of vitreous silica in aqueous media', *Journal of Colloid and Interface Science*, vol. 68, no. 3, pp. 492-500.
- Woolf, D.O. 1952, 'Reaction of aggregate with low-alkali cement', *Public Roads*.
- Worrell, E. 2008, 'Energy efficiency improvement opportunities for the cement industry'.
- Yamada, K., Sagawa, Y., Nagase, T., Ogawa, S., Kawabata, Y. & Tanaka, A. 2016, 'Importance of alkali-wrapping in concrete prism tests', *Proceedings of 15th International Conference on Alkali Aggregate Reaction, paper 15ICAAR2016_084*.
- Yamada, K., Tanaka, A., Oda, S., Sagawa, Y., Ogawa, S. & Ochiai, T. 2016, 'Exact effects of temperature increase and alkali boosting in concrete prism test with alkali

wrapping', *Proceedings of 14th International Conference on Alkali-Aggregate Reaction*, vol. 203.

Young, J.F., Mindess, S. & Darwin, D. 2002, *Concrete*, Prentice Hall.

Zheng, K. 2016, 'Pozzolanic reaction of glass powder and its role in controlling alkali-silica reaction', *Cement and Concrete Composites*, vol. 67, pp. 30-8.

Zwanenburg, G., Hoefsloot, H.C., Westerhuis, J.A., Jansen, J.J. & Smilde, A.K. 2011, 'ANOVA-principal component analysis and ANOVA-simultaneous component analysis: a comparison', *Journal of Chemometrics*, vol. 25, no. 10, pp. 561-7.

Appendix A

Factorial Analysis Outputs

The results from the principal component and ANOVA factorial analysis outlined in section 5.3.4 are presented in this appendix. The analyses were carried in OriginPro8 at a confidence level of 95% (The effect of the variables with a p-value less than 0.05 is to be considered significant).

Table A1 Correlation matrix table showing possible three principal components and their respective eigenvalues (*extracted from OriginPro8*).

	Eigenvalue	Percentage of Variance	Cumulative
1	8.89108	98.79%	98.79%
2	0.09248	1.03%	99.82%
3	0.01645	0.18%	100.00%
4	0	0.00%	100.00%
5	0	0.00%	100.00%
6	0	0.00%	100.00%
7	0	0.00%	100.00%
8	0	-0.00%	100.00%
9	0	-0.00%	100.00%

Table A2 Extracted principal components and their respective eigenvalues (*extracted from OriginPro8*).

	Coefficients of PC1	Coefficients of PC2	Coefficients of PC3
AK 2.5	0.32745	0.65776	0.63535
AK 3.0	0.33224	0.36037	-0.63215
AK 3.5	0.33493	-0.16777	0.01249
AK 4.0	0.33454	-0.21285	0.21146
AK 5.25	0.33536	-0.00659	-0.05805
T60	0.33205	-0.45863	0.12719
T38	0.33411	0.25652	-0.29246
AG 3	0.33481	-0.17899	-0.14981
AG 6	0.33444	-0.23622	0.15596

Table A3 ANOVA results table for alkali content and temperature factors (extracted from *OriginPro8*).

	DF	Sum of Squares	Mean Square	F Value	P Value
Alkali Content	2	0.1065	0.05325	4.66245	0.0371
Temperature	1	0.00437	0.00437	0.38252	0.55008
Interaction	2	0.00373	0.00186	0.16318	0.85166
Model	5	0.11332	0.02266	1.98432	0.16676
Error	10	0.11421	0.01142	--	--
Corrected Total	15	0.22753	--	--	--

At the 0.05 level, the population means of **Alkali Content** are **significantly** different.
 At the 0.05 level, the population means of **Temperature** are **not significantly** different.
 At the 0.05 level, the interaction between **Alkali Content** and **Temperature** is **not significant**.

Table A4 ANOVA results table for alkali content and age factors (extracted from *OriginPro8*).

	DF	Sum of Squares	Mean Square	F Value	P Value
Alkali Content	2	0.10214	0.05107	3.55053	0.04459
Age	3	0.01544	0.00515	0.35784	0.78393
Interaction	6	0.00792	0.00132	0.09175	0.99659
Model	11	0.1255	0.01141	0.79319	0.64513
Error	24	0.34521	0.01438	--	--
Corrected Total	35	0.47071	--	--	--

At the 0.05 level, the population means of **Alkali Content** are **significantly** different.
 At the 0.05 level, the population means of **Age** are **not significantly** different.
 At the 0.05 level, the interaction between **Alkali Content** and **Age** is **not significant**.

Appendix B

Expansion Tests

The expansion measurements for accelerated mortar bar tests and details of the concrete prism tests carried out in Chapters four, and six are presented in this Appendix. Measurement values presented here are an average of three specimens (mortar bars or concrete prisms).

Investigation of Alkali Limits and Aggregate Blends for Mitigating Deleterious ASR in Concretes (Chapter Four)

Accelerated Mortar Bar Test (AMBT)

Table B0 AMBT Expansion data at the standard ages as per AS 1141.60.1 for mortar bars cured in 0.6M, 0.8M, and 1.0M NaOH solution for 28 days

Sample ID	Mix Description	W/C Ratio	Storage Solution	Expansion (%)		
				10 Days	21 Days	28 Days
WT ¹	60% WT + 40% PR _F	0.47	0.6	0.262	0.650	0.773
			0.8	0.358	0.650	0.753
			1.0	0.368	0.578	0.662
WT ²	60% WT + 40% GW _F	0.47	0.6	0.242	0.635	0.767
			0.8	0.255	0.548	0.658
			1.0	0.300	0.548	0.652
GW _F	100% GW _F	0.47	0.6	0.005	0.018	0.050
			0.8	0.010	0.105	0.185
			1.0	0.023	0.200	0.295
WT	100% WT	0.47	0.6	0.167	0.520	0.683
			0.8	0.128	0.368	0.503
			1.0	0.298	0.580	0.698
RT	100% RT	0.47	1.0	0.350	0.5442	0.744
AS	100% AS	0.47	1.0	0.274	0.844	0.917

Concrete Prism Tests

Table B1 Concrete mix design for CPT and ACPT prisms. *Note: Cement content = 420 kg and water content = 189 kg*

Sample ID	Mix Description	Alkali Content (kg/m ³)	Added NaOH (kg/m ³)	Coarse Aggregate (SSD) (kg)	Fine Aggregate (SSD) (kg)	W/C Ratio	Slump (mm)	Fresh Density (Kg/m ³)	Air Content (%)	
WT ¹	PR _C = Coarse Aggregate	2.5	0.083	1239	411	274	0.45	70	2505	2.2
		3.0	0.728	1239	411	274	0.45	70	2502	2.1
		3.5	1.374	1239	411	274	0.45	75	2509	1.9
	WT ¹ = Fine Aggregate	4.0	2.019	1239	411	274	0.45	60	2519	2.4
		5.25	3.633	1239	411	274	0.45	70	2506	2.0
WT ²	GW _C = Coarse Aggregate	2.5	0.083	1101	410	273	0.45	55	2422	1.6
		3.0	0.728	1101	410	273	0.45	60	2423	1.7
		3.5	1.374	1101	410	273	0.45	60	2429	1.6
	WT ² = Fine Aggregate	4.0	2.019	1101	410	273	0.45	60	2427	1.8
		5.25	3.633	1101	410	273	0.45	65	2429	1.9
GW	GW _C = Coarse Aggregate	2.5	0.083	1101	751	0.45	55	2413	2.8	
		3.0	0.728	1101	751	0.45	50	2410	2.7	
		3.5	1.374	1101	751	0.45	40	2432	2.1	
	GW _F = Fine Aggregate	4.0	2.019	1101	751	0.45	40	2457	2.2	
		5.25	3.633	1101	751	0.45	45	2429	2.7	
RT	PR _C = Coarse Aggregate	2.5	0.083	1044	840	0.45	90	2530	1.9	
		3.0	0.728	1044	840	0.45	90	2519	1.9	
		3.5	1.374	1044	840	0.45	95	2521	2.0	
	RT = Fine Aggregate	4.0	2.019	1044	840	0.45	100	2522	2.2	
		5.25	3.633	1044	840	0.45	100	2514	1.9	
AS	GWC = Coarse Aggregate	2.5	0.083	----	----	0.45	50	2377	0.8	
		3.0	0.728	----	----	0.45	60	2381	1.2	
		3.5	1.374	----	----	0.45	70	2370	1.3	
	AS = Fine Aggregate	4.0	2.019	----	----	0.45	80	2366	1.6	
		5.25	3.633	----	----	0.45	85	2371	1.8	

Table B2 CPT Expansion data for concrete prisms at varying alkali content at the standard age of 12 month as per AS 1141.60.2

Sample ID	Alkali Content (kg/m ³)	12-month Expansion (%)
WT ¹	2.5	-0.017
	3.0	-0.013
	3.5	-0.001
	4.0	-0.001
	5.25	0.015
WT ²	2.5	-0.011
	3.0	-0.017
	3.5	-0.009
	4.0	-0.013
	5.25	-0.003
GW	2.5	-0.009
	3.0	-0.012
	3.5	-0.005
	4.0	-0.016
	5.25	-0.003
RT	2.5	-0.004
	3.0	-0.002
	3.5	0.002
	4.0	0.002
	5.25	0.051
AS	2.5	0.027
	3.0	0.044
	3.5	0.157
	4.0	0.441
	5.25	0.490

Table B3 ACPT expansion data for concrete prisms at varying alkali content after 3, 4, and 5 months. *Note:*

The recommended expansion age for reactivity classification as per RILEM AAR-4.1 is 4 months.

Sample ID	Alkali Content (kg/m ³)	Expansion (%)		
		3 M	4 M	5 M
WT ¹	2.5	0.000	-0.001	-0.001
	3.0	-0.003	-0.003	-0.004
	3.5	-0.001	0.002	0.001
	4.0	0.005	0.005	0.005
	5.25	0.014	0.030	0.042
WT ²	2.5	-0.010	-0.008	-0.009
	3.0	-0.009	-0.010	-0.010
	3.5	-0.006	-0.007	-0.005
	4.0	-0.007	-0.007	-0.007
	5.25	0.006	0.007	0.013
RT	2.5	-0.001	-0.003	-0.003
	3.0	-0.002	-0.001	-0.001
	3.5	0.004	0.000	0.002
	4.0	0.006	0.006	0.005
	5.25	0.023	0.030	0.035
AS	2.5	-0.004	-0.004	-0.003
	3.0	-0.008	-0.008	-0.009
	3.5	0.004	0.004	0.026
	4.0	0.141	0.159	0.169
	5.25	0.359	0.397	0.419

Investigating the ASR Mitigating Potential of Ground Reactive Aggregate Fines (Chapter Six)

Accelerated Mortar Bar Test (AMBT)

Table B4 AMBT expansion data at the standard ages for aggregates used as ground reactive aggregate fines (GRAFs) (Figure 6.20)

Sample ID	W/C Ratio	Expansion (%)		
		10 Days	21 Days	28 Days
WT	0.47	0.436	0.844	0.917
GW	0.47	0.096	0.240	0.340
RH	0.47	0.087	0.200	0.295
PR	0.47	0.002	0.005	0.008

Table B5 56-days AMBT expansion data at standard ages for mortar bars containing reactive test aggregates WT and RT, and cement replacement levels of GRAFs (Figure 6.21)

Sample ID	W/C Ratio	Dosage (%)	Expansion (%)		
			10 Days	21 Days	56 Days
WT-Control	0.47	----	0.415	0.58	0.932
WT_G	0.47	10	0.323	0.436	0.713
		25	0.097	0.200	0.392
		40	0.034	0.060	0.194
GW_G	0.47	10	0.230	0.376	0.632
		25	0.152	0.234	0.429
		40	0.100	0.134	0.248
RH_G	0.47	10	0.419	0.569	0.819
		25	0.267	0.405	0.588
		40	0.171	0.227	0.303
PR	0.47	10	0.409	0.534	0.894
		25	0.266	0.469	0.841
		40	0.254	0.431	0.797
RT-Control	0.47	----	0.350	0.544	0.933
WT_G	0.47	10	0.268	0.431	0.561
		25	0.122	0.245	0.519
		40	0.069	0.091	0.136
GW_G	0.47	10	0.280	0.514	0.926
		25	0.230	0.396	0.665
		40	0.100	0.200	0.309
RH_G	0.47	10	0.325	0.461	0.642
		25	0.319	0.436	0.596
		40	0.191	0.256	0.367

Concrete Prism Tests

Table B6 Concrete mix design for CPT and ACPT prisms containing reactive test aggregate WT and 25% cement replacement of GRAFs

Sample ID	Alkali Content (kg/m ³)	Added NaOH (kg/m ³)	Coarse Aggregate(SSD) (kg)	Fine Aggregate (SSD) (kg)	W/C Ratio	Slump (mm)	Fresh Density (Kg/m ³)	Air Content (%)
OPC	5.25	3.633	1251	660	0.42	55	2525	1.8
25% WT _G	5.25	3.633	1251	660	0.42	45	2467	2.1
25% RH _G	5.25	3.633	1251	660	0.42	50	2468	2.7
25% GW _G	5.25	3.633	1251	660	0.42	45	2485	2.5
25% FA	5.25	3.633	1251	660	0.42	65	2512	1.6

Table B7 CPT and ACPT expansion data for concrete prisms containing reactive test aggregate WT and 25% cement replacement of GRAFs

Sample ID	Expansion (%)			
	12 months CPT	ACPT at respective ages		
		3 months	4 months	5 months
WT-Control	0.045	0.048	0.007	0.076
25% WT _G	0.019	0.015	0.019	0.021
25% RH _G	0.036	0.028	0.033	0.039
25% GW _G	0.021	0.019	0.017	0.015
25% FA	-0.001	-8.E-04	0.004	-6.6E-04

Appendix C

Chemical Tests

The results on the dissolution and GAST chemical tests carried out in Chapters four and six are presented in this Appendix.

Table C0 Dissolution test results as per ASTM C 289 (Figure 4.2, Table 5.1)

Aggregate	Dissolved Silica (mmol/L)	Reduction in Alkalinity (mmol/L)	Reactivity (ASTM C289)
WT	124.9	40.1	Deleterious
GW	29.1	40.1	Innocuous
RT	146.2	38.7	Deleterious

Table C1 TGA results of aggregates after 28 days of GAST (Table 5.1)

Aggregate	Portlandite Content (Relative area under the curve)
WT	0.012
RT	0.038
GW	0.025
AS	0.019